Secular variation of the Earth's magnetic field in the South West Pacific

Thesis submitted in accordance with the requirements of
the University of Liverpool for the degree of Doctor in Philosophy
by
Florian Stark

September 2011

Abstract

The dearth of archaeomagnetic intensity data from the southern hemisphere is a limiting factor in evaluating models of global geomagnetic field evolution during the Holocene. High quality microwave archaeointensity data were obtained from 106 individual ceramic fragments (33 archaeological contexts) from Fiji, Vanuatu, New Caledonia, Bismarck Archipelago and Solomon Islands in the SW Pacific. Complementary Thellier-type experiments, corrected for anisotropy give good agreement with the microwave results. Magnetic mineralogical investigations were performed using a Variable Field Translation Balance (VFTB). Single Curie temperatures between 460°C to 580°C were typically found for most of the island regions indicating an impure to pure magnetite phase. The remaining samples revealed a second T_C around 350°C, which was primarily found in samples from the Island of Efate. SEM and EDX investigations have been carried out on selected samples and identified some large titanomagnetite grains (> 50 μm) which were probably introduced by adding beach or river sand to the clay matrix during the manufacturing of the pottery. The newly established archaeointensity curve covers a time interval from 1000 BC to 1750 AD and suggests a more distinctive geomagnetic field strength variation during the last three millennia than those predicted by current global models. The majority of the new data prior to 250 AD exhibit significantly lower intensity than predicted by current global field models (CALS3k.3 and ARCH3k) for the region, with an apparent intensity minimum at 250 BC reaching as low as 50% of the present-day field strength. Between 400 AD and 1500 AD, the data are broadly consistent with the global field models but with a 20% higher field between 1200 and 1400 AD. Two significant increases of the geomagnetic field strength between 200 AD and 400 AD as well as 1200 AD and 1400 AD correlate with intensity peaks found in French data sets and hint at an occurrence of archaeomagnetic jerks in the SW Pacific. Strong climatic variations around 1300 AD in the SW Pacific seem to fit to the second intensity peak and could support the hypothesis that archaeomagnetic jerks influence the climate. Nevertheless more data are needed for an unambiguous identification of such geomagnetic events and their correlation with the climate. For the first time in the SW Pacific this study has attempted to provide chronological information using archaeomagnetic dating. Three poorly dated archaeological sites on the Santa Cruz Islands, which are an important link between Near and Remote Oceania,

were investigated. Similar archaeointensity results found from sites RF-2 and RF-6 on Reef Island contrast with a significantly higher value obtained from Nendö (SZ-8) potsherds suggesting a different age for this site. The SW Pacific archaeointensity results highlighted the potential of a new and independent dating tool that can be used by archaeologists to solve problems that cannot be addressed using conventional dating methods, such as the timing of the advance of the Lapita peoples across Oceania.

Acknowledgements

First of all, I would like to thank my supervisors Mimi Hill, John Shaw and Richard Holme for their guidance and patience throughout the work for this thesis. I thank John Cassidy (University of Auckland) for his support, ideas and his help in improving my spoken and written English. In particular Mimi, John and John are thanked for scrutinizing the manuscripts of my first publication to Earth and Planetary Science letters and of this thesis. I am very grateful to Peter Sheppard (University of Auckland) for his help on archaeology and for organising the SW Pacific ceramics. In particular I would like to thank Peter White (University of Sydney) for Duke of York samples, Simon Best (University of Auckland) for Lau samples, Stuart Bedford (Australian National University) for samples from Vanuatu, Christophe Sande (Institute of Archaeology of New Caledonia) for samples from New Caledonia and Roger Green (University of Auckland) for samples from Santa Cruz and Solomon Islands. Monika Korte (GFZ Potsdam) is thanked for rerunning CALS3k.3 and ARCH3k with my data. William R. Dickinson (University of Arizona) is acknowledged for petrographical studies on a selection of samples and Paul Hands (University of Birmingham) for preparing thin sections for the SEM investigations. Betty Mariani and Carmen Pinnington are thanked for the introduction and help they provided with the SEM study. I would like to thank Andy Biggin, Andy Roberts, Ceri Davis, John Hakes, Laura Roberts Artal, Maxwell Brown, Megan Thomas, Müzeyyen Taspinar, Orhan Tatar, Pinar Ertepinar and Neil Suttie for many fruitful discussions about various topics (not only geomagnetism) and for showing me a great time in and outside the laboratory. Special thanks to Robin Aspey for his technical support, his introduction to the U.K. and showing me a life outside of the campus. I am thankful to John Piper for his support and field trips to Wales and the Yorkshire Dales. Many thanks to Andy Herries for his company during our measurement marathons in the lab and for a fantastic field trip to the caves of South Africa. Verena Hermann and Valerian Bachtadse are thanked for joining me on a wonderful expedition to Antarctica and Richard Chiverrell is thanked for a great time on Iceland. Nikolai Petersen is thanked for his help on the magnetic mineralogy and the VFTB and Stuart Gilder for giving me the opportunity to do some experiments at the Geomagnetism Laboratory in Munich. Special thanks to Roman Leonhardt, who actually brought me to archaeomagnetism and for umpteen points of advice on

the Thellier technique. I extend thanks to all the other friends that I have made during the course of my PhD study. Finally, last but not least, my heartiest thanks go to my parents for their unrestricted support and love. This study was supported by the Marsden Fund, Royal Society of New Zealand (grant number UOA0722) and the University of Liverpool.

Parts of this thesis are based on, or directly taken from a paper published in Earth and Planetary Science Letters:

Stark, F., Cassidy, J., Hill, M. J., Shaw, J., Sheppard, P., 2010. *Establishing a first archaeointensity record for the SW Pacific.* Earth and Planetary Science Letters 298 (1-2), 113 – 124.

Some results of this work were presented as contributions to national and international meetings. A selection is listed in temporal order in the following. The abstracts are documented in the abstract volumes of the meetings.

Stark, F., Cassidy, J., Gratton, M. N., Hill, M. J., Shaw, J., Sheppard, P. J., 2008. *Establishing a new Archaeomagnetic Record for the SW Pacific.* AGU Fall Meeting Abstracts, A690+, 2008AGUFMGP11A0690S.

Stark, F., Hill, M. J., Cassidy, J., Shaw, J., Sheppard, P., Dec. 2009. *Geomagnetic field strength variations derived from SW Pacific ceramics.* AGU Fall Meeting Abstracts , B4+, 2009AGUFMGP33B.

Stark, F., Hill, M., Cassidy, J., Shaw, J., Sheppard, P., July 2011. *Intensity of the Earth's magnetic field over the last 3000 years in Melanesia and the potential of archaeomagnetic dating.* IAGA Melbourne A043S2.

Contents

List of Figures

List of Tables

Abbreviations and symbols

Abbreviations

α_{95}	radius of cone of 95% confidence
δ(CK)	relative check error
δ(pal)	cumulative check difference
δ(TR)	intensity difference between first and repeated demagnetisation step
$\delta(t^*)$	true tail of a pTRM
σ_{hys}	shape parameter after Fabian (2003)
AC	additivity check
AD	Anno Domini
ARCH3k.3	continuous global geomagnetic field model for the last 3000 years based on archaeomagnetic data
ATRM	anisotropy of thermoremanent magnetisation
BSE	back scattered electrons
BC	before Christ
BP	before present
CALS3K.3	continuous global geomagnetic field model for the last 3000 years based on archaeomagnetic and palaeomagnetic data
ChRM	characteristic remanence
CR	cooling rate
CRA	conventional radiocarbon age
CRM	chemical remanent magnetisation
CT	context (archaeological)
DoY	Duke of York Islands
EDX	energy dispersive spectroscope
F	geomagnetic field strength (archaeointensity)
FMR	ferromagnetic resonance
IGRF	International Geomagnetic Reference Field
IRM	isothermal remanent magnetisation
MAD	maximum angular deviation
MD	multi domain

MSP	melting spot
MW	microwave
MWS	microwave system
NRM	natural remanent magnetisation
PS	potsherd
PSD	pseudo single domain
pT_MRM	microwave produced partial thermoremanent magnetisation
pTRM	partial thermoremanent magnetisation
S_{300}	coercivity parameter after Bloemendal et al. (1992)
SD	single domain
SEM	scanning electron microscope
SIRM	saturation isothermal remanent magnetisation
SP	superparamagnetic
SV	secular variation
SW	south west
TE	transverse electric
TM	titanomagnetite
TRM	thermoremanent magnetisation
VADM	virtual axial dipole moment
VFTB	variable field translation balance
VRM	viscous remanent magnetisation

Symbols and constants

B [T]	magnetic field strength
B_c [T]	coercive force
B_{cr} [T]	remanence coercivity
M $[Am^2kg^{-1}]$	specific magnetisation
M_r $[Am^2kg^{-1}]$	remanent magnetisation
M_{rs} $[Am^2kg^{-1}]$	specific saturation remanence
M_s $[Am^2kg^{-1}]$	specific saturation magnetisation
T_b $[°C]$	blocking temperature
T_C $[°C]$	Curie temperature
T_{ub} $[°C]$	unblocking temperature
$\mu_0 = 4\pi \cdot 10^{-7} \frac{Vs}{Am}$	magnetic permeability in a vacuum

Chapter 1

Introduction

The Earth is shielded by a magnetic field which largely deflects the incoming cosmic radiation like the solar wind. This geomagnetic field, however, is not stable and has undergone dramatic variations in space and time throughout the history of Earth. Probably the most remarkable variation is the reversal when the Earth's magnetic field changes its polarity. With some exceptions the phenomena of reversal has occurred at irregular intervals of several hundred thousand years during late Cenozoic times and the last reversal occurred around 780,000 years ago. Since the first investigations of the geomagnetic field strength conducted by Carl Friedrich Gauss in 1832 ongoing measurements have revealed a significant decrease of the global dipole field by more than 10% (McElhinny and Senanayake, 1982; Jackson et al., 2000). Notwithstanding, this short period of direct observations does not allow us to draw substantial conclusions about reasons for this decrease and its likely consequences. For a better understanding of the geomagnetic field information gathered by palaeomagnetic and archaeomagnetic data is needed to extend the observational time range back beyond direct field measurements. Whereas palaeomagnetism deals with the magnetic remanence in materials caused by natural geological processes such as sedimentation and volcanism archaeomagnetism is based on artefacts inadvertently left behind by ancient civilizations.

Archaeomagnetic measurements utilise the fact that burnt archaeological materials (e.g. pottery, bricks, kilns) contain a record of the magnetic field present during their last firing. Since the pioneering work of Thellier in the 1930's this kind of material has been recognised as an excellent recorder of the ancient geomagnetic field. If the burnt archaeological material is well dated, then the extracted geomagnetic information extracted contributes to a secular variation (SV) record which extending well beyond the short time of direct measurements obtained by satellites, observatories and historical data. Secular variation records are crucial for the investigation of physical processes occurring deep in the Earth, such as convection near the core-mantle boundary. Furthermore, if the SV for a particular region is well defined then undated burnt archaeological material can be dated by comparing the magnetic record it contains

with the existing SV curve (e.g. Kovacheva et al., 2004; Schnepp and Lanos, 2005). For an unambiguous assessment, however, the full archaeomagnetic vector (inclination, declination and intensity) is needed. This vector can often be obtained from kilns, whereas samples from displaced bricks, tiles and ceramics mostly only provide the intensity. Moreover a high resolution full vector description of the Earths magnetic field plays a key role in investigation of possible interactions between geomagnetic field variations and climate changes. For Western Europe, where the geomagnetic field is well constrained for the past three millenia, Gallet et al. (2003) were able to describe a remarkable coincidence between sharp changes in geomagnetic field directions and intensity maxima. These enhanced secular variations denoted as archaeomagnetic jerks (four have been detected so far $\sim$ 800 BC, $\sim$ 200 AD, $\sim$ 750 AD and $\sim$ 1400 AD) seem to appear in a time span within a century, which cannot be resolved for poorly constrained areas. Interestingly they seem to coincide with the occurrence of centennial cooling periods in the North Atlantic (Gallet et al., 2005). Moreover, major upheavals in civilised societies in Iran and Egypt as well as the decline of the Maya civilisation in South America coincide with the phenomena (Gallet et al., 2006). Anyway there is still the conundrum about what could cause an archaeomagnetic jerk and whether it is a local or global phenomena.

Whilst the database of archaeomagnetic measurements is continually growing (e.g. De Marco et al., 2008; Kovacheva et al., 2009; Donadini et al., 2009) and experimental methods have advanced such that data quality is improving (e.g. Leonhardt et al., 2003; Le Goff and Gallet, 2004; Walton, 2004; Biggin et al., 2007; Böhnel et al., 2009), there is considerable unevenness in the data distribution both spatially and temporally. On all time scales there is a notable lack of data from the southern hemisphere. In the SW Pacific region in particular, there is no comparable study to that presented here. The nearest regions from which directional SV studies have been obtained are lake sediment studies from Australia (e.g. Barton and McElhinny, 1982; Constable and McElhinny, 1985) and New Zealand (Turner and Lillis, 1994). There is a relative palaeointensity record from the NE Australian lake sediments available (Constable, 1985), but the nearest region for which there are absolute archaeointensity data is South Australia (Barbetti, 1983). Current global field models covering archaeological timescales such as CALS3k.3 (Korte et al., 2009), which use archaeomagnetic data from lake sediments and archaeological artifacts, are therefore strongly influenced by the northern hemisphere data and are not necessarily well constrained in regions such as the SW Pacific where there are few data. Nevertheless even a well constrained global field model and an archaeomagnetic master curve, respectively are only as good as their dataset. Every archaeo- and palaeomagnetic intensity determination bears potential sources of errors which are described by several studies (e.g. Bowles et al., 2002; Donadini et al., 2007). Besides experimental inaccuracities, neglecting magnetic

anisotropy can lead to a substantial scatter of data and therefore may obscure any real trends. Usually, archaeological materials bear an intrinsic anisotropy of TRM (ATRM) acquired during ancient firing. In particular, pottery samples often demonstrate strong magnetic anisotropy, generated from a preferential alignment of magnetic grains during manufacturing, which could lead to archaeointensity errors from 30% up to 60% for wheel thrown pottery (Rogers et al., 1979). Many studies dealing with archaeointensities derived from potsherds also take into account the differences between ancient and laboratory cooling that can have an effect on the archaeointensity determinations (e.g. Fox and Aitken, 1980; Halgedahl et al., 1980; Genevey and Gallet, 2002; Hill et al., 2007). Neglecting this effect can lead to an average error of 8% (Gallet et al., 2009). Nevertheless this effect depends on the burning technique and it is necessary to consider whether kilns, firing pits or simple open blazes were used to fire the pottery.

The key aim of this study is to determine for the first time the magnitude, range and rate of variation of field intensity over the past three millenia in the SW Pacific region. These new data will significantly improve the resolution of current generalised global field models in this region and subsequently contribute to modeling studies of the geodynamo. Ultimately, the aim of this project is to define a well constrained and statistically robust archaeointensity curve that can be used for dating SW Pacific ceramics. In particular ceramics from the Lapita people, which reached and colonized for the first time in history of mankind the archipelagos east of the Solomon island chain, are of major interest. Most of the Lapita sites cannot be dated by means of radiocarbon as the artefacts are from intertidal areas and are not stratigraphically constrained. Archaeomagnetic dating has the potential advantage of dating ceramics directly and is therefore a promising alternative for helping to shed new light on controversial theories about the colonization history of the SW Pacific during the Lapita era and beyond. In order to extract high quality archaeointensity data from SW Pacific ceramics, the latest state-of-the-art 14 GHz microwave system (MWS) has been used, and is unique in the world and housed at the Oliver Lodge building at the University of Liverpool. This MWS reduces magnetic mineralogical alteration during the trail of intensity determination since the sample is not heated as in conventional thermal-based techniques. Nevertheless, to cross check the MWS results, complementary Thellier (thermal-based) experiments were also conducted. Additionally, magnetic mineralogical investigations have been performed using a Variable Field Translation Balance (VFTB) to detect carriers of the thermoremanent magnetization (TRM). In order to gather more information about the potsherds SEM and petrographical investigations were carried out on polished thin sections of selected samples. For establishing an archaeointensity curve only sherds were used which were found in very well defined and sealed contexts, and dated by radiocarbon and/or pottery style to constrain the age uncertainty. The suite of samples encompasses the last three millenia and comes from several island groups

in Melanesia including the Bismarck Archipelago in the east to the Fiji islands in the west.

This thesis can be subdivided in to five sections. An introduction into archaeological and geographical settings in the SW Pacific and a description of the sampled materials can be found in Chapter 2. The methodology of the experiments and analysing techniques conducted in the laboratories are outlined in Chapter 3. The results of measurements and investigations of ceramics procured from the Fiji Lau Group, Vanuatu, New Caledonia and Bismarck Archipelago with the Solomon Islands are described in Chapters 4 to 7. The results of the heating experiments using a Thellier technique and examining cooling rate as well as anisotropy dependency are described in Chapter 8. The results and their implications are comprehensively discussed in Chapter 9 and a summary of the outcome of this PhD project as well as an outlook for future work is given in the final Chapter 10. During the course of this PhD project further archaeomagnetic investigations have been carried out and the results are outlined in the Appendix C and D. These investigations comprise archaeomagnetic dating of an historical Icelandic lava flow using palaeomagnetic directions, and successful MW intensity measurements on a contemporaneous Spanish hearth which are part of a submitted paper to the Journal of Quaternary Research.

An ample variety of supporting physical methods was employed to determine the magnetic mineralogical and archaeomagnetic characteristics of the samples. Theories and fundamental principles behind the applied methods are only outlined here since they are beyond the scope of this thesis. Nevertheless for a deeper understanding the reader is referred to the textbooks and papers noted at the beginning of a Chapter and/or a section.

Chapter 2

Archaeological and geographical settings

This chapter is divided into four parts. The first part outlines the prehistorical colonisation of the SW Pacific in particular focussing on the dispersion of the Lapita people and their descendants in Near and Remote Oceania. The second part discusses (pre)historic SW Pacific pottery. Original manufacturing techniques and source materials are explained. The third part describes provenances, contexts and dating of the ceramic series investigated for this thesis. The last part gives a short insight into the dating and calibration techniques used to determine the ages of the potsherds.

2.1 The colonisation of the SW Pacific and the expansion of the Lapita people

Around 50,000 years ago the first modern humans coming from mainland Asia migrated southward via Indonesia and settled in Australia and New Guinea, which were then connected. Supported by a lower sea level and the usage of simple rafts they also managed to reached the Bismarck Archipelago and the very east end of the Solomon island chain which was for many thousands of years the outermost post of mankind in the SW Pacific. Together with New Guinea and the Admiralty Islands, this region is also referred to as Near Oceania (Kirch, 2000).

The Lapita people, ancestors of all Austronesian speaking people in Remote Oceania, suddenly emerged in the Bismarck Archipelago (Near Oceania) around 1500 BC. Improved sailing skills and new innovations (outrigger canoe) enabled them to colonize Remote Oceania (comprising all areas east of the main Solomon Islands including the Polynesian islands of Samoa and Tonga) in the subsequent centuries (Fig. 2.1). Archaeologists assume that they are descendents of a branch of Austronesian speaking people which migrated from Taiwan to the south east ($\sim$ 5000 BC) and mingled with the indigenous Papuan inhabitants in the Bismarck Archipelago (Green, 1991; Bellwood, 1991). The Lapita are recognized as an agricultural and seafaring society who devel-

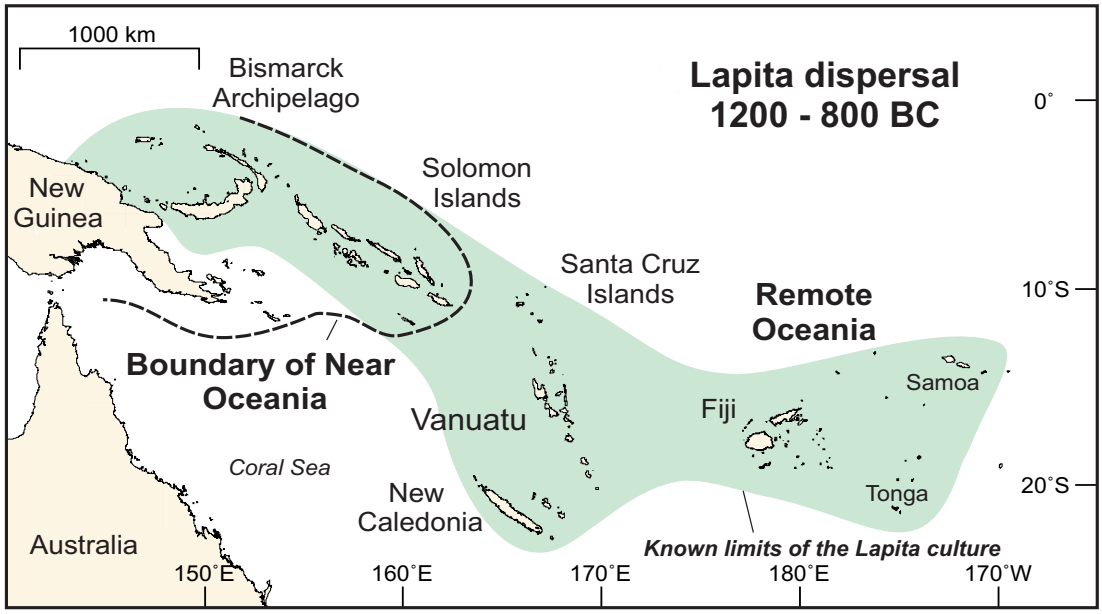

Figure 2.1: Maximal dispersal of the Lapita culture (green area) adapted from Kirch (2000). The dashed line divides Near and Remote Oceania (Green (1991).

oped a remarkable distinctive pottery style and maintained a trading network between their dispersed island communities.

It is still a conundrum how Remote Oceania was colonized. About three centuries after the first appearance of the Lapita in Near Oceania, they suddenly set out around 1200 BC to venture into Remote Oceania. Nearly instantaneously they colonized an area from the Bismarck Archipelago to the easternmost Samoan island (Fig. 2.1), implying a strong driving force (Kirch, 1997). Currently there are two major models to explain how the SW Pacific was populated. One describes a uniform wave of advance through the Solomons and out into Remote Oceania and the other suggests that early settlers leap-frogged (Sheppard and Walter, 2006) over 2000 km from the Bismarcks, and across the previously-settled Solomons, to Remote Oceania (e.g. Green, 1991). In order to evaluate these models the timing of settlements and the rate of migration must be known. Unfortunately, the age of most of the crucial Lapita sites are unknown. The reason is that archaeological artefacts (i.e. pottery) from these sites of obvious Lapita age in the main Solomon Islands are invariably found within inter-tidal deposits (Wickler, 2001) and lack intact contexts vital for effective dating by conventional means such as radiocarbon methods (Felgate, 2003). It is commonly assumed that the main Solomon Islands have been occupied by early Lapita settlers (Green, 1979), but as all known Lapita sites in the main Solomons are found as intertidal deposits, the dates of this early settlement and its link to the age of Lapita settlement in the south-east Solomons (Santa Cruz Islands) and Bismarck Archipelago, are hardly known. Once a geomagnetic reference curve has been set up for this region employing

Figure 2.2: Typical Lapita potsherd found on Santa Cruz (SE Solomon Islands), showing a characteristic dentate stamp pattern and a human face.

archaeomagnetic dating for such sites should help to establish the rate and pattern of settlement in both Near and Remote Oceania.

2.2 Prehistoric Lapita and SW Pacific pottery

The advent of Lapita culture goes along with the emerging of a new type of ceramic series. This so called Lapita pottery was decorated using a toothed (dentate) stamped method (Fig. 2.2) and the motifs were mainly showing human faces. The Lapita also produced plain vessels which were probably used for storing food, while decorated pottery was likely to be utilized for trading and ritual purposes (Kirch, 2000).

During the rapid expansion into Near and Remote Oceania, the knowledge of pottery manufacturing was brought to the new settlements and ceramics were produced all over from Island Melanesia to Tonga and Samoa. In the course of the following centuries, advanced isolation led to a cultural differentiation and SW Pacific pottery became gradually undecorated. Around the 10th century decorations disappeared entirely (Bellwood, 1978; Kirch, 2000). Nowadays, findings of potsherds along with radiocarbon dating play a key role in tracking down migration pattern during the Austronesian expansion in the SW Pacific. Nevertheless, the holistic picture is still vague, since most pottery is found within intertidal zones and cannot be reliably dated.

2.2.1 Manufacturing techniques of the pottery

Experimental archaeologists assume that ancient Lapita pottery was produced in a similar way as is still practiced in some Oceanian societies. Several publications describe early and recent pottery manufacturing in the SW Pacific area (e.g. Roth, 1935; Irwin, 1985; Kirch, 1997). Although the locations of the observations of Irwin (1985) on Mailu (Papua New Guinea) and Roth (1935) on Vitu Levu (Fiji) are separated by a distance of more than 3000 km from each other, there are striking similarities in the manufacturing techniques, which suggests a more or less similar process of pottery making throughout the SW Pacifc islands. Typical manufacturing stages of traditional pottery production are illustrated in Fig. 2.3a-f which were documented by Roth (1935). Clay, the starting material, was often mixed with beach or river sand (e.g. Kirch, 1997; Dickinson, 2006) which improves the workability and also stabilises vessels after firing. These deliberate added aplastic admixture is in the following denoted as temper or tempered material (Shepard, 1963). The ancient potters then formed the raw mass to "pencils" and pieced them together (coil method) to fabric the raw pot (Fig. 2.3a). The Lapita pottery was produced without the aid of a wheel but using a paddle-and-anvil method to thin out the walls of a vessel instead (Fig. 2.3b). Paddle and anvil technique simply involves striking the partially dry surface of the pot with a wooden "paddle" while holding a smooth flat stone "anvil"on the inside surface opposite the point struck. This is a way of thinning and smoothing a pot (pers. comment Peter Sheppard). Because there is no evidence for kilns, (e.g. Irwin, 1985; Kirch, 1997) it is suggested that pots were fired in simple open blazes. The raw pots are arranged either upside down (Irwin, 1985) or arbitrary (Roth, 1935) as shown in Fig. 2.3c and subsequently covered with palm tree leaves, coconut shells and wood (Fig. 2.3d), as was still practiced during the historic period in Island Melanesia. This rapid firing (around 25 min from air temperature to around 600°C to 800°C) can lead to incompletely oxidized grey or black inner surfaces on the pottery, whereas the outer surfaces are usually of reddish brown colour (Irwin, 1985; Kirch, 2000). Nevertheless there are also findings of potsherds showing a low intense firing with maximum temperatures around 500°C which has been discovered by experimental archaeologists (Kirch, 1997, and citations therein). Some pots were probably preheated before the proper firing, as practiced in some Papuan regions and removed from the blaze to cool down in the open air after final heating (Irwin, 1985). On the other hand Roth (1935) monitored no removal during heating and cooling. Nevertheless once the fire died out the compromised vessels (Fig. 2.3e) cooled down very fast within 30 min to air temperature (pers. comm. Geoff Irwin 2010). Occurring movements of pottery (deliberately or non deliberately) during the cooling process can be detected by monitoring the demagnetisation behaviour of the samples (see e.g. Section 3.5.3 "Microwave experimental procedure"). Some pottery was used for cooking (Fig. 2.3f). Although the temperatures reached are lower than during the manufacturing process, to

a certain extend there is an overprint of the original remanence. Regarding a potsherd as a recorder of the ancient geomagnetic field it is important to know how ancient pottery was produced and used, since the manufacturing technique crucially impacts on anisotropy of TRM and cooling rate effects (see Sections 3.4.2 "Anisotropy of TRM" and 3.4.3 "Cooling rate dependency").

2.2.2 Island geology and the effect on clay and temper

The south west Pacific region is characterised by a huge diversity of island types and landforms which are very well described in Brookfield and Hart (1971) and Kirch (2000). The large archipelagos ranging from the Bismarcks, Solomon Islands, Vanuatu, and Fiji are primarily andesitic island-arc formations whereas New Caledonia is a fragment of the ancient supercontinent of Gondwana. Different stages of volcanism, weathering, erosion, subsidence, formation of limestone etc. has led to the complex geological evolution in this area. The isolation of many islands and the absence of oceanic river systems resulted in the fact that the composition of clay and/or temper, which are products of weathering, is often highly distinguishable and can therefore be used as a tracer for inter-island ceramic transfer (Dickinson, 2006). After Dickinson (2006) the anlaysis of temper or clay is so far the only sure way to perceive a transfer of pottery. Scientists benefit from the information by tracing trading routes or knowing the provenance. In particular the latter is important for successful archaeointensity determinations with subsequent calculations of the Virtual Axial Dipole Moments (VADM's).

2.3 Investigated ceramic series from the SW Pacific

In the following paragraphs provenance, dating and contexts of the examined potsherds are described. Also possible dependencies on an anisotropy of a thermoremanent magnetisation (ATRM) and cooling rate (CR) differences between natural and laboratorial treatment are discussed.

2.3.1 Provenance of the potsherds

For the archaeomagnetic investigations (including investigations of archaeointensity and/or magnetic mineralogy) a total of 302 individual potsherds (PS) from 77 secured contexts (CT) were available. The potsherds were excavated from archaeological sites on various islands allocated all over Melanesia in the SW Pacific (Fig. 2.4). These islands can be roughly grouped together into five island regions of the Bismarck Archipelago (32 PS; 5 CT), the Solomon Islands with Santa Cruz Islands (69 PS; 9 CT), New Caledonia (81 PS; 21 CT), Vanuatu (62 PS; 19 CT) and the Fiji Archipelago (58 PS; 23 CT). Table 2.1 gives a short overview of the provenance of all examined potsherds. A more detailed overview for each island group can be found in chapters 4 to 7.

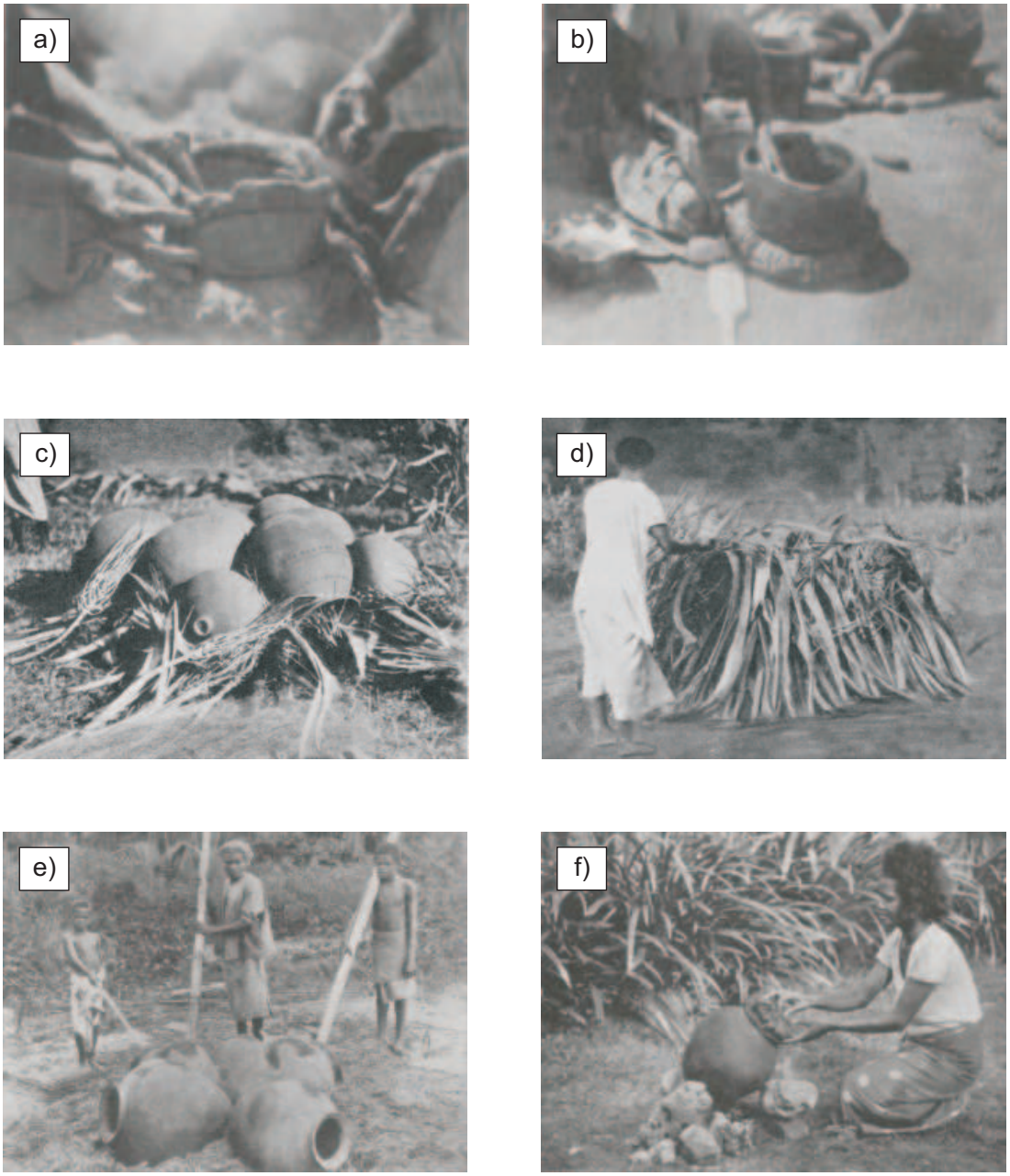

Figure 2.3: Traditional pottery manufacturing and usage observed on Viti Levu, Fiji archipelago (Roth, 1935). (a) Clay tempered with beach sand is formed to pencils which build up the raw pot. (b) Vessel wall thinning and smoothing by using a paddle and anvil technique. (c) Pots are arbitrary placed and ready for firing. (d) Pots covered with palm tree leaves and light firewood. (e) Removal of burnt pottery after a short firing process. (f) Cooking vessel in use.

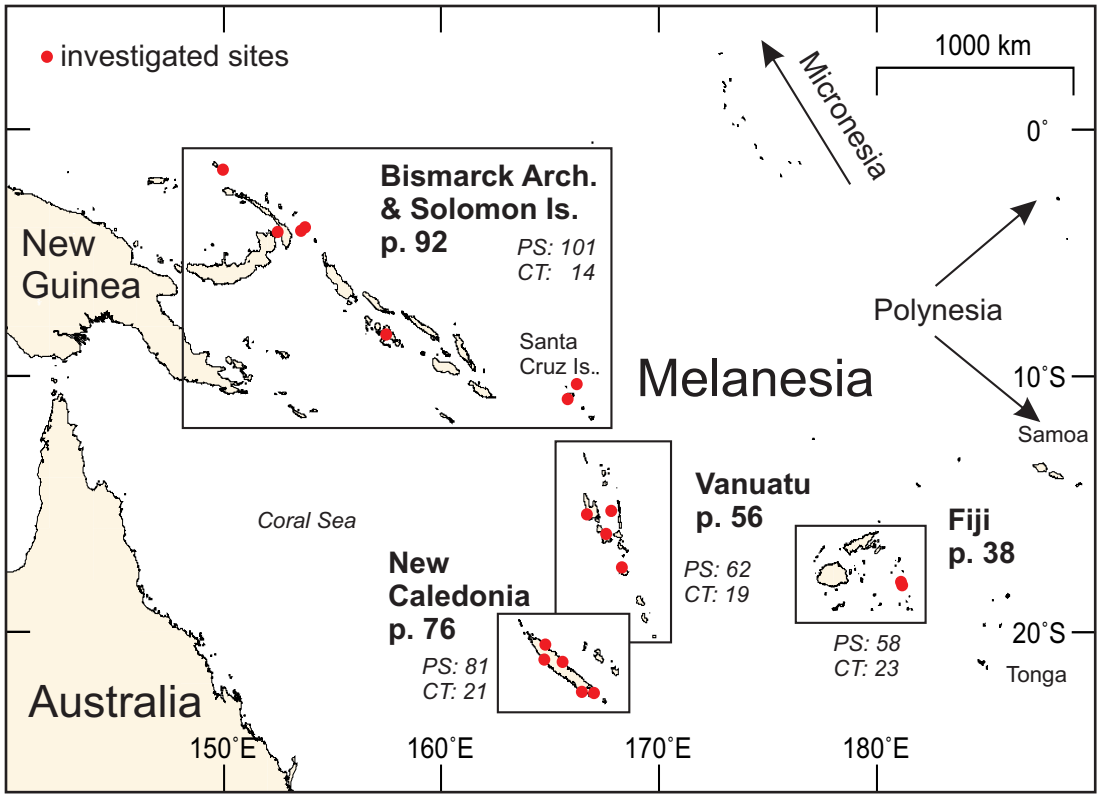

Figure 2.4: Overview map of the investigated regions and sites in the SW Pacific. Black boxes outline additional maps with referring pages found in the Chapters 4 to 7. Red dots indicate sites yielding Lapita and post Lapita pottery investigated for this study.

2.3.2 Context and dating of the potsherds

Well dated samples are a prerequisite for establishing an accurate archaeointensity curve. All bar one of the ceramic samples were selected from well stratified secure contexts with no evidence of mixing and with reliable age estimates. The exception is a pottery fragment from the Fiji archipelago and addressed in the Discussion section of Chapter 4. Every context is associated with a single date. Multiple fragments found in the same context are combined and referred to as a site. In order to date the pottery fragments a combination of radicarbon, stratigraphical order and ceramic seriation were taken into account. Radiocarbon ages obtained for the majority of the potsherds were given in BP (years Before Present) including an age uncertainty ranging from $\pm$ 33 to $\pm$ 130 years. The raw BP dates were calibrated using the software "*Oxcal 4.1*" (Bronk Ramsey, 2001, 2009) and the *ShCal04* (McCormac et al., 2004) or *Marine09* (Reimer et al., 2009) calibration curves. An age at the 95.4% confidence level (2σ) and a rounding of 10 years were chosen. The calibrated age was then generated by calculating a mean value out of the limits of the confidence interval (Fig.2.5a).

Table 2.1: Investigated prehistoric south west Pacific sites

Region	Island	Location/Site	Lat. & Long.	Contexts	Potsherds
Fiji Archipelago (1005 BC to 1795 AD)					
	Lakeba	Lakeba	18.2°S, 181.2°E	14	40
	Nayau	Nayau	18.0°S, 179.0°E	4	7
	Aiwa	Aiwa Levu & Lailai	18.3°S, 181.3°E	5	11
Vanuatu (1035 BC to 1775 AD)					
	Efate	Mangassi	17.6°S, 168.2°E	8	31
		Arapus	17.6°S, 168.2°E	1	4
		Teoma	17.8°S, 168.2°E	2	8
	Malekula	Chachan San	16.0°S, 167.2°E	1	4
		Sakau	16.5°S, 167.8°E	1	2
		Vao	15.9°S, 167.3°E	2	9
	Uripiv Island	Jimis	16.1°S, 167.5°E	1	1
	Ambae	Vatumeamu	15.4°S, 167.8°E	1	1
		Vatulawn	15.4°S, 167.8°E	1	1
	Espirito Santo	Vusi Vilae	15.4°S, 166.7°E	1	1
New Caledonia (900 BC to 1585 AD)					
	New Caledonia	Tiouandè	20.8°S, 165.1°E	9	36
		Pindai	21.3°S, 165.0°E	5	21
		Nouville	22.3°S, 166.4°E	2	4
		Kone	21.1°S, 164.9°E	1	6
		Nepou	21.4°S, 165.1°E	1	4
		Nessaidou	21.2°S, 165.5°E	1	4
		Goro	22.3°S, 167.0°E	2	6
Bismarck Archipelago (1265 BC to 665 BC)					
	Ambitle	Balbalankin	4.1°S, 153.6°E	1	6
	Babase	Kamgot	4.0°S, 153.7°E	2	12
	Duke of York	Duke of York	4.2°S, 152.5°E	1	8
	Emira	Emira	1.6°S, 150.0°E	1	6
Solomon Islands (675 BC and 1515 AD) with Santa Cruz (*1175 BC to 545 BC)					
	New Georgia	Hoghoi	8.3°S, 157.4°E	1	3
		site 25	8.3°S, 157.4°E	1	3
	Nendo	SE-SZ-8	10.7°S, 165.9°E	4	33
	Reef Island	SE-RF-2	10.3°S, 166.3°E	2	20
		SE-RF-6	10.3°S, 166.3°E	1	10

Table 2.1: Listing of provenances and covering ages of the investigated prehistoric ceramic series from the Southwest Pacific. The oldest and youngest dates from an island region shown in brackets are given in calibrated calendar ages. *For the Santa Cruz Islands only limited dated material is available (see Chapter 7). Undated potsherds are used for archaeomagnetic dating experiments. The last two columns describe the number of secured archaeological contexts and number of individual pottery fragments.

Depending on the given BP age uncertainty and the standard calibration curve age uncertainties of the final calendar years can vary. As the radiocarbon calibration curve exhibits a distinct plateau between ca. 750 BC to 350 BC, age calibration leads to bigger uncertainties (Fig.2.5b). Most of the radiocarbon dated material consisted of unidentified wood charcoal which ideally sticked on a potsherd or were found in the same context. Although it is standard practise to identify the tree species in order to avoid old wood problems, as a general rule this is not a problem in the Pacific as most species are short lived. Most of these dates pre-date any concern over this issue (pers. comm. P. Sheppard). Two potsherds from Nayau (Fiji) were dated using the radiocarbon source of a human bone and one potsherd from Aiwa Levu (Fiji) using a bird bone.

Some pottery fragments were dated using marine shells found in the same context. For the case where the radiocarbon age was determined using marine shells, then an appropriate regional marine ΔR correction was applied, based on calculations from islands in the local region (Petchey et al., 2004; Sheppard and Walter, 2006; Green et al., 2008). An example for calibrating a radiocarbon date is shown in Fig. 2.5c. For more information on ^{14}C radiocarbon dating, calibration and marine reservoir effects (ΔR correction) the reader is referred to Ulm (2006) and Reimer and Reimer (2007).

For five potsherds from Fiji (see Chapter 4) no radiocarbon age determination was available. For these the age was estimated by pottery style analysis and an uncertainty of $\pm$ 250 years was assigned. For the whole suite of investigated ceramic samples from the SWP calibrated radiocarbon ages range from 1265 $\pm$ 145 cal BC found on Babase (Bismarck Archipelago) to 1775 $\pm$ 125 cal AD found on Malekula (Vanuatu) (Table 2.1 and Chapter 4 to 7). The ages have precision at the 95.4% confidence level of $\pm$ 75 to $\pm$ 300 years. All radiocarbon dates are consistent with archaeologically assigned ages.

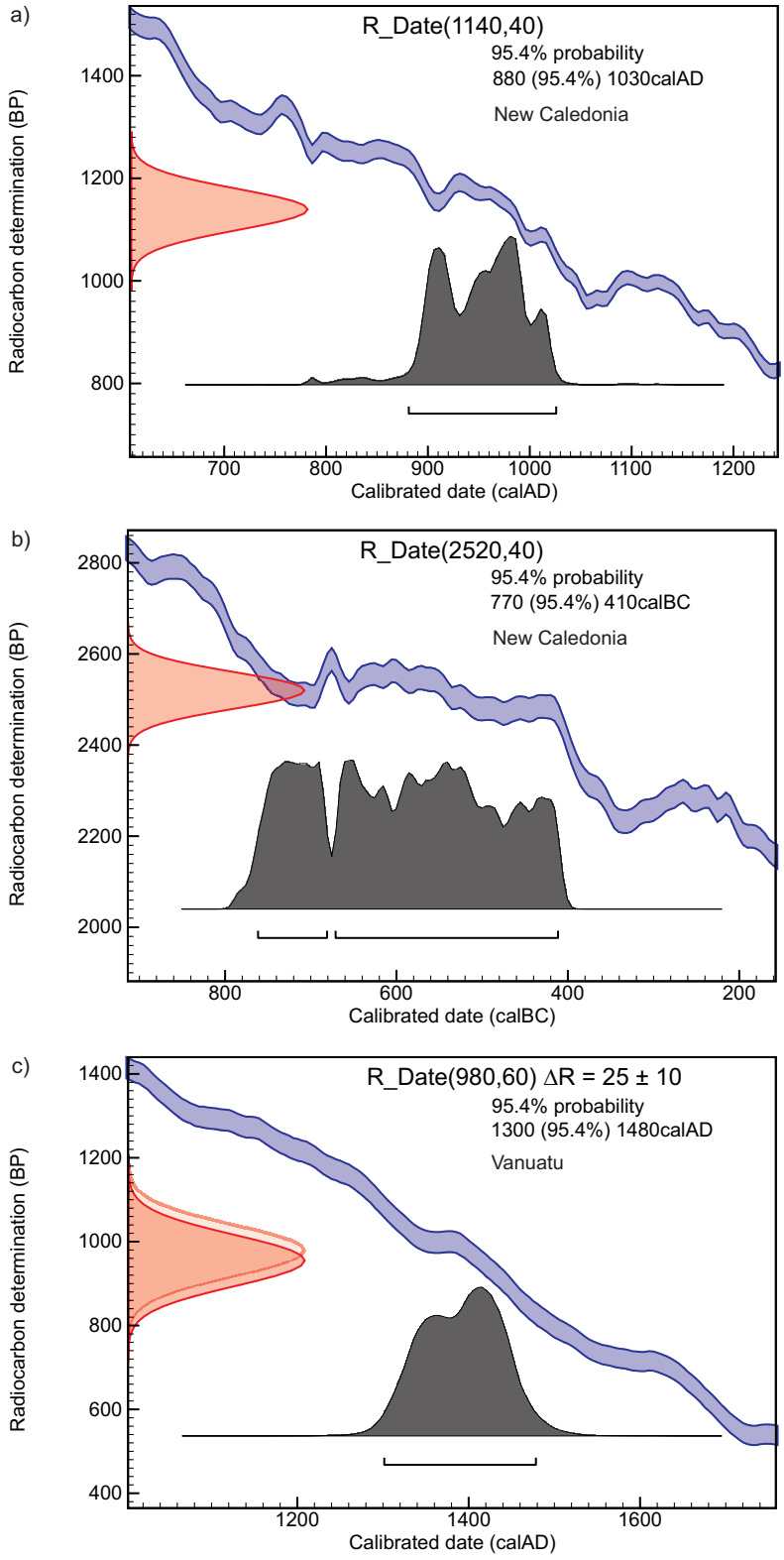

Figure 2.5: Three typical results from calibrating radiocarbon data using OxCal4.1 (Bronk Ramsey (2009)). The blue, red and black curves indicate the calibration curve, the raw BP date with uncertainties and the calibrated BP date with uncertainties. Panel (a) illustrates an age result with relative small age uncertainties. (b) A plateau of the calibration curve around 700 BC to 300 BC causes bigger age uncertainties. Panel (c) shows a result using ΔR marine correction.

Chapter 3

Methodology

This chapter describes the methodologies of taking samples from pottery fragments, laboratory treatment of samples and processing of obtained data. Investigations of the magnetic mineralogy, microwave and Thellier palaeointensity techniques, anisotropy of the thermomagnetic remanence (ATRM) and cooling rate effects are delineated in detail. Theories of the microwave and Thellier technique as well as descriptions of consistency checks and data analysis are only touched on, since it would go beyond the scope of this thesis. For more detailed information about magnetic mineralogical investigations see Dunlop and Özdemir (1997). Coe et al. (1978), Tauxe (1998) and Leonhardt et al. (2004a) are suggested for introductions to palaeointensity determinations using Thellier-type methods and the application of analysing techniques. PhD theses from Hill (2000), Gratton (2004), Brown (2008) and Suttie (2010) give an excellent insight into theoretical and experimental archaeo- and palaeointensity determinations using microwaves.

3.1 Sampling technique and preparation

At least three 5 mm diameter and $\sim$ 4 mm length sister samples from each potsherd were drilled perpendicular to the sherds surface (Fig. 3.1). One was subject to a set of standard rock magnetic measurements. The other two cores were cut into half and $\sim$ 2 mm specimen were used for demagnetisation and archaeointensity experiments on the 14 GHz microwave system. Some potsherds were too soft to drill, therefore small arbitrarily orientated pieces were broken from the potsherd by hand and trimmed with a diamond tipped blade (water cooled) to fit the sample holders of the various instruments. Selected potsherds revealing reasonable archaeointensity values and stable, non-friable minicores were chosen for a cross-check with the Thellier method. Thus another two 5 mm diameter and $\sim$ 4 mm length sister samples were investigated. In order to harden six friable samples for the Thellier experiments, they were imbued with an aqueous solution of "water glass", the compound sodium metasilicate Na_2SiO_3. For testing the accuracy of the anisotropy correction one sample was drilled perpendicular

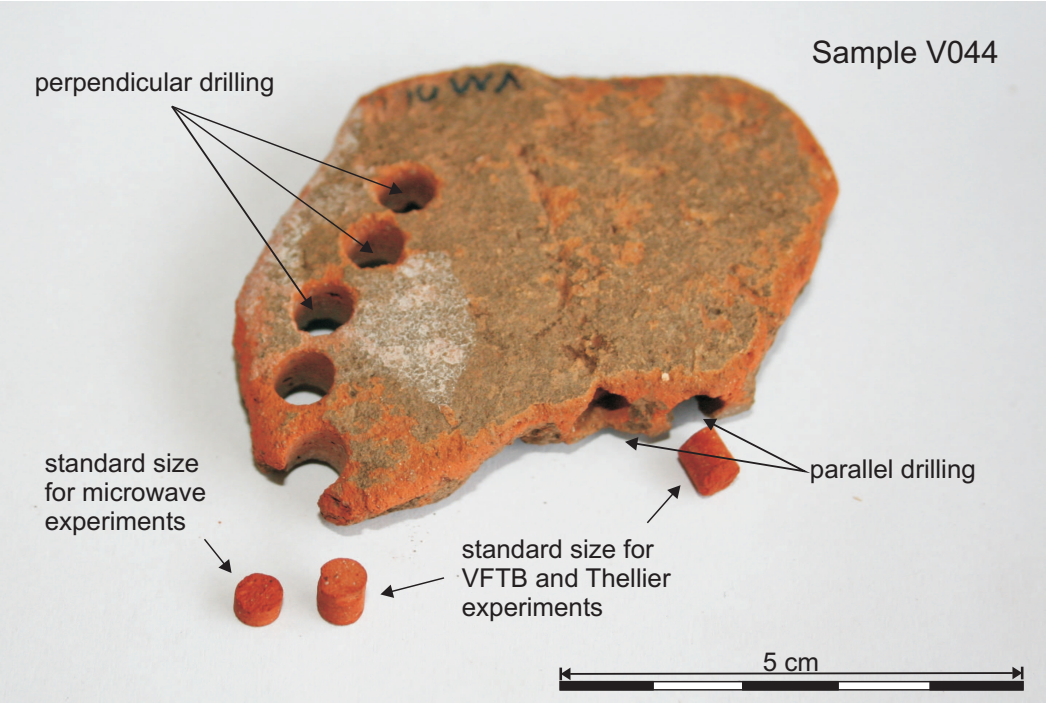

Figure 3.1: Sampled potsherd from Vanuatua (V044) with different sized specimen. Sister samples for rock magnetic and microwave investigations were taken perpendicular to the sherds plane whereas for Thellier experiments including anisotropy and cooling rate experiments sister samples were taken both perpendicular and parallel to the sherds surface.

the other parallel to the sherds surface (Stark et al., 2009). After intensity determination and successfully applying the ATRM correction, these two values from a sherd need to converge.

3.2 Rock-magnetic investigations

The investigation of the magnetic mineralogical properties of a sample aims to identify magnetic phases and their domain states as well as testing the stability of the samples during heating, which is of particular importance for the thermal-based Thellier experiments. A comprehensive description of fundamental principals of rock-magnetic techniques are found in textbooks such as Butler (1992), Dunlop and Özdemir (1997) and Tauxe (1998).

Generally (pre)historic artefacts like earthenware, ceramics, bricks and tiles were made of clay. For the SW Pacific ceramics shell and/or sand temper were added to enhance the workability during manufacturing and stabilise them after the firing process. Clay source and tempering material may vary due to different geological settings

on the widespread islands. Therefore, depending on the provenance of the source material used for pottery manufacturing, the magnetic mineralogy may also differ (see Chapter 2). Besides clay minerals, this heterogeneous mix also contains a variety of iron oxides such as magnetite (Fe_3O_4) and haematite (α-Fe_2O_3) as well as miscellaneous iron(oxy)hydroxides such as goethite and lepidocrocite. During the firing of the clay these iron containing oxides and hydroxides respectively can be transformed into magnetite, maghemite (γ-Fe_2O_3) and haematite depending on the reduction/oxidation (redox) conditions.

In order to determine the magnetic mineralogy of the potsherds, rock magnetic measurements were carried out using a Variable Field Translation Balance (VFTB) (Krása et al., 2007). A $\sim$ 150 mg sample from each sherd was in sequence subject to isothermal remanent (IRM) acquisition, hysteresis and backfield coercivity measurements and magnetisation with temperature (M_s(T)) determinations, heating up to 700°C in an ambient field of up to 800 mT. The results were then analysed using "RockMagAnalyzer 1.0" software by Leonhardt (2006).

3.2.1 Isothermal remanent magnetisation

Ferro(i)magnetic substances acquire an IRM if their coercivity is smaller than an ambient magnetic field. In other words such samples subjected to an external magnetic field preserve a remanent magnetisation even when this field is removed. This IRM can be used to distinguish between ferro(i)magnetic minerals. If an applied field is strong enough to reach the maximum of remanence, then an IRM is saturated (sIRM), which is also denoted as saturation remanence M_{rs}.

In order to characterise an IRM using a VFTB an acquisition of a remanent magnetisation is measured by applying incrementally increasing fields (1 to 800 mT) to an untreated sample. The field strength which is needed to saturate a remanence depends on the magnetic minerals and their grain size. Whereas samples containing low coercive minerals like magnetite, maghemite or titano(magnetite/maghemite) saturate in fields between 100 to 300 mT, high coercive minerals such as haematite or goethite ($FeO(OH)$) usually do not saturate at fields up to one Tesla.

3.2.2 Hysteresis and backfield measurements

Measurements of a hysteresis loop are based on the ability of magnetic minerals to retain a magnetisation after applying a field. Various rock magnetic parameters can be determined by analysing hysteresis curves.

During the VFTB measurements hysteresis experiments are conducted after the IRM investigation. A step by step incrementing field H is applied from 0 mT to 800 mT and then an anti-parallel field to -800 mT, and finally back to 800 mT again.

Throughout this procedure the magnetisation M of the sample is measured in-field in contrast to IRM experiments. Hence as well as ferro(i)magnetic fractions, paramagnetic phases are also measured. These are indicated by the slope of the closed loop at high fields (χ_{hf}). The intersection of the extrapolated slope and the y-axis then gives the measure for the saturation magnetisation M_s of the ferro(i)magnetic components. The ratio of the observed saturation magnetisation and remanence of saturation remanence M_{rs} (interception of the descending curve with the y-axis) can be utilised to estimate the grain size of the remanence carrier, with decreasing values indicating increasing grain sizes. The coercive force B_c is measured at the interception of the descending or ascending curve with the x-axis (M=0) and the remanence coercive force B_{cr} is the strength of an anti-parallel field required to switch back to the intercept with the origin. Here B_{cr} is determined using backfield coercivity measurements, which are conducted after the hysteresis run and can be regarded as a part of the IRM experiments. Therefore after acquiring an SIRM an increasing field is applied anti-parallel and M_r is measured. Depending on the ferro(i)magnetic minerals and grain sizes, a certain force (B_{cr}) is needed to reduce a remanent magnetisation in a sample to zero ($M_r = 0$). From the backfield curves a so-called S_{300} parameter (Bloemendal et al. (1992)) can be obtained which is calculated as $S_{300} = (1 - M_{-300\ mT}/M_{rs})/2)$. This is a measure for estimating high coercive components from the backfield curves.

3.2.3 Magnetic domain estimation

Characterising magnetic grain sizes and thus estimating magnetic domain states of the remanence carrying minerals can help to understand and interpret archaeomagnetic results. Since non-interacting magnetic particles do not affect archaeointensity determinations, a single domain (SD) behaviour is a prerequisite (Néel, 1955; Coe, 1974). Yet the analysis of bulk rock magnetic parameters concerning the domain state is often ambiguous and consequently limits their value for preselecting suitable samples for intensity determinations. In particular samples from pottery fragments often exhibit a variety of different magnetic minerals with different stability and concentration parameters. Interpreting indigenous pottery from the SW Pacific with a complicated geological setting concerning the clay and temper source allows only a tentative diagnosis.

Day et al. (1977) suggested to plot M_{rs}/M_s against H_c/H_{cr} since both ratios are sensitive to grain size variations. This so-called Day-plot defines areas which indicate predominant SD or MD behaviours of the remanence carrier. The transition zone between the SD and MD areas is referred to as the pseudo single domain PSD remanence area. This area belongs to magnetic minerals like magnetite with larger grain sizes than the crucial SD size of ~ 0.1 μm , but carrying a TRM which is significant harder and more intense than predicted for MD particles (Dunlop and Özdemir, 1997). Dunlop and Özdemir (1997) discuss several possibilities for this behaviour, where SD-like moments

in larger MD grains are related to dislocations, surface pinning due to formation of crystallites and/or mixtures of SD, SP and MD grains. The latter was investigated theoretically and experimentally by for example (Dunlop, 2002a,b) and the mixing curves of SD/MD and SD/SP were applied on the Day-plot. There are further ideas for plotting hysteresis parameters in order to estimate the domain state but they are not used here as their application is restricted and they do not give additional information relevant to this project. For further reading see Dunlop and Özdemir (1997) and Tauxe (1998). The magnitude of demagnetisation tails are significant for classifying the domain state (Shashkanov and Metallova, 1972; Bol'shakov and Shcherbakova, 1979; Shcherbakov et al., 1993), therefore in order to determine any non SD behaviour, pTRM tail checks were incorporated in microwave and Thellier experiments and these are described later in the sections of microwave experimental procedures and the Thellier MT4 technique. Cooling rate dependencies of TRM's (described later) are also governed by the domain state of investigated potsherds and can give a hint of the prevailing domain state (e.g. Leonhardt et al., 2010).

3.2.4 Thermomagnetic measurements

Investigations of the thermomagnetic behaviour are conducted as the last step in the sequence of VFTB measurements. Information about the magnetic phases and possible alteration of the magnetic mineralogy during heating/cooling can be gathered from thermomagnetic curves (M(T)) of the sample. Since backfield measurements were performed prior to thermomagnetic investigations, a so-called prefield conforming to an IRM_{800mT} was applied in the same direction as the applied field during the thermomagnetic measurements. A high powered prefield removes the magnetic history of previous measurements and prevents unambiguous M(T) curves, especially when conducting M(T) experiments using low fields ($\sim$ 33 mT). Besides avoiding overheating of the Helmholtz coils, the use of low magnetic fields also suppresses paramagnetic magnetisations in the permanent ambient magnetic field during the M(T) measurements. For some samples a high field of 800 mT was applied. This leads to a saturation of low coercive minerals like magnetite and these thermomagnetic curves are therefore denoted as ($M_S(T)$). For the heating and cooling steps a rate of 30°C/min was chosen in order to keep temperature hysteresis to a low level. Differences of the conductivity and heat capacity between thermocouple and sample lead to a temperature hysteresis which increases with higher heating and cooling rates. The Curie temperatures (T_C) were finally determined using the method of Moskowitz (1981) in the "RockmagAnalyzer".

3.3 Scanning electron microscopy

In addition to the results of the VFTB measurements, an imaging device scanning electron microscope (SEM) has been used to study the magnetic mineralogy of selected potsherds from the SW Pacific. The aim of using a SEM is to detect and identify large magnetic grains probably brought into the clay by using tempers. They are usually > 5 μm and can also influence a TRM. SEM is also used to investigate whether a texture or pattern of preferential alignment of clay minerals generated during fabrication can be identified. This feature is responsible for anisotropy effects potentially influencing a recorded TRM.

The SEM (Philips XL30) housed in the School of Environment Sciences of the University of Liverpool, is equipped with an Oxford Instruments Energy Dispersive Spectroscope (EDX) for quantitative geochemical analysis. Polished thin sections were prepared by Paul Hands at the University of Birmingham. Thirteen samples sized $\sim$ 5×5 mm were selected by their provenance representing an island group or region. Also some samples measured hitherto were chosen because of their success and non-success during archaeointensity determination. Prior to SEM investigations the polished samples were coated with carbon. Primarily back scattered electrons (BSE) were used to image the polished surface of the potsherd samples. Secondary electron (SE) imaging was applied for observing a melting spot on an unpolished sample which may occur during microwave archaeointensity determination. This sample was coated with a gold-palladium alloy in order to obtain a higher resolution. Depending on the method the maximum resolution varies from $\sim$ 5 μm to $\sim$ 1 μm for BSE and SE imaging, respectively. EDX element mapping was applied for some selected samples to determine the distribution of mainly iron, oxygen and titanium. The maximum resolution for the EDX function is $\sim$ 1 μm. For detailed information on SEM investigation and EDX analysis the reader is referred to Goldstein et al. (1992).

Prof. William R. Dickinson (emeritus University of Arizona) a specialist in temper determination in SW Pacific pottery (e.g. Dickinson, 2006) kindly investigated the petrography of 10 thin sections from potherds from Efate (Vanuatu) using reflecting light microscopy. The results are presented in Chapter 5 and in the Appendix B.

3.4 Absolute archaeointensity determination on ceramics

3.4.1 Basic theory of archaeointensity determination

All methods dealing with determination of archaeointensities are based on a linear relationship between an applied magnetic field, which is about the magnitude of the geomagnetic field strength, and an acquired TRM and NRM, respectively (Nagata, 1943).

$$NRM = \alpha_1 \cdot H_{anc} \tag{3.1}$$

$$TRM = \alpha_2 \cdot H_{lab} \tag{3.2}$$

H_{anc} describes the field strength of the Earth during the acquisition of an NRM, where the applied laboratory field is denoted as H_{lab}. The parameters α_1 and α_2 are constants relating to magnetic attributes of the investigated samples. Assuming during the course of time no magnetic mineralogical alteration occurred which means $\alpha_1 = \alpha_2$, then the equations (3.1) and (3.2) can be rearranged:

$$H_{anc} = H_{lab} \cdot \frac{NRM}{TRM} \tag{3.3}$$

Utilising equation (3.3) Thellier and Thellier (1959) developed a method to determine archaeo/palaeointensities. As a prerequisite for reliable intensity determinations the pTRM's and/or pNRM's acquired in a certain temperature interval must follow the law's of independence, additivity and reciprocity. "The Law of Independence" Thellier (1938) assumes that pTRM's acquired during cooling between two arbitrary temperature steps T_1 and T_2 are independent of pTRM's acquired during cooling between other temperature steps T_3 and T_4. This is valid for both intensity and direction. Following this assumption "The Law of Additivity" assumes that the total TRM is the sum of all the independent pTRM's. "The law of reciprocity" states that the blocking and unblocking temperatures are the same ($T_b = T_{ub}$), which assumes that an acquired pTRM to a temperature step can be completely replaced by reheating to the same temperature step.

3.4.2 Anisotropy of TRM

Moulded archaeological artefacts i.e. ceramics, tiles, bricks can contain a strong magnetic anisotropy (e.g. Rogers et al., 1979; Aitken et al., 1981; Veitch et al., 1984). As a consequence an acquired TRM and/or pTRM varies with the orientation of the investigated objects in an ambient magnetic field. Neglecting to include the effect of the magnetic anisotropy into the determination of archaeointensities can lead to errors between 30% to 40% and for wheel-thrown pottery even up to 60% (Rogers et al., 1979). The ATRM effect in pottery is generated by preferential alignment of magnetic grains during fabrication of the clay material and could be enhanced by subsequent firing. Rogers et al. (1979) observed that this alignment generally results in a hard direction perpendicular, and an easy plane parallel, to the sherd surface and also suggested applying a laboratory field within 10° to the direction of the NRM. This idea was accomplished and refined by Aitken et al. (1981). They describe a method where the anisotropy of TRM is corrected for, and is embedded in, Thellier-experiments by remagnetising the samples in the direction of their ancient magnetisation. This technique has been successfully employed in microwave measurements of ancient ceramics

(e.g. Shaw et al., 1996) and is also used in this study as described in section 3.5.3 "Microwave experimental procedure". Another enhanced version of this technique is used in the three-axis vibrating sample magnetometer (Le Goff and Gallet, 2004), which additionally considers the fact that the measured NRM is not parallel to the ancient magnetic field and also biased by magnetic anisotropy.

A different method to deal with the magnetic anisotropy effect is correcting raw intensity values with an ATRM correction factor. In this case the ATRM tensor is determined by successively acquiring and measuring a pTRM in six orthogonal directions (Veitch et al., 1984), which was successfully practiced by for example Selkin et al. (2000), Genevey and Gallet (2002) and Hill et al. (2007). This method was also used in this thesis for correcting the intensity values obtained from Thellier experiments using the approach of Leonhardt et al. (2006). A detailed description is found in section 3.6.2 "Thellier experimental procedure".

3.4.3 Cooling rate dependency

Studies on cooling rate (CR) effects have shown theoretically and experimentally that for an assemblage of single domain (SD) particles, the TRM increases with slower cooling (e.g. Fox and Aitken, 1980; Halgedahl et al., 1980; Dodson and McClelland-Brown, 1980; McClelland-Brown, 1984). The relationship for pseudo-single domain (PSD) and multi-domain (MD) particles however is less clear. Typically, pottery fired in a kiln has a natural cooling time of about 1.5 days (e.g. Chauvin et al., 2000). It has been argued that this causes, on average, an overestimation in archaeointensity of $\sim$ 10% when compared to laboratory cooling of around 30 min (e.g. Genevey and Gallet, 2002). However, this is often highly variable and can range from zero to over 10% (Genevey et al., 2008). For the MWS, where a heating and cooling cycle takes up to 90 s, there is only one published study where the cooling rate effect has been investigated and both under- and overestimation of archaeointensity results were found (Shaw et al., 1999). As described earlier (Chapter 2), the burning technique used for the present samples would lead to a faster natural cooling time than if fired in a kiln, probably less than 30 min (pers. comm. Irwin 2010). In this case, this is similar to the cooling rate used during the Thellier experiments and therefore it is likely that the correction for cooling rate is negligible. Notwithstanding this fact, CR experiments were conducted in this study to investigate remanence acquisition behaviour. These CR experiments were performed subsequent to Thellier and ATRM experiments at 550°C and 580°C. With a cooling fan, the minicore samples cooled down to room temperature within 10 to 20 min during the Thellier experiments. To simulate a slow CR, the cooling fan was switched off, leaving the samples to cool to room temperature in the oven, which took about 8 h.

3.4.4 Archaeointensity acceptability criteria

For both microwave and Thellier experiments similar selection criteria to those described by Brown et al. (2006) and Leonhardt et al. (2004a) were used. Archaeointensity values are calculated from the slope, determined by least squares analysis, of the so called Arai plot (Nagata et al., 1963), where the NRM lost versus the partial TRM (pTRM) gained (or pT_MRM, where T_M is acquired remanence in the MWS) is plotted. Parameters used for assessing the quality of archaeointensity data are described in Tauxe (1998). The following selection criteria are applied:

1. A stable NRM direction with an intercept at the origin of an orthogonal vector plot;
2. At least 5 data points (N) to fit a single slope;
3. A regression coefficient (r^2) of the best-fitting slope ≥ 0.98;
4. The ratio of the standard error in the best-fit straight line to the slope of the same line should be less than or equal to 10% ($\beta \leq 0.10$);
5. A quality factor (q) as defined by Coe et al. (1978) of 4 or larger;
6. A gap factor of (g)$\geq$ 0.5;
7. $pT_{(M)}RM$ checks differing from the original value by $\leq$ 10% using the DRAT criteria of Selkin and Tauxe (2000);
8. $pT_{(M)}RM$-tail checks $\leq$ 10% difference between two zero field power steps;
9. An NRM fraction (f)$\geq$ 0.5, as suggested by Biggin and Thomas (2003), to detect MD curvature. However (f) $\geq$ 0.3 is accepted if there is a sister sample with a fraction $\geq$ 0.5 and no evidence of curvature.

3.5 Archaeointensity determination using microwaves

All SW Pacific ceramics investigated for this thesis were subject to demagnetisation and subsequent archaeointensity experiments using a 14 GHz microwave system (MWS) combined with a Tristan Technologies SQUID magnetometer (Shaw and Share, 2007). For comprehensive descriptions of the microwave methodology and equipment see Hill (2000), Gratton (2004), Brown (2008) and Suttie et al. (2010).

3.5.1 The concept of the microwave technique

In contrast to the conventional thermal techniques (e.g. Thellier and Thellier, 1959; Coe, 1967b), where heating the bulk sample leads to increased vibrations of the lattice

(phonons) generating in turn electron spin waves (magnons), the microwave technique demagnetises samples by directly exciting magnons in the magnetic particles without substantially heating the bulk sample (Walton et al., 1992, 1993). This keeps thermochemical alteration, which is often a limiting factor for conventional thermal based techniques (e.g. Coe, 1967a), to a low level. In order to excite magnons in the MWS high-frequency microwaves are employed at a ferromagnetic resonance (FMR) frequency. Ideally this would take a few milliseconds (Walton et al., 1992), but practically the exposure time for the archaeointensity experiments is between 3 s and 30 s, which enables some magnons to be converted into phonons and can cause some light heating (Suttie et al., 2010). As the matrix of the samples is often composed of non conducting materials, dielectrical heating in the range of 150 °C to 250 °C, depending on the mode used in the cavity, can occur (e.g. Hill, 2000; Suttie et al., 2010). Although the equivalence between thermal and microwave unblocking has not been described theoretically, comparative studies of microwave and conventional techniques (e.g. Hill et al., 2002; Thomas et al., 2004) have already shown that a pTRM acquired during thermal demagnetisation is equivalent to a pT_MRM acquired during microwave demagnetisation. Besides the advantage of limiting alteration, samples can be treated individually (i.e. considering their particular blocking spectra and sensitivity to a VRM). Moreover archaeointensity determinations are conducted significantly faster than using conventional methods.

3.5.2 The 14 GHz Microwave system

The 14 GHz Microwave system (MWS) with a Tristan Technologies, Inc. DRM-300 SQUID magnetometer housed in the Oliver Lodge Laboratories of the University of Liverpool was used to de/remagnetise the samples. For generating microwaves a MG3692B 20 GHz synthesised signal generator amplified by a custom built set of solid state 80 W microwave amplifiers with an operational range between 14.0 - 14.5 GHz was used. The microwaves are channelled via a horizontal waveguide into the cavity. The cavity itself is surrounded by three pairs of Helmholtz coils in X, Y and Z direction, enabling the application of an artificial magnetic field in any direction. The cavity and field coils are covered by a mu-metal shield and thus are positioned together with the magnetometer in a low field cage which nearly eliminates the present geomagnetic field by generating a magnetic field anti-parallel to it.

The specimen is mounted to a quartz glass tube using negative pressure from a vacuum pump and then inserted vertically into the MWS. Using a vacuum technique for holding the specimen minimizes material inside the tuned microwave cavity. The Tristan technologies "low" temperature liquid helium SQUID magnetometer has a maximum sensitivity of $\sim 1 \times 10^{-11} Am^2$ (Shaw and Share, 2007). The sensitivity of the magnetometer can be adjusted to the magnetic strength of an investigated sample.

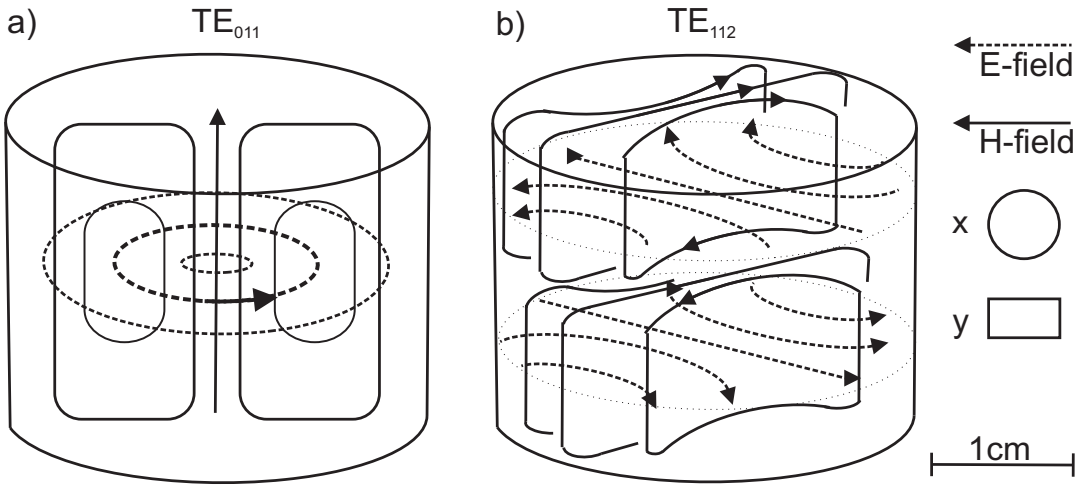

Figure 3.2: Electric and magnetic fields of (a) mode TE_{112} and (b) mode TE_{011}in a cavity based on Fuller (1987) and adapted from Suttie et al. (2010). x and y showing top and side view of a typical sample size. Dashed line and solid lines delineate electric and magnetic fields.

Therefore a prior sensitivity test is performed where an appropriate gain for the magnetometer is determined. Measurements are conducted automatically in the X,Y and Z directions (in core coordinates) accompanied by determination of the background noise before and after a measurement.

Mode of the cavity

The size of the cylindrical cavity (radius 15 mm) is dimensioned so that microwaves resonate at a frequency of $\sim$ 14 GHz. The internal length can be varied by an adjustable end cap (18 mm to 22 mm). The cavity can be run in two main modes (Fig. 3.2). The main experiments were conducted in the TE_{011} (transverse electric) mode corresponding to a cavity length of $\sim$ 20 mm (Fig. 3.2a). The three numbers correspond to the number of azimuthal wavelength, the number of radial maxima and the number of half wavelengths along the axis of the cavity (z-axis). In this mode samples with a typical size of 5 mm in diameter and $\sim$ 2-3 mm in length are permeated with magnetic fields parallel to their z-axis when placed in the middle of the cavity. The electrical field grows radially from the center of the core and can cause a rapid heating due to dielectrical loss of energy on the outer rim of a sample (Suttie et al., 2010). Setting the cavity to a length of $\sim$ 22 mm results in the TE_{112} mode (Fig. 3.2b) where the fields in the cavity vary distinctly along the x-axis and can be separated in areas of electrical and magnetical field maxima. Suttie et al. (2010) utilized that fact to demonstrate dielectrical heating due to electrical fields as well as demagnetising samples by magnetic fields.

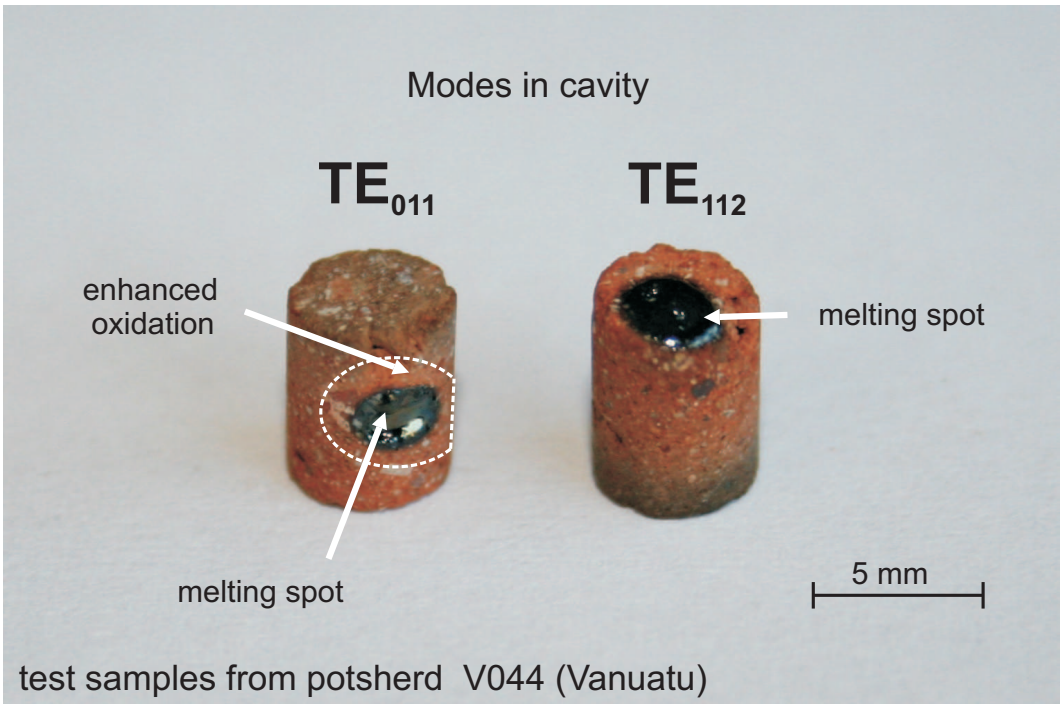

Figure 3.3: Demonstration of dielectrical heating creating melting spots on samples from a Vanuatu potsherd. It is clearly shown that a melting spot generated in the TE_{011} mode manifested on the side of a sample, where it is close to the half maximum of the ambient electric field. In contrast the mode TE_{112} with a larger electrical field on the top and bottom of a sample exhibited a melting spot in one of these areas.

Although the mode TE_{011} is more likely to produce dielectrical heating, it was preferred to the TE_{112} mode since resonance and demagnetisation of a sample were easier to handle. Dielectrical heating which sometimes manifests in a melting spot on the surface of a sample can be limited to a certain extent by adjusting power and exposure time during measurement. Depending on the mode, melting spots can occur either on the top/bottom (TE_{112}) or on the side (TE_{011}) of a sample (Fig. 3.3a, b). Thus the nature of a melting spot is not yet clear. It seems that due to the strong and focused temperature rise a vitrification process is launched. In order to shed some light on this phenomena SEM investigations were undertaken on a melting spot. Results and interpretations are given in Chapter 5.

Tuning of the cavity

Since samples vary in size and the resonant characteristics of bulk material will change, the cavity needs to be (re)tuned. At the beginning of a measurement cycle the sample is placed in the center of the cavity. A computer controlled "wide" frequency sweep at low power (1 W) between 14 GHz and 14.5 GHz is performed to localise the area of a

resonance frequency which is in turn followed by a "narrow" sweep to identify the exact value of the resonance frequency. The computer automatically records the frequency where the reflected power is at a minimum. In order to test the quality of a resonance frequency the reflected power is plotted against the applied frequencies. For getting best results a minimum of reflected power is desirable. If there is a significant amount of reflected power the position of the sample can be adjusted along the z-axis to find the ideal resonance.

Differences in (magnetic) mineralogical compositions and grain sizes of the (magnetic) particles can lead to the fact that not all of the incoming power is absorbed and some amount of the power is reflected. Notwithstanding, these samples are still usable and can provide reliable archaeointensities, but they are also more likely to alter due to undesirable heating effects. For both cases the resonance frequency needs to be checked after every step, since the optimal frequency can vary due to temperature changes and/or slightly different positions in the cavity as well as thermochemical alteration of a sample, which would lead to spurious consistency checks and intensity determinations.

3.5.3 Microwave experimental procedure

Demagnetisation experiments

Prior to intensity determinations, demagnetization experiments on sister samples from the same pottery fragment were conducted in order to resolve their magnetic nature and to preselect suitable potsherds for the trial of archaeointensity determination. The demagnetisation experiments were analysed using "PlotCore" (written by Alan McCormack). Theoretically the shorter the exposure of samples to the microwaves, the less likely is alteration due to heating (Walton, 1988). Experimentally, 5 seconds were chosen since it kept unwanted heating on a low level but was long enough to avoid high power steps (> 35 W) which were found to result in alteration in the ancient Pacific ceramics. Depending on the behaviour of the samples, the power was incrementally increased by 2-3 Watt for every step.

Between 8 and 12 power steps were performed starting with 8 W for 5 seconds. Most samples lost about 80% of their NRM at ~ 30 W for 5 seconds. In order to demagnetise more than that, much higher powers are needed resulting in thermochemical alteration. Demagnetisation experiments provide information about the components of the remanent magnetisation. If no characteristic remanence (ChRM) is found, then the sample was rejected. For many samples a viscous remanent magnetisation (VRM) was identified and could be removed in order to isolate the ChRM.

Demagnetisation experiments were also used to determine the distribution of the (un)blocking spectrum, which helps to adjust the range of power steps used for archaeointensity determination performed on sister samples. Some samples exhibited a

very narrow blocking spectrum. In order to get a reasonable amount of measurements for a linear segment in the Arai plot, the 5 seconds were reduced to 3 seconds. Other samples were hard to demagnetise. Therefore the exposure time was extended up to 30 seconds. In this case heating effects (up to 300°C) caused by dielectric loss (Suttie, 2010) is exploited to cause some additional demagnetisation. During this procedure powers were kept below 25 W. Samples which could not be demagnetised by more than 30% of their NRM, were rejected and did not undergo archaeointensity analysis.

Microwave protocol

For the archeointensity experiment in the MWS the Coe (1967a) protocol, describing a double-heating method, was used which is a modification of the original Thellier and Thellier (1959) method and was also employed in an alternated form for the later described Thellier-type experiments (Leonhardt et al., 2003). A sample is demagnetised by applying microwaves with a certain energy (power times exposure time) and subsequently measuring the remaining NRM. This is followed by a remagnetisation step at the same energy level, where contemporaneously a known field is applied in the direction of the NRM until the sample moves out of the cavity to be measured in the magnetometer. As a prerequisite the same amount of energy needs to be absorbed by magnetic particles during de- and remagnetisation. This is not always straight forward, since the applied energy is not necessarily the same as the absorbed energy. The cavity can get out of tune during measurements due to alteration and/or movement of the samples causing differences in the amount of absorbed energy.

Since most of the investigated pottery fragments come from an area close to the equator with typical intensities between $\sim$ 20 μT to $\sim$ 40 μT, a rather low laboratory field H_{lab} of 30 μT was chosen throughout this study so that the expected laboratory field is in the range of an expected ancient field (Kono and Tanaka, 1984) or lower (Yu et al., 2004). For the samples from New Caledonia ($\sim$ 22° S) H_{lab} was set to 40 μT. Applying the field in the direction of the NRM, keeps possible anisotropy of TRM effects on a low level (e.g. Le Goff and Gallet, 2004). Considering the information gathered from prior demagnetisation, de(re)magnetisation steps were repeated with increasing powers until the sample is fully demagnetised or could not be demagnetised further without altering the magnetic mineralogical composition. After the first three power step, and then subsequently after every second power step repeated infield steps (pT_MRM checks (Coe, 1967b)) were carried out to monitor possible alteration. Repeated zero field checks were also made as an additional alteration check and also used to detect MD sensitivity if $B_{NRM} \neq B_{LAB}$, (Yu et al., 2003). Analogously these consistency checks are also performed during the Thellier experiments, where a more detailed explanation is given in Section 3.6.1.

TRM anisotropy effects during microwave experiments

The magnetic anisotropy bias is limited by applying a laboratory field parallel to the NRM. This field is generated by three pairs of Helmholtz coils, surrounding the cavity and can be applied in any direction. Since an NRM is also subject to a magnetic anisotropy effect and thus not parallel to an ancient magnetic field direction (H_{anc}), an ATRM bias is not fully compensated (e.g. Le Goff and Gallet, 2004). In other words when applying (H_{lab}) in the NRM direction, the resulting direction of a TRM is not necessarily consistent with the NRM. Nevertheless, for moderate anisotropy effects which are expected for non-wheel thrown pottery this method sufficiently reduces this bias to a negligible extent.

3.6 Archaeointensity determination using a Thellier-type method

In order to cross-check the Microwave results, additional Thellier-type (MT4) experiments (Leonhardt et al., 2004a) were conducted on selected sister samples at the Geomagnetism Laboratory of the University of Munich. In the following, the theory and experimental procedure of the Thellier technique as well as investigation of the Anisotropy of TRM (ATRM) and cooling rate dependency are described.

3.6.1 Modified Thellier-technique MT4

The method used here to determine absolute archaeointensities is based on a Thellier-technique refined by Coe (1967a). It describes a double heating zero field/in field (ZI) procedure. During the experiment the investigated sample is first heated and subsequently cooled in a zero field to a temperature $T_i < T_C$. Afterwards the remaining NRM is measured. During the following heating step to T_i a known field is applied and a pTRM acquired. This procedure is repeated with increasing T_i until the complete NRM is replaced by a pTRM.

The frequent heating and cooling steps can lead to chemical alteration of the magnetic mineralogy in the samples which in turn causes spurious archaeointensity determinations. In order to monitor possible alteration so called “infield” pTRM-checks after Coe (1967b) were employed. Therefore a sample is heated to a temperature $T_k < T_i$ and cooled to room temperature in an ambient field which is the same as for all other steps. These checks were performed after every second heating/cooling cycle. This incremental procedure is based on the assumption that between each temperature step the acquired pTRM’s are independent. This is also denoted as the “Law of independence” Thellier (1938).

Besides alteration, the presence of MD particles, if unrecognised, can result in false interpretations of Arai diagrams. A pTRM carried by MD particles in a certain

temperature inverval ($T_n < T_m < T_C$) is not fully removed after a repeated heating/cooling step in a zero field up to a temperature T_m. The remnant of the last pTRM is denoted as pTRM-tail and can crucially affect the shape of an Arai curve. In contrast to SD particles, where blocking and unblocking temperatures T_b and T_{ub} are identical, the T_{ub} can differ from T_b for MD grains. If $T_{ub} > T_b$ ($T_{ub} < T_b$) then the shape of a curve in the Arai diagram is convex (concave) and a superposition of both effects in a sample can lead to S-shaped Arai diagrams (Leonhardt et al., 2004b). In order to estimate the influence of MD particles, acquisition of a pTRM at a temperature T_i is followed by a repeated demagnetisation step (TR) at T_i which is denoted as a pTRM tail check and concurrent to a check of the law of independence (Riisager and Riisager, 2001; Leonhardt et al., 2004b). The intensity difference ($\delta(TR)$) is calculated using the primary and repeated demagnetisation steps. Whether the intensity increases or decreases due to a pTRM-tail depends on the angular difference between the magnetisation of a sample and an applied laboratory field. Using the angular difference and ($\delta(TR)$) the measure of the true pTRM-tail ($\delta(t^*)$) can be determined (Leonhardt et al., 2004b).

A further possibility for detecting MD bias is the use of an additivity-check (AC) after Krása et al. (2003). This check works analogously to the pTRM-check but is performed in a zero field environment. A combination of these results from both checks helps to verify the "law of additivity".

In summary the modified Thellier technique MT4 comprises a field-off first method with accompanying pTRM-checks, as well as pTRM-tail and additivity checks.

3.6.2 Thellier experimental procedure

Thirty one individual potsherds were selected based on the microwave demagnetization behaviours of sister samples. Two 5 mm diameter and 4 mm length sister samples from each potsherd were investigated. To test the efficiency of the ATRM correction, one of the samples was drilled perpendicular to the sherd surface and the other parallel. After applying an ATRM correction, factor convergence of the archaeointensity values of these sister samples is a powerful way of testing for the accuracy of the anisotropy correction (e.g. Stark et al., 2008; Genevey et al., 2009). In total 62 samples from 31 individual fragments were subject to Thellier experiments.

The cylindric mini-cores were inscribed and the Z-direction was marked using a heat resistant white ink (Fig. 3.4a). Afterwards the samples were subjected to the procedure of the MT4-method. Therefore a maximum of 31 samples were inserted in a quartz glass tube (Fig. 3.4b) which was then placed in an MMTD thermal demagnetiser. It is important that the samples always occupy their same position since there is a small temperature gradient in the oven. The samples were also always orientated in the same direction throughout the whole experiment. The laboratory field $H_{lab} = 30$

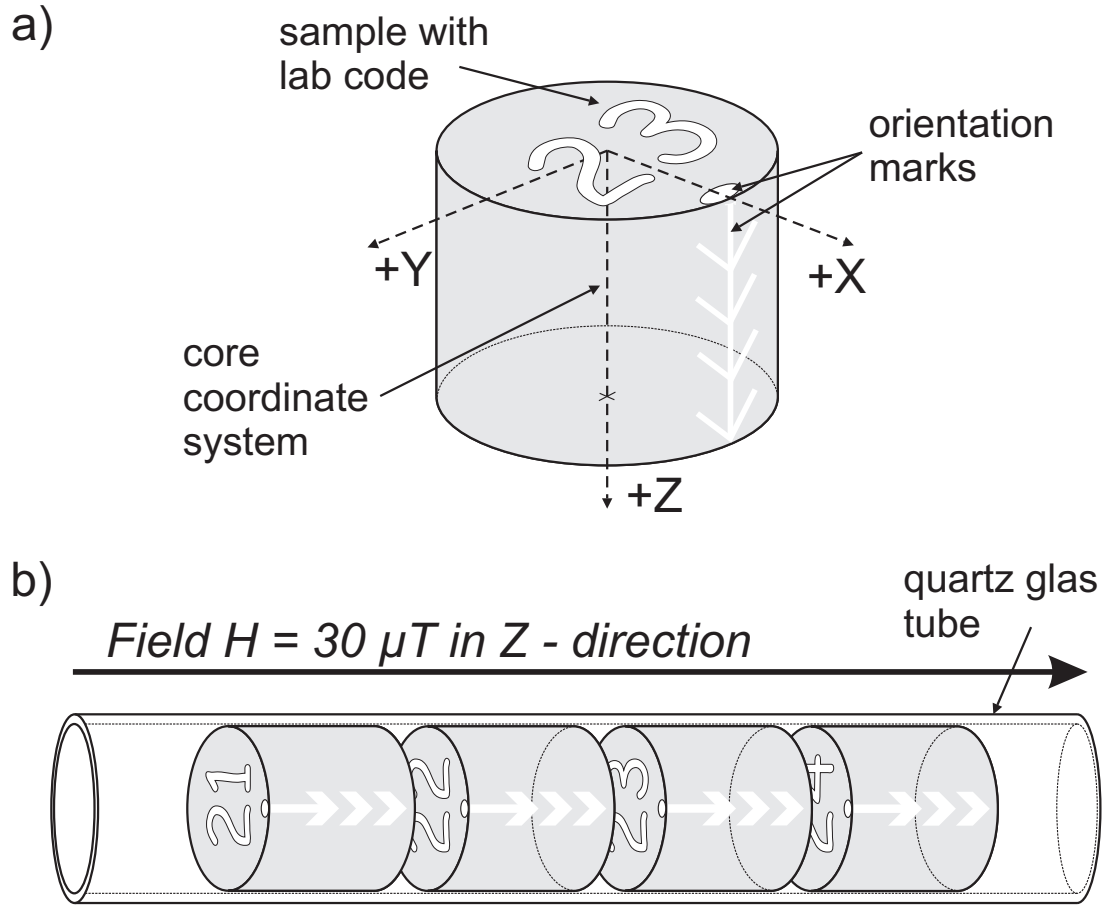

Figure 3.4: Thellier experiments on mini-cores extracted from potsherds. (a) shows an illustration of a typical mini-core used for Thellier and ATRM experiments with an inscribed coordinate system in x, y and z-directions. (b) illustrates mini-cores inserted in a quartz glass tube for heating. A laboratory field H_{lab} of 30 μT is applied in +z - direction (core-coordinates).

$\pm$ 0.1 μT was applied in the Z-direction (core coordinates) during a complete heating and cooling cycle, which took about 45 to 60 minutes depending on the maximum temperature. After every single de(re)magnetisation step the direction and intensity of the remanent magnetisation was determined using a 2G cryogenic magnetometer. In order to compensate the noise and interfering fields, every sample was measured in two positions anti-parallel to each other. If the offset was bigger than 5% the measurement was repeated. Up to 12 double heating steps were applied between 100°C and 580°C (11 for samples heated up to 550°C) with pTRM checks after every second, tail checks every third and additivity checks every fourth temperature step. The specimens were remagnetised along the Z-direction (core coordinates). For the vector subtraction, only values of the measured Z component are used and all parameters were determined using the "ThellierTool4.1" (Leonhardt et al., 2004a).

3.6.3 ATRM determination in the Thellier-type experiment

The nature of the ATRM's in ceramics is usually to a large extent characterised by an oblate anisotropy ellipsoid (e.g. Rogers et al., 1979; Aitken et al., 1981), with the hard direction of the magnetisation pointing perpendicular and an easy plane of directions parallel to the sherds surface. Thus for perpendicular drilled mini-cores the easy plane of magnetisation corresponds to the x-y-plane and the hard direction to the z-direction in core-coordinates (Fig. 3.4a).

The technique of sampling potsherds along both their major and minor axes of magnetisation (Fig. 3.1) and comparing the intensities before and after anisotropy correction is a powerful way to test the accuracy of the anisotropy correction. Depending on the degree of ATRM, an archaeointensity determination of both sister samples would lead to more or less different results. After applying a correction utilising a calculated tensor of anisotropy of the thermoremanent magnetisation (ATRM), the results of sister samples need to converge.

During the Thellier experiments, the laboratory field was applied parallel to the long axis of the arbitrarily orientated mini cores. Therefore for these measurements, we determined an ATRM tensor, using the approach of Veitch et al. (1984), and applied an appropriate correction (e.g. Genevey and Gallet, 2002; Leonhardt et al., 2006; Hill et al., 2007). The applied fields and atmospheric conditions were the same as for the Thellier and cooling rate experiments. ATRM measurements were performed in +z, +y, −y, +x, −x and −z directions (core coordinates) at 550°C and 580°C, respectively (Fig. 3.5a). Finally the measurement in the +z direction was repeated to monitor possible alteration. In order to use the maximum possible blocking spectrum of a sample the ATRM experiments were performed when more then 95% of the original NRM was removed. The applied method (Veitch et al., 1984) is based like the Thellier method, on the same physical principals that for weak fields the induced magnetisation is proportional to an applied field, where the proportionality factor k_{ij} is the tensor of susceptibility (e.g. Soffel, 1991; Butler, 1992; Tauxe, 1998).

$$\begin{bmatrix} M_1 \\ M_2 \\ M_3 \end{bmatrix} = \begin{bmatrix} k_{11} & k_{12} & k_{13} \\ k_{21} & k_{22} & k_{23} \\ k_{31} & k_{32} & k_{33} \end{bmatrix} \begin{bmatrix} H_1 \\ H_2 \\ H_3 \end{bmatrix} \tag{3.4}$$

H_1, H_2 and H_3 are the components of the applied field along the x, y and z-axes, and M_1, M_2 and M_3 are the corresponding components of the magnetisation M. For $(i \neq j)$ $k_{ij} = k_{ji}$ the equation (3.6) can be simplified as:

$$M_j = k_{ij} H_i \tag{3.5}$$

By analogy, a susceptibility of TRM can be defined as:

$$M_j^{TRM} = k_{ij}^{TRM} H_i \tag{3.6}$$

For convenience the anisotropy of TRM k_{ij}^{TRM} is indicated as ATRM. After determination of an ATRM-tensor the ancient magnetic field (H_{anc}) can be calculated. M_{ChRM} denotes a characteristic magnetisation of the investigated linear segment during the archaeointensity determination and H_{anc} describes a unit vector.

$$H_{anc} = \frac{ATRM^{-1} \cdot H_{anc}}{|ATRM^{-1} \cdot H_{ChRM}|} \tag{3.7}$$

In order to correct for any anisotropy error obtained during the trial Thellier experiments a correction factor f_{ATRM} was calculated utilising the relationship between the ancient (H_{anc}) and laboratory (H_{lab}) magnetic field with respect to the ATRM - tensor (e.g. Veitch et al., 1984; Selkin and Tauxe, 2000; Leonhardt et al., 2006).

$$f_{ATRM} = \frac{|ATRM \cdot H_{anc}|}{|ATRM \cdot H_{lab}|} \tag{3.8}$$

The ATRM corrected archaeointensity H_{ATRM} is then calculated using:

$$H_{ATRM} = f_{ATRM} \cdot H_{anc} \tag{3.9}$$

To estimate uncertainties due to orientation problems and/or progressive alteration during the ATRM experiments the correction factor was not only calculated from the average of the components of the axes, but also from the positive (+x, +y and +z) and negative (−x, −y and −z) components. The redundancy of the correction factor was then deduced after Leonhardt et al. (2006) using equation (3.12):

$$\sigma(f_{ATRM}) = \left| f_{ATRM}^{pos} - f_{ATRM}^{neg} \right| \tag{3.10}$$

3.6.4 Determination of cooling rate effects

As described in Chapter 2 the use of open fires for burning pottery leads to significantly shorter cooling times in contrast to kiln fired earthenware. Nevertheless the cooling rate dependency is determined in order to learn more about the prevailing magnetic domain states.

The manufacturing techniques and the compositions of magnetic minerals can be distinct for SW Pacific pottery. Therefore each sample needs to be investigated individually for the influence of cooling time differences on the TRM acquisition. Examinations of CR were conducted after the Thellier and ATRM experiments. To determine the CR effect of the samples a similar approach was chosen as described by Genevey and Gallet (2002). Prior to this experiment only a NRM of $\sim 5\%$ for all samples remained.

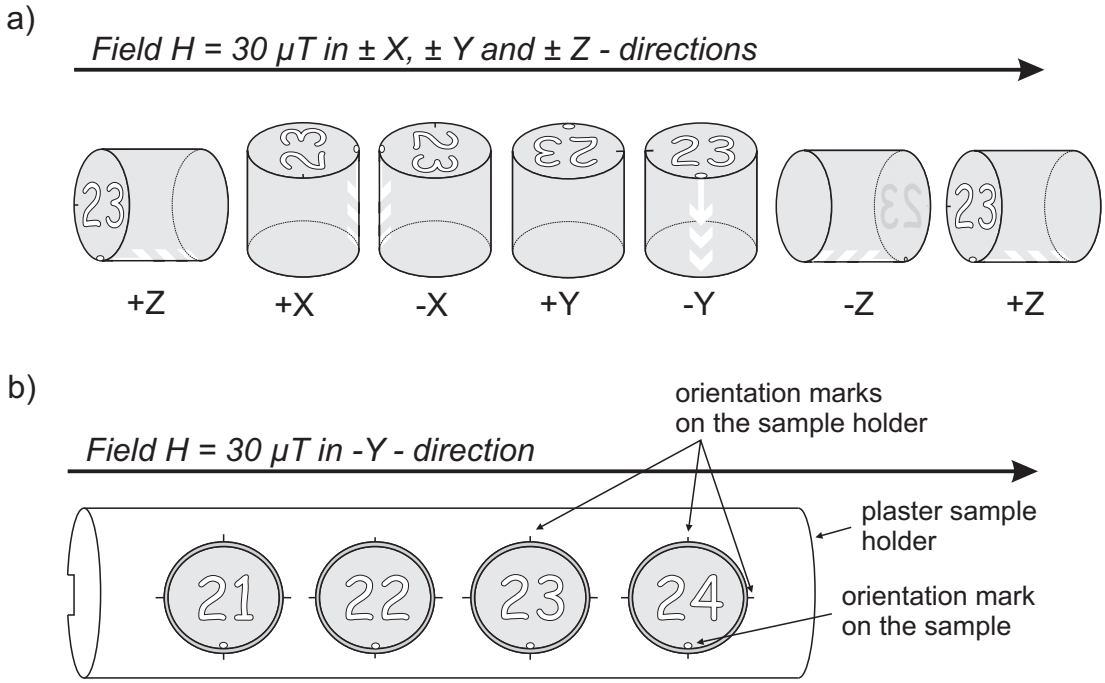

Figure 3.5: Illustration of anisotropy of thermoremanent magnetisation experiments. (a) For the ATRM experiments the samples are positioned back to back to a H_{lab} in ±x, ±y and ±z - directions. The +z step is repeated in the end to monitor possible alteration. (b) In order to apply a field in ±x and ±y directions samples are mounted on a plaster sample holder with orientation marks prior heating. The example shown in the figure below illustrates a field (H_{lab}) applied in −y -direction.

In a first fast cooling step (TRM_{FC1}) the samples were heated in an ambient magnetic field (30 ± 0.1 μT) to 550°C and 580°C, respectively and subsequently cooled down using a cooling fan to room temperature. The samples were cooled down within 20 min from the maximum temperature to ∼ 25°C. In a second slow cooling step (TRM_{SC}) the applied field and end temperature were the same, but now the cooling fan was switched off and the samples cooled down within ∼ 8 h to room temperature. In order to monitor alteration during this procedure the fast cooling step was repeated (TRM_{FC2}). The CR experiments were like the Thellier and ATRM experiments conducted in an MMTD20 thermal demagnetiser and the acquired TRM's were measured in a 2G cryogenic magnetometer. In order to correct archaeointensities obtained from samples where $H_{lab} \neq H_{anc}$, a CR correction factor f_{cr} can be calculated as following:

$$f_{CR} = \frac{\|TRM_{FC1}\| + \|TRM_{FC2}\|}{2 \cdot \|TRM_{SC}\|} \tag{3.11}$$

In order to incorporate a cooling rate correction factor into the obtained ATRM corrected archaeointensities, the following equation can be applied:

$$H_{ATRM,CR} = H_{ATRM} \cdot f_{CR} \tag{3.12}$$

The degree of alteration of the magnetic mineralogy during these experiments can be measured by comparing first (TRM_{FC1}) and repeated (TRM_{FC2}) fast cooling steps and estimated from equation (3.13) after Chauvin et al. (2000):

$$alt(\%)_{FC1 \rightarrow FC2} = abs \frac{\|TRM_{FC1}\| - \|TRM_{FC2}\|}{\|TRM_{FC1}\|} \cdot 100 \tag{3.13}$$

Chapter 4

Results from the Fiji Lau Group

Chapter 4 to 7 describe results from laboratory investigations conducted on samples from different island regions in the SW Pacific. Each chapter starts with an description of the investigated region and the sample material. Subsequently results of VFTB, SEM and microwave experiments are presented.

4.1 Study area

The Fiji Lau Group is located south-east of the two major islands Viti Levu and Vanua Levu in the Fiji archipelago and comprises around one hundred islands of variable sizes (Fig. 4.1a). Whereas the northern Lau Group consists of mainly mountainous islands containing a volcanic center the southern Lau Group is dominated by flat islands of Carboniferous origin (Ladd and Hoffmeister, 1945). The studied potsherds from this region come from the islands Lakeba, Nayau and Aiwa (Fig. 4.1 b). Lakeba located at 18.2° S, 181.2° E has a size of $\sim$ 56 km^2. The main part of the island dates from the Miocene and has an andesitic volcanic origin which is in turn surrounded by karstic limestone (Ladd and Hoffmeister, 1945). Nayau (18.0° S, 179.0° E) with a size of about 22 km^2 lies $\sim$ 28 km to the north-west of Lakeba and is composed of exposed volcanics and weathered limestone whereas the small Aiwa islands Levu (1.12 km^2) and Lailai (1.0 km^2) are $\sim$ 12 km to the south-east to Lakeba and consist entirely of limestone (Franklin et al., 2008, and citations herein). The Fiji archipelago was discovered and settled between 1200 BC and 1000 BC by immigrating people of the Lapita culture (Best, 2002). The typical dentate-stamped pottery became rapidly less and changed into plain ware with some paddle-impressings in the first millenium BC (Kirch, 2000). Lakeba is of particular interest for archaeologists, since the island was settled around 1000 BC and displays many of the key stylistic changes in ceramics found elsewhere in Fiji (Best, 1984; Kirch, 2000). The first Europeans to sight Fiji were Dutch sailors in the 17th century and the first exploration of the archipelago was undertaken by Capt. William Bligh in 1792 (Encyclopaedia Britannica, 2011a).

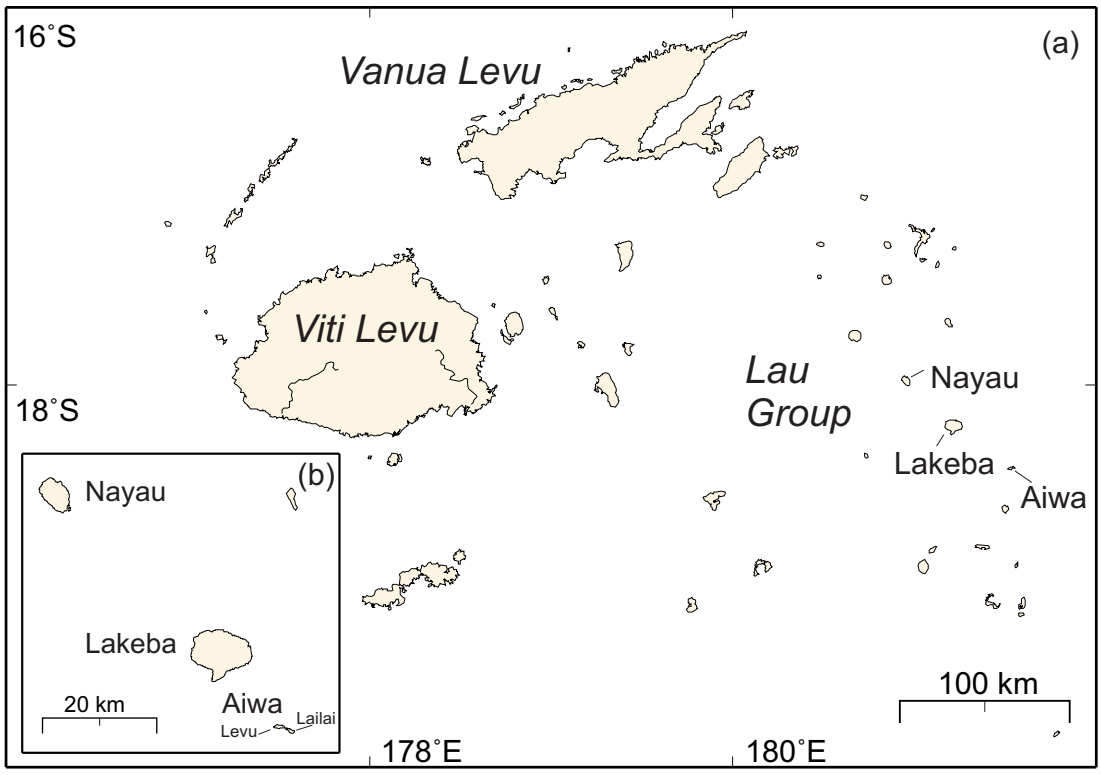

Figure 4.1: (a) Outline map of the Fiji archipelago illustrating the main islands Vanua Levu and Viti Levu as well as the islands of the Lau Group. Embedded map (b) shows the three islands Nayau, Lakeba and Aiwa providing ancient potsherds investigated for this study.

4.2 Sample description

From the Fiji archipelago a suite of 40 individual potsherds from Lakeba, 7 from Nayau and 11 from Aiwa were available and represent 23 different archaeological contexts (Table 4.1). The radiocarbon ages given in BP were obtained mainly from marine shell and charcoal. Two potsherds from Nayau and one from Aiwa have CRA dates from human bone and bird bone, respectively. The entire radiocarbon dates are consistent with archaeologically assigned ages. CRA data of potsherds yielding successful archaeointensities were calibrated as described in Chapter 2 and reveal dates in calendar years from 1005 ± 95 cal BC to 1555 ± 95 cal AD (Table 4.2). The ages have precision at the 95.4% confidence interval of ± 95 to ± 195 years. All CRA data from Lakeba used for this study have been recently revised by the Rafter Radiocarbon Laboratory in New Zealand, since the old measurements were based on the former Libby half-life of ^{14}C. For the revised data the more accurate figure of 5730 ± 40 years (Cambridge half-life) was applied. Unfortunately no new lab codes were assigned and some publications still refer to the old ages (Clark and Anderson, 2009). For five potsherds from Lakeba no radiocarbon age determination are available. For these the age was determined from the archaeological context and a conservative age uncertainty of ± 250 years assigned. Throughout the region, archaeologists can ascertain the age of ceramics in the 3200 to 2800 BP period, because the Lapita pottery is very distinctive and changes fairly uniformly over the entire Lapita region. After 2800 BP different island groups begin to follow different sequences with some better understood than others. As a general rule, archaeologists in Vanuatu can tell within about 300 years the age of ceramics by their stylistic characteristics. The sequence from Lakeba can be estimated stylistically in the 300 – 500 year range. Although the ceramic seriation is not as precise as it is in many parts of the world, nonetheless Pacific archaeologists are fairly confident in their ability to date these decorated ceramics within 500 years (pers. comm. P. Sheppard 2010). No ages were available for 4 samples from Nayau and 9 samples from Aiwa. These samples were only subjected to magnetic mineralogical experiments.

4.3 Magnetic mineralogical investigations

In order to determine the magnetic mineralogy of the potsherds, rock magnetic measurements were carried out using a Variable Field Translation Balance (VFTB). A ∼ 150 mg sample from each sherd was subject to isothermal remanent (IRM) acquisition, backfield coercivity measurements, hysteresis loops and magnetisation with temperature ($M(T)$) determinations, heating up to 700°C in an ambient field of up to 800 mT. The complete results of these investigations are shown in Appendix A.

Table 4.1: Investigated ceramic series from the Fiji archipelago

Island/Context	Pottery Group	N_P	^{14}C Age/Error (BP)	CRA Reference	Dated Material
Fiji, Lakeba (18.2° S, 181.2° E)					
196-19-B19(a)	F2800	7	$\sim$ 2800*	–	–
197-3-T-1	F2700	3	$\sim$ 2700*	–	–
197-3-T-2	F2700	1	2855/36	†NZ4589	marine shell
197-3-T-1-3+4	F2700	1	2540/127	†NZ4596	charcoal
197-1-N-1-1	F2250	2	2260/80	†NZ4808	charcoal
197-1-N-2-2	F2250	1	$\sim$ 2250*	–	–
197-1-N-1-4	F2250	2	2873/67	†NZ4594	charcoal
197-3-K-4	F2230	4	2498/35	†NZ4591	marine shell
2(b)-1-M4-3	F1930	4	1937/116	†NZ4040	charcoal
197-3-F-1	F1500	5	2065/34	†NZ4588	marine shell
47-17-B2 c43	F930	2	$\sim$ 900*	–	–
47-15-B2 (45-55)	F930	1	1228/33	†NZ4581	marine shell
47-17-B2	F930	1	1266/33	†NZ4582	marine shell
101-7-(3,44,125)	F500	6	$\sim$ 500*	–	–
Fiji, Nayau (18.0° S, 179.0° E)					
G6 III/13 N31-(1-2)	FN	2	2570/40	β-235993	human bone
G7 Feature 3 N44-18	FN	1	2580/40	β-235994	charcoal
D8 II/8 N15-20	FN	1	–	–	–
G7 I/4 N36-(4,17,18)	FN	3	–	–	–
Fiji, Aiwa Levu & Aiwa Lailai(18.3° S, 181.3° E)					
TP-1 II/7 30-9	FAL	1	200/70	β-164260	charcoal
TP-1 II/7 30-25	FAL	1	360/40	β-164258	bird bone
TP-1 II/7 30-(10,13,29)	FAL	3	–	–	–
TP-4 II/2 93-(3,4)	FAL	2	–	–	–
TP-1 I/3 129	FAL	4	–	–	–

Table 4.1: Island/Context describe the islands with their latitudes, longitudes and the context code of the investigated potsherds. Pottery Group describes the lab code of a site and N_p the number of individual potsherds from a context. The conventional radiocarbon age (CRA) with errors are given in BP. Dates labeled with an asterisk(*) are archaeological ages and were obtained from a combination of pottery style and archaeological context. CRA Reference describes the lab code of the samples used for determining the CRA. †Revised dates using new half-life but no new date reference was issued. Dated Material is charcoal bird and human bone. In the case where marine shell was used a ΔR marine correction factor of 43 $\pm$ 12 was applied.

IRM and Backfield measurements

IRM experiments revealed two different types of IRM curves. Type 1 represented by sample F2800-5 almost completely saturated ($\geqq$ 98%) in a magnetic field of 300 mT indicating "soft" ferro(i)magnetic remanence carrier like (titano)magnetite and/or maghemite (Fig. 4.2 solid line). Curves of type 2 exhibited a saturation between 89% and 97% at 300 mT but were not fully saturated at a maximum field of 800 mT . This behaviour suggests a presence of both low and high coercivity minerals with the low coercivity minerals dominating the magnetic fractions in type 2. The sample F2230-2 shown in Fig. 4.2 (dashed line) describes the lower-most saturation level (89%) at 300 mT of all investigated samples from the Fiji Lau region. All investigated sites of Lakeba, Nayau and Aiwa revealed both types of IRM curves. Utilizing backfield curves (Fig. 4.2) the remanence coercivity force B_{cr} (Fig. 4.2) and S_{300}-parameter (Bloemendal et al., 1992) are calculated for each specimen. The B_{cr} values for the Fiji sites range between 18.8 mT (F1930-4) and 67.6 mT (F1500-5) with an average value of 37.0 mT and a standard deviation of 10.23 (Lakeba: 37.9 $\pm$ 10.9 mT; Nayau: 36.3 $\pm$ 6.2 mT; Aiwa: 37.0 $\pm$ 7.6mT). The S_{300} values range between 0.89 and 1 with their distribution corresponding to the spectrum of the IRM curves. Nearly 75% of the values range between 0.98 and 1 suggesting a strong presence of low coercivity minerals. For the remaining specimens an increasing number of "hard" magnetic minerals (i.e haematite) are present. The presence of haematite is plausible since it is an oxidation and/or weathering product of magnetite and maghemite.

Magnetic hysteresis

Hysteresis measurements revealed a dominant ferrimagnetic component, with some indication of paramagnetism. The shape of the hysteresis loop classified by calculating a shape parameter σ_{Hys} after Fabian (2003) showed, all bar one, pot-bellied shapes with typical PSD dimensions (see Subsection "Domain state estimations") throughout the investigated sites from Fiji (Fig. 4.3a). The absence of constricted hysteresis loops also indicates that besides a soft ferrimagnetic component no significant amount of SP and/or high coercive magnetic phases are present (Tauxe et al., 1996). Only sample F2230-3 revealed a minor constricted hysteresis (Fig. 4.3b). This can be explained by the presence of both low and high coercive magnetic grains which are already suggested by the relatively low S_{300}-parameter. Plotting the shape parameter against the S_{300}-parameter shows a relationship between the shape of the hysteresis loop and the coercive fractions (Fig. 4.4) and suggests that sample F2230-3 follows this trend. This favours the assumption that the constricted loop is more likely to be generated by an amount of high coercive minerals than by the presence of SP particles.

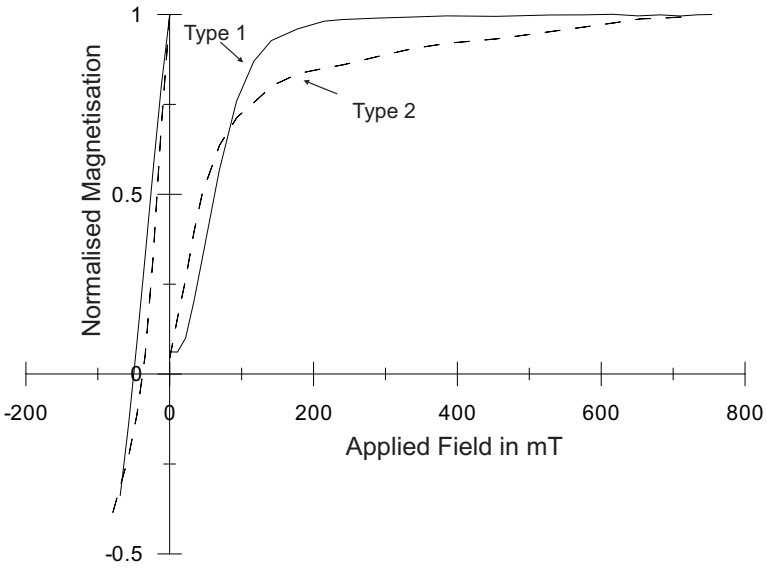

Figure 4.2: IRM and corresponding backfield curves of sample F2800-5 (solid line) and F2230-2 (dashed line). Whereas F2800-5 saturates around 300 mT, an applied field of up to 800 mT was not enough to saturate sample F2230-2. A remanence coercivity force B_{cr} was determined by the interception of backfield curves and ordinates.

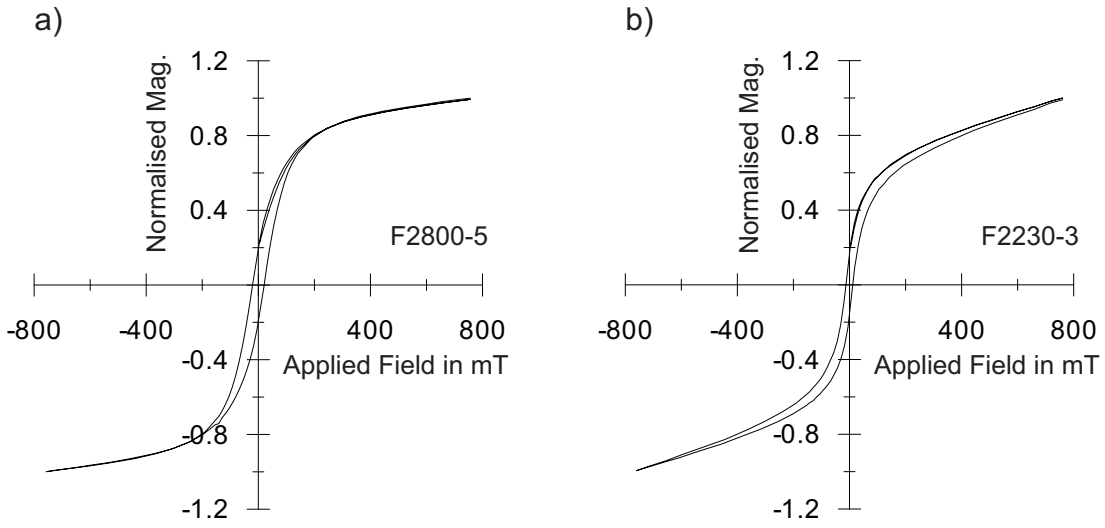

Figure 4.3: Curve (a) illustrates a typical hysteresis loop for samples from the Fiji Lau Group. (b) Sample F2230-3 revealed a near wasp-waisted hysteresis where the loop does not close. This behaviour was not found in other potsherds from this region.

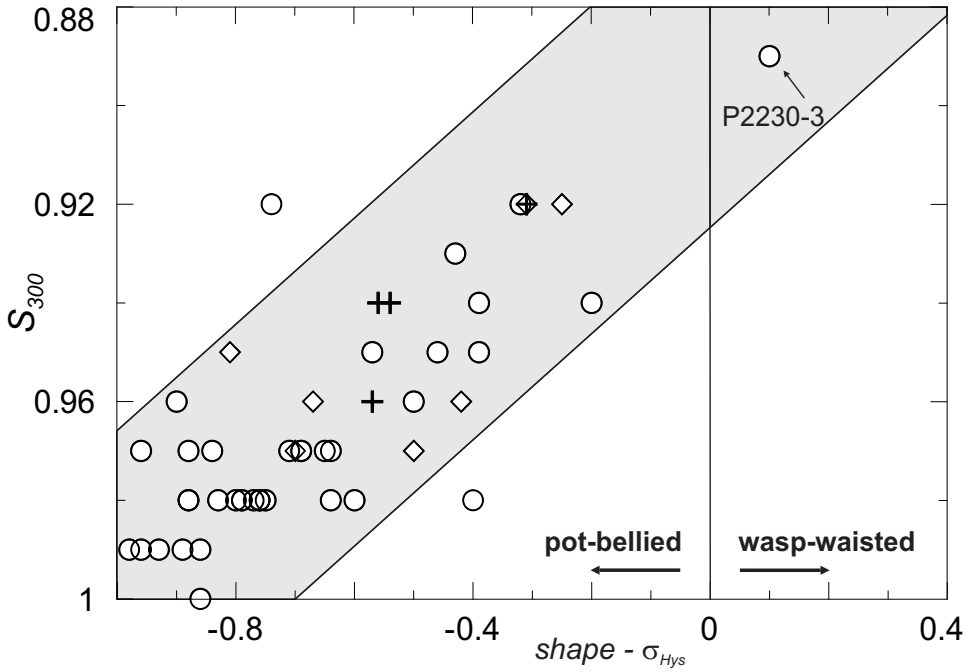

Figure 4.4: Dependency of the shape parameter σ_{Hys} (Fabian, 2003) from the coercivity spectrum of the magnetic minerals represented by the S_{300}-parameter (Bloemendal et al., 1992). Samples from Lakeba, Nayau and Aiwa are plotted in circles, diamonds and crosses, respectively. The grey shaded area indicates a trend channel.

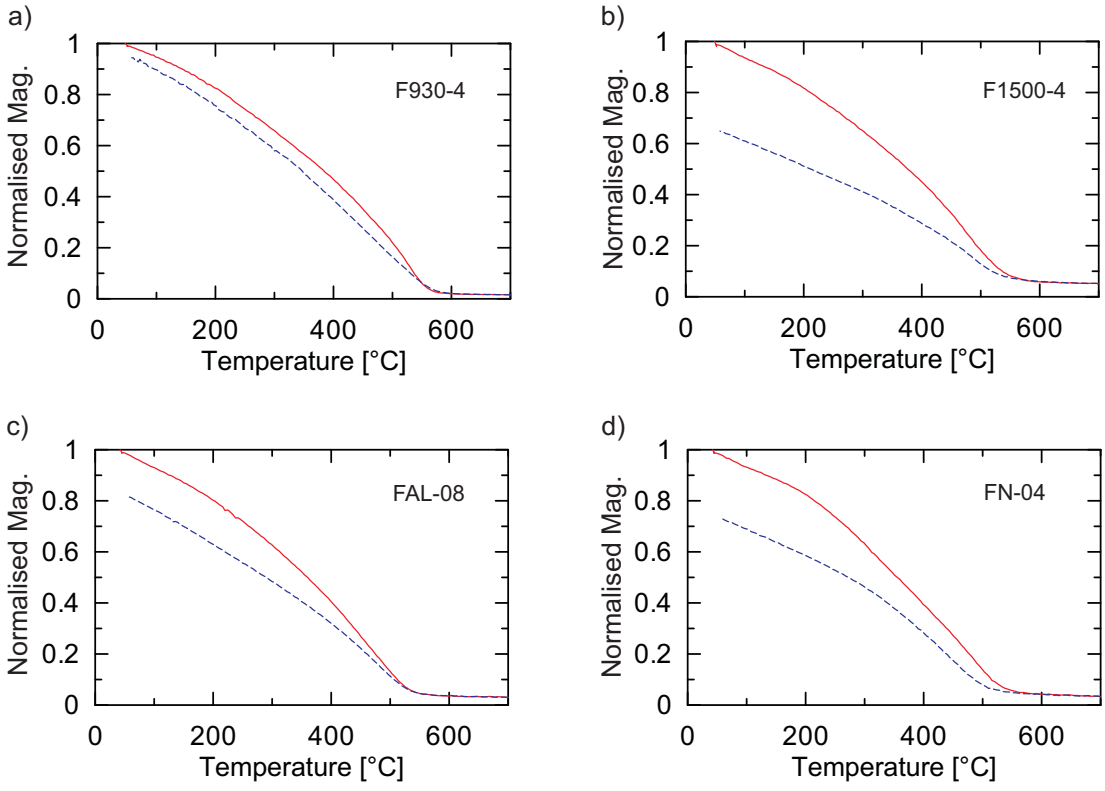

Figure 4.5: All thermomagnetic curves obtained from Fijian samples are dominated by a single T_C with different degrees of reversibility. Typical curves from Lakeba (a and b), Aiwa Islands (c) and Nayau Island (d).

Thermomagnetic curves

All investigated samples from the Fiji region exhibited common behaviours with a single Curie temperature T_C and decreasing magnetisation in the subsequent cooling curve (Fig. 4.5a-d). The Curie temperatures range from 493°C to 574°C with an average T_C of $\sim$ 528°C (Lakeba: $\sim$ 532°C, Nayau: $\sim$ 513°C, Aiwa: $\sim$ 521°C) suggesting magnetite and/or impure magnetite is the dominant magnetic mineral. Assuming Ti^{4+} ions cause the impurities, the unblocking temperatures correspond to a Ti-poor titanomagnetite $Fe_{3-x}Ti_xO_4$ with x ranging from $\sim$ 0 (nearly pure magnetite) to $\sim$ 0.1 (O'Reilly, 1976). Besides Ti^{+4} ions also substitutions of iron ions with foreign ions i.e. Mg^{2+} and/or Al^{3+} from the surrounding silica phases are also possible and can lower the Curie temperature of pure magnetite (Brabers, 1995).

A less magnetic phase in the cooling curve is explained by alteration of the magnetic mineralogy during heating up to 700°C likely to be some of the (titano-)magnetite oxidised to a lesser magnetic haematite phase. An increased reddish colouring, in particular of black and/or grey samples, supports this idea. No haematite fraction is detected in the thermomagnetic curves (Fig. 4.5a-d) which, however, can be obscured by the much stronger magnetic (titano-)magnetite fraction. The decline of the magnetisation M varied from nearly reversible (Fig. 4.5a) to a reduction of more then one third of its maximum value in the heating curve (Fig. 4.5b).

It is further worth mentioning that about 30% of the thermomagnetic curves revealed a more or less prominent kink in the heating curve at $\sim$ 200°C which was not found in the subsequent cooling runs (Fig. 4.5d). This phenomena was found in samples from all three islands. One explanation for this is could be stress release of titanomaghemite (Krása and Herrero-Bervera, 2005).

Domain state estimation

Plotting the hysteresis parameters M_{rs}, M_s, B_{cr} and B_c in the (Day et al., 1977) plot (Fig. 4.6) suggests an assemblage of PSD particles in the ceramic samples, though this division is only strictly valid for magnetite and titanomagnetite (Tauxe et al., 1996). Comparison with theoretical mixing curves after Dunlop (2002a) shows that the data distributes within, as opposed to along, any of the SP+SD and SD+MD mixing curves. This seems to be typical for ceramics (e.g. Dunlop, 2002b). Nevertheless the results of the Day-plot are only valid to a certain extent since minor contributions of maghemite and/or high coercitive minerals like haematite can hamper a precise determmination. One sample from Nayau (FN005) exhibited bulk sample hysteresis properties indicating larger magnetic grains than the others.

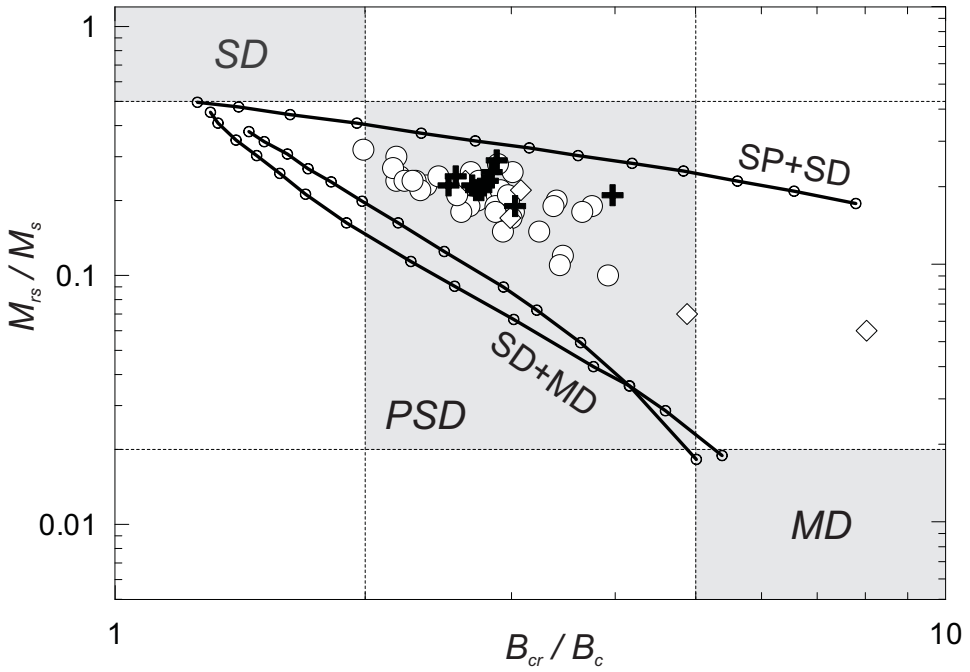

Figure 4.6: Day plot for Lakeba (circles), Nayau (diamonds) and Aiwa Islands (crosses) showing bulk sample hysteresis parameters. With the exception of one sample from Nayau all results plot within the PSD range.

4.4 Microscopic investigations

Scanning electron analysis was performed on three samples from Lakeba (F500-6, F2250-3 and F2800-4). In each thin section large (titano)magnetite grains ($\sim$ 50 μm to $\sim$ 250 μm) were observed. These grains were often interstratified with ilmenite lamellae due to high temperature oxidation which is typically seen in volcanic rocks (Fig 4.7a). Some grains also showed evidence of hydrothermal erosion (Davies, 2009, and citations herein). EDX analysis of Fe (Fig 4.7b) and Ti (Fig 4.7c) distributions illustrates enrichments of titanium in the ilmenite lamellae and only a little presence of titanium in the (poor Ti) titanomagnetite sections. The large iron-oxide grains are found in the tempered material added during manufacturing of the pottery (Dickinson, 2006). It is questionable to what extent these microlites contribute to the NRM. Their grain sizes are typical of MD particles. Exsolved paramagnetic ilmenite lamellae can divide a grain into small cells of (titano)magnetite with magnetic domains in the SD to PSD range (Dunlop and Özdemir, 1997). But it is more likely that these huge grains only acquire an induced magnetisation. It is assumed that a dominating second fraction of microlites coming from the clay mass is responsible for the magnetic remanence. This fraction cannot be resolved by the SEM and therefore restricts identification of SD particles ($\sim$ 0.05 to 1 μm for magnetite (Butler and Banerjee, 1975)).

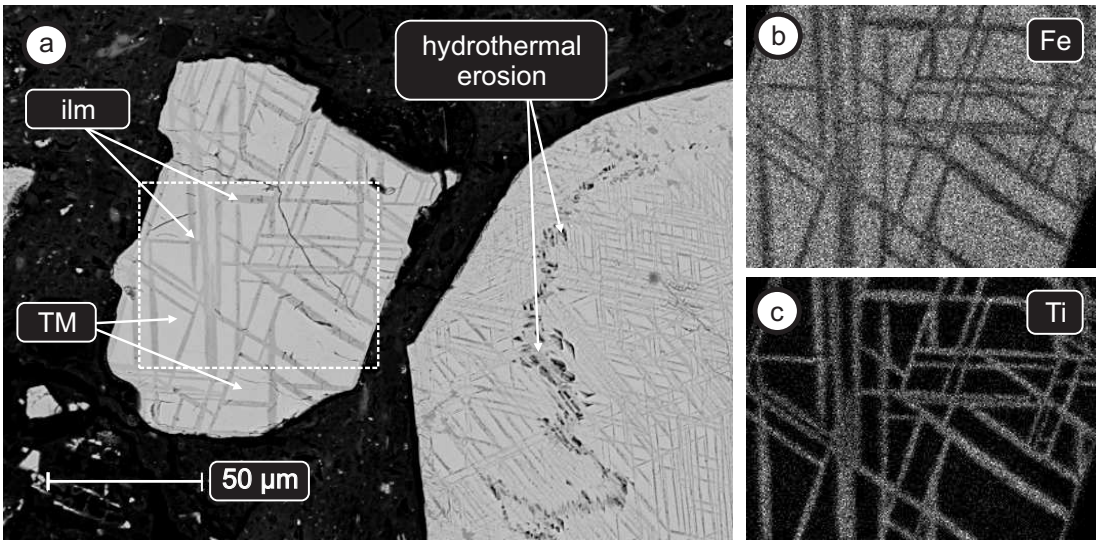

Figure 4.7: SEM and EDX mapping images from a Fijian sample. (a) shows two grains of Ti-poor titanomagnetite (TM) with densely crowded exsolved ilmenite (ilm) lamellae. (b) and (c) delineate an EDX map of Fe and Ti contents. Investigated area is illustrated by the dashed area in (a). Brightness indicates an increased population of the investigated elements.

4.5 Results of the archaeointensity determination

Demagnetisation experiments

Prior to the archaeointensity measurements, demagnetization experiments were conducted on 45 potsherds. As a result of these, 20 individual potsherds (Lakeba: 16, Nayau: 2 and Aiwa: 2) were chosen for archaeointensity experiments (44% of total). Half of all investigated potsherds revealed a more or less pronounced viscous remanent overprint. Nevertheless the samples are accepted if a clear ChRM can be identified (Fig. 4.8a). The remainder of the samples were rejected, primarily because they lacked a stable component of remanence, which was possibly caused by insufficient heating, pot movement during firing, or intensive use as cookware (Fig. 4.8b). Two potsherds were rejected as they could not be successfully demagnetized by more then 30% (Fig. 4.8c). For sample F2700-2 it was not possible to find a resonable resonance frequency, hence most of the incoming microwave energy was reflected. Even though sample F900-1 absorbed about a third of the applied microwave energy the sample could not be demagnetised.

Microwave archaeointensity experiments

From 40 microwave archaeointensity experiments (on 20 potsherds), 20 samples from 10 individual potsherds (Lakeba: 18, Nayau: 2 and Aiwa: 0) passed the selection criteria. This corresponds to a success rate at the sample level of 50%. Fig. 4.9 shows examples of accepted Arai plots. Some samples contained a viscous remanent magnetization,

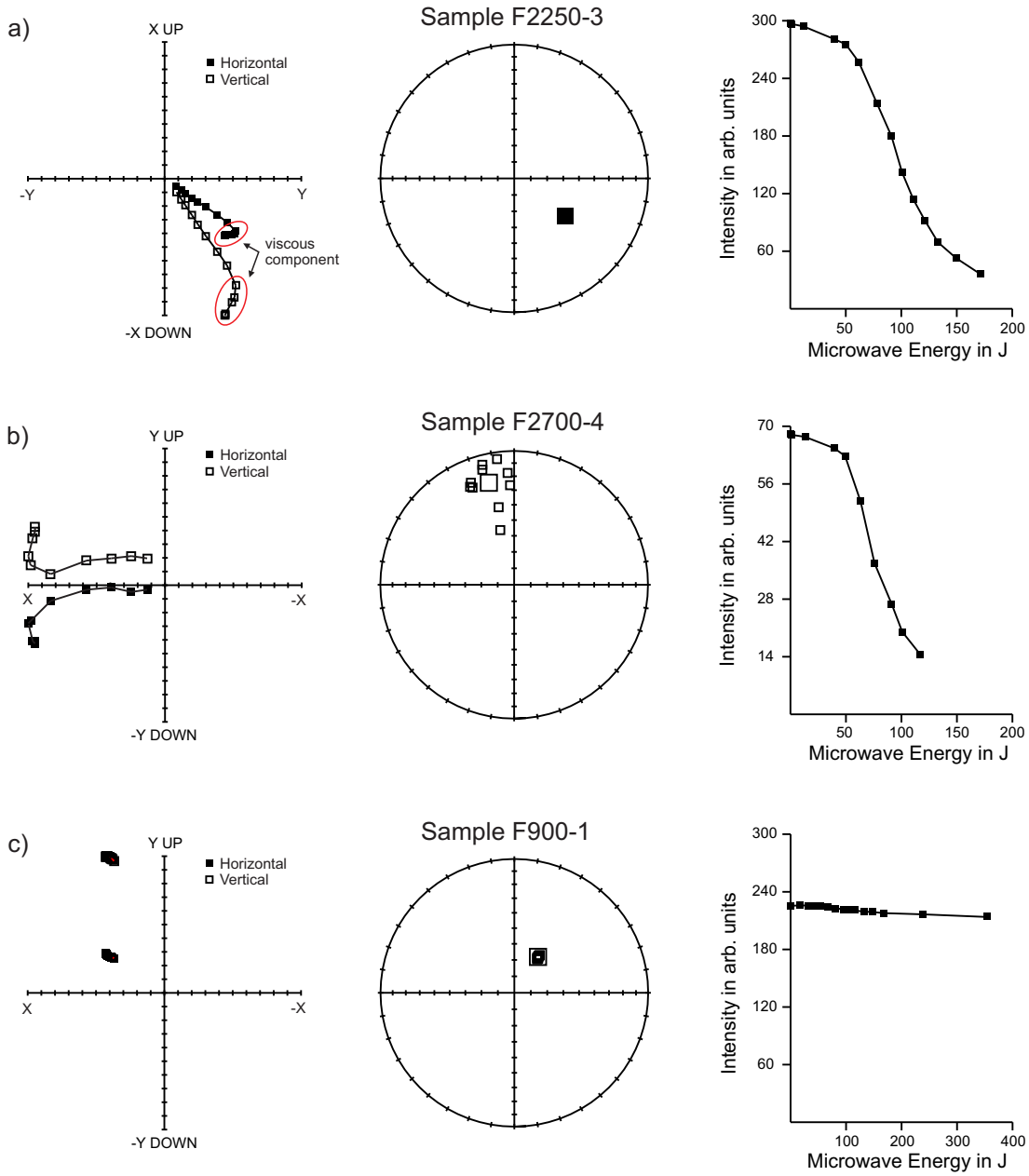

Figure 4.8: Representative results from demagnetisation experiments on potsherds from Fiji. From left to right: orthogonal plot in core coordinates, circular plot and decay of the NRM. (a) represents an accepted result with a pronounced VRM and a ChRM. (b) and (c) are examples for rejected potsherds due to lack of a ChRM and/or failing response to the demagnetising microwave energy.

clearly identified in the orthogonal vector plots, and therefore not used as part of the analysed segment to determine archaeointensity. Samples from potsherd F2250-4 were hard to demagnetise using the microwave and only 37% and 49%, respectively of the NRM fraction could be used to determine the intensity. Results from this sherd thus strictly fail selection criteria 9 (Chapter 3, Section 3.4.5), however they were accepted, since a similar archaeointensity value was reproduced on sister samples during Thellier experiments for F225-4.

Most rejected samples did not exhibit reproducible behaviour between sister samples and showed large scatter in their Arai plots, where the best fitted segment had a correlation coefficient (r^2) less than 0.98 and a β value > 0.10 (Fig 4.10). This often came along with lacking repeatability of the applied power during the experiments. Some samples exhibited alteration during the experiment, especially where high microwave powers were needed to de(re)magnetize (Fig 4.10a). The effect of alteration is most often manifested in a melting spot on the sample with a red oxidized area, indicating a strong local temperature rise. This is most likely due to dielectric heating and is probably localised to the outer skin of the sample (Suttie et al., 2010). Despite preselection by the demagnetisation experiments a few samples revealed several magnetic components in their orthogonal vector plots which can be associated with different slopes in the Arai plot (Fig 4.10b). Although it is assumed that the last component is the ChRM this fraction was too small to be analysed. This can be explained by the fact that some pottery was used as cooking pot which leads to a stronger magnetic overprint on parts of the vessel which were most exposed to the fire. Five potsherds where discarded because they had a large intra-sherd scatter (>20%).

4.6 Discussion of the archaeointensity results from the Fiji archipelago

Successful results from the microwave measurements are listed in Table 4.2 and range from 25.9 μT to 51.1 μT which corresponds to VADM's of 4.3 to 12.8 ($\times 10^{22}$ Am^2). All accepted samples show good within-sherd consistency, with mean deviation of only 8% (Fig 4.11a). The distribution of the q-factor (Coe et al., 1978) ranges from 4 to 72 with an average around 27 which is an excellent result for archaeointensity determinations (Fig 4.11b). The contexts of the entire suite are well defined with the exception of context 197-1-N-1-4 (potsherd F225-4) which was out of stratigraphic sequence (i.e. lower layers had younger dates). There is a possibility that potsherd F225-4 dates from $\sim$ 2250 BP instead of 2873 BP (as used in this study). However, comparing the result from potsherd F225-4 (51.1 μT) with potsherd F225-3 (25.9 μT) from context 197-1-N-2-2 which dates from $\sim$ 2250 BP, there is a significant difference in their intensity. This supports the idea of different ages between these contexts and a radiocarbon age of 2873 BP, although further data are needed to verify this.

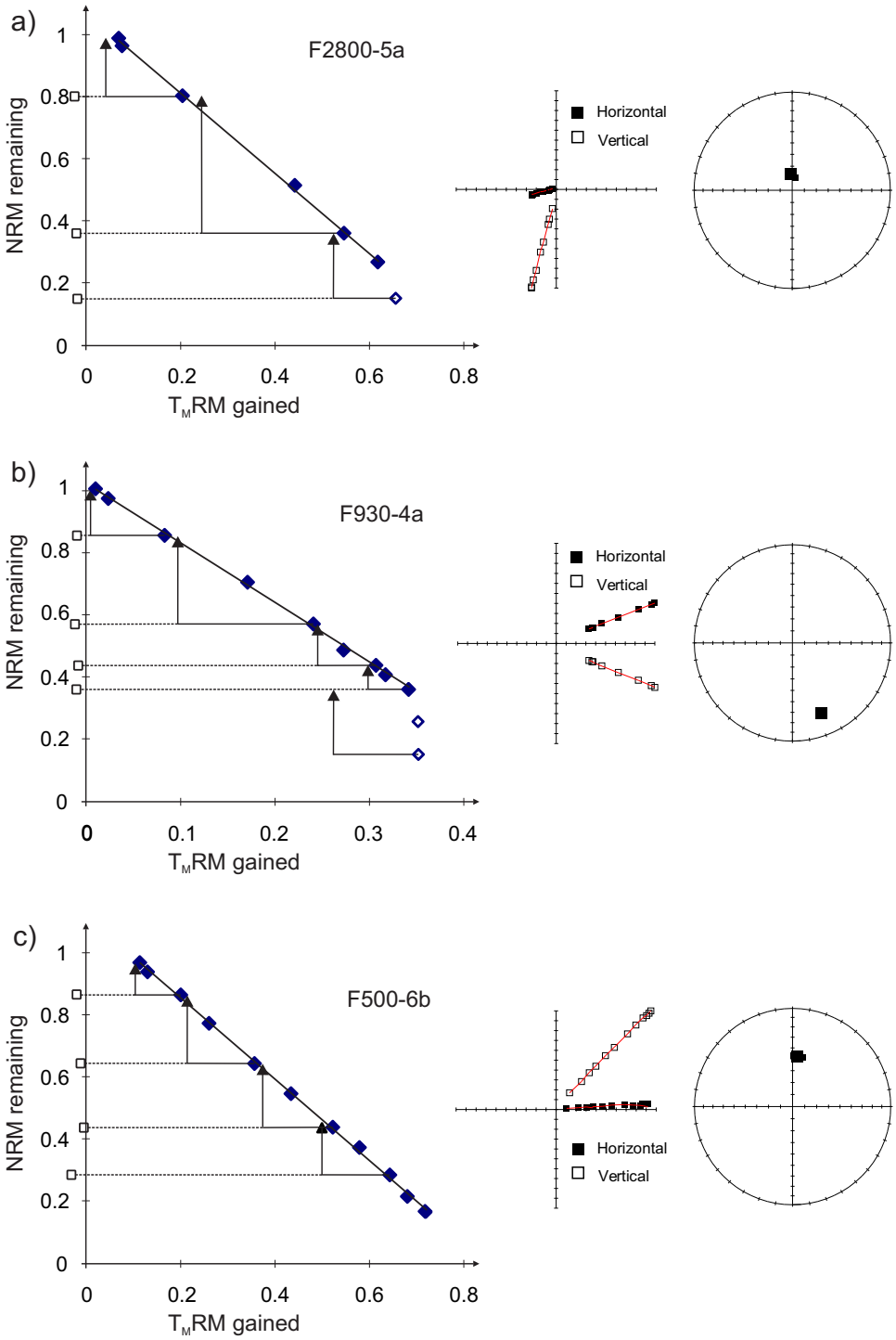

Figure 4.9: Three representative successful arai-diagrams together with their orthogonal vector and circular plots from an (a) early ($\sim$ 800 BC), (b) intermediate ($\sim$ 1160 AD) and (c) late stage of settlement on Lakeba ($\sim$ 1500 AD). Filled (open) diamonds are accepted de/remagnetisation steps used for determining the linear segment. Triangles and squares indicate pTRM and MD checks.

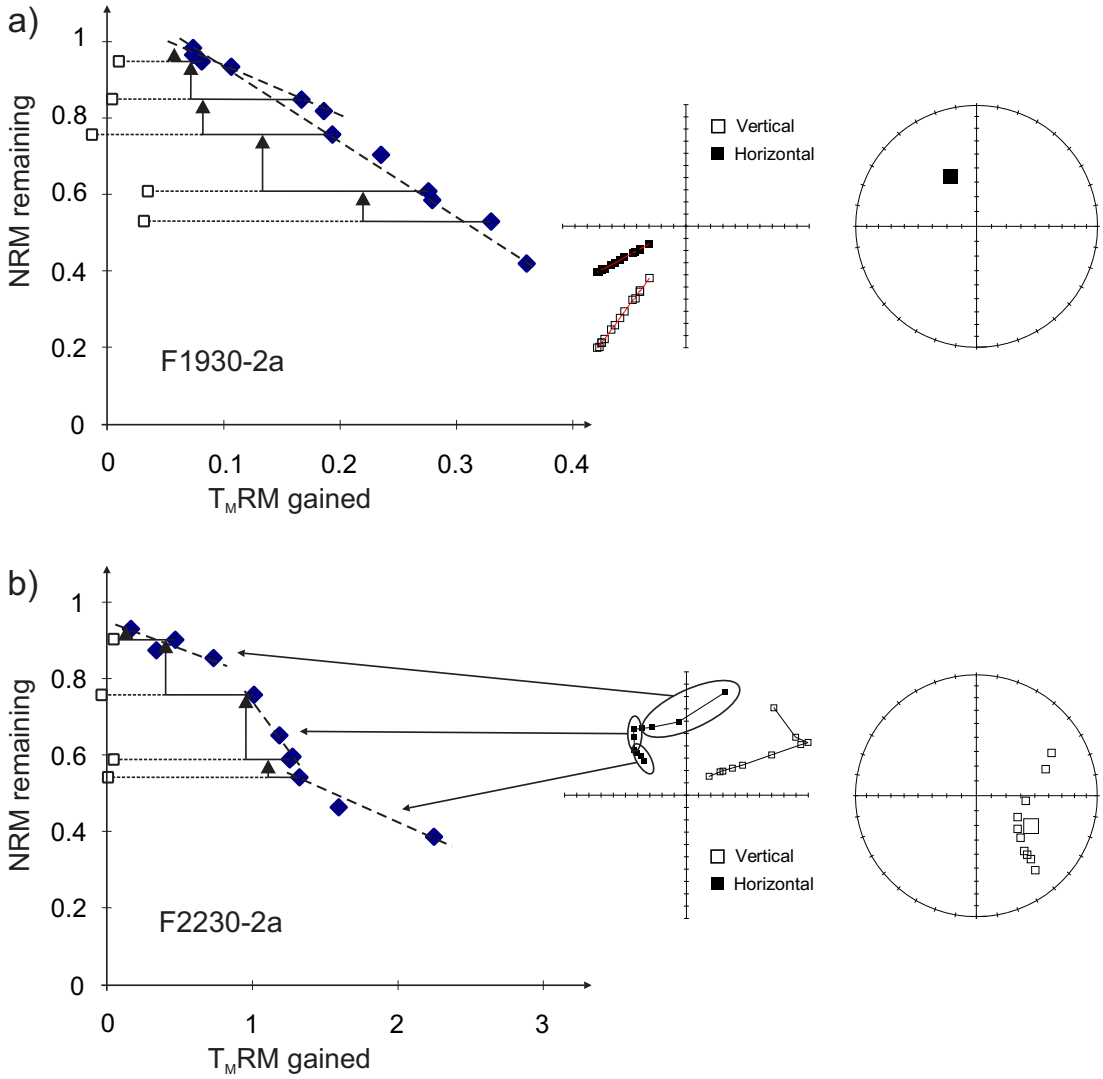

Figure 4.10: Examples for rejected Fijian samples. (a) F1930-2a represents a typical sample revealing a melting spot with ongoing alteration. Panel (b) illustrates a typical sample (F2230-2a) with several components of magnetisation.

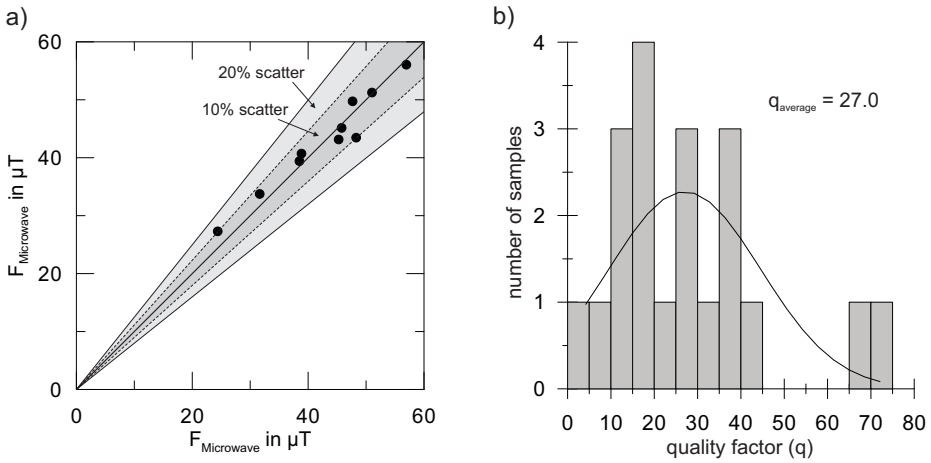

Figure 4.11: Scatter and q-factors of microwave intensity results of sister samples from Fijian potsherds. (a) Grey shaded area shows intensity differences of less than 20% (bright grey) and 10% (dark grey). (b) illustrates the distribution of the quality factors (q) after Coe et al. (1978).

For three sites two different potsherds were investigated. A scatter within these sites from 10% to 20% can be explained because the sherds are of different ages (within the age uncertainty). Furthermore, as described below, there were significant field strength variations around 900 BC and during the period from 420 BC to 180 AD. All archaeointensity values have been relocated to Lakeba, Fiji (18.2° S, 181.2° E) and are plotted in Fig. 4.12 along with the present-day field strength in Fiji (42.2 μT after IGRF 2011) and the global field models CALS3k.3 and ARCH3k (Korte et al., 2009). For illustration purposes the archaeointensity values obtained from each potsherd are connected with a dotted line. Between 1000 BC and 250 BC five intensity values from four sites (Lakeba 3 and Nayau 1) are available. They indicate a strong decay of the geomagnetic field strength for this period of time. The field decreases from 51.1 μT in 1005 BC to 25.9 μT around 250 BC which is a decay of $\sim$ 50%. From the minimum around 250 BC to 1160 AD three intensity values from two different sites suggest a strong increase of the field strength to a maximum of 56.5 μT around 1160 AD. Two archaeointensites from one site dating around 1500 AD show values around the present field strength of 42 μT. Although there are still few data from the Fiji Archipelago, the obtained data set exhibits a more distinct variation of the geomagnetic field strength than predicted by the field models ARCH3k and CALS3k.3 from Korte et al. (2009). In particular, the low field intensity around 250 BC is not indicated in both models which are not very well constrained for the SW Pacific region.

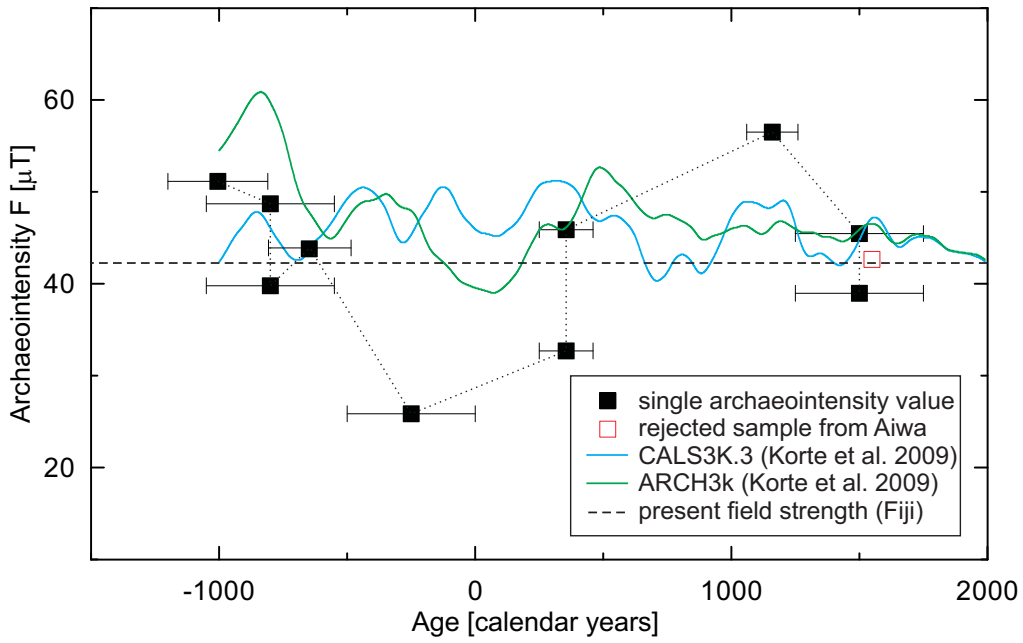

Figure 4.12: Archaeointensity results from the Fiji archipelago. Blue (CALS3k.3) and green (ARCH3k) lines represent intensity models after Korte et al. (2009) calculated for Fiji, Lakeba. Dashed black line shows the present geomagnetic field strength in Fiji, Lakeba. Black squares represent mean values of successful potsherds. Red square indicates the mean value of the rejected potsherd from Aiwa islands.

4.7 Summary

The potsherds from the Fiji Lau Group are found to be excellent recorders of the ancient geomagnetic field strength. The remanence carrier is a low-Ti titanomagnetite with grain sizes ranging from SD to PSD. Large titanomagnetite particles (> 5 μm), which partly underwent high temperature oxidation, were probably introduced by the tempering process and seem not to contribute significantly to the thermoremanence.

More then 90% of the investigated ceramics show a good response to the microwave treatment with more then half of them carrying a ChRM. Final archaeointensity determinations yield a good success rate of 50% and together with radiocarbon and/or archaeological ages result in high quality data.

Table 4.2: Archaeointensity results from the Fiji Archipelago.

Site/Context	Potsherd	Age ± (2σ) (cal. yrs)	N	f	g	β	q	$F_{specimen}$ (μT)	F_{mean} (μT)	VADM × 10^{22}(Am^2)
Fiji, Lakeba (18.2° S, 181.2° E)										
196-19-B19(a)	F280-5a	-800 ± 250*	6	0.72	0.73	0.02	36.4	38.85	39.78	9.03
	F280-5b		9	0.72	0.81	0.03	31.5	40.71		
196-19-B19(a)	F280-3a	-800 ± 250*	10	0.47	0.82	0.02	28.4	47.67	48.70	11.06
	F280-3b		8	0.5	0.81	0.02	10.4	49.73		
197-1-N-1-4	F225-4a	-1005 ± 195	6	0.49	0.78	0.06	17.1	51.02	51.14	11.61
	F225-4b		5	0.37	0.72	0.04	8.0	51.25		
197-1-N-2-2	F225-3a	-250 ± 250*	7	0.66	0.71	0.02	20.9	24.4	25.85	5.87
	F225-3b		7	0.48	0.78	0.02	17.7	27.3		
47-17-B2	F930-4a	1160 ± 100	8	0.63	0.78	0.03	36.5	56.95	56.50	12.83
	F930-4b		9	0.62	0.83	0.02	38.6	56.05		
197-3-F-1	F150-4a	355 ± 105	10	0.56	0.85	0.03	16.6	31.64	32.69	7.42
	F150-4b		6	0.65	0.79	0.02	25.4	33.74		
197-3-F-1	F150-3a	355 ± 105	7	0.62	0.77	0.05	16.9	48.29	45.88	10.41
	F150-3b		9	0.56	0.86	0.02	41.8	43.46		
101-7-3	F500-6a	1500 ± 250*	10	0.73	0.86	0.01	66.0	38.5	38.96	8.84
	F500-6b		11	0.8	0.89	0.01	72.1	39.42		
101-7-3	F500-5a	1500 ± 250*	7	0.72	0.81	0.07	12.5	45.78	45.46	10.32
	F502-5b		7	0.43	0.82	0.02	11.7	45.15		
Fiji, Nayau (18.0° S, 179.0° E)										
G6 III/13 N31-2	FN 3a	-650 ± 150	5	0.48	0.68	0.09	4.2	44.86	43.91	9.96
	FN 3b		9	0.80	0.86	0.04	28.0	42.96		
Fiji, Aiwa Levu (18.2° S, 181.2° E)										
TP-1 II/7 30-25	Fal 13b	1555 ± 95	3	0.14	0.50	0.08	1.2	†44.33	†42.60	–
	Fal 13d		4	0.34	0.61	0.07	4.0	†40.87		

Table 4.2: Microwave archaeointensity results yielded from potsherds from three islands (Lakeba, Nayau and Aiwa) in the Fiji Lau Group. The ages with uncertainties are given in calendar years. N is the number of points used to define a linear segment in the Arai diagram. f, g, β and q stand for the fraction of NRM, gap factor, normalised error of the slope and quality factor according to Coe et al. (1978). F is the intensity result for individual specimens in μT. F_{mean} values are the arithmetic mean of F, and VADM describes the Virtual Axial Dipole Moment in Am^2. *For the archaeological ages an uncertainty of ± 250 years is assigned. †These are the only results from the Aiwa Islands. Since they failed the acceptance criteria they were not considered for further analysis.

Chapter 5

Results from Vanuatu

5.1 Study area

The Vanuatu group of islands is mainly of volcanic origin, is mountainous and stretches over a distance of around 800 km from the northern most Torres islands to the southern most island of Aneityum (Fig. 5.1). The closest neighbors of Vanuatu are the Solomon Islands with Santa Cruz in the north, the Fiji archipelago in the east, and New Caledonia in the southwest. The archipelago was first settled by the Lapita people around 3500 years ago with pottery sherds dating back to 1300-1100 BC (Kirch, 1997). The Europeans first discovered Vanuatu (Espiritu Santo) in 1606 AD (Encyclopaedia Britannica, 2011d).

5.2 Sample description

A series of 62 individual pottery fragments was obtained from the Vanuatuan Islands of Efate (43), Malekula (6) with the offshore islands Uripiv (1) and Vao (9), Espiritu Santo (1) and Ambae (2) collectively representing 19 different archaeological contexts (Table 5.1). The quality of these contexts includes a good age control as described in Chapter 2 Section 2.3. The only potsherd (V059) with an estimated archaeological age comes from site Wusi Vilae on the island of Espiritu Santo, which is also the youngest of the Vanuatuan ceramic series ($<$ 100 BP). Since this potsherd failed the selection criteria for archaeointensity determinations no effort for assigning an age uncertainty was made. Ages from potsherd V061 and V062 were provided in cal BP but without error estimation and CRA lab code to trace back. No age uncertainty was assigned for these samples. All other potsherds with ages from 1035 $\pm$ 165 cal BC to 1775 $\pm$ 125 cal AD were dated by means of ^{14}C radiocarbon using either charcoal or marine shells as dated material. The ages are within the 95.4% confidential interval and the calculated precisions vary between $\pm$ 90 to $\pm$ 300 years. For marine shells a ΔR correction of 25 $\pm$ 10 years (Burr et al., 1998) was applied.

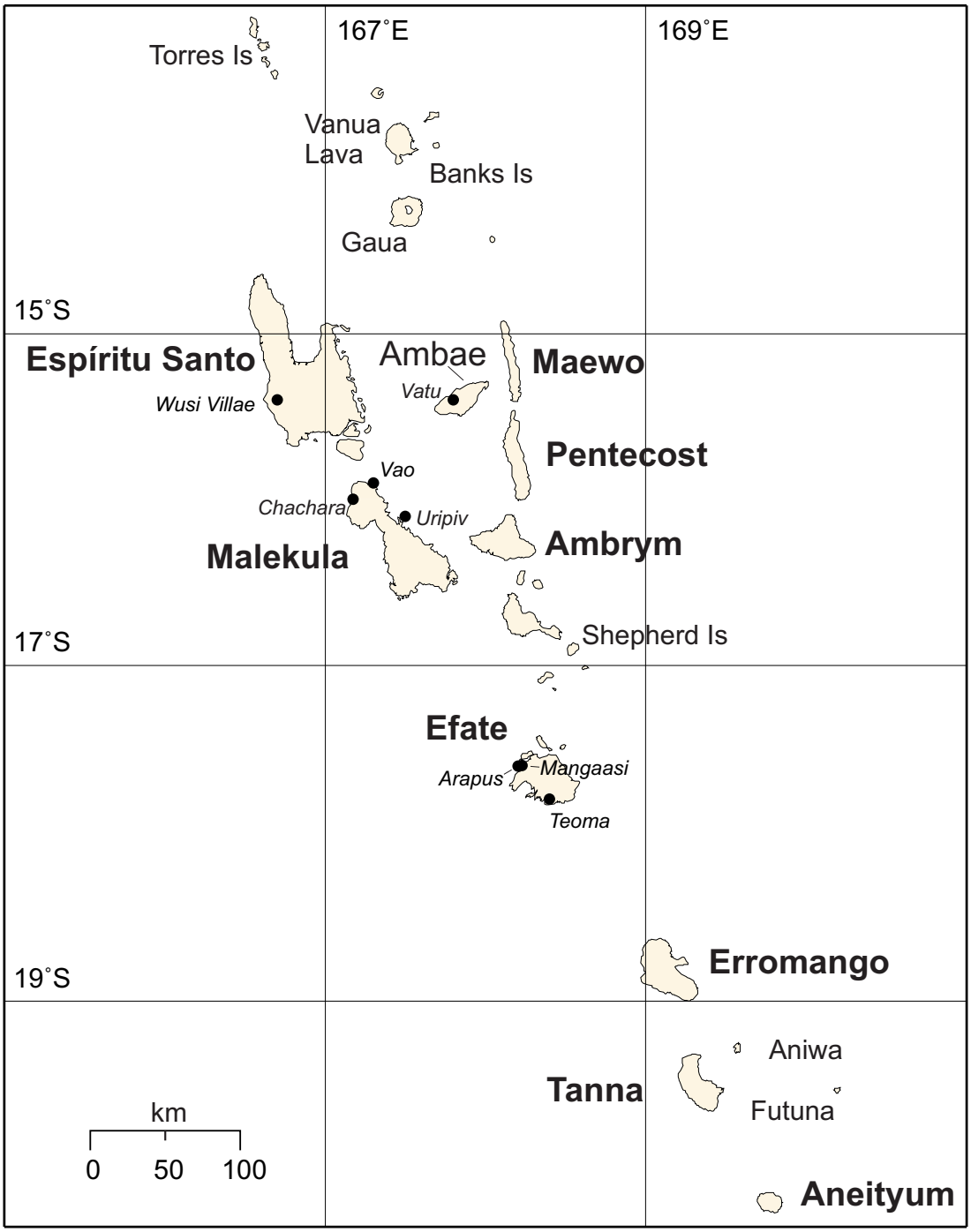

Figure 5.1: Map showing islands of Vanuatu and the location of the investigated sites (black dots) on Espiritu Santo, Malekula Efate and Ambae.

Table 5.1: Investigated ceramic series from the Vanuatu archipelago

Island/Context	Pot. Group	N_P	CRA Ref.	CRA/Err.	Cal. Age ± (2σ)			Dated Material
Island Efate, Site Mangaasi (17.6° S, 168.2° E)								
TP 9.4 130-150	V001-004	4	WK-6603	2790/50	-555	±	165	marine shell
TP 9 L3.1 165-175	V005-008	4	ANU-10798	2420/80	-560	±	210	charcoal
TP 9 175-185	V009-011	3	ANU-10798	2420/80	-560	±	210	charcoal
TP 9 155-165	V012-015	4	ANU-10800	2550/130	-635	±	285	charcoal
TP 9 195-205	V016-018	3	ANU-10799	2790/110	-1000	±	260	charcoal
TP 9.2 80-100	V019-022	4	WK-6602	2820/50	-575	±	165	marine shell
TP 9 60-80	V023-027	5	ANU-10801	2180/130	-120	±	300	charcoal
TP 1 70-90	V028-031	4	ANU-10640	1310/130	785	±	245	charcoal
Island Efate, Site Arapus (17.6° S, 168.2° E)								
ST 17 140-160	V032-035	4	ANU-11159	3200/50	-1035	±	165	marine shell
Island Efate, Site Teoma (17.8° S, 168.2° E)								
3B 3-5 L3 spit 3	V036-039	4	WK-16831	3139/36	-940	±	120	marine shell
3B 4-9 L3 spit 2	V040-043	4	WK-16831	3139/36	-940	±	120	marine shell
Island Malekula, Site Chachara (16.0° S, 167.2° E)								
TP C2 0-30	V044-047	4	ANU-10525	980/60	1390	±	90	marine shell
Island Malekula, Site Sakau (16.5° S, 167.8° E)								
TP-1 20-40	V048-049	2	WK-18953	201/41	1775	±	125	charcoal
Island Malekula, Site Vao (15.9° S, 167.3° E)								
Area A A.6 140-150	V050-054	5	WK-14040	2776/38	-890	±	90	charcoal
ST 11 170-180	V055-058	4	WK-14041	2839/40	-935	±	115	charcoal
Island Espiritu Santo, Wusi Villae (15.4° S, 166.7° E)								
Survey 19 surface	V059	1	–	<100	†1900	±	–	––
Island Malekula, Uripiv (Jimis) (16.1° S, 167.5° E)								
TP 9 120-130	V060	1	WK-10414	2681/74	-745	±	235	charcoal
Island Ambae, Vatulawn/Vatumeamu (15.4° S, 167.8° E)								
TP-1 245-265	V061	1	–	1800*		–		charcoal
Tp-1 40-60	V062	1	–	800*		–		charcoal

Table 5.1: Ceramic suite from Vanuatu. Island/Context describes location (sites) and context codes. Pot. Group denotes lab code and N_p the number of the individual potsherd available from each context. CRA Ref. and CRA/Err. are reference code and the conventional radiocarbon age with uncertainty (in BP). †An estimated archaeological age was assigned for potsherd V059. Cal. Age states the calibrated CRA in calendar years. *No exact CRA were given for potsherds V061 and V062. Dated Material gives the source of ^{14}C used for dating. Best estimate for ΔR is 25 ± 10 (Burr et al., 1998).

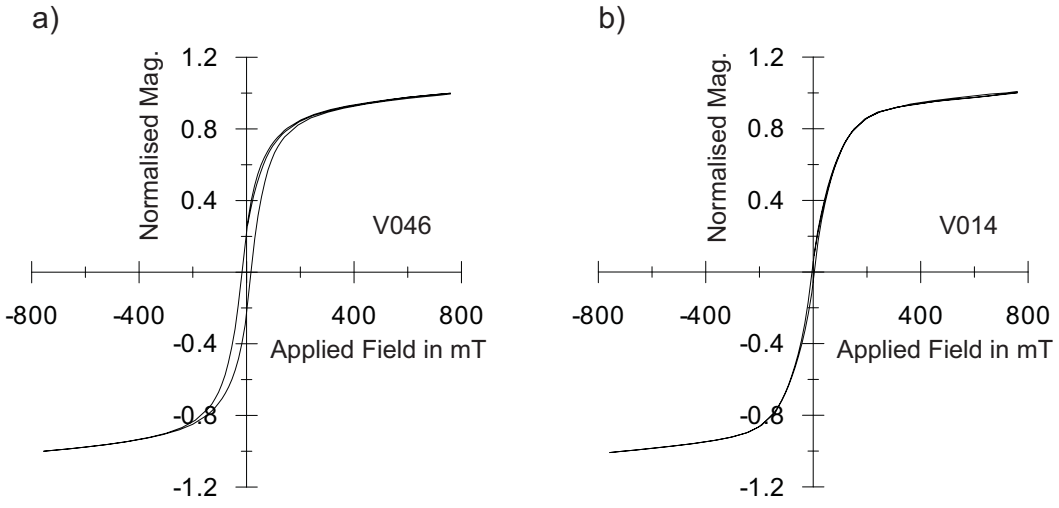

Figure 5.2: Curve (a) illustrates a typical hysteresis loop for samples from Malekula . (b) Sample V014 represents ceramics carrying two Curie temperatures from Island Efate.

5.3 Magnetic mineralogical investigations

In order to investigate the magnetic mineralogical behaviour of the pottery fragments from Vanuatu, 62 individual samples (43 from Efate, 9 from Vao, 6 from Malekula, 2 from Ambae, 1 from Uripiv and 1 from Espiritu Santo) have been subjected to VFTB measurements.

IRM, Backfield and magnetic hysteresis measurements

IRM results from Vanuatu exhibit magnetic phases close to saturation (between 93% to 100%) at an ambient magnetic field of 300 mT. This behaviour highlighting low coercivity magnetic material with only small contributions of a high coercive magnetic phase is comparable to IRM curves found from Fiji (Fig. 4.2). The B_{cr} values range between 17.2 mT (VE011) and 69.7 mT (VA061) with an average value of 31.6 mT and a standard deviation of 10.4 (Efate: 28.9 $\pm$ 8.6 mT, Malakula: 36.8 mT $\pm$ 9.9 mT, Ambae: 69.7 mT and 34.5 mT, Uripiv: 30.5 mT and Espiritu Santo: 38.5 mT). Although all hysteresis loops from the Vanuatuan sites were classified after Fabian (2003) as pot-bellied two different types of curves were observed (Fig. 5.2). Besides a loop with a well defined pot-bellied shape with typical PSD dimensions (Fig. 5.2 a) loops with very weak pronounced pot-bellied shape were also found (Fig. 5.2 b) indicating PSD to MD grain sizes (Tauxe, 1998). In particular the latter was found in samples from the island Efate exhibiting two Curie temperatures.

Thermomagnetic curves

Three types of thermomagnetic curves were identified (Fig. 5.3). Type 1 is characterized by a nearly perfectly reversible curve and is found in samples from Efate and Malekula including the offshore island of Vao (Fig. 5.3a,b). Type 2 curves show alteration during heating producing a lesser magnetic phase on cooling. All investigated islands revealed some pottery fragments belonging to type 2. In particular sample VA061 and VA062 excavated on Ambae were characterized by strong decay of saturation remanence during heating up to 700°C (Fig. 5.3c,d). Both type 1 and 2 curves have single Curie temperatures (T_C) ranging from 490°C to 574°C suggesting magnetite or Ti-poor titanomagnetite as remanence carrier. Type 3 curves (Fig. 5.3e) exhibit a first T_{C1} between 464°C and 518°C, but a second T_{C2} between 328°C and 372°C was also found. During cooling from 700°C both T_C's are replaced by a new single T_{C3}, slightly higher than T_{C1}. Repeated heating and cooling cycles with increasing temperature indicate that these lower Curie temperatures (T_{C1}) are genuine and not caused by decaying of unstable magnetic minerals such as maghemite or some titanomagnetites (Fig. 5.3f). Curves of type 3 appear to be reversible to around 400°C. Between 400°C and 450°C this magnetic phase, which is assumed to be a Ti-poor titanomagnetite ($\sim$ TM35), seems to transform into a titanomagnetite ($\sim$ TM20) with an even lower amount of Ti resulting in a stronger magnetisation (blue cooling curves run above the red heating curves). Some thermomagnetic curves still show little remainding saturation remanence with of a T_{C2}, which indicates that heating up to 700°C within around 30 min is not intense enough to alter all of the TM20. Nevertheless, there is a progressive decay of magnetic material when heating in 50°C and 100°C intervals, respectively from 200°C to 600°C. This procedure results in a more magnetic fraction during each cooling. After the final heating/cooling run to 600°C, T_{C2} vanished in nearly all samples of type 3. Interestingly only those samples from Efate with small coercivities ($B_c < 10$ mT) exhibit this behaviour. This could be due to differences in the source material and/or manufacturing of the pottery (e.g. differences in the tempering material and/or insufficient firing). Since samples with two T_C's are revealed to be very susceptible to alteration during heating up to 400°C and beyond, conventional methods like the Thellier-technique are only to a limited extent suitable for obtaining reliable archaeointensities.

Domain state estimation

Day-Plot analysis (Fig. 5.4) suggests domain states in the PSD range and plot between the SD-MD and SP-SD mixing lines proposed by Dunlop (2002a). Nevertheless compositions of different magnetic minerals (titano)magnetite, haematite etc. hamper a firm conclusion (e.g. Tauxe et al., 1996). It is noteworthy that samples from Efate exhibit a broad spectrum of grain sizes with a cluster close to the MD area. In particular,

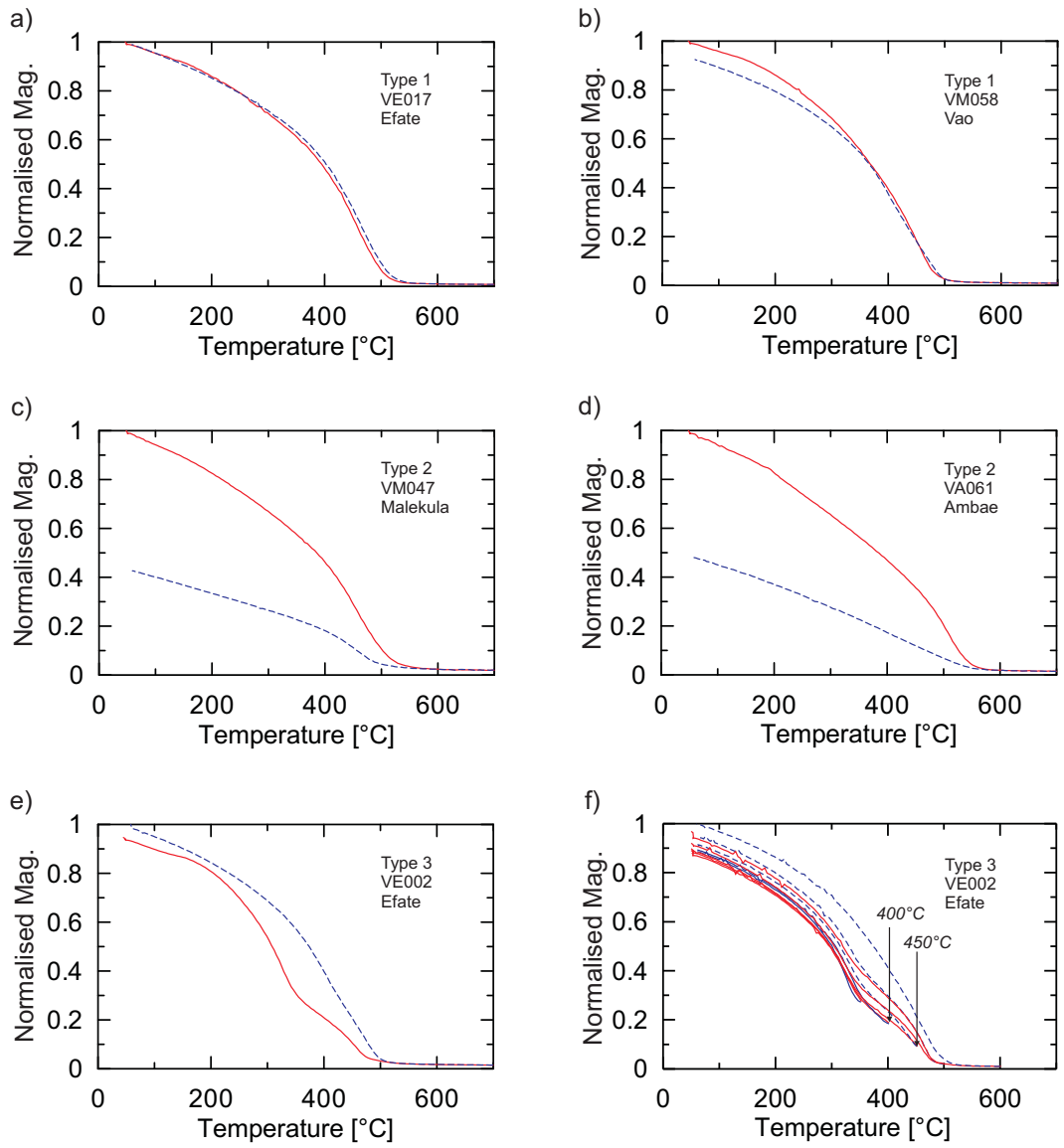

Figure 5.3: Representative thermomagnetic curves obtained from pottery fragments from Vanuatu. Panel (a) and (b) describe (nearly) reversible curves from Vao (Malekula) and Efate. Curves in (c) and (d) show samples from Malekula and Ambae revealing strong alteration during heating up to 700°C. Panel (e) exhibit two different Curie temperatures in the heating curve which have transformed to a single Curie temperature visible in the cooling curve. (f) Step by step heating up and cooling down with incrementally increasing temperatures reveals that the lower Curie temperature is genuine, but the magnetic phase starts to alter in an interval between around 400°C to 450°C.

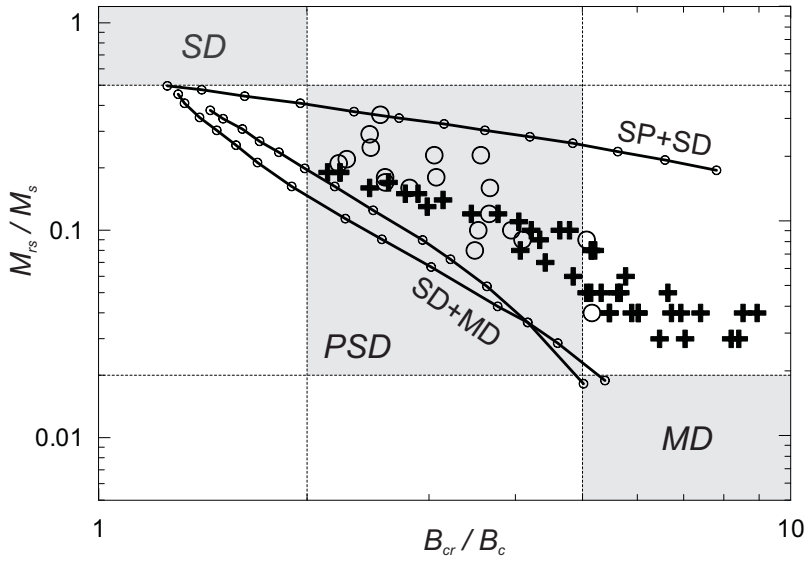

Figure 5.4: Day-plot for the investigated samples from the investigated sites of Vanuatu. Crosses mark the results of island Efate whereas circles denote the remaining islands.

samples with two Curie temperatures fall in this area. The remaining samples plot distinctly closer to the SD border. One sample from Ambae plots on the SP + SD mixing curve, although a significant presence of SP particles is unlikely since no constricted hysteresis loop typical of SP domains was found.

Examining two different coloured layers of a potsherd

Some potsherds from Efate exhibit both a reddish (oxidised) and a greyish layer (Fig. 5.5 a). Deduced from the shape of the pottery fragment, the reddish layer belongs to the outer rim which was probably more exposed to an oxidising environment then the interior surface during firing. In order to investigate the magnetic mineralogy two minicores were drilled from the reddish and greyish coloured layers (Fig. 5.5 b) and subjected to hysteresis and thermomagnetic experiments. After obtaining the thermomagnetic curves repeated backfield and hysteresis measurements were performed. Investigating the greyish layer revealed thermomagnetic curves similar to type 3 with two distinct Curie temperatures around 350 °C and 480 °C (Fig. 5.5 c). The thermomagnetic curve of the reddish layer, however, is type 2 exhibiting a single Curie temperature around 490 °C and a cooling curve slightly below (Fig. 5.5 d). Nevertheless both cooling curves of the reddish and greyish specimens exhibited similar behaviours with a final single Curie temperatures around 495 °C. This suggests a very similar magnetic phase in both specimens after heating up to 700 °C which is supported by the fact that the former greyish specimen turned reddish. Hysteresis measurements of both layers revealed differences in their magnetic domain states before heating (Fig. 5.5 e,f) where the reddish layer yields parameters closer to the SD region and the greyish closer to the MD region.

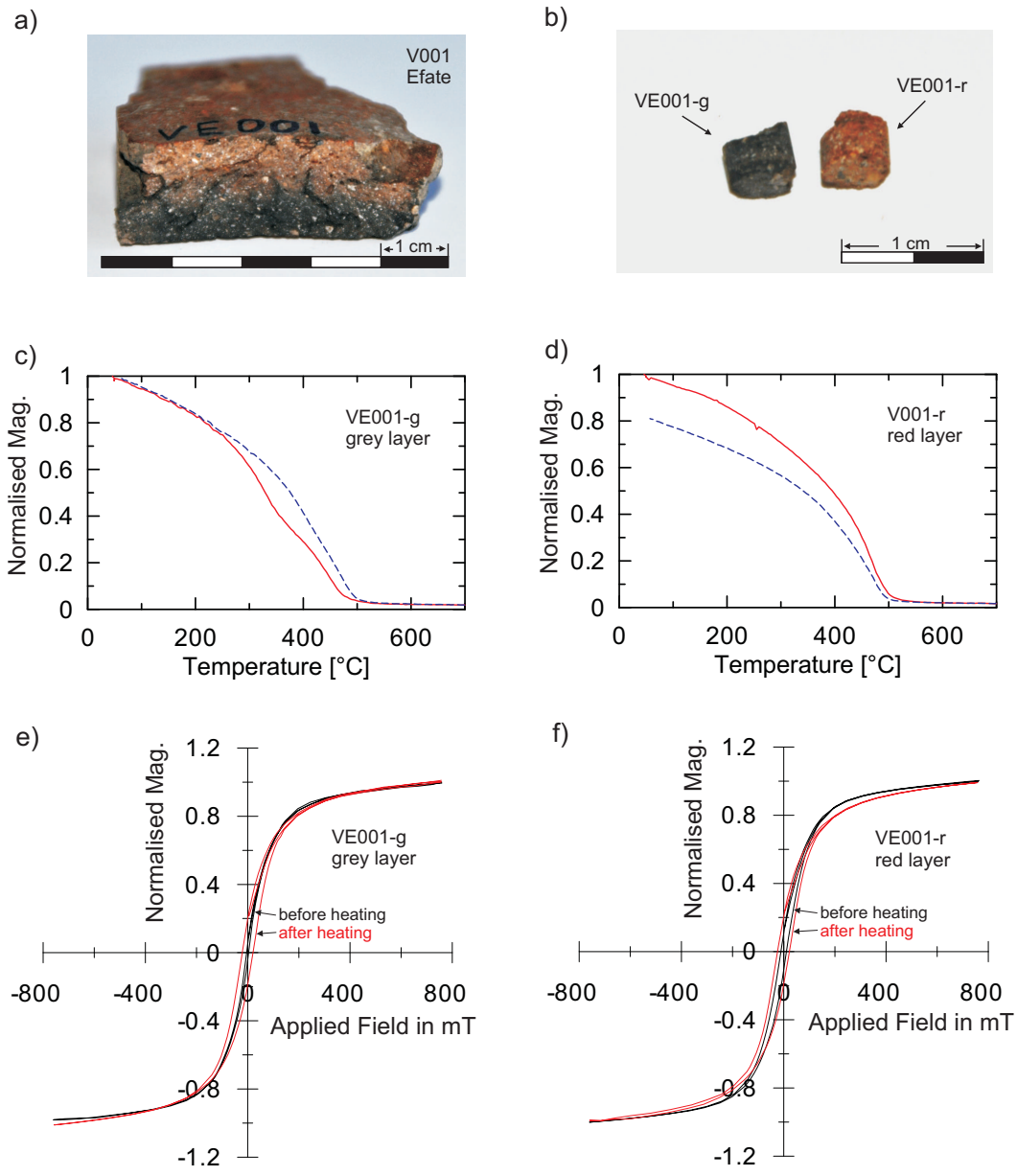

Figure 5.5: Rock magnetic examination of a pottery fragment from Efate (Vanuatu) exhibiting both reddish and greyish layers. (a) The two different coloured layers are clearly visible in potsherd V001 from Efate. Two specimen (VE001-grey and VE001-red) were drilled from the reddish and greyish layer, respectively and subject to additional magnetic mineralogical investigations (b). Panels (c) and (d) show thermomagnetic curves of the probed grey and red layers, respectively. Panel (e) and (f) delineate hysteresis loops of the grey and red layer before heating (black) and after heating (red).

5.4 Microscopic investigations

SEM investigations

Scanning electron analysis was performed on three samples from Vanuatu (V009, V013, V046). In each thin section large titanomagnetite grains ($\sim$ 50 μT to $\sim$ 300 μT) are identified by EDX. In particular in sample V009 a relative high aggregation of TM was found (Fig. 5.6a). These grains were probably introduced by the temper material (i.e. volcanic sands) during ceramic production and exhibited hardly any alteration due to high or low temperature oxidation (Fig. 5.6b).

In order to investigate the phenomena of a melting spot which sometimes occurred during microwave experiments (see Section "3.5.3 Microwave experimental procedure") a mini-core from sample V20 exhibiting a MSP was coated with a gold-palladium alloy and secondary electron (SE) imaging was applied in order to enhance the spatial resolution. EDX analysis revealed contributions of iron, oxygen and titanium suggesting a concentrated assemblage of titanomagnetite over the whole area of the MSP. An accumulation of regrown idiomorphic titanomagnetite crystals in the range of several microns is found in particular at the edge of a melting spot (Fig. 5.6c,d). In the center of a MSP are smaller crystals (< 1 μm) which exhibit a more pronounced vitrification.

Petrographic evaluation of Efate samples

Ten potsherds from Efate exhibiting different magnetic mineralogical and archaeomagnetic results (passing or failing the acceptance criteria and revealing single or multiple T_C's) were sent to the University of Arizona for petrographic investigations (Appendix B.1). The aim was to find out whether any aspects of sand temper and/or clay paste have a significant impact on the reliability of archaeointensity determinations. Magnetic mineralogical results obtained from VFTB measurements cannot be unambiguously interpreted in order to draw firm conclusions about the reasons for failure or success of these experiments. Additionally two Curie temperature behaviour was only found in some potsherds from Efate yielding both successful and unsuccessful archaeointensity results. As samples with two Curie temperatures were found on sites besides samples with a single Curie temperature it is unsure whether this phenomena is due to different tempered material and/or clay source or burning technique. In order to shed some light on this problem the petrographer W. R. Dickinson examined ten polished thin section at the University of Arizona. Areal frequency counts of 100 temper sand grains per thin section were made to detect compositional variability of the sherd tempers (Appendix B.2). After Dickinson (pers. comm. 2010) the Mangassi and Arapus sherds contain closely similar feldspathic tempers (Appendix B.3), which are similar to already investigated tempers studied previously in sherds from Mangassi, Erueti and Mele Plain on Efate (Dickinson, 2006). Also the tempers he found in the Teouma

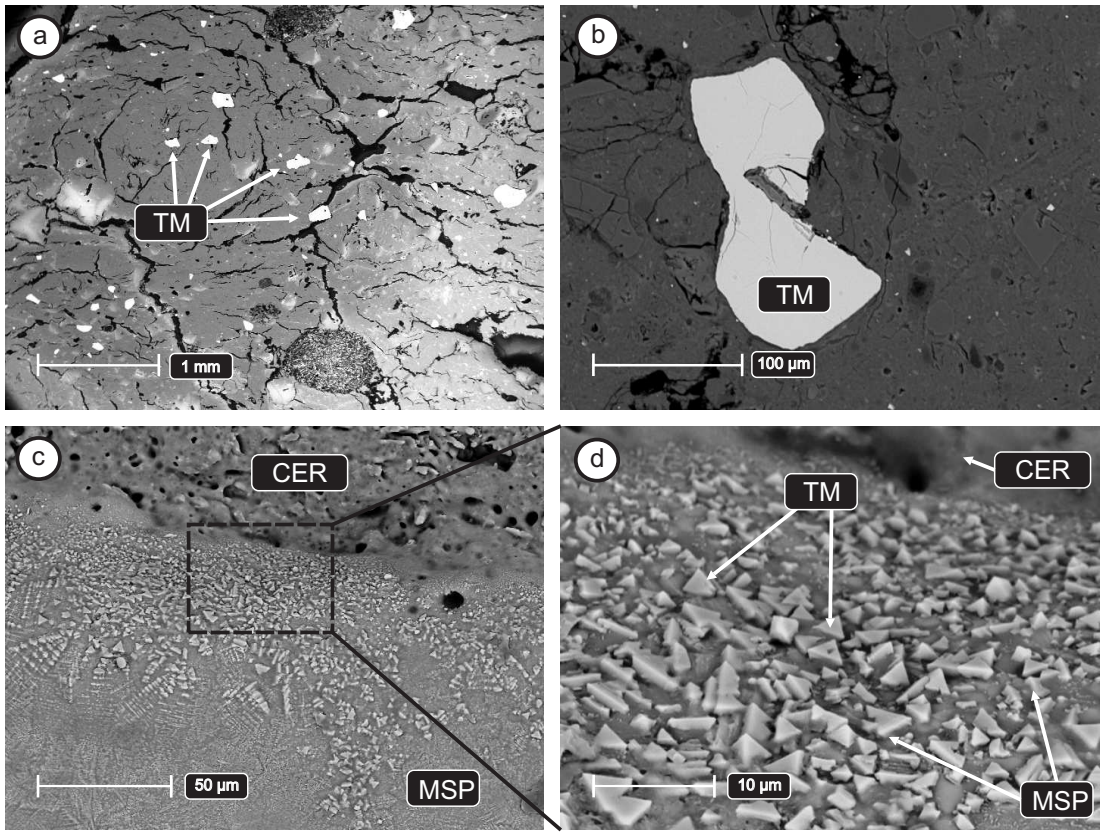

Figure 5.6: SEM investigation of thin sections and melting spots from Vanuatuan samples. Panel (a) shows a relative high concentration of large titanomagnetite (TM) grains within the clay matrix. Panel (b) illustrates a typical TM grain showing no evidence of alteration. Panel (c) and (d) delineate a melting spot with regrown titanomagnetite crystals on the rim to unmolten ceramic material (CER) using SE imagination.

sherds is similar to known results from previously investigated Teouma pottery studied by Dickinson (2009). Comparing the results of tempered material with failed and/or successful archaeointensity results as well as the presence of one or two Curie temperatures reveals no consistent correlations. The two sherds from Mangassi yielding reliable archaeointensities lack any clinopyroxene temper grains. Nevertheless this seems to be coincidental, since after Dickinson (pers. comm. 2010) there is no feasible way that the absence of clinopyroxene grains from a temper sand could influence an archaeomagnetic signal derived from ferromagnetic grains. On the other hand the two sherds from Teouma failing the archaeointensity experiments exhibit the highest amount of clinopyroxene of the investigated thin sections. There is also no significant link between the abundance of the opaque iron oxide sand grains and the archaeomagnetic and magnetic mineralogical results. The failure to detect any petrographic differences in the tempers of the sherds with different archaeomagnetic behaviours suggests that variable conditions during firing control the magnetic record in the pottery.

5.5 Results of the archaeointensity determination

Demagnetisation experiments

Demagnetisation experiments were carried out on 62 potsherds. Of these 40 individual potsherds were selected (Efate: 22, Malekula with Vao and Uripiv: 15, Ambae: 2, Espiritu Santo: 1) for archaeointensity experiments (64.5% of total). The rest were mainly rejected because no characteristic remanent magnetisation was found. Also two samples could not be demagnetised more then 30%. Fig. 5.7a illustrates a typical example for an accepted sample with an easily identified ChRM. A typical example for some accepted marginal cases is shown in Fig. 5.7b. Two magnetic components are identified with one pointing to the origin of the orthogonal vector plot interpreted as the ChRM. The figure further illustrates the advantage of prior demagnetisation experiments. The plot showing the decay of the magnetisation reveals a very narrow unblocking spectrum for sample V061. This additional information is exploited during archaeointensity experiments, where the de(re)magnetisation steps are adjusted to the individual nature of a sample. Fig. 5.7c shows a rejected samples lacking a ChRM.

Microwave archaeointensity experiments

From 114 microwave archaeointensity experiments (on 40 potsherds), 48 samples from 24 individual potsherds (Efate: 26, Malekula (incl. Vao and Uripiv): 22, Espiritu Santo: 0, Ambae: 0) revealed reliable archaeointensities within the acceptance criteria. This corresponds to a success rate of 50.0% at the potsherd level and 42.1% at the sample level. Typical Arai plots of accepted samples are shown in Fig. 5.8. Some samples strictly failed the acceptance criteria since less then 50% of the NRM fraction could be removed. Nevertheless these samples were accepted when a sister sample fulfilled this criteria and showed consistency. All sister samples of potsherd V046 could not be demagnetised more than 38% and 40%. Also these samples were accepted since they revealed consistency, together with a high quality factors over 10 and 35. In order to identify a slope, a ChRM is carefully isolated and secondary components like a VRM visible in the orthogonal vector plots are removed (i.e. Fig. 5.8a and b). Around 50% of the samples revealed a VRM overprint. Some samples developed melting spots when powers exeeded 25 Watt with an exposure time of 5 seconds were applied. Increasing the exposure time and keeping powers below 20 Watt was a remedy for some samples and a fraction of the NRM and/or pTRM of more then 50% was obtained. Nevertheless at powers > 35 Watt (at 5 or more seconds) two thirds of the samples start to develop a melting spot recognised to a certain extend in the changing reflected power. The archaeointensity experiment was cancelled when there was strong evidence of a melting spot. The last de/remagnetisation steps are visible as open diamonds in Fig. 5.8b,c and d. A shifting of these results to the left can be explained

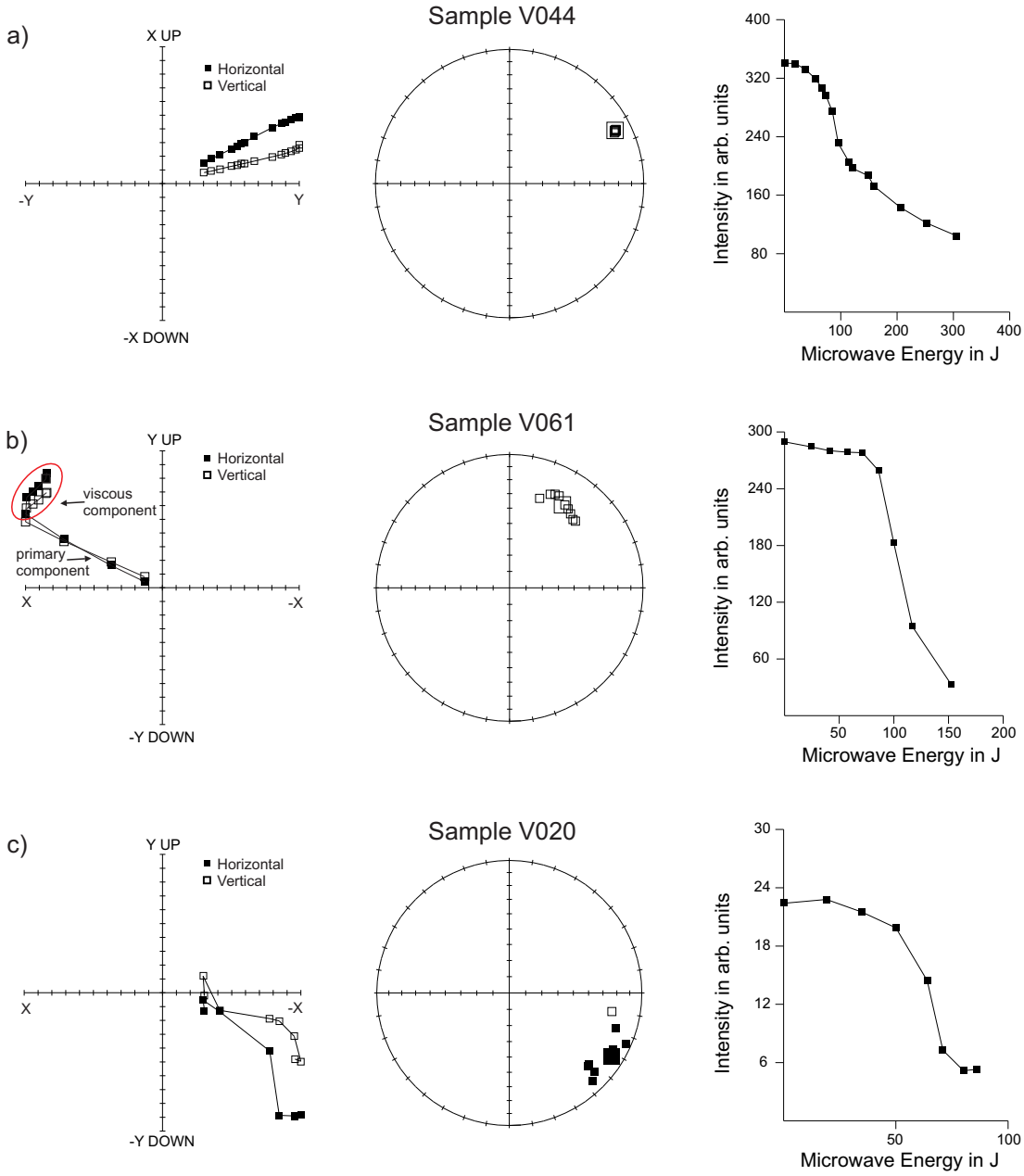

Figure 5.7: Representative results from demagnetisation experiments on potsherds from Vanuatu. From left to right orthogonal plot, circular plot and decay of the magnetisation. a) represents an accepted result, b) an accepted marginal case and c) an example of a rejected potsherd.

that some (titano)magnetite decayed into the magnetically weaker haematite which is clearly visible as a red rim around the melting spot. Alteration is also indicated by pTRM-checks. For the remaining samples no significant curved Arai plots (2-slope behaviour) were identified suggesting no significant MD effect.

Samples were mainly rejected because of a strong scatter of data points with a correlation coefficient of the analysed linear segment < 0.98 (Fig. 5.9a,b). Also a creation of MSP decreasing the number of reliable de(re)magnetisation measurements in a linear segment as well as the analysable fraction, was a main problem for samples from Vanuatu. Fig. 5.9b describes an Arai plot of a sample from potsherd V061 which was already described before as a marginal case after the demagnetisation experiments. Unfortunately the ChRM could not be isolated for this sample and was therefore rejected. Three samples were rejected due to ongoing alteration monitored by failing pTRM-checks and two due to an intra-sherd scatter of more then 20%.

5.6 Discussion of the archaeointensity results from the Vanuatu archipelago

Accepted results from the microwave archaeointensity determinations are listed in Table 5.2 and range from 18.7 μT to 55.0 μT which corresponds to VADMs of 4.3 to 12.7 ($\times 10^{22}$ Am^2). All selected samples show good within-sherd consistency with a deviations less then 10% for 17 potsherds and less then 20% for 7 potsherds. (Fig. 5.10a). The distribution of the q-factor (Coe et al., 1978) ranges from 2.4 to 46.9 with an average around 15 underpinning solid archaeointensity determinations (Fig. 5.10b).

Six contexts yielded archaeointensities from two or more individual potsherds. For four of them with three or more results, the deviation was smaller than 10% showing very good consistency within a context. Three results from context TP 9 60-80 revealed different intensities. Whereas two potsherd V026 and V027 revealed similar results ($\sim$ 30 μT and $\sim$ 32 μT), potsherd V024 exhibited a $\sim$ 40% lower intensity around 19 μT. This can be explained by a rather big age uncertainty of $\pm$ 300 years. Strong intensity variations around 0 AD give a hint that these potsherds very likely date from different time periods. Besides 0 AD a strong intensity variation is monitored around 1000 BC. Around this time period two individual archaeointensity values obtain from two potsherds V057 and V058 from the same context also reveal divergent results.

Fig. 5.11a illustrates all results obtained from individual potsherds from Efate and Malekula. In Fig. 5.11b context mean values were determined whenever possible and a possible trend is indicated. For both panels the calculated CALS3K.3 and ARCH3k models (Korte et al., 2009) as well as the present day field strength of Efate 17.6° S and 168.2° E (44.3 μT) are inserted. All results were recalculated for Efate (17.6° S and 168.2° E). Archaeointensity values plotting between 1000 BC and 0 AD suggest a significantly lower geomagnetic field strength then predicted by both field models,

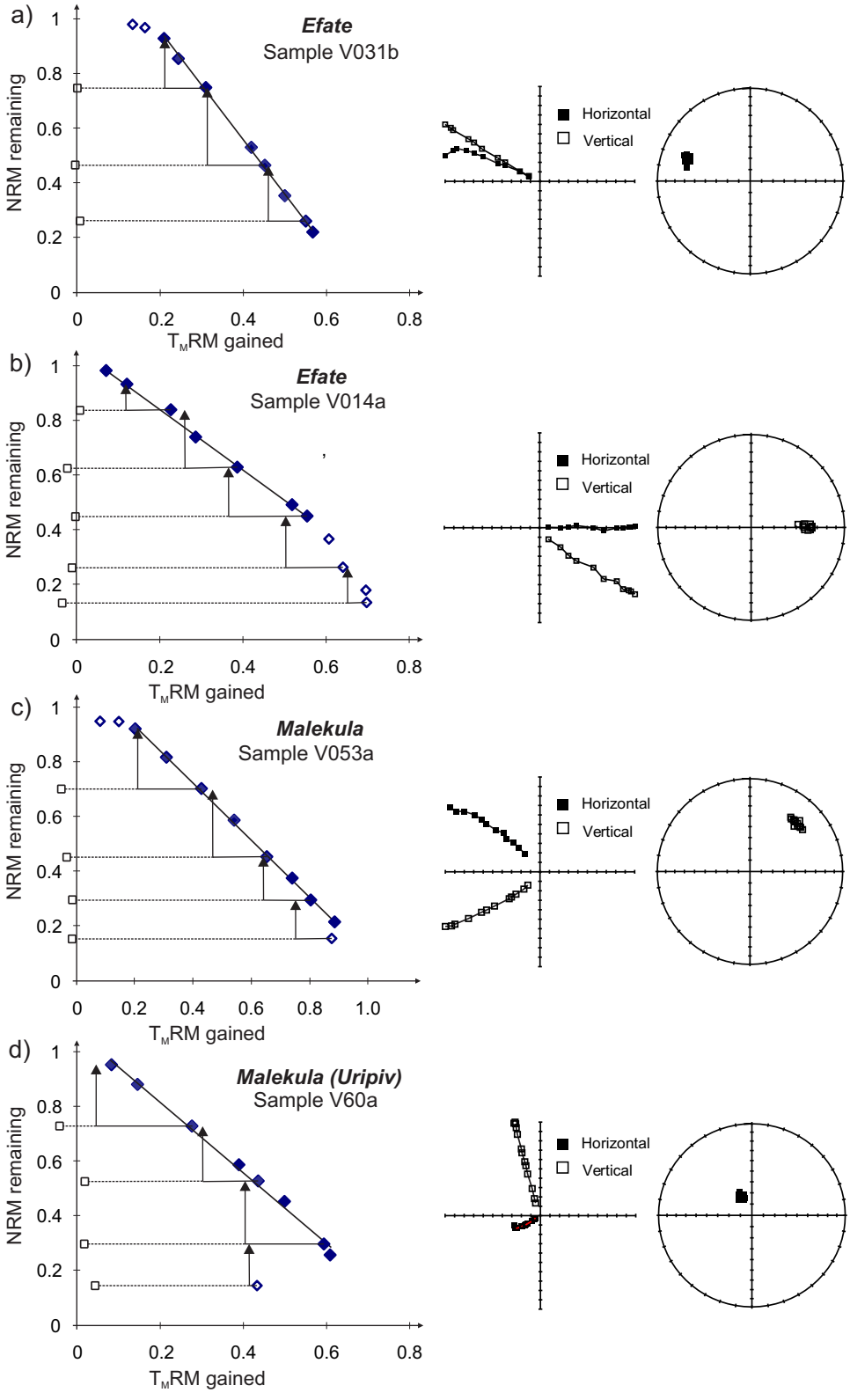

Figure 5.8: The panel shows four representative successful Arai plots together with their orthogonal vector and circular plots from Efate and Malekula. Closed (open) diamonds indicate accepted rejected data points for calculating a slope. Arrows and open squares represent alteration and MD sensitive checks.

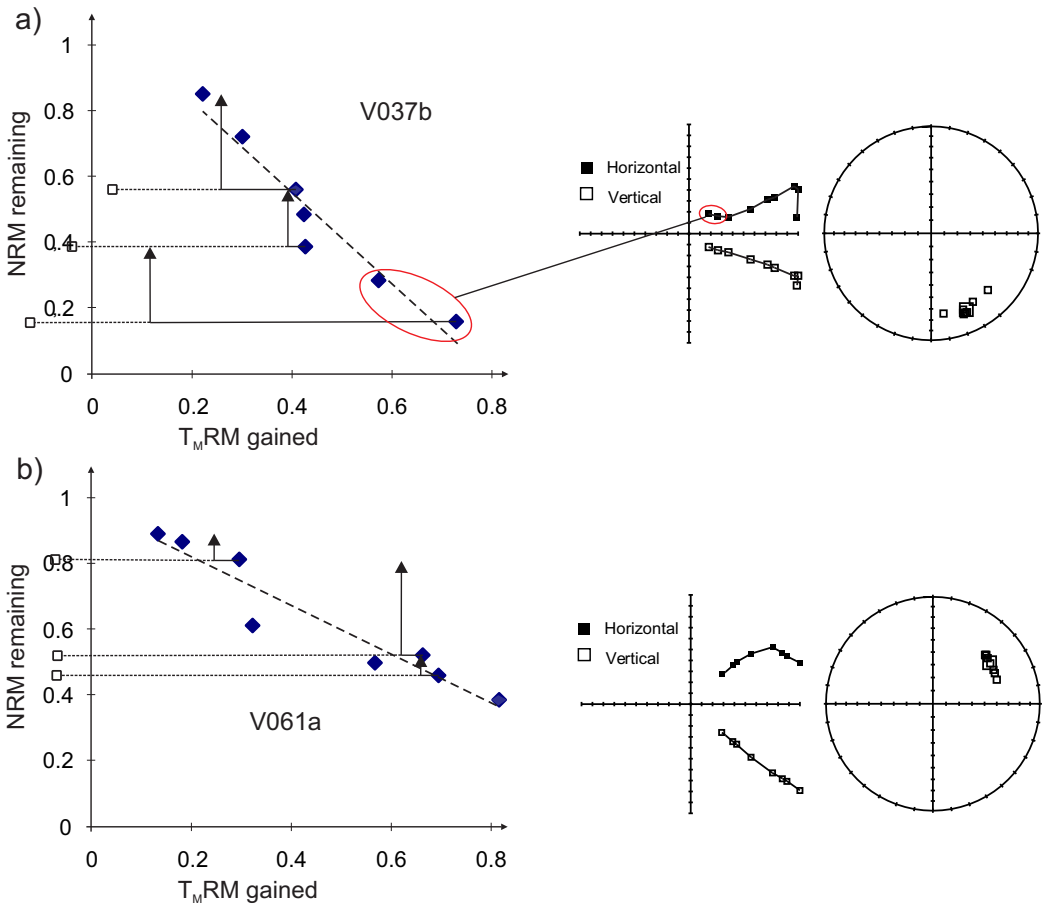

Figure 5.9: Examples of rejected Vanuatu samples. Panel (a) illustrates a sample with strong scatter within the linear segment and additionally exhibiting a MSP resulting in the creation of new magnetic material (red ellipses). (b) This sample exhibits two components of magnetisation. There is also ongoing alteration during the experiment indicated by failing pTRM-checks.

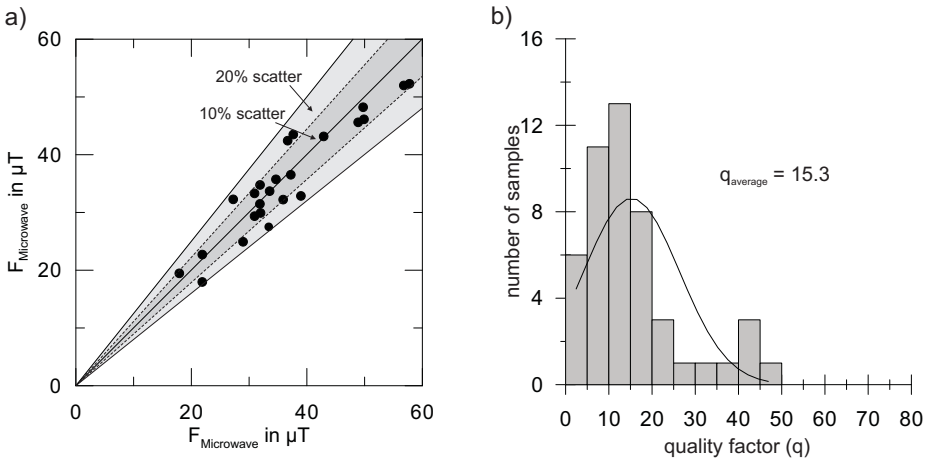

Figure 5.10: Scatter and q-factors of microwave intensity results of sister samples from Vanuatu potsherds. (a) The grey shaded area shows intensity differences of less than 20% (bright grey) and 10% (dark grey). (b) illustrates the distribution of the quality factors (q) after Coe et al. (1978).

where the field decreases from over 40 μT to a minimum around 25 μT. Between 0 AD and 1800 AD the field increases again with a maximum of 50 μT around 1400 AD. It needs to be mentioned that for the last millennia only five individual results were available and no results for the period between 0 AD and 800 AD. Here the obtained archaeointensities plot closer to the field models, but indicate a stronger field around 1400 AD. As mentioned before they indicate strong intensity variations around 1000 BC and 0 AD which are not observed in the CALS3k.3 model. Nevertheless the ARCH3k model gives a better hint of an enhanced variation during these periods of time. A single value (potsherd V032) found around 1000 BC exhibits a very low intensity which contrasts with the other results in this time period (Fig. 5.11b). Interestingly this is the only result from site Arapus on island Efate. It is also worth mentioning that the whole site Teoma on Efate, comprising 8 individual potsherds, yielded no reliable archeointensity results. Most of them were already sorted out during demagnetisation experiments since they were lacked a stable remanence.

5.7 Summary

The ceramics from Vanuatu in particular from the islands Efate, Malekula, Vao and Uripiv were able to yield high quality archaeointensities. Rock magnetic investigations revealed that a Ti-poor titanomagnetite (TM20) is the main carrier of the TRM and the grain sizes range from SD to PSD. Some sherds from Efate contain two types of titanomagnetite (TM20 and TM35) with hysteresis measurements suggesting grain sizes in the PSD close to the MD area. The TM35 is only stable to temperatures around

400°C and is then transformed to a TM20. This indicates a less intense firing during manufacturing the vessel. Petrographic analysis on Efate potsherds found tempers typical for this region but no significant relationship between tempered material and the success/failure of archaeointensity determinations. SEM investigations revealed some large titanomagnetite grains similar to Fiji but, no sign of high temperature alteration. A success rate of 42.1% on the sample level was possible due to a painstaking preselection during prior demagnetisation experiments. The archaeointensity results indicate a stronger variation than predicted by the current field models with a tendency to plot around 25% lower between 1000 BC and AD.

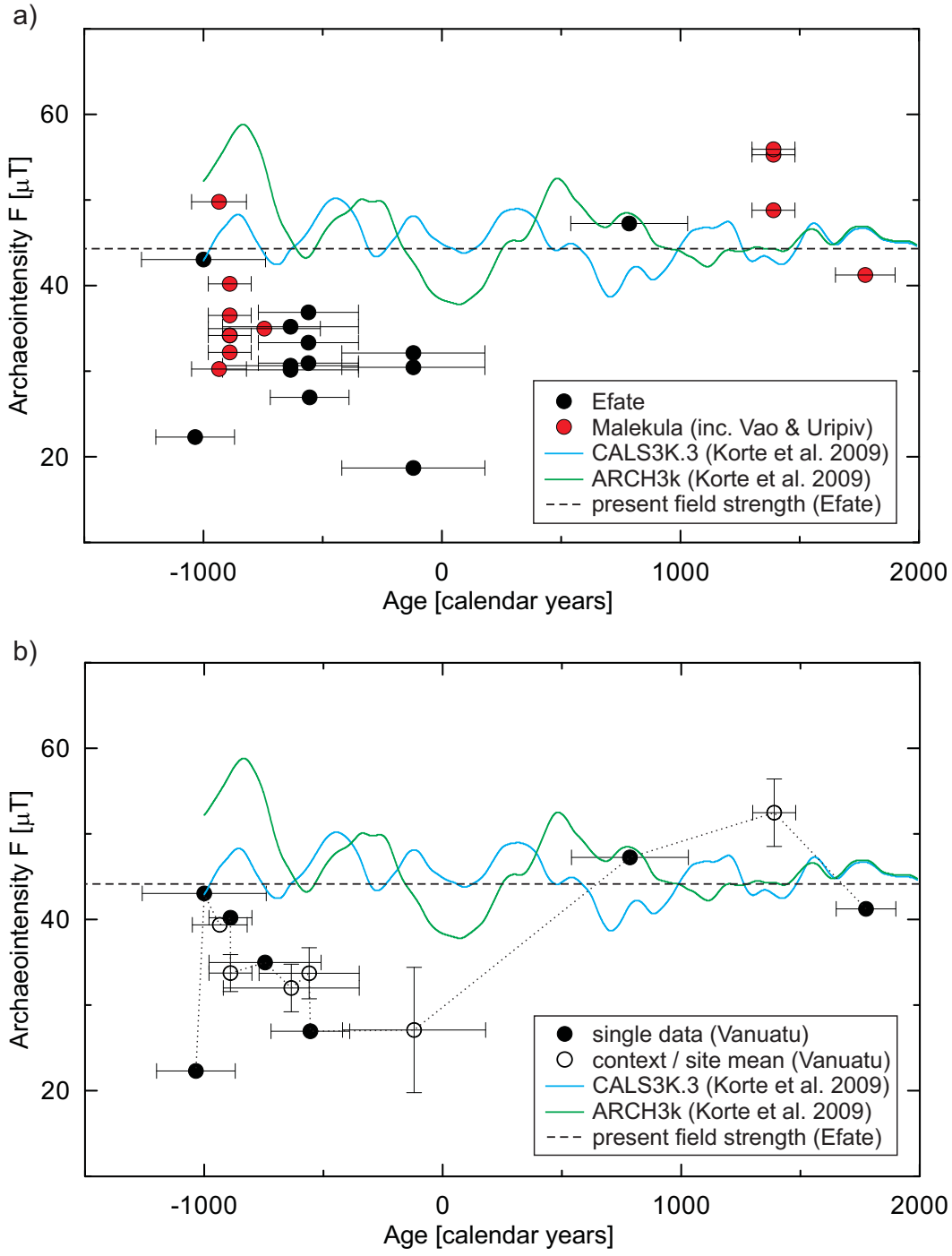

Figure 5.11: Archaeointensity results from Vanuatu. (a) Black and red dots show single data from the island regions of Efate and Malekula recalculated for Efate. Panel (b) shows relocated site mean archaeointensity results (open circles), black dots indicate sites which yield only one reliable intensity value. In both panels blue (CALS3k.3) and green (ARCH3k) lines represent intensity models after Korte et al. (2009) calculated for island Efate in the island group of Vanuatu. Dashed black line shows the present geomagnetic field strength in Efate, Vanuatu. The dotted faint line indicates a possible trend.

Table 5.2: Archaeointensity results from Vanuatu.

Site/Context	Potsherd	Age ± (2σ) (cal. yrs)	N	f	g	β	q	$F_{specimen}$ (μT)	F_{mean} (μT)	VADM × 10^{22}(Am^2)
Island Efate, Site Mangaasi (17.6°S, 168.2°E)										
TP 9.4 130-151	V002a	-555 ± 165	8	0.69	0.8	0.02	12.35	28.95	26.94	6.25
	V002f		6	0.52	0.78	0.02	20.6	24.92		
TP 9 L3.1 165-175	V005a	-560 ± 210	6	0.4	0.76	0.07	4.39	31.97	30.94	7.18
	V005f		8	0.6	0.83	0.05	10.53	29.91		
TP 9 175-185	V009a	-560 ± 210	7	0.78	0.8	0.07	10.84	37.22	36.87	8.56
	V009b		9	0.81	0.86	0.06	18.2	36.53		
TP 9 175-185	V010f	-560 ± 210	9	0.71	0.84	0.04	16.53	31.9	33.33	7.74
	V010b		7	0.75	0.81	0.05	9.26	34.76		
TP 9 155-165	V012f	-635 ± 285	7	0.61	0.81	0.08	7.21	34.65	35.19	8.17
	V012b		9	0.62	0.86	0.05	11.96	35.74		
TP 9 155-165	V013f	-635 ± 285	8	0.72	0.8	0.05	10.99	30.94	30.15	7
	V013b		8	0.73	0.82	0.04	11.57	29.36		
TP 9 155-165	V014a	-635 ± 285	8	0.61	0.84	0.03	23.09	33.88	30.64	7.11
	V014f		7	0.53	0.74	0.03	10.76	27.39		
TP 9 195-205	V016a	-1000 ± 260	7	0.72	0.67	0.07	10.24	42.91	43.04	9.99
	V016f		8	0.6	0.83	0.08	9.4	43.17		
TP 9 60-80	V024a	-120 ± 300	6	0.56	0.71	0.04	5.63	17.91	18.69	4.34
	V024f		6	0.56	0.77	0.05	5.36	19.46		
TP 9 60-80	V026f	-120 ± 300	8	0.53	0.79	0.1	4.58	33.4	30.45	7.07
	V026b		5	0.34	0.62	0.05	3.6	27.51		
TP 9 60-80	V027a	-120 ± 300	10	0.75	0.86	0.04	16.36	30.94	32.12	7.46
	V027f		6	0.46	0.78	0.09	4.38	33.3		
TP 1 70-90	V031a	785 ± 245	6	0.61	0.79	0.04	21.91	48.88	47.25	10.97
	V031b		8	0.62	0.82	0.02	40.56	45.61		
Island Efate, Site Arapus (17.6°S, 168.2°E)										
ST 17 140-160	V032a	-1035 ± 165	6	0.61	0.78	0.03	18.63	21.89	22.3	5.18
	V032b		8	0.63	0.82	0.04	10.49	22.71		

Continued on Next Page...

Table 5.2 – Continued

Site/Context	Potsherd	Age ± (2σ) (cal. yrs)	N	f	g	β	q	$F_{specimen}$ (μT)	F_{mean} (μT)	VADM × 10^{22}(Am^2)
Island Malekula, Site Chachara (15.9° S, 167.3° E)										
TP C2 0-30	V044a	1390 ± 90	5	0.34	0.72	0.1	4.2	56.79	54.39	12.57
	V044f		7	0.5	0.82	0.04	14.72	51.99		
TP C2 0-30	V045a	1390 ± 90	6	0.39	0.75	0.09	5.63	49.89	48.01	11.09
	V045b		7	0.5	0.55	0.04	9.53	46.13		
TP C2 0-30	V046a	1390 ± 90	6	0.38	0.78	0.05	10.97	57.77	55.02	12.71
	V046h		6	0.4	0.75	0.01	35.44	52.28		
TP-1 20-40	V049a	1775 ± 125	6	0.69	0.69	0.08	7.52	37.65	40.57	9.37
	V049b		9	0.73	0.87	0.03	34.84	43.49		
Island Vao, Site Vao (15.9° S, 167.3° E)										
Area A A.6 140-150	V050b	-890 ± 90	5	0.74	0.68	0.03	19.84	38.97	35.92	8.3
	V050f		9	0.79	0.86	0.04	19.97	32.86		
Area A A.6 140-150	V051f	-890 ± 90	10	0.63	0.88	0.03	2.44	33.55	33.62	7.77
	V051c		5	0.36	0.74	0.09	5.93	33.69		
Area A A.6 140-150	V053a	-890 ± 90	8	0.7	0.85	0.01	46.89	31.87	31.67	7.32
	V053f		5	0.38	0.69	0.05	7.4	31.48		
Area A A.6 140-150	V054a	-890 ± 90	8	0.69	0.84	0.04	17.38	36.68	39.55	9.14
	V054f		7	0.52	0.85	0.01	42.34	42.43		
ST 11 170-180	V057a	-935 ± 115	7	0.66	0.8	0.03	28.96	49.74	48.98	11.32
	V057b		7	0.58	0.79	0.06	11.82	48.22		
ST 11 170-180	V058a	-935 ± 115	7	0.79	0.78	0.03	18.43	27.24	29.76	6.88
	V058b		7	0.6	0.79	0.05	11.27	32.27		
Island Uripiv, Jimis (16.1° S, 167.5° E)										
TP 9 120-130	V060a	-745 ± 235	6	0.5	0.77	0.01	40.68	35.9	34.06	7.99
	V060b		6	0.65	0.76	0.03	6.83	32.23		

Table 5.2: Microwave archaeointensity results obtained from pottery fragments found on the islands Efate, Malekula, Espiritu Santo and Ambae from the Vanuatu archipelago. The ages with uncertainties are given in calendar years. N is the number of points used to define a linear segment in the Arai diagram. f, g, β and q stand for the fraction of NRM, gap factor, normalised error of the slope and quality factor according to Coe et al. (1978). F values are the intensity results for individual specimens in μT. F_{mean} values are the arithmetic mean values of F and VADM describes the Virtual Axial Dipole Moment in Am^2.

Chapter 6

Results from New Caledonia

6.1 Study area

The archipelago of New Caledonia is located around 1300 km to the east of Australia and around 400 km west of the island chain of Vanuatu. The mainland, also referred to as La Grande Terre, is a narrow and oblong island stretching about 400 km from northwest to southeast. It is surrounded by a group of minor islands i.e. the Loyalty Islands, Belep and Île des Pins (Fig. 6.1). In contrast to the minor islands, the mainland is mountainous with the highest peaks reaching over 1500 m (Encyclopaedia Britannica, 2011b). New Caledonia is a fragment of the ancient continent Gondwana which explains its complex and distinctive geological characteristics (Sand, 2001). The first human settlement in New Caledonia is archaeologically related to the expansion of Austronesian-speaking people into Remote Oceania and dates around 1200 BC (Green, 1993; Sand, 1997). These first settlers were named after the archaeological site Lakeba (WKO013A) found near Koné which has become a type-site for a whole cultural complex. Spriggs (1997) defines this region as the southern Lapita province. The first European contact was in 1774 AD by Capt. James Cook and the archipelago was annexed by the French in 1853 (Encyclopaedia Britannica, 2011b).

6.2 Sample description

All investigated samples come from archaeological sites located on the mainland Grande Terre (Fig. 6.1). They comprise a suite of 81 individual potsherds (Tiouandé: 36, Pindai: 21, Nouville: 4, Goro: 6, Nepou: 4, Nessaidou: 4 and Koné: 6) and represent 21 different archaeological contexts (Table 6.1). Radiocarbon ages are available for all samples and determined exclusively from charcoal. The uncalibrated CRA values range from 2780 BP to 310 BP with an age uncertainty of 40 to 70 years. For potsherds yielding reliable archaeointensities the CRA were calibrated as described in Chapter 2. The dates calibrated in calendar years range from 900 ± 100 cal BC to 1585 ± 95 cal AD. The precision of the calibrated ages conforms to a 95.4% confidence level with age

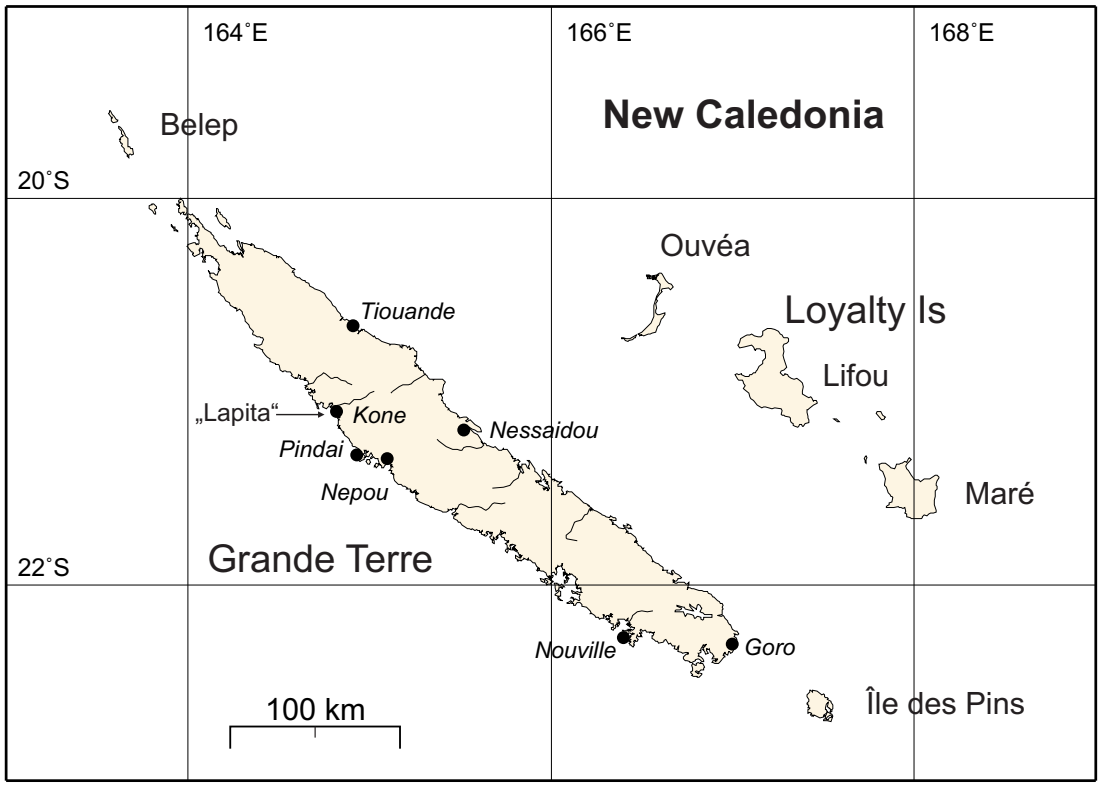

Figure 6.1: Overview map of New Caledonia and the nearby Loyalty Islands. The investigated sites are indicated with black dots.

uncertainties from ± 75 to ± 160 years.

6.3 Magnetic mineralogical investigations

A set of rock magnetic investigations as described in Chapter 3 were carried out on sister samples from all 81 potsherds. In the following subsections the main outcome of IRM, backfield, hysteresis and thermomagnetic experiments are documented. The full results are given in Appendix A. Some results are repetitive and therefore comparable to studies of the Fijian and Vanuatuan samples. In this case only the main outcome is summarised and the reader is referred back to Chapters 4 and 5 for a more detailed explanation.

IRM, backfield and hysteresis measurements

IRM and backfield measurements exhibited similar curves (type 1 and 2) as already described for the Fiji samples (see Fig. 4.2) with saturation of 92% or more, at a field of 300 mT indicating a low coercivity ferrimagnetic remanence carrier with some minor contributions of high coercive minerals. Running magnetic hysteresis loops showed predominantly ferrimagnetic behaviours with some paramagnetic contributions (Fig. 6.2). All loops are pot-bellied after Fabian (2003) and exhibit typical PSD dimensions (Tauxe, 1998). Plotting bulk sample hysteresis parameters in the Day-plot together with the Dunlop (2002a) mixing curves show an assemblage of SD to PSD particles without following any trend of the mixing curves (Fig. 6.3).

Thermomagnetic curves

Although the investigated pottery fragments come from various sites on New Caledonia, nearly all thermomagnetic curves exhibit similar behaviours with a single T_C between 518°C and 590°C and reversible or nearly reversible curves (Fig. 6.4a and b) where the cooling curve is always below the heating curve (compare Fig. 4.5). These behaviours identify magnetite and/or Ti-poor titanomagnetite as the main remanence carrier. Only one sample revealed a T_C around 409°C indicating a bigger amount of Ti in the titanomagnetite. Two samples from Tiouandé with single T_C's around 520°C exhibited an increased magnetisation after heating up to 700°C with cooling curves running above the heating curves (Fig. 6.4a and b). Both samples were rejected after the demagnetisation experiments since they did not carry a ChRM remanence. Further, their paramagnetic contribution was significantly higher than in other samples. Only one sample revealed at least two T_C's with the first T_C around 574°C suggesting a nearly pure magnetite phase. A second T_C around 622°C gives a hint of a second magnetic fraction interpreted to be maghemite (γ-Fe_2O_3), a conclusion supported by a kink around 200°C often found in (titano)maghemite-containing samples (Krása and

Table 6.1: Investigated ceramic series from New Caledonia

Location/Context	Pottery group	Sample Code	N_P	CRA/Err.(BP)	CRA Ref.
Location Tiouandé (20.8° S, 165.1° E)					
EHI-73A (137) A 30-40 cm	T-137-(1-4)	NC25-NC28	4	1250/40	β-136958
EHI-13 (141) II 20-30 cm	T-141-(1-4)	NC29-NC32	4	930/40	β-136962
EHI-13 (142) II 90-105 cm	T-142-(1-4)	NC33-NC36	4	1840/40	β-136963
EHI-22A (143) A 30-40 cm	T-143-(1-4)	NC37-NC40	4	1780/40	β-136964
EHI-13 (169) A 10-20 cm	T-169-(1-4)	NC44-NC47	4	1140/40	β-155191
EHI-13A (170) A 40-50 cm	T-170-(1-5)	NC48-NC52	5	1330/70	β-155192
EHI-13A (171) A 100-110 cm	T-171-(1-5)	NC53-NC57	5	2520/40	β-155193
EHI-22A (173) 0-10 cm	T-173-(1-5)	NC58-NC62	5	310/40	β-155195
EHI-22A (174) A 90-95 cm	T-174-(1)	NC63	1	2590/40	β-155196
Location Pindai (21.3° S, 165.0° E)					
WNP038 (191) G2 80-90 cm	P-191-(1-5)	NC64-NC68	5	2240/40	β-167904
WNP038(192) B1 90-100 cm	P-192-(1-4)	NC69-NC72	4	2180/40	β-167905
Cave C (216) TP1 50-60 cm	P-216-(1-4)	NC75-NC78	4	1640/40	β-184379
Cave F (217) 40-50 cm	P-217-(1-4)	NC79-NC82	4	2240/40	β-184380
WNP038 (250) 70-80 cm	P-250-(1-4)	NC83-NC86	4	2060/40	β-197911
Location Nouville (22.3° S, 166.4° E)					
Nouville (196) 80 cm	N-196-(1-2)	NC73-NC74	2	940/40	β-171955
SNA 020 (255) E1 70-80 cm	N-255-(1-2)	NC91-NC92	2	740/40	β-197916
Location Goro (22.3° S, 167.0° E)					
SG015 (163) A 80-90 cm	G-163-(1-3)	NC41-NC43	3	2760/40	β-154623
GN2005-8 (264) I 30 cm	G-264-(1-3)	NC97-NC99	3	380/40	β-227657
Location Nepou (21.4° S, 165.1° E)					
Nepou B 50-60 cm	N-252-(1-4)	NC87-NC90	4	1950/50	β-197913
Location Nessaidou (Ferme Aqua Nessa) (21.2° S, 165.5° E)					
3 40-50 cm	N-260-(1-4)	NC93-NC96	4	1040/40	β-201696
Location Koné (21.1° S, 164.9° E)					
SK013A (133) zone II G3	K-133-(1-6)	NC19-NC24	6	2780/50	β-136954

Table 6.1: Location/Context describe the location of the site with their latitude and longitude as well as the context code of the investigated potsherds. The pottery Group describes the lab code of a context and N_p the number of individual potsherds from a context. The conventional radiocarbon age (CRA) with errors are given in BP. The Date Reference describes the lab code of the samples used for determining the CRA. Dated material was exclusively charcoal.

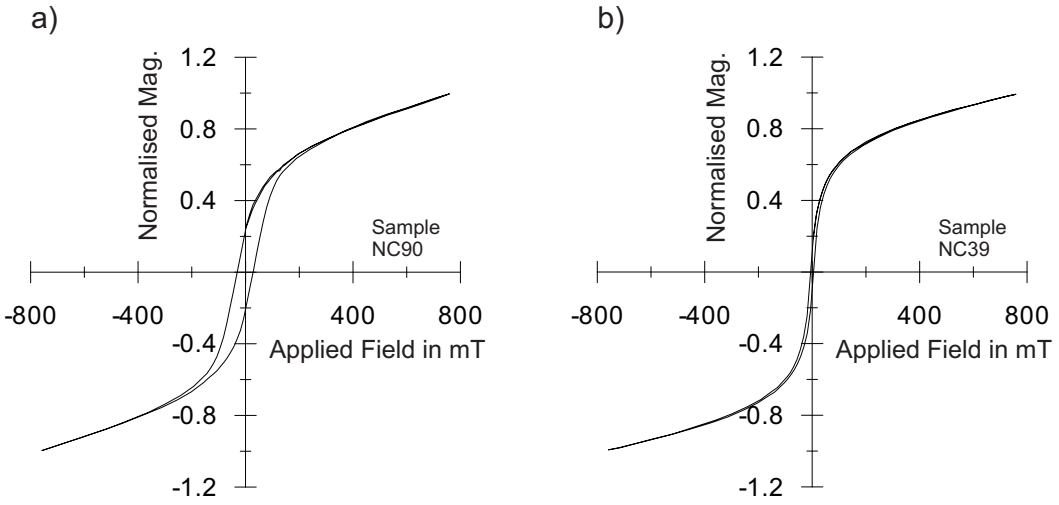

Figure 6.2: All hysteresis curves determined from samples from New Caledonia exhibit potbellied behaviours and varied between (a) curves indicating grain sizes close to SD and (b) curves indicating grain sizes in the PSD region.

Herrero-Bervera, 2005). Nevertheless this sample was rejected after demagnetisation experiments due to lack of a ChRM.

6.4 Microscopic investigations

Scanning electron investigations were carried out on two samples from Koné (NC19) and Tiouandé (NC33). The sample from Tiouandé revealed shrinking cracks ($\sim$ 1 mm in length) parallel to the sherd surface which seem to be a result of the manufacturing technique (Fig. 6.5a). No typical titanomagnetite grains could be identified, which suggests grain sizes smaller then the resolution of the SEM ($<$ 1 μm). Hysteresis parameters with ratios of $B_{cr}/B_c = 2.91$ and $M_{rs}/M_s = 0.16$ support small grain sizes for NC33, which plot in the PSD range close to the SD range. The thin section NC19 revealed only one titanomagnetite grain with a length of $\sim$ 100 μm (Fig. 6.5b) and some dispersed smaller grains $<$ 5 μm.

6.5 Results of the archaeointensity determination

Demagnetisation experiments

Sister-samples from 81 individual potsherds were subjected to demagnetisation experiments. Of these we chose 42 potsherds (Tiouandé: 23, Pindai: 8, Nouville: 3, Goro: 3, Nessaidou: 2, Nepou: 1) for archaeointensity experiments (52.5% of total). Half of the other potsherds were mainly discarded because no characteristic remanence was found. The other half of the rejected samples could not be demagnetised more then 30%. A

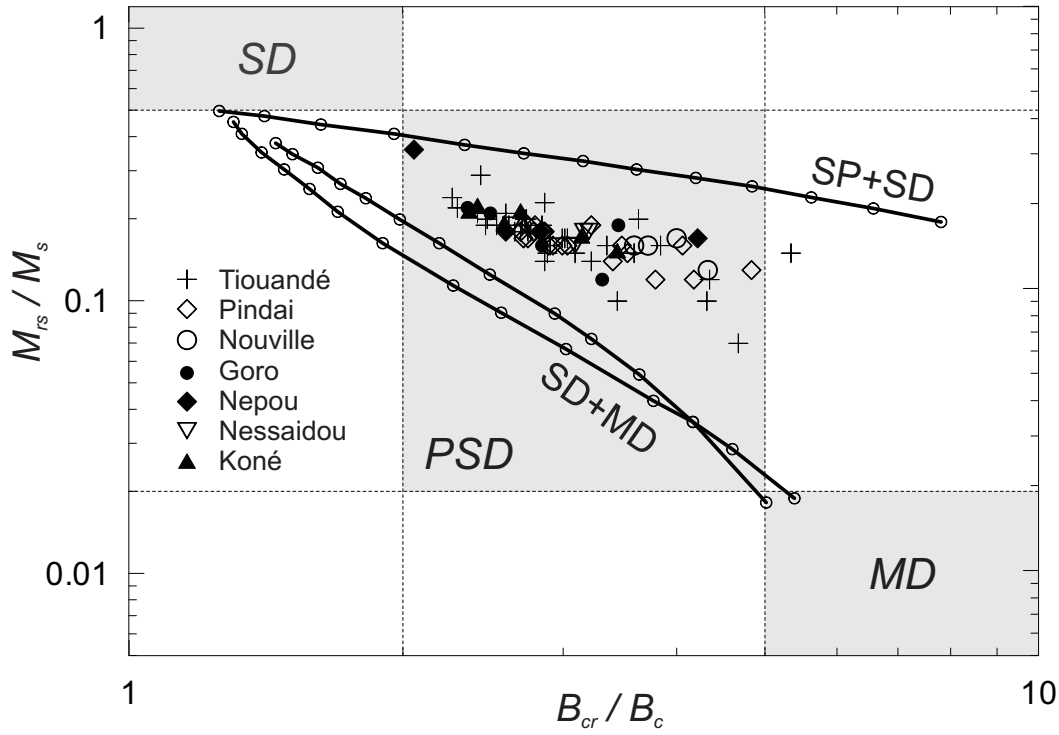

Figure 6.3: Day-plot for New Caledonia showing bulk sample hysteresis parameters for samples from different locations.

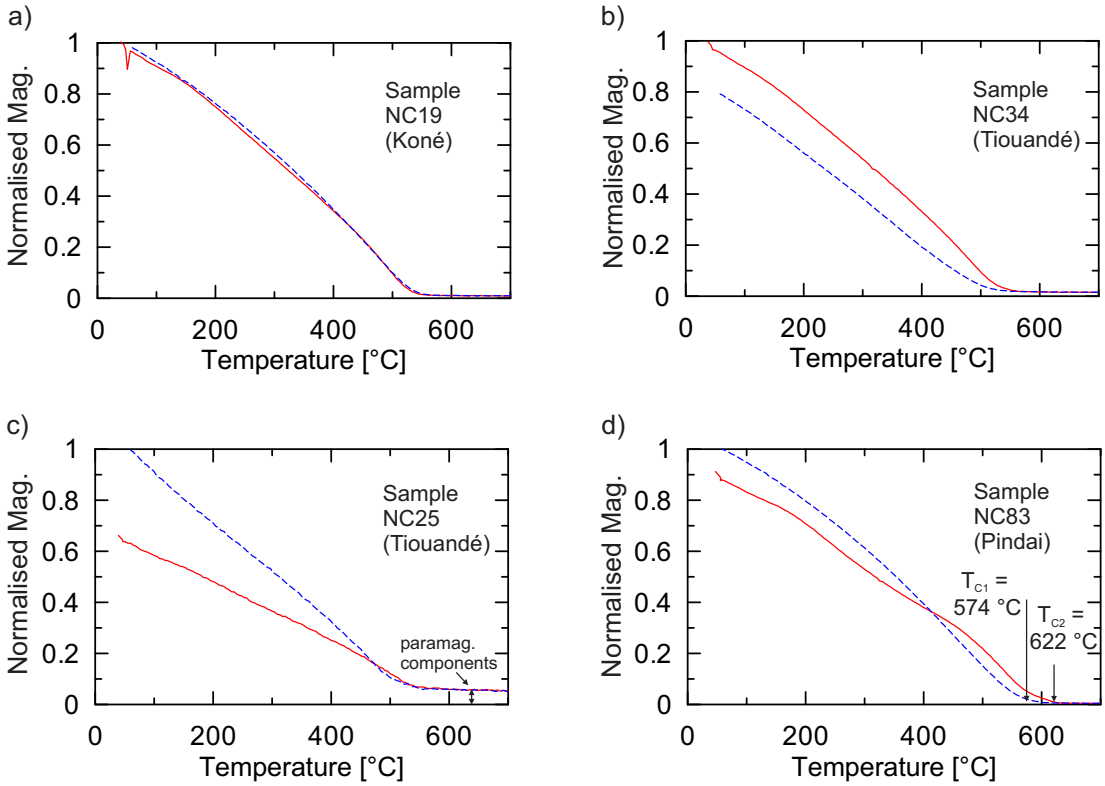

Figure 6.4: Typical thermomagnetic curves obtained from potsherds from New Caledonia. (a) and (b) show reversible or nearly reversible M(T)-curves found in nearly all potsherds. (c) Two samples exhibit strong alteration during heating resulting in a stronger magnetic fraction during cooling. (d) One sample revealed a second T_C around 622° which was not found in the cooling cycle.

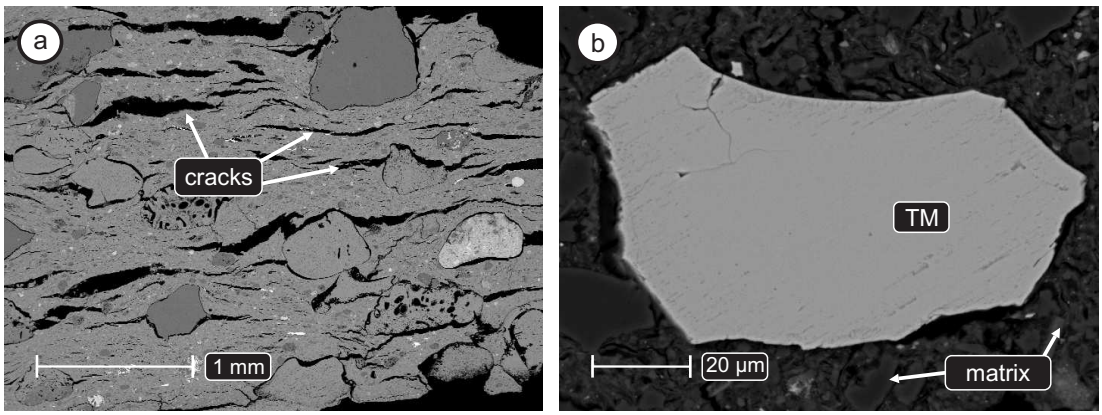

Figure 6.5: SEM investigation of two thin sections of samples from New Caledonia. (a) shows an overview picture of sample NC33 from Tiouandé. Shrinking cracks parallel to the plane of the sherd as indicated by arrows are found in the burnt clay matrix and are probably a result of the manufacturing technique. No (titano)magnetite particles were identified within the resolution of the SEM. (b) in a thin section from a potsherd from Koné (NC19) a titanomagnetite grain was found.

typical accepted sample (NC29) is shown in Fig. 6.6a exhibiting a characteristic remanence. Fig. 6.6b is representative of rejected samples lacking a ChRM and Fig. 6.6c is an example of a sample which could not be demagnetised even with powers of more than 30 W applied over more then 10 seconds.

Microwave archaeointensity experiments

From 85 microwave archaeointensity experiments on 42 potsherds, 34 samples from 17 individual potsherds (Tiouandé: 12, Nessaidou: 2, Pindai: 1, Nouville: 1, Koné: 1, Nepou: 0, Goro: 0) revealed reliable archaeointensities. This corresponds to a success rate at the sample level of 40%. Acceptance criteria 2 and 9 were adjusted in order to improve the outcome. Therefore results with an N of 4 and/or a fraction f of 0.3 or bigger are accepted, when similar intensity values were reproduced within the selection criteria (Chapter 3, Section 3.4.5). Typical Arai-diagrams of accepted samples from five different archaeological sites are shown in Fig. 6.7. A ChRM was isolated as described in Chapters 4 and 5. Similar to the experimental procedure in Chapter 5, an increase of the exposure time and keeping powers below 25 W helped to minimise the occurrence of melting spots and to gain a bigger fraction f.

Despite pre-selection most potsherds were rejected because none of their sister-samples were able to demagnetise more then 50% of their NRM. Some samples also revealed two or more components which are identified in the orthogonal vector plot and the circular plot. They were discarded when it was not possible to isolate the ChRM in the linear segment (Fig. 6.8a). One sample revealed two slope behaviour and was therefore rejected (Fig. 6.8b). Tail-checks and hysteresis parameters do not suggest MD behaviours. The curvature is probably a consequence of lack of a ChRM, which can also be observed in the circular plot. Ongoing alteration during the de/remagnetisation process and poor consistency of the intensity results leads to the exlusion of several potsherds (Fig. 6.8c).

6.6 Discussion of the archaeointensity results from New Caledonia

Successful archaeointensity results from the microwave experiments are listed in Table 6.2. The intensity values range from 23.5 μT to 52.2 μT which corresponds to VADM's of 5.2 to 11.5 ($\times$ 10^{22} Am^2). All accepted samples from New Caledonia exhibit good within-sherd consistency with deviations of the intensity values less then 10% for 11 potsherds and less then 20% for 7 potsherds (Fig. 6.9a). The distribution of the q-factor (Coe et al., 1978) ranges from 2.1 to 56.2 with an average around 13 (Fig. 6.9b). Six archaeological contexts yielded two intensity values from individual potsherds with all of them showing a good consistency within a context with devia-

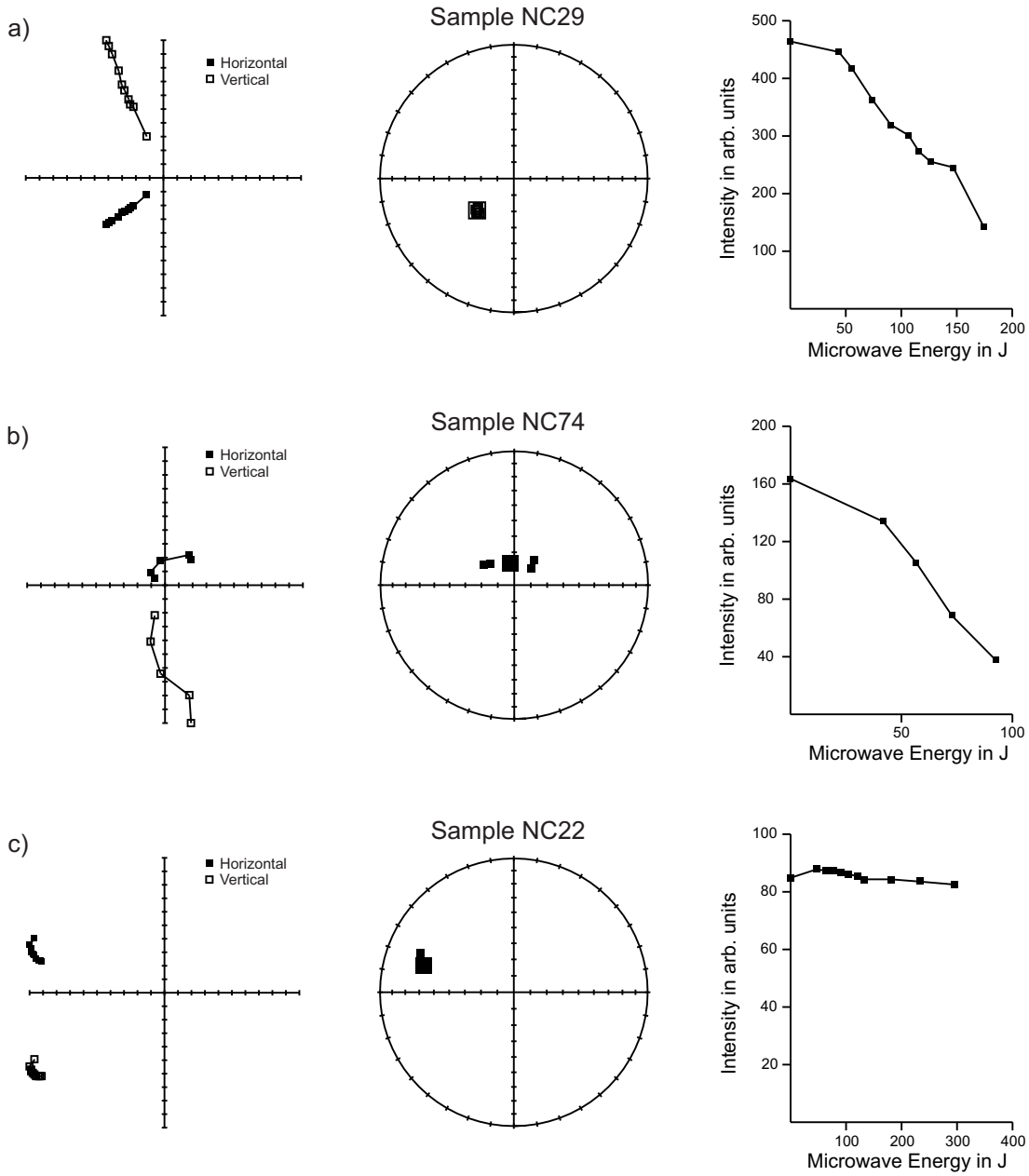

Figure 6.6: Representative results from demagnetisation experiments on potsherds from New Caledonia. From left to right the figures illustrate an orthogonal plot, a circular plot and decay of the NRM. (a) represents an accepted result with a stable a ChRM. (b) and (c) are examples for rejected potsherds due to lack of ChRM and/or failing response to the demagnetising microwave energy.

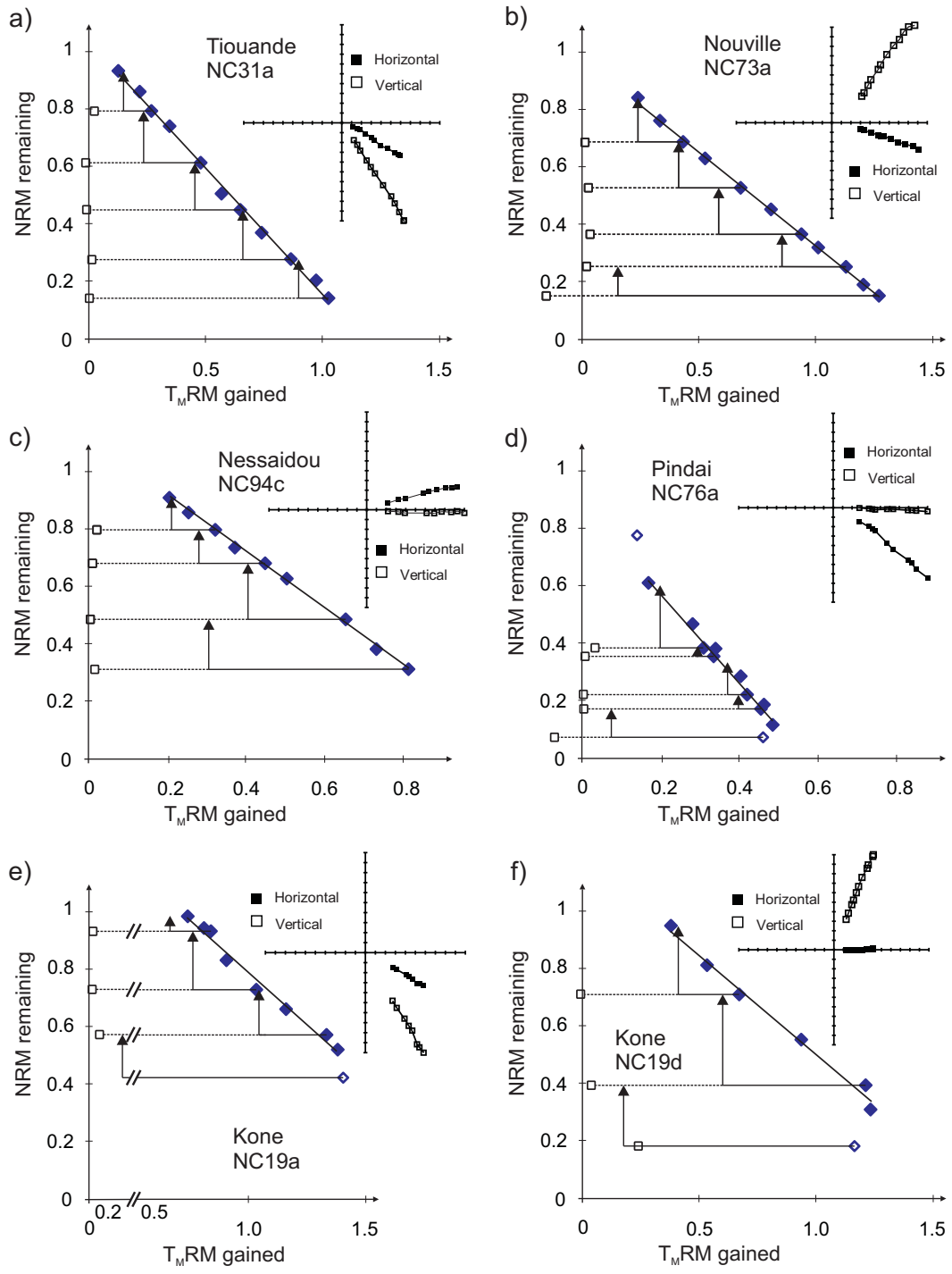

Figure 6.7: Panels (a)to (f) show six representative successful Arai-diagrams together with their orthogonal vector and circular plots obtained from New Caledonian potsherds from five different archaeological sites. Panel (e) shows a sample strictly failing the selection criteria (f < 0.5) which was accepted after a successful second archaeointensity determination of a sister sample (f) with a fraction f > 0.5

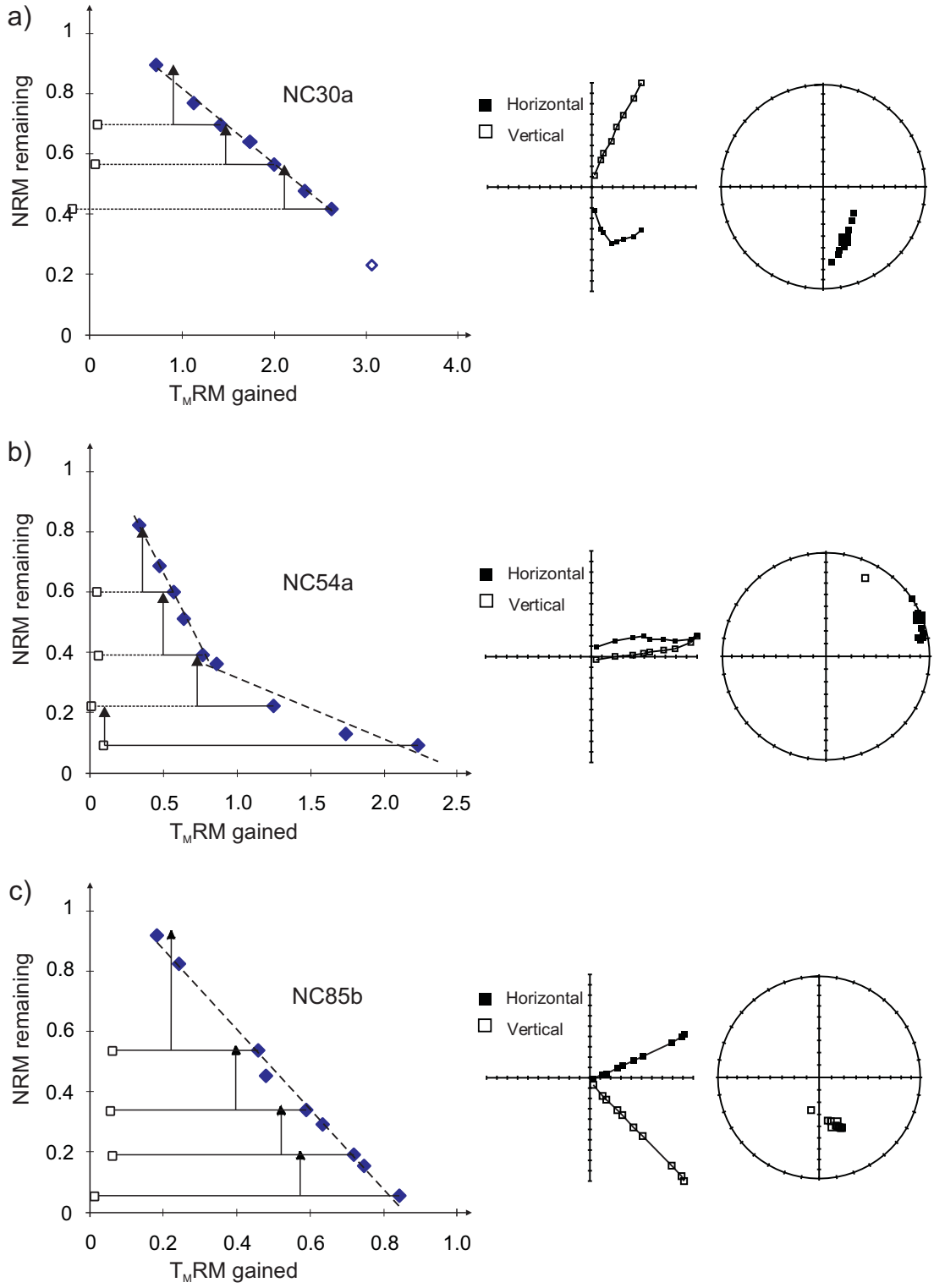

Figure 6.8: Examples of rejected samples from New Caledonia. Panel (a) illustrates a sample (NC30a) with two components. (b)Sample NC54a revealed a two slope behaviour presumably produced by several magnetic components. In panel (c) ongoing alteration leads to spurious archaeointensity results.

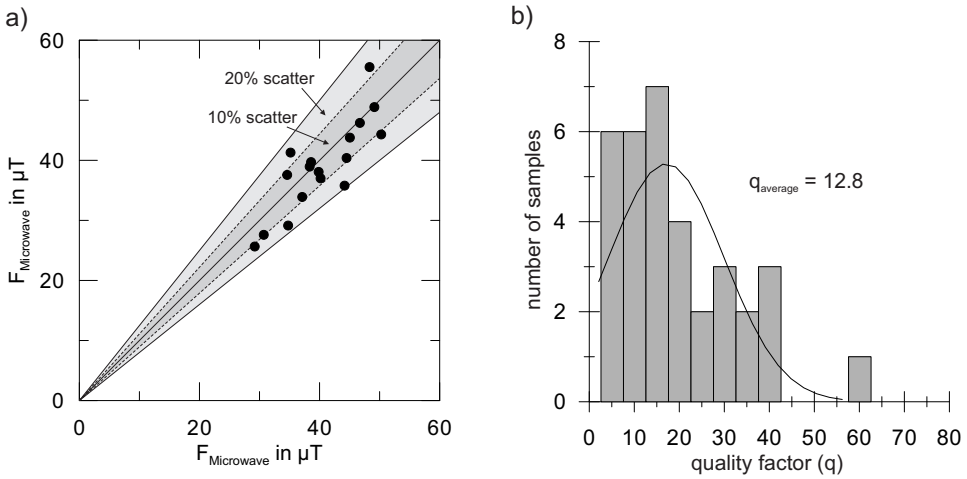

Figure 6.9: Scatter and q-factors of microwave intensity results of sister samples from New Caledonia potsherds. (a) Grey shaded area shows intensity differences of less than 20% (bright grey) and 10% (dark grey). (b) illustrates the distribution of the quality factors (q) after Coe et al. (1978).

tions $< 14\%$. The results of the single potsherds from different sites on New Caledonia are shown in Fig. 6.2a. For Fig. 6.2b site/context mean values are calculated and a possible trend of the geomagnetic field strength is interpolated. Since the sites on New Caledonia are widely distributed over the island (Fig. 6.1), all results are recalculated for the site on Tiouandé as are the global field models CALS3k.3 and ARCH3k (Korte et al., 2009) as well as the present field strength (46.8 μT after IGRF 2011).

Between 1000 BC and 0 AD three intensity values from single potsherds indicate a significantly lower field of ~ 30 μT than predicted by the global field models CALS3K.3 and ARCH3k (Korte et al., 2009) followed by a sharp increase of the field strength between 0 AD and 300 AD by around 50% to ~ 52 μT. From this maximum the field again decreases gradually to values of about 35 μT around 1000 AD. Compared with the data set, the ARCH3k model indicates some similarities for the time period 0 AD to 1600 AD. Nevertheless it seems that there is consistent overestimation of around 5 to 8 μT and/or offset of the timing by around 250 years. For the time period 300 AD to 800 AD CALS3k.3 seems to be better constrained than ARCH3k, however, the minima around 250 BC and 1000 AD cannot be identified although it is at least hinted at by ARCH3k. A site mean value of ~ 46 μT around 1585 AD plots close to the present field strength of around 47 μT and is also within the range of the global field models. In total it appears that both models are better constrained for the time period after 0 AD than prior to this.

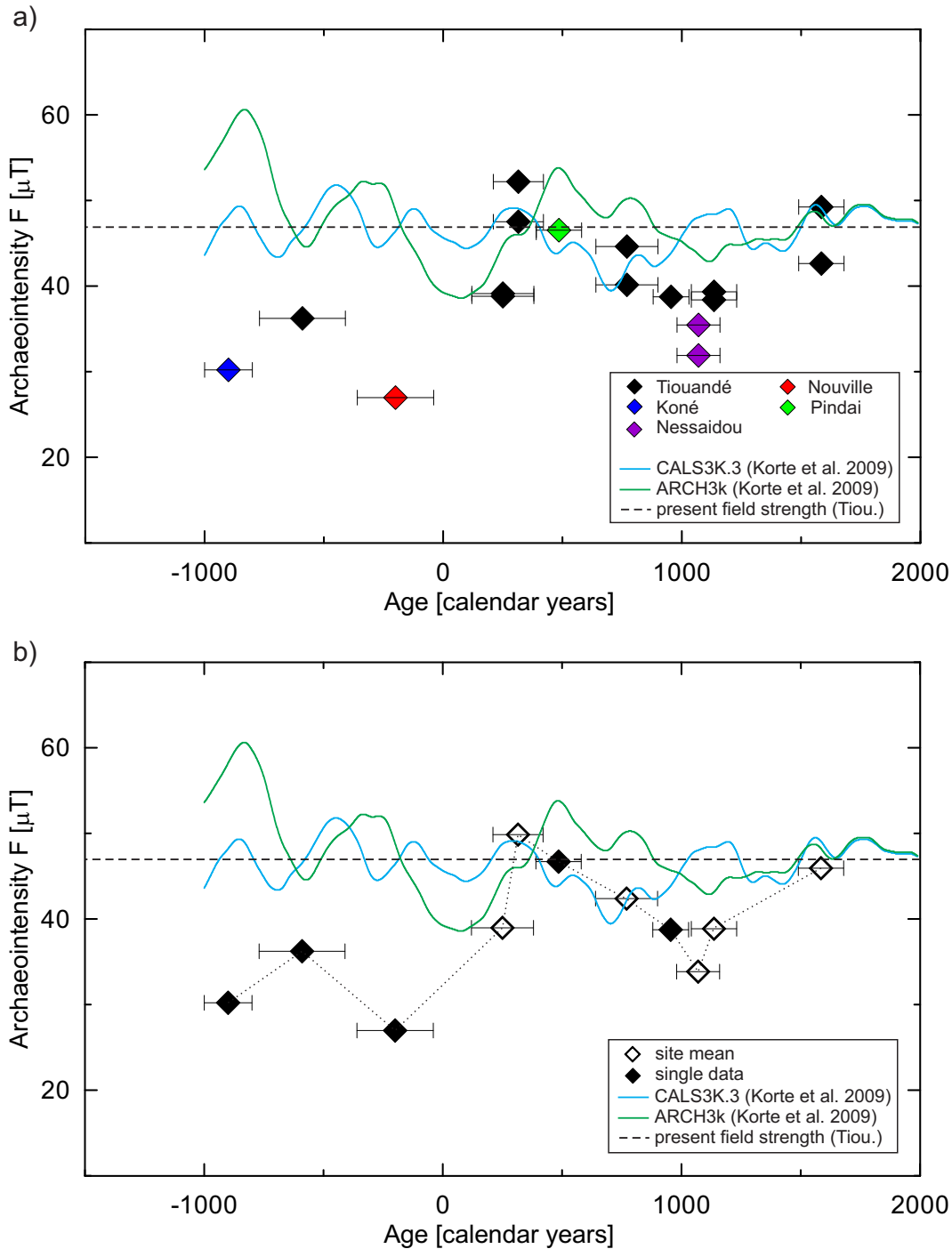

Figure 6.10: Archaeointensity results from New Caledonia. Panel (a) illustrates single data from various archaeological sites. Panel (b) shows relocated site mean archaeointensity results (open symbols), black diamonds indicate sites which yield only one reliable intensity value. In both panels blue (CALS3k.3) and green (ARCH3k) lines represent intensity models after Korte et al. (2009) calculated for the Tiouandé site. Dashed black line shows the present geomagnetic field strength in Tiouandé, New Caledonia.

Table 6.2: Archaeointensity results from New Caledonia.

Site/Context	Potsherd	Age ± (2σ) (cal. yrs)	N	f	g	β	q	$F_{specimen}$ (μT)	F_{mean} (μT)	VADM $\times 10^{22}$(Am^2)
Tiouandé (20.8° S, 165.1° E)										
EHI-13 (141) II 20-30 cm	NC29a	1135 ± 95	5	0.32	0.70	0.07	3.1	38.63	39.31	8.46
	NC29e		6	0.57	0.69	0.04	10.2	39.99		
EHI-13 (141) II 20-30 cm	NC31a	1135 ± 95	11	0.79	0.89	0.02	38.4	35.18	38.38	8.44
	NC31c		9	0.60	0.85	0.04	16.0	41.59		
EHI-13 (142) II 90-105 cm	NC33a	250 ± 130	9	0.82	0.83	0.02	29.2	38.39	38.81	8.53
	NC33b		6	0.50	0.68	0.02	15.5	39.23		
EHI-13 (142) II 90-105 cm	NC34a	250 ± 130	4	0.19	0.61	0.04	2.9	39.90	39.12	8.60
	NC34b		4	0.38	0.72	0.07	3.6	38.34		
EHI-22A (143) A 30-40 cm	NC37a	315 ± 105	6	0.44	0.73	0.04	11.0	50.40	47.52	10.45
	NC37b		6	0.36	0.75	0.10	3.8	44.63		
EHI-22A (143) A 30-40 cm	NC39a	315 ± 105	6	0.63	0.77	0.10	7.3	48.44	52.19	11.48
	NC39b		4	0.32	0.57	0.09	2.1	55.94		
EHI-13 (169) A 10-20 cm	NC46a	955 ± 75	8	0.47	0.85	0.03	11.7	40.22	38.74	8.52
	NC46b		5	0.25	0.74	0.01	12.1	37.26		
EHI-13A (170) A 40-50 cm	NC48a	770 ± 130	9	0.39	0.87	0.02	20.1	45.14	44.62	9.81
	NC48e		12	0.72	0.89	0.02	38.7	44.10		
EHI-13A (170) A 40-50 cm	NC49a	770 ± 130	6	0.31	0.79	0.02	10.4	44.25	40.14	8.83
	NC49b		6	0.53	0.74	0.05	9.4	36.04		
EHI-13A (171) A 100-110 cm	NC53a	-590 ± 180	8	0.69	0.82	0.02	27.4	34.61	36.23	7.96
	NC53d		8	0.70	0.75	0.02	29.8	37.84		
EHI-22A (173) 0-10 cm	NC58a	1585 ± 95	11	0.76	0.87	0.05	16.5	44.59	42.63	9.37
	NC58b		6	0.45	0.79	0.07	2.6	40.68		
EHI-22A (173) 0-10 cm	NC60a	1585 ± 95	13	0.67	0.90	0.02	31.9	49.25	49.24	10.83
	NC60d		8	0.63	0.82	0.02	37.0	49.22		

Continued on Next Page...

Table 6.2 – Continued

Site/Context	Potsherd	Age ± (2σ) (cal. yrs)	N	f	g	β	q	$F_{specimen}$ (μT)	F_{mean} (μT)	VADM $\times 10^{22}$(Am^2)
Nessaidou (21.2°S, 165.5°E)										
(260)3 40-50 cm	NC94b	1070 ± 90	5	0.74	0.66	0.02	20.0	34.77	32.06	7.01
	NC94c		9	0.60	0.86	0.02	30.5	29.34		
(260)3 40-50 cm	NC95c	1070 ± 90	6	0.47	0.76	0.04	7.9	37.14	35.64	7.80
	NC95d		7	0.60	0.82	0.04	14.3	34.14		
Pindai (21.3°S, 165.0°E)										
Cave C (216) TP1 50-60 cm	NC75a	485 ± 95	5	0.26	0.68	0.01	18.1	46.82	46.70	10.22
	NC75b		10	0.51	0.82	0.08	7.6	46.57		
Nouville (22.3°S, 166.4°E)										
Nouville (196) 80 cm	NC73a	-200 ± 160	7	0.45	0.80	0.02	14.6	29.16	27.49	6.04
	NC73b		11	0.68	0.89	0.01	56.2	25.82		
Kone (21.1°S, 164.9°E)										
(133) Zone II G3	NC19a	-900 ± 100	8	0.44	0.83	0.04	6.8	30.68	29.23	6.40
	NC19d		6	0.64	0.79	0.04	9.4	27.78		

Table 6.2: Microwave archaeointensity results from the New Caledonian sites. The age with uncertainties is given in calendar years. N is the number of points used to define a linear segment in the Arai diagram. f, g, β and q stand for the fraction of NRM, gap factor, normalised error of the slope and quality factor according to Coe et al. (1978). F values are the intensity results for individual specimens in μT. F_{mean} values are the arithmetic mean values of F and VADM describes the Virtual Axial Dipole Moment in Am^2.

6.7 Summary

Potsherds from the New Caledonian sites Tiouandé, Nessaidou, Pindai, Nouville and Koné yielded reliable archaeointensities. Rock magnetic investigations identified Ti-poor titanomagnetite and magnetite as dominant remanence carriers, with grain sizes ranging from SD to PSD. One sample from Pindai indicates a further magnetic phase which is interpreted as maghemite with a Curie temperature around 622°C. Shrinkage cracks parallel to the surface were observed during SEM investigations. They are likely to be a result of the manufacturing technique. In contrast to samples from other island regions in the south west Pacific, large titanomagnetite grains were less abundant. Only one titanomagnetite grain could be found in a thin section using the SEM. A success rate of 40% was only achieved because of a reajustment of the acceptance criteria 2 and 9. Between 250 AD and 1600 AD the results plot close to the ARCH3k and CALS3K.3 models. Around 1200 AD the samples indicate a minimum of the geomagnetic field strength. For the time period between 1000 BC and 0 AD only three results from 3 different sites were obtained, which indicate a $\sim$ 25% lower field then the present magnetic field strength.

Chapter 7

Results from the Bismarck and Solomon archipelagos

7.1 Study area

The island chains of the Bismarck Archipelago and the Solomon Islands stretch about 2000 km from northwest to southeast and cover an area from near the equator to 10° S (Fig. 7.1). Both island groups are mountainous with several active volcanoes. The Bismarck Archipelago is also regarded as the cradle of the Lapita culture and was already settled by hunters and gatherers in the late Pleistocene more than 36,000 years ago. With simple rafts and supported by lower sea levels they managed to occupy the inter-visable Solomon island chain (Irwin, 1992). This was then the ultimate border until around 3,500 years ago when near-instantaneous waves of migration of Lapita people occurred in Melanesia. One of the stepping stones in between this settling history was Santa Cruz with the Lapita sites Nenumbo (RF-2) and Ngamanie (RF-2) on Reef Islands and Nanggu (SZ-8) on Nendö. The process leading to the first occupation of Remote Oceania is still unclear. Unfortunately crucial sites like the Santa Cruz sites are not sufficiently well dated using radiocarbon. Therefore a first attempt by archaeomagnetic dating is performed on samples from the three sites on Santa Cruz as is described in Chapter 9. Whereas the Solomon islands were discovered by Álvaro de Mendaña de Neira in 1568 coming from Peru, the Bismarck Archipelago were discovered by Willem Schouten in 1616 coming from Europe (Encyclopaedia Britannica, 2011c; Firth, 1983). Nevertheless both archipelagos were ignored until the middle of the 19th century when colonialists and missionaries settled this region, a place notorious for human sacrifice and cannibalism (Knauft, 1999).

7.2 Sample description

All investigated samples are so-called plain ware without any decoration. With the exception of the potsherds from DoY, all of them are very friable and soft. In particular

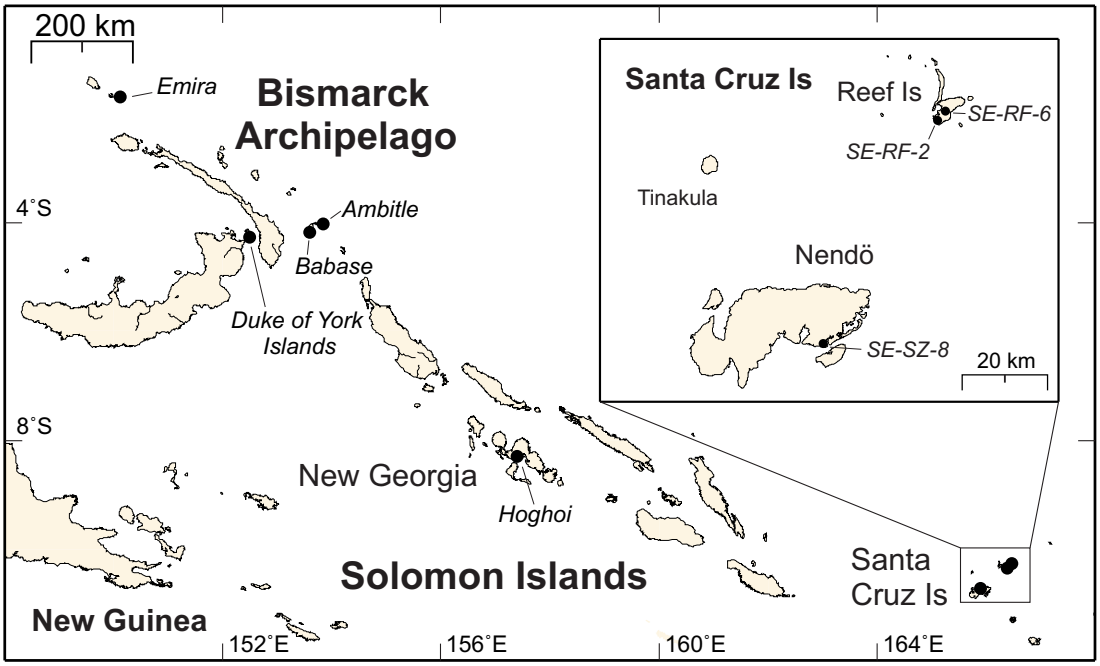

Figure 7.1: Maps of the investigated sites (black dots) on the Bismarck Archipelago and Solomon Islands.

the samples from the Bismarck Archipelago revealed coarse admixtures in their matrix.

Bismarck Archipelago

From the Bismarck Archipelago a suite of 32 individual potsherds were available. Eight came from the Duke of York Islands (DoY), 12 from Babase Island, 6 from Ambitle Island and 6 from Emira Island comprising in total 5 archaeological contexts (Table 7.1). All bar one were dated by means of radiocarbon using pieces of charcoal. Only the samples from DoY were dated using marine shells. Therefore a ΔR correction of 39 $\pm$ 68 was performed. Their uncalibrated radiocarbon ages vary from 3075 $\pm$ 45 BP to 2620 $\pm$ 110 BP.

Solomon Islands

Sixty-nine individual potsherds come from the Solomon Islands (Table 7.1). Six of them were found on the island of New Georgia and originate from two different archaeological contexts with uncalibrated ages of 2619 $\pm$ 45 BP and 468 $\pm$ 62 BP. The age was determined by means of radiocarbon using charcoal.

The remaining samples were excavated from the Santa Cruz Islands with 33 from Nendö and 30 from the Reef Islands. The dating of these ceramics is vague. Nevertheless the settlements of sites RF-2 and RF-6 on the Reef Islands and SZ-8 on Nendö are associated with the Lapita period (Green et al., 2008) and consequently indicate a time period. At the moment the settling history of these sites is highly

Table 7.1: Investigated ceramic series from Bismarck Archipelago and Solomon Islands.

Island/Context	Pottery Group	N_P	^{14}C Age/Error (BP)	CRA Reference	Dated Material
Bismarck Archipelago					
Duke of York Islands (4.2° S, 152.5° E)					
SDP TP1 Spit 7	Y2940-(1-8)	8	2940/60	SUA-3061	marine shell ΔR 39±68
Babase Island (4.0° S, 153.7° E)					
Test Pit 1 Spit 6	BB-6-(1-6)	6	3035/45	WK-7561	charcoal
Test Pit 1 Spit 9	BB-9-(1-6)	6	3075/45	WK-7563	charcoal
Ambitle Island (4.1° S, 153.6° E)					
Test Pit 1 Spit 5	BA-(1-6)	6	2620/110	ANU-11188	charcoal
Emira Island (1.6° S, 150.0° E)					
Test Pit 1 Spit 10	BE-(1-6)	6	3044/31	WK21349	charcoal
Solomon Islands					
New Georgia (Hoghoi) (8.3° S, 157.4° E)					
Hoghoi	HG-(1-3)	3	2619/45	NZA-1253	charcoal
Site 25	HG25-(1-3)	3	468/62	NZA-6235	charcoal
Santa Cruz (Nendö) (10.7° S, 165.9° E)					
SE-SZ-8 86 SS54	SZ-(1-3)	3	–	–	–
SE-SZ-8 158 YY53	SZ8-(1-10)	10	–	–	–
SE-SZ-8 GG64	SZS-(1-10)	10	–	–	–
SE-SZ-8 174 U54	SE-(1-10)	10	–	–	–
Santa Cruz (Reef Islands) (10.3° S, 166.3° E)					
SE-RF-6 P24-9-XP	RF6-(1-10)	10	–	–	–
SE-RF-2 S38-51-XP	R51-(1-11)	10	–	–	–
SE-RF-2 252	R25-(1-10)	10	–	–	–

Table 7.1: Island/Context describe the islands with their latitudes, longitudes and the context code of the investigated potsherds. Pottery Group describes the lab code of a site and N_p the number of individual potsherds from a context. The conventional radiocarbon ages (CRA) with errors are given in BP. Dates labeled with an asterisk(*) are archaeological ages and were obtained from a combination of pottery style and archaeological context. CRA Reference describes the lab code of the samples used for determining the CRA. Dated Material is charcoal and marine shell. ΔR values are given for DoY and Santa Cruz Islands.

Table 7.2: Occupation periods of the Santa Cruz Islands during the Lapita expansion.

Site	Occupation Begin (BP)	Occupation End (BP)	Est. Potsherd Age (cal. yrs) ± Error	Reference
SE-SZ-8	3650	2600	-1175 ± 525	Green et al. (2008)
SE-RF-2	3270	2720	-1045 ± 275	Green and Jones (2008)
SE-RF-6	2910	2080	-545 ± 415	Green and Jones (2008)

Table 7.2: The occupation period of the Lapita sites on the Santa Cruz Islands are given in BP and conform at a 95.4% confidence level. In order to get rough age estimations of the investigated potsherds mean values are calculated and given together with their errors in calendar years.

controversial (e.g. Best, 2002; Felgate, 2003; Jones et al., 2001; Green and Jones, 2008). In order to get an idea of the age of each site, and therefore for the investigated pottery groups from the Santa Cruz Islands, the latest Bayesian analysis of the older and newer radiocarbon age determinations is used (Green and Jones in prep.). In Table 7.2 the estimated beginning and ending of each occupation in BP and cal. yrs., together with their references, are given. The dates conform at a 95% confidence level. Although this procedure leads to relatively high age uncertainties up to ±525 years it helps to range in the archaeointensities obtained from the Santa Cruz Islands.

7.3 Magnetic mineralogical investigations

Rock magnetic investigations as described in Chapter 3 were performed on sister samples from 101 potsherds using a VFTB. The following sections present the major results of the IRM, backfield, hysteresis and thermomagnetic measurements. A detailed overview of the results is given in Appendix A.

IRM, Backfield measurements and Hysteresis measurements

Analyzing IRM's at a present magnetic field of 300 mT revealed saturations between 92% to 100% which suggest low coercivity magnetic minerals mixed with very small amounts of high coercive minerals. These results are comparable with curve types 1 and 2 in Fig. 4.2. B_{cr} results obtained from backfield measurements revealed values around 31 ± 4.2 mT for the samples from the Bismarck Archipelago and 29 ± 4.4 mT for samples from the Solomon Islands. Following Fabian (2003), all measured hysteresis loops exhibited pot-bellied shapes. The various shapes further indicate grain sizes ranging from SD-PSD to PSD-MD (Tauxe, 1998) comparable to the New Caledonian samples in Fig. 6.2. This is also supported by Day-plot analysis (Fig. 7.3). It is also noteworthy that the Bismarck and Duke of York samples plot closer to the PSD-MD region than the Santa Cruz and New Georgia samples.

Thermomagnetic curves

Around 80% of the analyzed thermomagnetic curves revealed similar behaviours. They exhibit a reversible or near reversible heating cycle with single Curie temperatures ranging between 484°C and 585°C (Fig. 7.2a,b,c and e). These curves are associated with low-Ti titanomagnetite or magnetite. One third of them also showed a kink around 200°C as already described in Chapter 4. Some samples revealed two or more Curie temperatures and/or some degree of decay which can be misinterpreted as T_C's (Fig. 7.2d and f). Nevertheless all of them showed a cooling curve above the heating curve which indicates development of a more magnetic component. All archaeointensity experiments on these samples failed due to the lacking of a ChRM. It is possible

that insufficient firing and/or acquiring a chemical remanence (CRM) due to weathering caused this behaviour. Although only six samples were investigated from New Georgia, four different types could be identified (Fig. 7.2e-h). Besides the already described types, two curves revealed a second T_C around 610°C which was interpreted as maghemite (γ-Fe_2O_3) and explicitly found on the site of Hoghoi. There are various suggestions of T_C's for maghemite (590°C - 695°C) depending on the impurities (e.g. Al^{3+}) (Dunlop and Özdemir, 1997). There are also different observations of the inversion temperatures T_{inv} of maghemite (250°C to $\geq$ 750°C) with naturally occurring maghemites having higher T_{inv} then synthetic maghemites (e.g. Dunlop and Özdemir, 1997). This explains the stability when heating to $\sim$ 610°C. Nevertheless when heating up the sample to 700°C the maghemite phase inverts to the magnetically weaker heamatite and can not be identified in the subsequent cooling run. The curve described in (Fig. 7.2h) was only found in one sample from Hoghoi. Between 450°C and 550°C the magnetisation in the heating curves increases significantly. The subsequent decrease indicates a T_C around 610°C which suggests a maghemite phase. The cooling run shows a single T_C around 580°C and a $\sim$ 25% stronger magnetisation. A decay of maghemite around 550°C is reported in Özdemir and Dunlop (1988), but what is the reason for the strong increase of the magnetisation starting around 460°C? It is possible that besides some amount of magnetite, antiferromagnetic lepidocrocite (γ-FeOOH) is also present in the sample, which dehydrites during heating to maghemite. Since this phenomena was observed in only one sample no further investigations were carried out.

7.4 Microscopic investigations

Scanning electron microscope analysis was carried out on three thin sections of samples from the Bismarck and Solomon Archipelagos (BB-9-1 (Babase), Y2940-2 (DoY) and SZ-1 (Nendö)) (Fig. 7.4a,b and c). All three thin sections revealed large titanomagnetite grains ($\sim$ 20 μm to $\sim$ 250 μm) which are identified using EDX. The titanomagnetite grains are probably introduced by the temper. The amount of temper in these samples was significantly higher than in the other investigated samples from the SW Pacific. Little islands like Babase, Duke of York Islands have only limited sources of clay. It is known that for instance, for the Reef Islands clay was imported from neighbouring islands (pers. comm. P. Sheppard 2011). In order to overcome the dearth of clay more and more temper is added. It is noteworthy that samples with a higher amount of temper did not couple with the microwave energy so that only poor resonance characteristics were obtained. Samples from Babase in particular exhibited this unusual behaviour by reflecting almost all of the microwave energy (see Section 7.5) and consequently were not able to demagnetise. The occurance of shrinkage cracks in the matrix parallel to the sherd surface (Fig. 7.4b and c) is presumably a result of the manufacturing technique. The preferential directions of cracks are probably governed

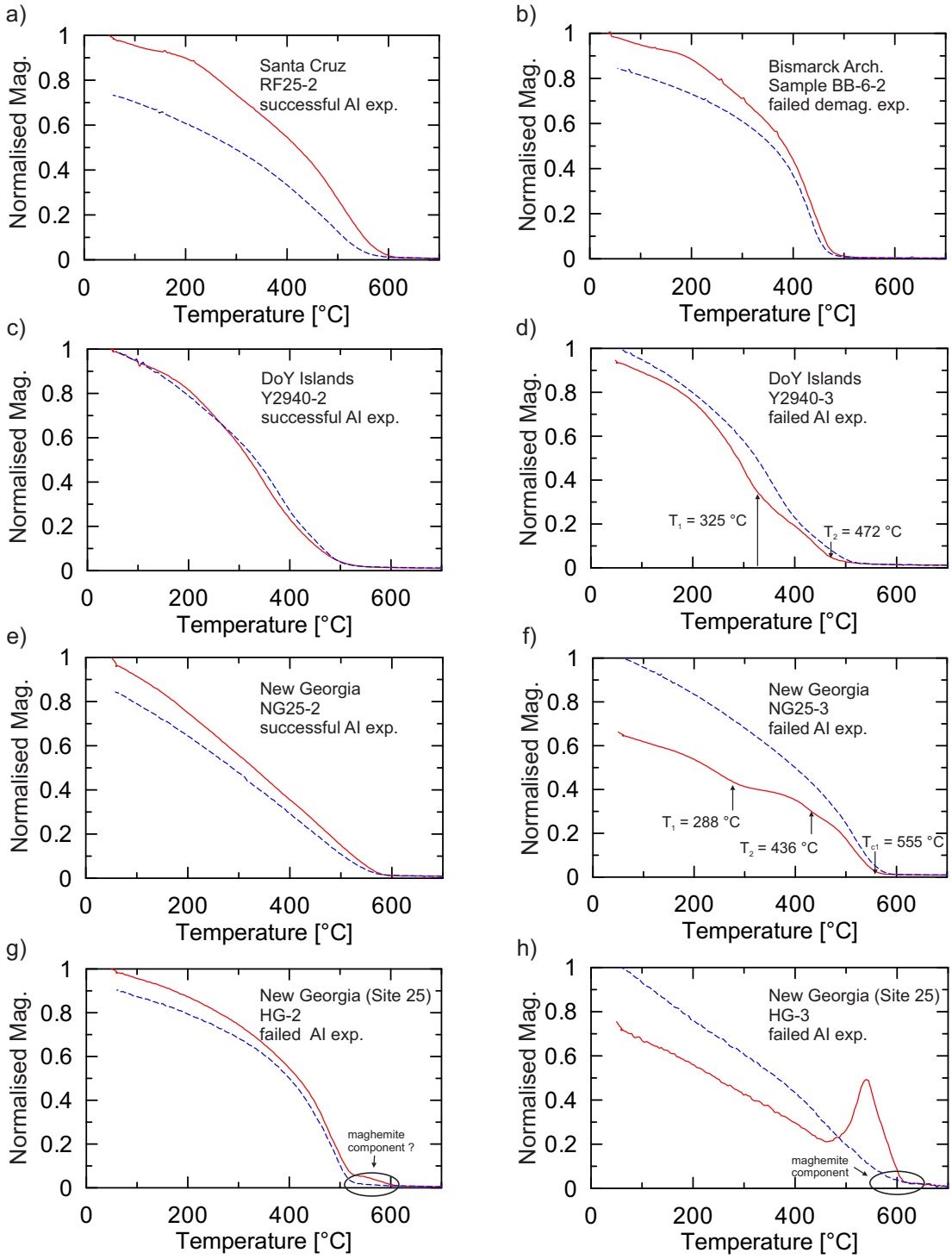

Figure 7.2: Representative thermomagnetic curves obtained from pottery fragments from Bismarck Archipelago and Solomon Islands yielding both reliable and/or no reliable archaeointensities. a) shows a sample from Santa Cruz with a single T_C and a prominent kink around 200 °C found in nearly all samples from this area: it was also more or less pronounced in samples from Ambitle and Babase from the Bismarck Archipelago (b). For the Bismarck Archipelago only samples yielding a single T_C were able to yield reliable archaeointensities (c-f). Samples (g) and (h) show results from Site 25 on New Georgia.

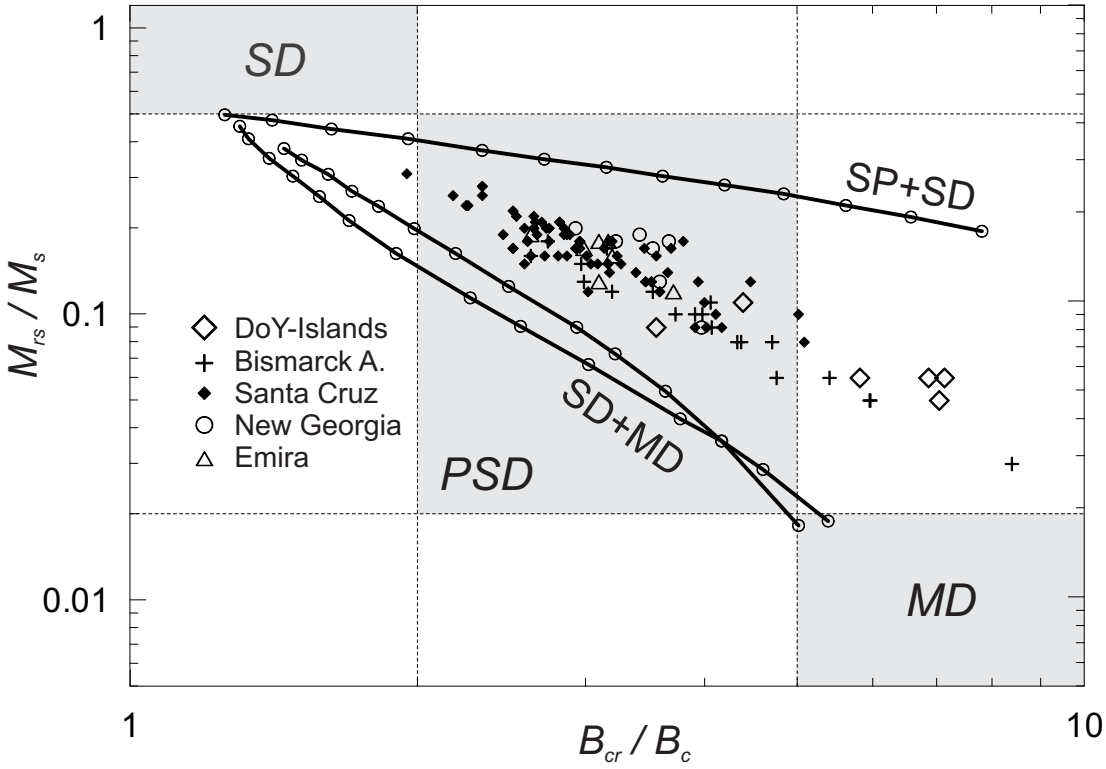

Figure 7.3: Day plot for potsherds from the Bismarck Archipelago and Solomon Islands showing bulk sample hysteresis parameter.

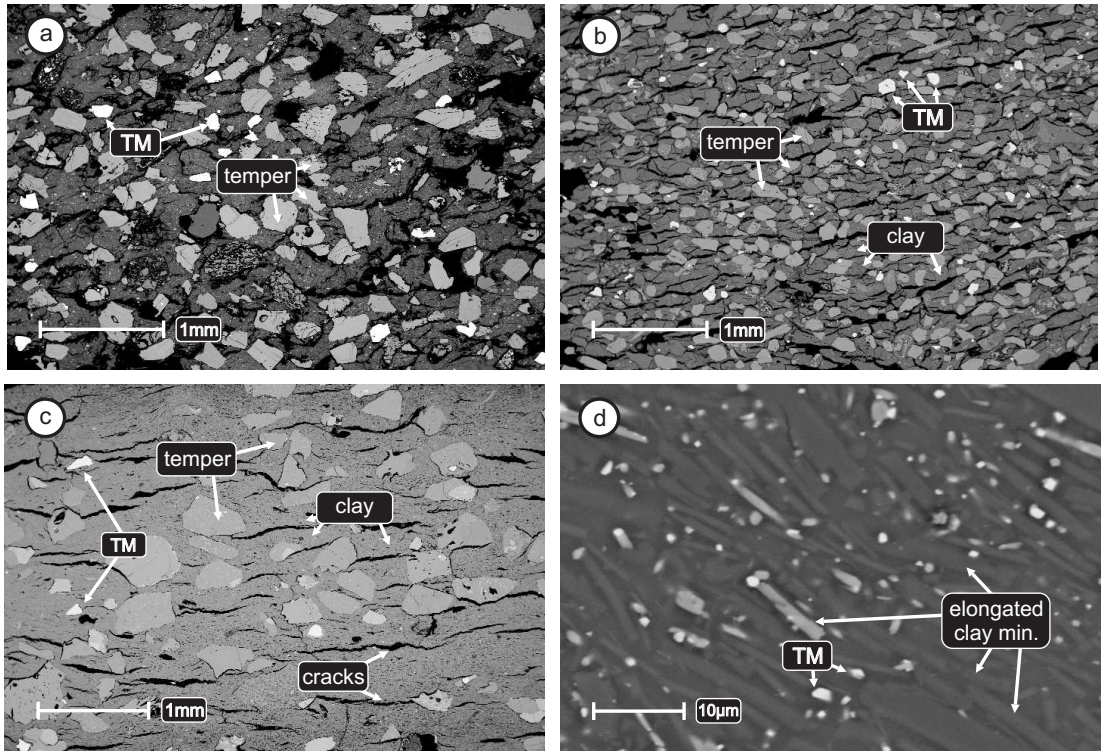

Figure 7.4: Images (a) to (c) show thin sections of samples from Nendö (Santa Cruz), Babase and Duke of York Islands (Bismarck Archipelago). Clearly visible is the high amount of temper within the clay matrix. In all thin section huge titanomagnetite grains (TM) can be found. Shrinking cracks parallel to the surface are visible. (d) A magnification of the clay matrix of the DoY sample reveals elongated crystals and fine dispersed titanomagnetite grains.

by shaping and smoothing the surface of the pottery. Firing the pottery dehydrates the clay matrix and leads to a decrease of volume and lead to cracks. Whereas Fig. 7.4a and b are thin sections from rejected samples Fig. 7.4c represents a sample yielding successful archaeointensity results. Fig. 7.4d shows a magnification of an arbitrary area in the clay matrix. Clearly visible are tiny titanomagnetite particles ($\sim$ 1 μm to $\sim$ 3 μm) dispersed within the burnt clay. This image also shows elongated clay minerals revealing a preferential alignment. It is not clear whether these clay minerals grew during the firing process and/or were brought into alignment during the manufacturing of the pottery. This feature was only observed for the sample Y2940-2. As shown in the next chapter this sample exhibited a distinctive anisotropy of the thermoremanent magnetisation.

7.5 Results of the archaeointensity determination

Demagnetisation experiments

Demagnetisation experiments were performed on all 101 pottery fragments. From the 32 individual sherds of the Bismarck Archipelago only the Duke of York potsherds

exhibited a good coupling to the microwave energy and a resonance frequency was unambiguously determined. From them only potsherd Y2940-2 revealed a characteristic component. Although using both modes (TE_{011} and TE_{011}) of the cavity, placing the samples on different positions in the cavity it was not possible to find a resonance frequency for most of them. The remaining samples showed some response and absorbed around 50% of the microwave energy but also using high powers (>35 W) together with an exposure time of more than 15 seconds the samples were not able to demagnetise more than 30%. Only when melting spots occurred then dielectrical heating caused further demagnetisation. This results in alteration of the magnetic mineralogy and thus makes archaeointensity determinations impossible. Reasons for these different behaviours are not very clear. Magnetic mineralogical investigations show no significant differences between the samples from DoY and the remaining samples from the Bismarck Archipelago. The only striking difference was the quality of pottery samples. Whereas the DoY potsherds seem to be well burnt with a firm and robust body, the remaining fragments from Babase, Ambitle and Emira islands are of a very soft and fragile nature. This is probably because of the high amount of temper material like beach sand (see Section 7.4). This high amount of tempered material might have an influence on the ability to absorb the microwave energy. Similar behaviours were also observed for samples from the Santa Cruz islands and New Georgia. From 63 samples from Santa Cruz islands 44 revealed a very friable nature and were very hard to demagnetise (f < 30%). From the remaining 19 samples, 13 possessed a ChRM and were chosen for archaeointensity experiments. Of 6 samples from New Georgia only 3 were chosen. It was not possible to demagnetise two of the rejected sherds by more than 30% and the other rejected sample did not contain a ChRM. In total, from 101 investigated potsherds 18 were selected for archaeointensity investigations.

Microwave archaeointensity experiments

From 51 microwave archaeointensity determinations (on 18 potsherds), 18 samples from 9 individual potsherds (DoY 2:, New Georgia 4, Nendö 4, Reef Islands 8) yielded reliable archaeointensities. This corresponds to a success rate of 50% at the potsherd level and 35% on the sample level. All dated samples from DoY and New Georgia passed the selection criteria, whereas undated samples R51-9a, R51-9b and R25-1b strictly failed criteria 2 and/or 9 (Chapter 3.4.4). As they fit well to other data from the same site/context and their purpose is for testing archaeomagnetic dating only, they were accepted. A third sister sample was measured when one of the first two sister samples were not able to be demagnetised by more than 50%. Typical Arai-plots of accepted samples from four island regions are shown in Fig. 7.5. Since most of the samples were hard to demagnetise, high MW energies were needed. This sometimes led to melting spots and the experiment was terminated when it was noticed that a melting

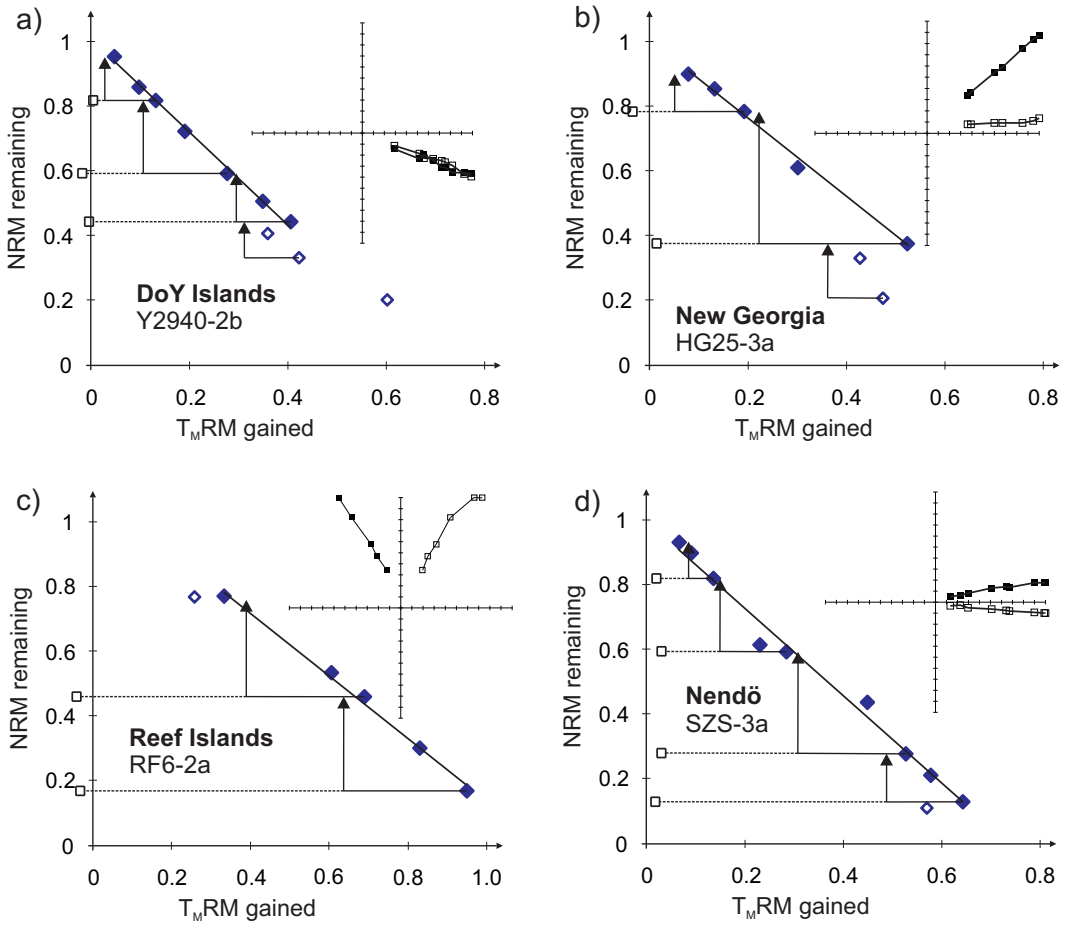

Figure 7.5: Four representative successful Arai-diagrams together with their orthogonal vectors obtained from samples of DoY Islands, New Georgia, Reef Islands and Nendö. (a) early ($\sim$ 800 BC), (b) intermediate ($\sim$ 1160 AD) and (c) late stage of settlement on Lakeba ($\sim$ 1500 AD).

spot had formed. When the linear segment was long enough (f factor high enough) to determine reliable archaeointensities these experiments were accepted (Fig. 7.5a and b). Around 75% of the rejected samples did not show reproducible behaviours between sister samples and showed a large scatter in their Arai-plots (Fig. 7.6a) which was often accompanied with the presence of several magnetic mineralogical components. The remaining samples were rejected because they could not be demagnetised by more than 30% and/or no ChRM could be isolated (Fig. 7.6b).

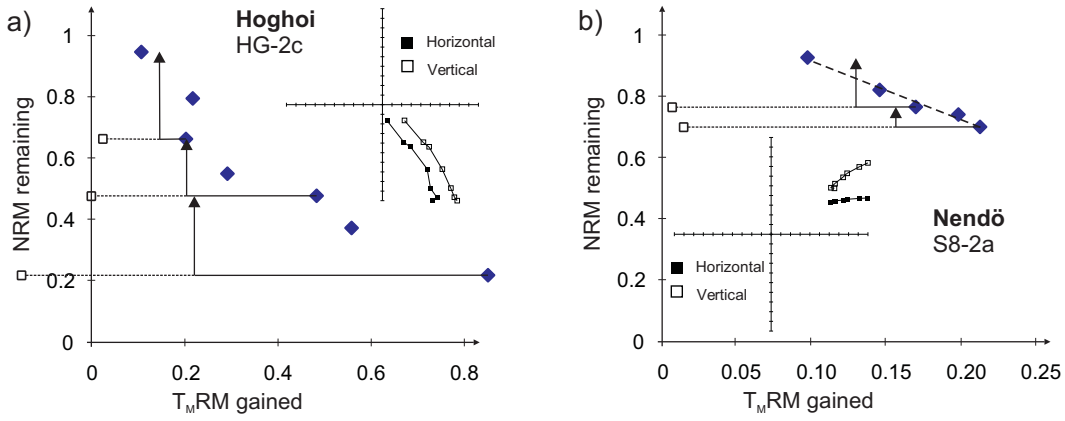

Figure 7.6: Examples of rejected samples. Panel (a) illustrates a typical sample (F2230-2a) with several magnetic components. (b)Sample F1930-2a represents a typical sample revealing a melting spot with ongoing alteration.

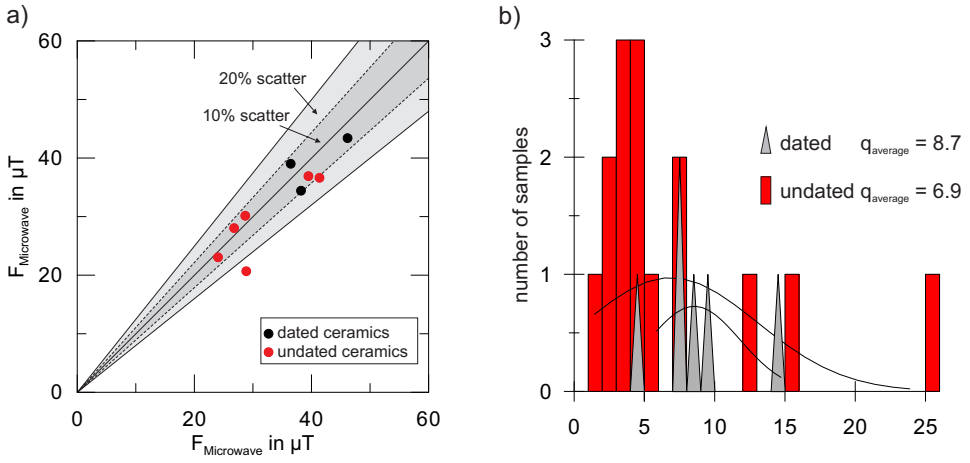

Figure 7.7: Scatter and q-factors of microwave intensity results of sister samples from potsherds from Bismarck Archipelago and Solomon Islands. (a) Grey shaded area showing intensity differences of less than 20% (bright grey) and 10% (dark grey), where black (red) dots illustrate deviations of dated (undated) ceramics. (b) shows the distribution of the quality factors (q) after Coe et al. (1978).

7.6 Discussion of the archaeointensity results from the Bismarck and Solomon archipelagos

Dated ceramics

Successful microwave archaeointensity determinations from Duke of York Islands and New Georgia are listed in Table 7.3 and range from 36.3 μT to 44.8 μT which corresponds to VADM's of 9.1 to 11.47 ($\times$ 10^{22} Am^2). All accepted samples show good within-sherd consistency, with deviations $< 10\%$ (Fig. 7.7a). The distribution of the quality factor after Coe et al. (1978) reveals significantly lower values (average 8.7) compared to other island regions in the SW Pacific (see Chapters 4 to 6). For the site 25 on New Georgia two different potsherds yielded reliable archaeointensities which deviate less than 4% showing good intra-site consistency. Fig. 7.8 shows results from New Georgia with archaeointensity values from the Duke of York Islands, global field models CALS3k.3 and ARCH3k (Korte et al., 2009), as well as the present field strength recalculated for New Georgia (8.3° S, 157.4° E). The single data from the DoY sherd (-665 $\pm$ 245 cal. yrs) plot within the variation of the ARCH3k.3 model and suggest an underestimation of the geomagnetic field strength by the CALS3K.3 for this time period. The samples from New Georgia (1515 $\pm$ 115) indicate a $\sim$ 10% lower field strength than indicated by both models with the ARCH3k model again ploting closer to the experimental data.

Undated ceramics

Since the undated ceramics do not contribute to an archaeointensity curve, the acceptance criteria were loosened. The threshold for the q factor was reduced to 1 instead of 4, the fraction f of the analysed NRM was reduced to 0.25 and the number of points N used to define a linear segment in the Arai-plot was reduced from 5 to 4. Selkin and Tauxe (2000) and Teanby et al. (2002) for instance suggest less strict acceptance criteria with N = 4, f = 0.3 and q = 1. All bar one of the undated sherds revealed a good within-sherd consistency with deviations $< 11\%$ (Fig. 7.7a). Only potsherd RF6-2 with intensity values of 28.9 μT and 20.7 μT exhibited a difference of more than 20%. This was the only sherd from site RF-6 passing the acceptance criteria and was therefore kept in order to compare the results with the other sites. With quality factors q (Coe et al., 1978) ranging from 1.45 to 25.1 (average is 6.9) the quality of the archaeointensity determinations are significantly lower than results from other island regions in the SW Pacific. In particular, sherds from the Reef Islands yielded low q-factors with 75% below 4 (Fig. 7.7b).

All archaeointensity results from the Santa Cruz Islands are recalculated for New Georgia. Two potsherds from Nendö (SZ-8) revealed similar archaeointensities with 36.3 μT and 37.7 μT. Three potsherds from site RF-2 revealed intensities between 23.6

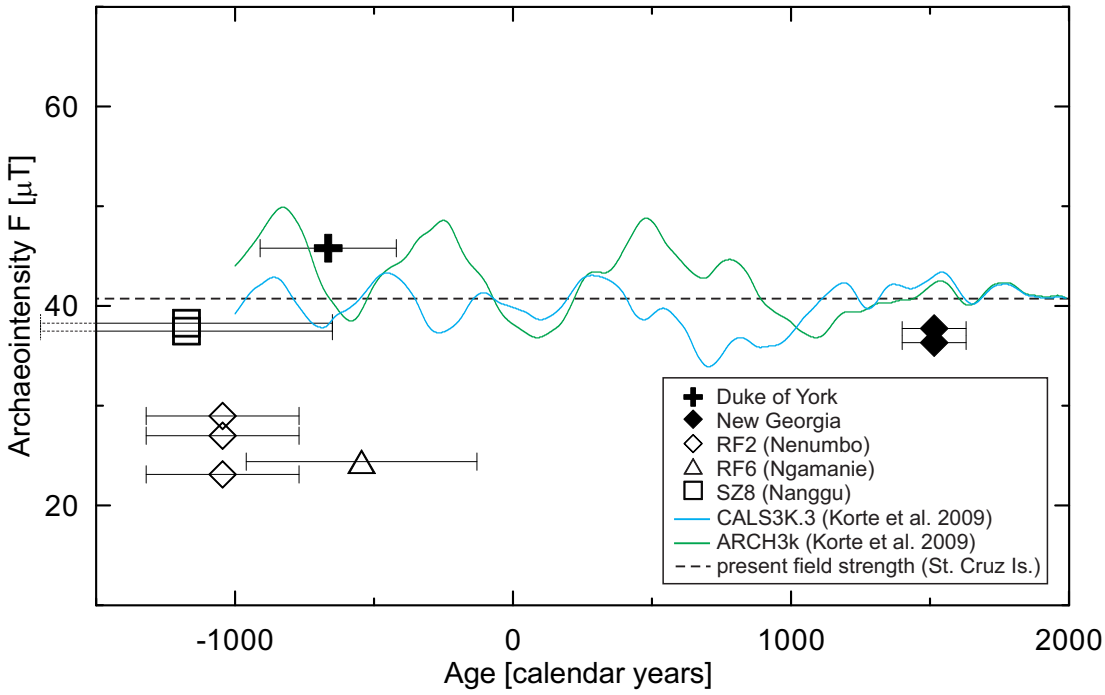

Figure 7.8: Archaeointensity values from Duke of York Islands (Bismarck Archipelago), of New Georgia (Solomon Islands) and the Santa Cruz Islands Nendo and Reef Island (Solomon Islands). Open symbols represent results from Santa Cruz with unclear age estimations in contrast to the well dated results from DoY Islands and New Georgia (cross and pentagon). The blue (CALS3k.3) and green (ARCH3k) curves represent intensity models after Korte et al. (2009) calculated for site Nendö, Santa Cruz. The dashed black line shows the present geomagnetic field strength in Nendö, Santa Cruz.

μT and 29.4 μT. A difference of around 20% can be explained by strong variations of the geomagnetic field strength around 1000 BC as is observed from the data from Fiji and Vanuatu (see Chapters 4 and 5). The only potsherd yielding reasonable results from RF-6 exhibited a sherd mean value of around 25 μT which is similar in magnitude to the RF-2 pottery. For a more detailed accomplishment and the evaluation of archaeomagnetic dating see Chapter 9.

Table 7.3: Archaeointensity results from Bismarck Archipelago and Solomon Islands.

Site/Context	Potsherd	Age ± (2σ) (cal. yrs)	N	f	g	β	q	$F_{specimen}$ (μT)	F_{mean} (μT)	VADM × 10^{22}(Am^2)
Bismarck Archipelago										
Duke of York Islands (4.2°S, 152.5°E)										
SDP TP1 Spit 7	Y294-2a	-665 ± 245	9	0.67	0.82	0.09	9.8	46.16	44.78	11.47
	Y292-2b		7	0.52	0.82	0.04	14.7	43.40		
Solomon Islands										
New Georgia (8.3°S, 157.4°E)										
Site 25	NG25-2x	1515 ± 115	5	0.55	0.81	0.08	7.25	38.21	36.32	9.09
	NG25-2y		7	0.68	0.73	0.07	8.35	34.42		
Site 25	NG25-3a	1515 ± 115	5	0.53	0.66	0.06	7.50	36.45	36.74	9.45
	NG25-3c		6	0.53	0.65	0.10	4.43	37.02		
Santa Cruz (Nendo) (10.7°S, 165.9°E)										
SZ8 86 SS54	SZ-3a	-1175* ± 525	7	0.84	0.77	0.03	25.13	39.47	38.19	9.42
	SZ-3b		6	0.42	0.66	0.05	4.83	36.91		
SE-SZ8 GG64	SZS3a	-1175* ± 525	9	0.81	0.82	0.06	15.83	41.37	39.00	9.61
	SZS3b		4	0.35	0.63	0.04	7.13	36.62		
Santa Cruz (Reef Islands) (10.3°S, 166.3°E)										
RF6 P24-9-XP	RF6-2a	-545* ± 415	5	0.59	0.71	0.03	12.31	28.86	22.53	5.56
	RF6-2c		5	0.50	0.72	0.06	3.85	20.67		
RF2 S38-51-XP	R51-9a	-1045* ± 275	4	0.30	0.62	0.10	1.45	24.04	23.55	5.81
	R51-9b		5	0.28	0.53	0.04	3.24	23.05		
RF2 252	R25-1a	-1045* ± 275	6	0.47	0.63	0.09	2.04	26.79	27.41	6.76
	R25-1b		5	0.38	0.59	0.07	3.14	28.03		
RF2 252	R25-9a	-1045* ± 275	5	0.74	0.67	0.09	5.41	28.69	29.42	7.25
	R25-9b		5	0.67	0.73	0.08	2.70	30.14		

Table 7.3: Microwave archaeointensity results from the Bismarck Archipelago and Solomon Islands. The ages with uncertainties are given in calendar years. Ages labeled with an asterisk (*) are a combination of multiple dates with limited validity. N is the number of points used to define a linear segment in the Arai diagram. f, g, β and q stand for the fraction of NRM, gap factor, normalised error of the slope and quality factor according to Coe et al. (1978). F values are the intensity results for individual specimens in μT. F_{mean} values are the arithmetic mean values of F and VADM describes the Virtual Axial Dipole Moment in Am^2.

7.7 Summary

Two reliable archaeointensity values from New Georgia (Solomon Islands) and one from Duke of York Islands (Bismarck Archipelago) were obtained. With values between ~ 37 μT and $\sim 45\mu$T they plot close to the corresponding global field models ARCH3k and CALS3k.3 with ARCH3k plotting closer to the three values. For the poorly dated sites on the Santa Cruz Islands the acceptance criteria 2, 5 and 9 were adjusted in order to obtain archaeointensites. Significant differences of the archaeointensities between the site SZ-8 on Nendö (~ 39 μT) and sites RF-2 and RF-6 on the Reef Islands (~ 23 μT and ~ 27 μT) indicate a distinct settling history. Magnetic mineralogical experiments revealed a single Curie temperature for most of the samples indicating low-Ti titanomagnetite as the main magnetic phase. The remaining samples revealed more complex magnetic behaviours with several magnetic phases indicating both different phases of titanomagnetite and/or an additional maghemite phase.

In total, archaeointensity determinations on potsherds from the Bismarck and Solomon archipelagos reveal a low success rate compared to other island regions in the south west Pacific. In particular old potsherds from the Lapita culture ($\sim$ 2600 BP to 3000 BP) found on Babase, Ambitle and Emira Island in the northern part of the Bismarck Archipelago and the Santa Cruz Islands in the Solomon Group could not be demagnetised using microwave energy since no resonance frequency was found. These potsherds exhibited a very fragile and coarse nature which seem to be a result of the high amounts of tempered material observed by the microscopic investigations.

Chapter 8

Multi-heating experiments

The multi-heating experiments encompass MT4 Thellier experiments (Leonhardt et al., 2004a) following the Coe protocol with alteration and MD checks, as well as correction for anisotropy and investigation of the cooling rate. The experiments, were performed in the Geomagnetism Laboratory at the Ludwig-Maximilians-University of Munich using a 2G cryogenic magnetometer and an MMTD thermal demagnetiser. For a detailed description of the experimental procedure and analysis see Chapter 3.

8.1 Thellier archaeointensity experiments on preselected samples

Thirty-one individual potsherds from Fiji and Vanuatu were selected based on successful microwave archaeointensity determinations of sister samples. For each potsherd two sister samples were investigated. From 62 full MT4 Thellier-type experiments, 14 samples exhibited acceptable results (i.e. with a success rate of 23%) which are listed in Table 8.1. Typical Arai-plots of accepted samples are shown in Fig. 8.1 (b,d,f) and juxtaposed with sister-samples from MW measurements (Fig. 8.1a,c and e). Using mini-cores entails the disadvantage that already little deviations in the x,y-plane (core coordinates) during the measurements in the cryogenic magnetometer lead to significant errors which are sometimes observed as a zig zag pattern in the orthogonal vector plot (see Fig. 8.1 (d,f)). In order to overcome this orientation problem only values of the measured Z-component were accepted for vector subtractions. In order to select and analyse linear segments in the Arai-plots the software "ThellierTool4.1" (Leonhardt et al., 2004a) was used. This software allows categorization of the quality of results as class A, B or C using the acceptance criteria, where samples exhibiting a class C result were rejected.

Two thirds of the samples were rejected because of magnetic mineralogical alteration and/or loss of sample material during the experiments (Fig. 8.2a). Using alteration checks two samples were check-corrected after Valet et al. (1996) using the "ThellierTool4.1". The corrected samples were then denotated as class A* or B*.

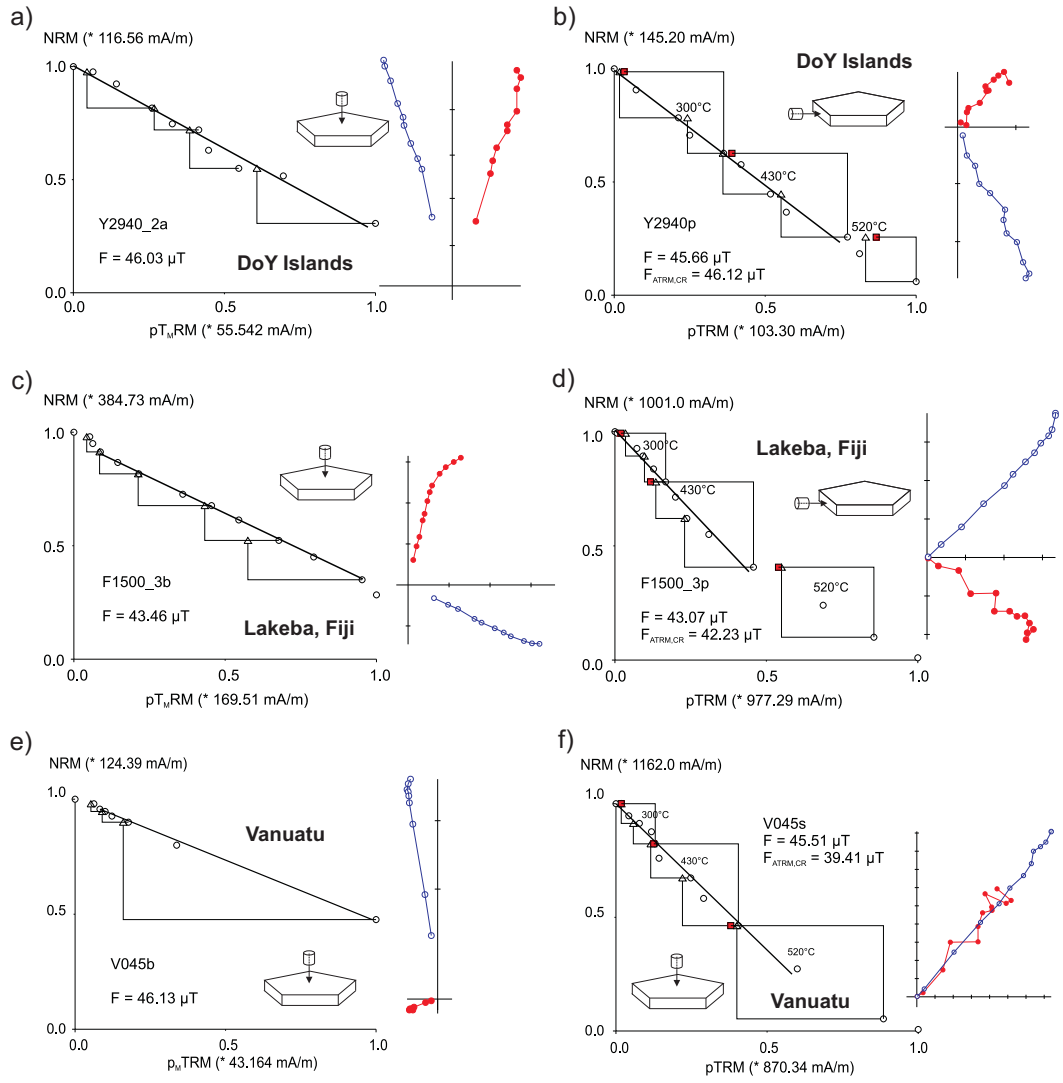

Figure 8.1: Examples of accepted Arai diagrams obtained from sister samples of the same potsherd using (left) MW and (right) corresponding Thellier experiments. Sketch figures indicate orientations of the extracted samples. FATRM,CR denotes archaeointensities corrected for anisotropy as well as cooling rate. Orthogonal vector plots show the demagnetization steps where solid (open) circles represent the horizontal (vertical) plane in core coordinates. Arrows and red squares represent pTRM and additivity checks respectively (Krása et al., 2003).

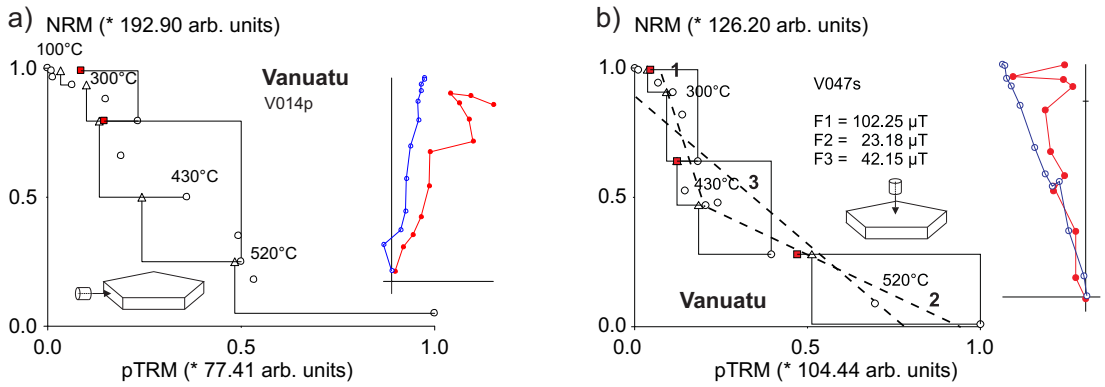

Figure 8.2: Rejected examples of sister samples from the Thellier experiments. Panel (a) shows typical samples with ongoing alteration during the Thellier experiment. Arrows indicate pTRM alteration checks and the red squares are additivity checks. In (b) both failing pTRM checks as well as a curved Arai plot made a reliable intensity determination impossible. The dashed line illustrates a possible fit to the data with intensity estimation, however interpretation is ambiguous (see Discussion in text).

Check-corrections were only performed when a non-corrected accepted sister sample was available. All samples from Vanuatu having a second T_C around 350° were affected by a strong decay and growth of new magnetic minerals, which occurred during the heating steps. Two samples from one potsherd show concave-up Arai diagrams (Fig. 8.2b). They were rejected since an ambiguous multi-slope behaviour results in multiple intensity values between 102 μT and 23 μT for the slopes (1) to (3) (see Fig. 8.2b).

8.2 Anisotropy of TRM experiments

The ATRM correction factor for the Thellier results ranges from 1.37 to 0.89 (for perpendicular to and parallel to the plane of drilled cores, respectively) (Fig. 8.3a), which indicates an oblate ellipsoid with a minor (hard) axis perpendicular to the sherd surface. Without an ATRM correction, intensities obtained from specimens drilled perpendicular (parallel) to the surface would therefore be overestimated (underestimated), respectively. After ATRM correction, the intensity difference between two orthogonally drilled sister samples decreased significantly, which confirmed a successful ATRM correction. All applied ATRM correction factors are listed in Table 8.1.

Fig. 8.3b shows the ATRM effect in % against the alteration during the ATRM experiments in %. With the exception of samples F1500-3p and V045p the ATRM effect dominated the alteration effect on the samples. In cases where the alteration effect is dominant, the archaeointensity results are not ATRM corrected.

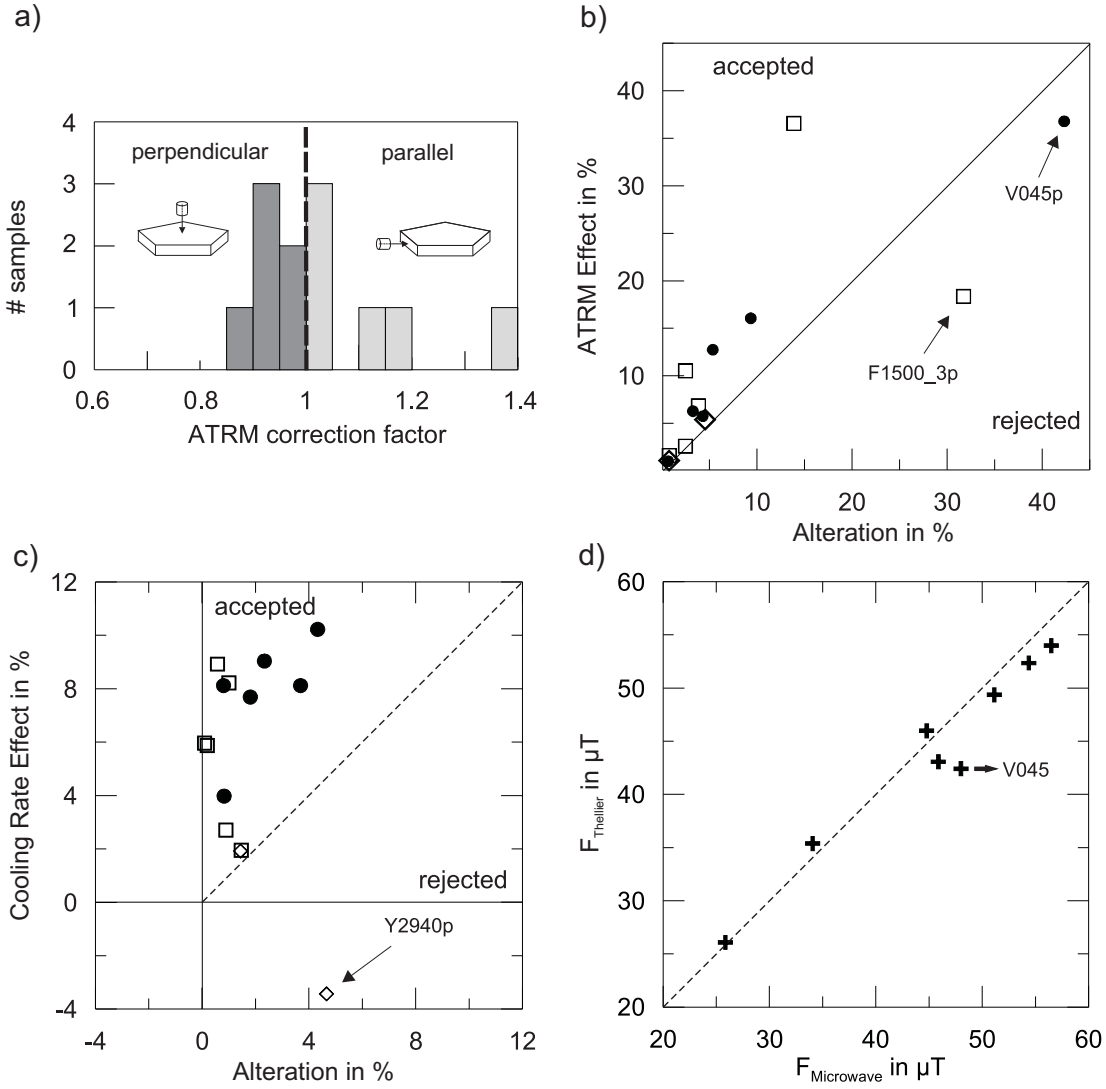

Figure 8.3: Results of the heating-experiments. (a) Distribution of ATRM correction factors for samples drilled parallel and perpendicular to the sherd surface. (b) ATRM effect and (c) CR effect versus alteration. Results below the diagonal were rejected, since alteration obscures the ATRM and/or CR correction factors. Diamonds, squares and dots represent DoY, Fijian and Vanuatuan specimens. (d) Cross-check of intensities yielded by the MWS with intensities obtained from Thellier experiments corrected for ATRM effect.

8.3 Cooling rate experiments

The CR experiments reveal that a cooling time of $\sim$ 8 h leads to an average decrease of 6% (ranging from 1.9% to 10.2% for individual potsherds) in the archaeointensities, which is consistent with a single domain behaving remanence carrier (Fig. 8.3c). CR experiments were successful when the cooling rate effect was bigger then the alteration effect. This was the case for all bar one investigated sample. Only sample Y2940p revealed a dominant alteration and was therefore excluded. As anticipated, CR correction factors were generally similar for sister samples. Since cooling rate dependency is related to the dimensions of the magnetic particles, this implies a reasonably homogenous distribution of grain sizes within the investigated ceramics. As previously discussed however, the cooling rate of the pots during their remanence acquisition is likely to have been of the same order as that experienced during the Thellier experiments, so it is not valid to apply this correction to our results. All applied CR correction factors are listed in Table 8.1.

8.4 Discussion of the multi heating results

The key purpose of the Thellier experiments was to cross-check the microwave results (see Fig. 8.3d). For eight common potsherds, archaeointensities determined from the MWS are on average 3.7% higher (range from -3.9% to 11.6% for individual potsherds) than the non cooling rate-corrected Thellier results. This difference may be explained by differences in experimental cooling, although further measurements are needed to verify this. The lower Thellier intensity of V045 can be attributed to the fact that one of the two specimens (V045p), drilled parallel to the surface, was not corrected for anisotropy since alteration occurred in this sample and obscured any anisotropy effects. Assuming an oblate shape for the anisotropy ellipsoid as before, the lack of correction will give an underestimation of the intensity as observed. In Fig. 8.4 successful microwave results are plotted together with corresponding Thellier results. A convergence of the ATRM corrected Thellier data to the microwave data underlines the importance of regarding ATRM effects in ceramics.

8.5 Summary

Thellier-type MT4 experiments after Leonhardt et al. (2004a) corrected for anisotropy of TRM were performed on selected samples from DoY, Fiji and Vanuatu. The accepted results are consistent with the microwave experiments. A success rate of 23% is not a desirable result considering the fact that the Thellier experiments were conducted on samples from ceramics which have already yielded good microwave intensities. Determining an ATRM tensor after Veitch et al. (1984) revealed anisotropy effects which

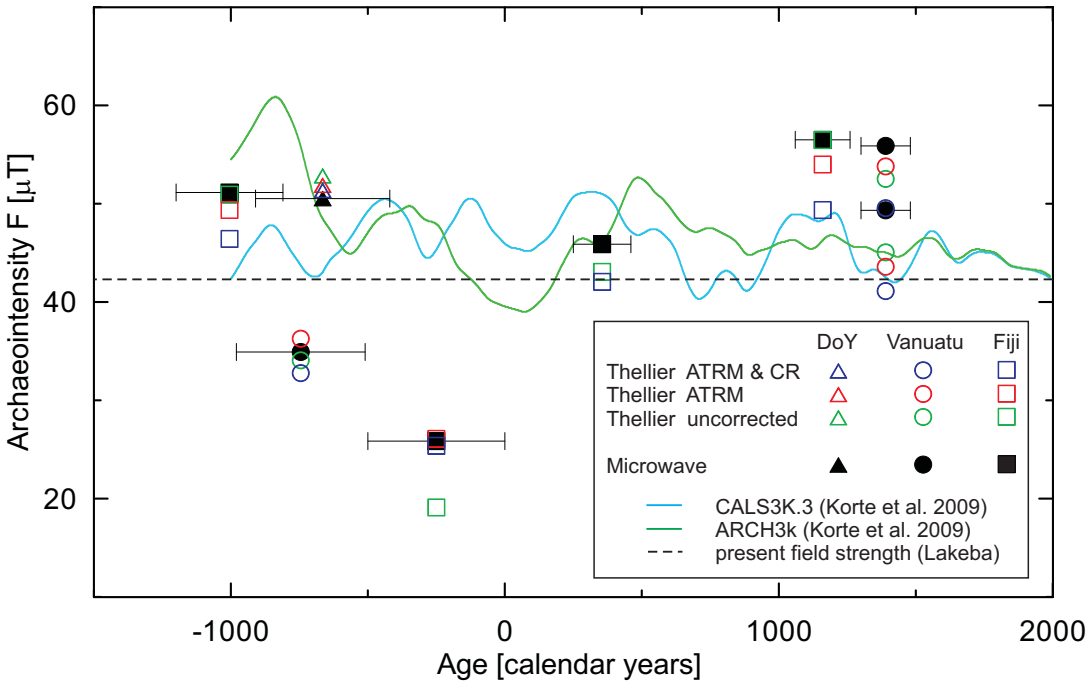

Figure 8.4: Thellier results from Fiji (squares), Vanuatu (circles) and DoY Islands (triangle). Black symbols represent corresponding Microwave results. Green, red and blue symbols indicate uncorrected, ATRM corrected and both ATRM and CR corrected values. The blue (CALS3k.3) and green (ARCH3k) curves represent intensity models after Korte et al. (2009) calculated for the Fijian island Lakeba. Dashed black line shows the present geomagnetic field strength in Lakeba.

cannot be neglected and a correction factor helps to improve the results. No cooling rate was applied since the ancient pottery cooled down within 30 minutes which is in the range of the laboratory procedures. In summary comparing microwave results with Thellier results revealed no significant difference between the methodologies.

Table 8.1: Results of the Thellier experiments.

Potsherd	**$T_{int.}$**	**N)**	**f**	**g**	**q**	**Class**	**F_{spec} (μT)**	**f_{ATRM}**	**F_{ATRM} (μT)**	**f_{CR}**	**$F_{ATRM,CR}$ (μT)**	**$F_{ATRM,MEAN}$ (μT)**
Y2940p	20 - 460	9	0.62	0.85	17.6	B	45.7	1.01	46.1	1.00†	46.1	45.5
Y2940s	20 - 490	10	0.72	0.87	11.6	B	48.0	0.95	45.8	0.98	44.9	
F2250-4p	20 - 580	13	0.92	0.82	16.7	B	45.6	1.02	46.3	0.94	43.5	46.4
F2250-4s	20 - 580	13	0.92	0.85	16.1	B*	56.3	0.93	52.4	0.94	49.3	
F2250-3p	350 - 550	6	0.74	0.72	7.2	B	19.1	1.37	26.1	0.97	25.4	25.4
−−												
F930-4p	20 - 490	10	0.72	0.85	41.3	A	53.0	1.03	54.6	0.91	49.8	49.4
F930-4s	100 - 520	10	0.92	0.86	31.8	A	60.0	0.89	53.3	0.92	49.0	
F1500-3p	20 - 490	10	0.62	0.84	11.2	B	43.1	1.00†	43.1	0.98	42.1	42.1
−−												
V044p	20 - 550	12	1	0.85	13.7	B	45.2	1.13	51.0	0.92	46.8	48.2
V044s	20 - 520	11	0.88	0.88	15.9	A*	57.0	0.94	53.8	0.92	49.6	
V045p	300 - 580	9	0.99	0.79	5.9	B	42.2	1.00†	42.2	0.96	40.7	40.0
V045s	20 - 550	12	0.99	0.83	17.6	B	45.5	0.94	42.6	0.92	39.4	
V060p	20 - 580	13	1	0.78	7.8	B	29.1	1.16	33.8	0.91	30.8	32.0
V060s	390 - 580	7	0.89	0.75	4.6	B	37.3	0.99	36.9	0.90	33.2	

Table 8.1: Thellier archaeointensity results from selected potsherds. T_{int} and N describe the temperature interval selected to define a linear segment in the Arai diagram. For N, f, g, and q, see Table 7.3. Class defines the quality of determination regarding the determination criteria of Leonhardt et al. (2004a). F_{spec} values are the intensity results of individual specimens. The anisotropy correction factor f_{ATRM}, the cooling rate correction factor f_{CR} and the corrected intensities F_{ATRM} and $F_{ATRM,CR}$ values are given in the next columns. $F_{ATRM,MEAN}$ values refer to the arithmetic mean intensities for individual sherds, corrected for anisotropy. * denotes classes with an applied pTRM-check correction (Leonhardt et al., 2004a). †Due to alteration no f_{CR} and f_{ATRM} were determined for samples Y2940p, F1500-3p and V045p, respectively.

Chapter 9

Discussion

9.1 Reliablility of the results

In order to interpret absolute archaeointensity data for their reliability and hence the suitability for archaeomagnetic dating and global field modeling, it is crucial to consider and account for several possible error sources. This helps to reduce the scatter within data sets which would otherwise obscure any real trends (e.g. Bowles et al., 2002; Donadini et al., 2007).

When establishing an archaeointensity curve and thus comparing archaeointensity data to a time scale, a reliable age control is important. For this study only samples from a well secured context dated by means of radiocarbon and/or pottery style were chosen. All dated and accepted potsherds exhibit age uncertainties $\leq$ 300 yrs with more than 54% having age uncertainties $\leq$ 150 yrs. This is comparable to the available data in the GEOMAGIA50 database (Korhonen et al., 2008) with 86% of the data between 1005 BC and 1775 AD having uncertainties $\leq$ 300 yrs. Though not all age uncertainties in the data base conform to a 95% confidence level.

As already found out by Rogers et al. (1979) a disregard of the magnetic anisotropy of remanence could lead to spurious determinations or archaeointensities with errors of more than 30%. For this study ATRM effects were limited by applying the magnetic fields in the direction of the NRM. Although is has been pointed out (e.g. McClelland-Brown, 1984) that for an assemblage of SD particles CR effects can lead to a systematic overestimation of a TRM, a CR correction was not performed, since the cooling time differences between the MW treatment in the laboratory and the ancient cooling in the open are similar and would otherwise introduce additional measurement errors (see Chapter 8).

To determine the archaeointensities the latest state of the art microwave technique was applied (see Chapter 3). In contrast to the traditional thermal-based methods alteration of the investigated samples is limited. Additional alteration and MD checks as well as strict acceptance criteria were applied in order to maintain a good quality control of the results. Moreover, samples were rejected when exhibiting an intra-sherd

scatter of the intensity values > 20%. Cross-checking the results with a different determination technique (MT4 Thellier-type after Leonhardt et al. (2004a)) yielded similar results for sister-samples and showed no significant bias between methods. In summary, the obtained dataset for the SW Pacific represents high quality data which can be unrestrictedly used for modeling purposes.

9.2 Archaeointensity variations in the SW Pacific

9.2.1 Inter-island variations

To compare the archaeointensity results of the investigated island regions (Fiji, Vanuatu, New Caledonia, DoY and Solomon Islands) all values have been relocated to Efate, Vanuatu (17.6° S, 168.2° E). They are plotted in Fig. 9.1a along with the present-day field strength in Efate (44.3 μT) and the global field models CALS3k.3 and ARCH3k (Korte et al., 2009) (calculated for Efate). Site mean values are shown in Fig. 9.1b and a running average was calculated using a 200 yrs gliding window to determine a trend of the geomagnetic field strength in the south west Pacific. Relocation of these results assumes that a geocentric axial dipole is valid over the geographical spread of the sites (3500 km), however it is acknowledged that there could be significant non dipole contributions over this area resulting in relocation errors (Casas and Incoronato, 2007).

For the time period between $\sim$ 1000 BC to $\sim$ 500 BC samples from Fiji, DoY, Vanuatu and New Caledonia indicate a strong intensity variation. Whereas samples from Fiji and DoY suggest intensities close to the suggested values of the CALS3k.3 model ($\sim$ 45 μT), samples from Vanuatu and New Caledonia plot significantly lower ($\sim$ 35 μT). Around 250 BC data from Fiji, Vanuatu and New Caledonia indicate a minimum of $\sim$ 25 μT which is around 40% lower than the present field strength. None of the global field models after Korte et al. (2009) resolve this minimum. Data from Fiji and New Caledonia suggest a strong increase of the intensity up to $\sim 50\mu$T around 250 AD which is followed by a gradual decrease to $\sim$ 30 μT around 1000 BC only shown by samples from New Caledonia. A near contemporaneous increase of more then 35% to $\sim$ 55 μT is marking a maximum of the geomagnetic field strength over the last 3 millenia in the SWP. This maximum is suggested by two sites from Fiji and Vanuatu between 1200 AD and 1400 AD. Unfortunately there are no results from New Caledonia for this time period. Therefore different field evolution between New Caledonia, Fiji and/or Vanuatu cannot be excluded since the distances between those islands range from 500 km to 1000 km. Between 1500 AD and 1750 AD data from Fiji, New Georgia, Vanuatu and New Caledonia reveal intensities close to the global field models (CALS3k.3 and ARCH3k) with a tendency to plot around 5% to 10% lower. In summary, archaeointensity values from the different islands are broadly consistent

Table 9.1: Archaeointensity values and CRA data from south east Australia

Code	CRA Ref.	^{14}C Age/Err.(BP)	Age$\pm(2\sigma)$ (cal. yrs)	F_{old} (μT)	F_{recal} (μT)	ΔF (μT)
GF4	ANU-678	2440/80	-565 $\pm$ 215	42.7	35.4	2
F3	ANU-664	2060/170	0 $\pm$ 400	59.9	49.6	5.9
GF3	ANU-655	2010/100	-45 $\pm$ 235	44.8	37.1	7.8
MB4	ANU-661	1610/110	455 $\pm$ 215	42.9	35.5	4.8
GF1	ANU-653	1420/100	660 $\pm$ 230	55.9	46.3	3.9
MR1	ANU-690	1400/110	700 $\pm$ 200	48.8	39.0	2.9
AL2	ANU-671	1390/80	725 $\pm$ 165	66.0	54.7	2.9
UF1	ANU-674	990/70	1105 $\pm$ 125	54.8	45.4	3
F2	ANU-663	950/120	1100 $\pm$ 210	41.7	34.5	2
UF2	ANU-675	750/70	1305 $\pm$ 105	43.8	36.4	2.7
MR3	ANU-691	400/70	1545 $\pm$ 115	65.9	52.6	3.6

Table 9.1: The radiocarbon ages and archaeointensity values are obtained from Barbetti and Polach (1973) and Barbetti (1977, 1983), respectively. Code denotes archaeomagnetic samples. CRA Ref. describes the lab code of the samples used for determining the CRA. The CRA (^{14}C Age) with errors are given in BP. The calibrated age is given in calendar years. F_{old}, F_{recal} and ΔF values are archaeointensity values for Australia, the recalculated values for Efate and corresponding uncertainty values of the original archaeointensity determination, respectively. All values are given in μT.

within comparable time periods.

9.2.2 Comparison with absolute archaeointensity data from Australia

The nearest archaeointensity data set to the SWP has been obtained from ancient Aboriginal fireplaces and baked clay in south east Australia by Barbetti (1977, 1983). In order to compare these results with the SWP data the Australian archaeointensities were recalculated for Efate (Fig. 9.1b). Since Barbetti (1977, 1983) applied the former Libby half-life of ^{14}C, the radiocarbon ages needed to be recalibrated using the original CRA data of Barbetti and Polach (1973) and the same procedure as described in Chapter 2. The CRA data, as well as original and recalculated archaeointensity data, are shown in Table 9.1. Although the Australian data set encompasses a time interval from 4190 BC to 1545 AD, only data back to 565 BC cover the investigated time period of the SWP samples.

The intensity value around 565 BC fits well to the available data from the SWP. The SWP minimum around 250 BC is not resolved by the Australian data set, however archaeointensity values around 45 BC and 0 AD indicate strong intensity variations between $\sim$ 37 μT and $\sim$ 50 μT, which can also be found for the data from the SWP during the same period from around 250 BC to 250 AD. Strong intensity variations are also observed for a time period around 750 AD, with an intensity maximum of $\sim$ 55 μT. For the remaining data between 0 AD and 1500 AD the Australian intensities indicate similar behaviour to the SWP data and in addition reveal a small minimum around 1000 AD which is also suggested by the data from New Caledonia. A comparison between Australian and SWP data has only a limited value since distances between these sites (up to 3900 km for Fiji) are beyond the resolution of local secular variations

(Casas and Incoronato, 2007). Also dating and measurement errors as well as the lack of good data coverage hamper a more in-depth interpretation.

9.3 Calculation of VADM's and comparison with data from other regions

In order to compare the south west Pacific data with data sets from other regions and continents the SWP archaeointensity values (F) are recalculated to virtual axial dipole moments (VADM's) using the following equation (e.g. Tauxe, 1998):

$$F = \frac{\mu_0 \, VADM}{4\pi R^3} \cdot \sqrt{1 + 3cos^2\theta} \tag{9.1}$$

where μ_0 is the permeability of free space, R the average radius of the Earth and θ the geographic colatitude. The VADM values from other regions were obtained from the GEOMAGIA50 data base (Donadini et al., 2006; Korhonen et al., 2008) and divided into data from Europe, South America, Asia and the World (all data) (Fig. 9.2). All peer reviewed data without ranking or weighting were selected. To cancel out non-dipole components a running average spanning a 500 year time window was calculated for all data sets similar to McElhinny and Senanayake (1982), Yang et al. (2000) and Knudsen et al. (2008). To test the efficiency of this method the World data (violet line with crosses) is compared to the VADM reconstruction of Knudsen et al. (2008) (dashed black line) which is also based on the GEOMAGIA50 data. It needs to be mentioned that Knudsen et al. (2008) further used an optimal least-squares fit to the palaeointensity data and omitted data from sun-dried objects (55 values) and iron slags (12 values). Both curves exhibit a very good correlation and validate this approach of comparing data from other regions with the SWP data. Additionally to the curve of Knudsen et al. (2008) the VADM models of Korte et al. (2009) (ARCH3k and CALS3k.3) are shown.

An estimated curve of the VADM obtained from south west Pacific data is shown in Fig. 9.2 (red line and dots). All bar one time period reveal VADM's above the present VAMD of 7.8 ($\times 10^{22}$Am^2). A minimum of ~ 6 ($\times 10^{22}$Am^2) is given for the time period around 250 BC $\pm$ 500 yrs. Between 250 AD and 1750 AD the VADM's are around 15% higher then the present VADM.

A comparison of the calculated VADM's from the south west Pacific with data from Europe, Asia, South America and the models show only small similarity. Among all data the SWP curve reveals the lowest VADM's from 1250 BC to 750 AD. Between 1000 AD and 1750 AD the curve trends between the South American and European VADM's and closer to the models of Knudsen et al. (2008) and Korte et al. (2009). In contrast to all other data, only the South American data sets, which are besides the SWP data the only data sets incorporating mainly southern hemisphere data, reveal a significant minimum around 250 BC similar to the SWP data.

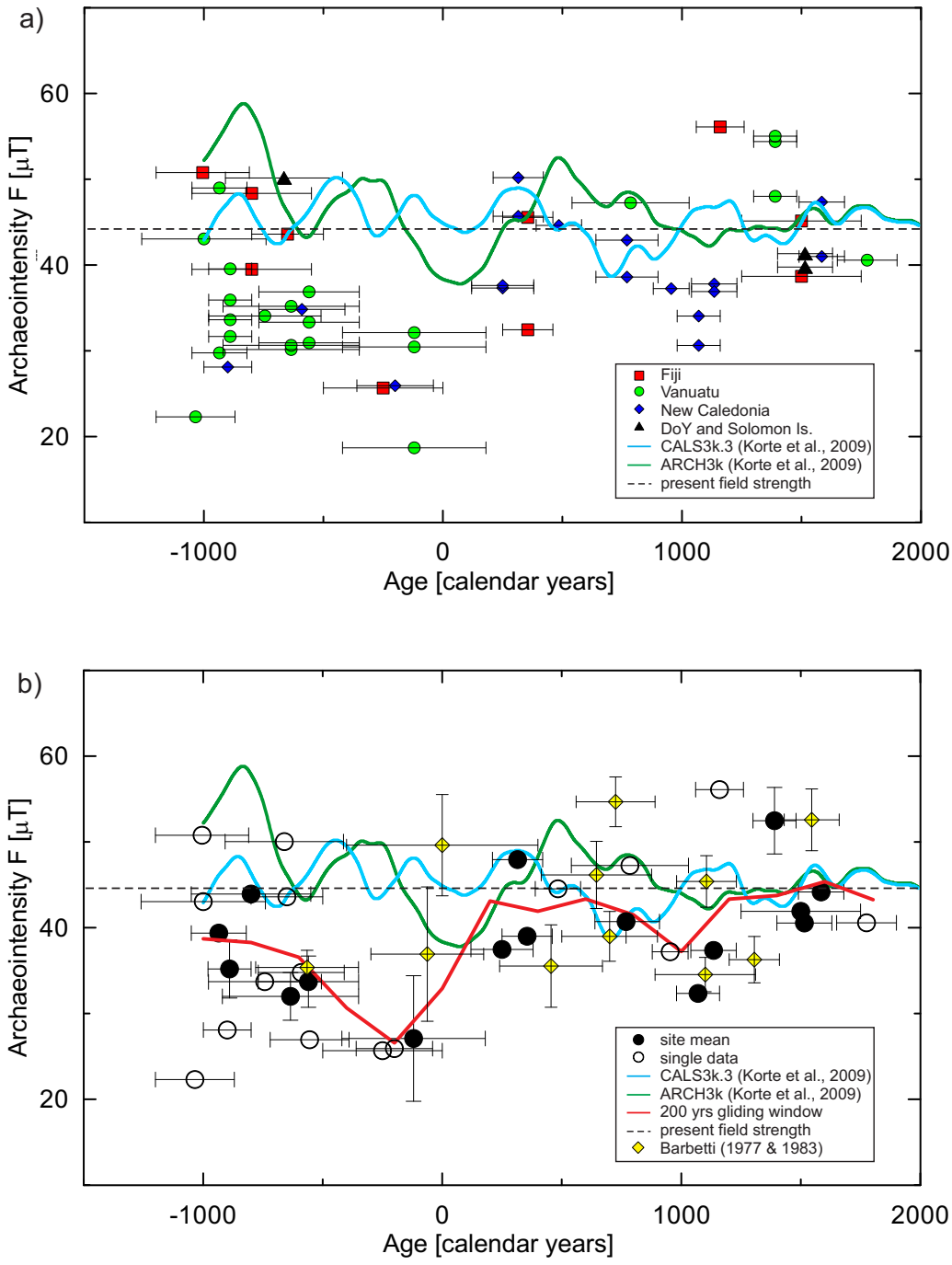

Figure 9.1: Diagrams showing all successful single archaeointensity results (Panel (a) and/or their mean values Panel (b) obtained from samples from Fiji, Vanuatu, New Caledonia, Bismarck Archipelago and Solomon Islands. All samples were recalculated for Island Efate in the Vanuatu group. The green (blue) curves illustrates the ARCH3k (CALS3k.3) models after (Korte et al., 2009). The red curve conforms to a 200 years gliding average of all single values. Crosses represent samples from the Santa Cruz islands with unsure dating.

Although Knudsen et al. (2008) conclude that the geographical distribution of the data has no significant impact on the estimated VADM's, the curves from the south west Pacific and South America suggest otherwise. This is probably a result of a low data density in these regions comparing to Europe and Asia where much more data are available.

Regarding those differences between VADM's from different continents it is worth mentioning that by calculating an average value over 500 years it is not possible to cancel out the secular variation, because the non-dipole fields do not necessarily point to the same direction as the dipole field (Yang et al., 2000; Korte and Constable, 2005). Only the components of the non-dipole field which are parallel to the dipole field can be eliminated, whereas components perpendicular to a dipole field are added to a total field strength. This means that for regions with a pronounced non-dipole field anomaly the averaged magnitude is higher than in regions with low non-dipole field activity (Yang et al., 2000). Another error source is the fact that for these calculations an axial dipole moment is assumed. Since none of the SWP and most of the other archaeointensities in the GEOMAGIA50 database have no assigned directions (at least no inclination) it is not possible to calculate a virtual dipole moment (VDM). Therefore it is possible that discrepancies between regional data sets are a result of neglecting a wobbling (non-parallel) dipole moment (Yang et al., 2000). A further, not to be neglected, fact is that many data in the GEOMAGIA50 data base are not adjusted for cooling rate differences which can lead to an overestimation of more than 8% (Genevey et al., 2009) and may explain to a some extent higher VADM estimates to some extent in other data sets. Between 1000 AD and 1750 AD the dipole reconstruction of Knudsen et al. (2008) plot close to the models of Korte et al. (2009), whereas between 1250 BC and 1000 AD those models plot significantly lower although following Korte et al. (2009) the CALS3k.3 and ARCH3k models have slightly higher dipole moments than their previous models. Valet et al. (2008) have already pointed out the significantly lower VADM estimations from the previous models e.g. CALS7k.2 (Korte and Constable, 2005) for the past two millenia Korte et al. (2009) also highlight the limited use of VADM's because a measure of geomagnetic dipole moments as VADM's calculated directly from data are always higher then spherical harmonic dipole moments.

9.4 Impact of the south west Pacific data on global field models

The scarcity of archaeointensity data is a limiting factor for the construction of global field models. In particular for regions on the southern hemisphere with a low density of data those models are not very well constrained. In order to test the impact of the first data from the south west Pacific, archaeointensity values obtained from the Duke of York Islands, Lakeba (Fiji) and Vanuatu were added to the original dataset used for

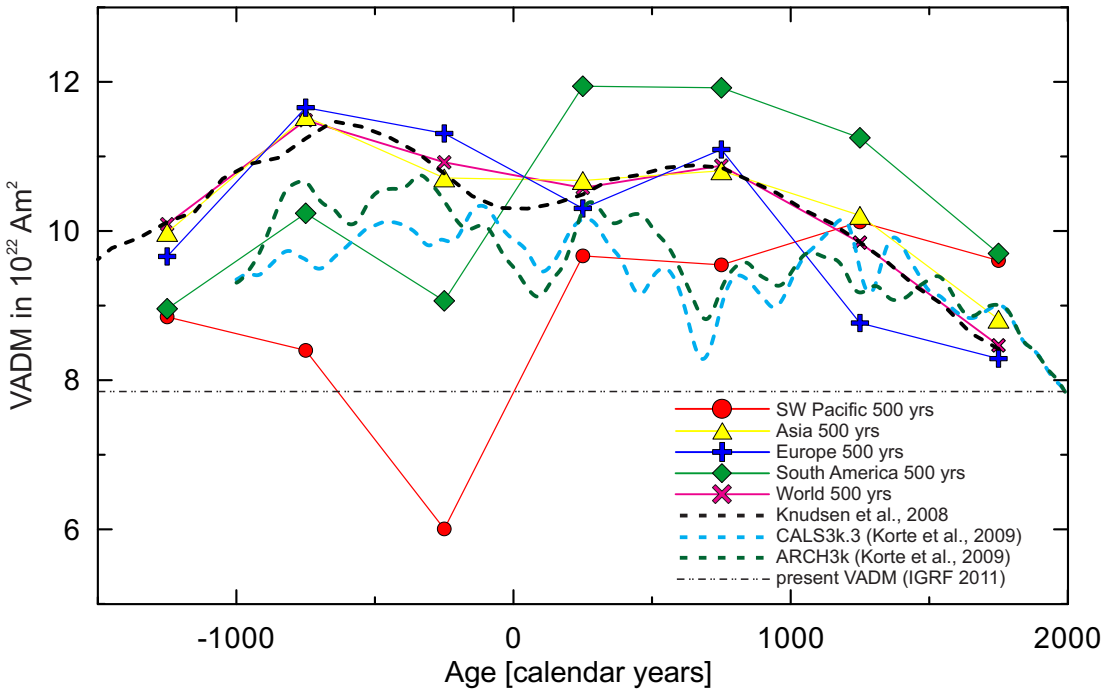

Figure 9.2: Variations of VADM's from different regions obtained from the GEOMAGIA50 data base (Donadini et al., 2006; Korhonen et al., 2008). VADM reconstruction of Knudsen et al. (2008), VADM models of Korte et al. (2009) and the present VADM are shown. Whereas VADM curves from Europe and Asia with a higher data densities plot close to the reconstruction of Knudsen et al. (2008), VADM curves from South America and SW Pacific deviate from this.

CALS3k.3 and ARCH3k. The models were rerun by M. Korte (2010) making no other modifications to the old data set or the modelling strategy and parameters.

The new curves (dashed lines) are denoted as modified CALS3k and ARCH3k and again plotted for Lakeba, Fiji (Fig. 9.3). There are noticeable changes to both models where the ARCH3k curve is more affected than the CALS3k curve. The reason for this is that the ARCH3k is governed only by archaeointensity data whereas the CALS3k.3 curve incorporates both archaeo- and sedimentary intensity data. In the first millenia BC where there are most new data, both modified models move towards these data reducing the intensity compared to CALS3k.3 and ARCH3k. In particular the modified ARCH3k model indicates occasionally a more then 30% lower field strength than predicted by the original model for this time period. Although the modified CALS3k.3 model did not change as drastically, a significant hump in the CALS3k.3 vanished in the modified model. In this region, CALS3k.3 is largely constrained by relative palaeointensities from NE Australia lake sediments (Constable and McElhinny, 1985) and clearly the south west Pacific data are not consistent with this relative palaeointensity record.

Although the intensity data presented here are preliminary, they have demonstrable impact on the behaviour of the CALS3k.3 and ARCH3k global field models in this region. They clearly show that the current models are not well constrained in the SW Pacific region and how even a small dataset can result in significant changes. To further improve the global field models, many more data from a wider geographical spread of the southern hemisphere are required. Likewise, to determine statistically robust field behaviour for the last few millenia for the SW Pacific and investigate non dipole behaviour, many more data are needed.

This set of archaeointensity results appears to display serial correlation through time which, if shown to be statistically significant, would further support them as representing geomagnetic field variations. In order to apply some quantitative non-parametric test for serial correlation in our dataset, a Non-Random-Ordering (NRO) factor was calculated for the archaeointensity (F) and VADM values from Duke of York Islands, Lakeba (Fiji) and Vanuatu (Biggin et al., 2008). Both NRO factors given for F and VADM are significant at the 95% level of confidence indeed indicating statistically significant serial correlation.

9.5 Potential of archaeomagnetic dating of Lapita sites.

For the first time an attempt at archaeomagnetic dating of south west Pacific pottery has been undertaken. Samples from sites RF-2, RF-6 and SZ-8 on the Santa Cruz Islands were investigated and the obtained archaeointensities compared to the SWP data set (Fig. 9.4). As already mentioned in Section 7.7, significant differences in the estimated archaeointensities of the sites RF-2 and RF-6 compared to site SZ-8 suggest

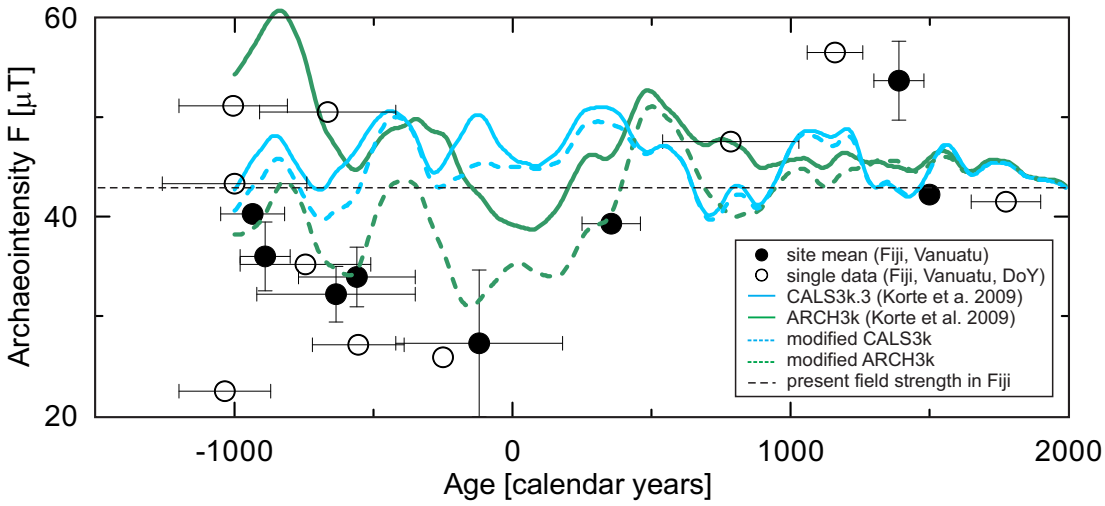

Figure 9.3: Archaeointensity results relocated to Fiji, Lakeba obtained from Fijian, Vanuatuan and Duke of York potsherds. When possible mean values were calculated. Blue (CALS3k.3) and green (ARCH3k) lines represent intensity models after Korte et al. (2009) calculated for Fiji, Lakeba. The modified models using data from Fiji, Vanuatu and DoY are shown in dashed blue (CALS3k.3) and dashed green (ARCH3k) lines. The dashed black line illustrates the present field strength in Fiji, Lakeba

different ages. The intensities of sites RF-2, RF-6 and SZ-8 ($\sim$ 39 μT) were compared with a curve averaged over a 200 yrs gliding window. An error envelope of this curve was calculated from the standard deviations of values within an averaged interval (window). Using an average over 200 years has the advantage of limiting possible outliers and age uncertainties without losing too much information about the regional geomagnetic secular variation. Big uncertainties with standard deviations of more then 10 μT are shown for the time period around 1000 BC, 0 AD and 1200 AD.

Intensity from site RF-6 ($\sim$ 23 μT thick blue line) indicates ages of around 1000 BC and/or between 250 BC and 0 AD. The validity of the result from site RF-6 is limited since it comprises only a mean value from a single sample and also the acceptance criteria were loosened. An intensity mean value obtained from three individual potsherds from site RF-2 ($\sim$ 27 μT thick green line) gives a more robust intensity result of around 27 μT and indicates ages of around 1000 BC and/or between 500 BC and 0 AD. For both sites RF-2 and RF-6 ages after 0 AD are unlikely. Comparing the intensity mean value from site SZ-8 ($\sim$ 39 μT thick orange line) to the averaged SWP data curve hardly gives a clue about the age. It can be nearly any age but probably not between around 500 BC and 200 BC.

Despite the fact that there are not enough data yet to establish a statistically-robust master curve for reliable dating, the example given from sites RF-2 and SZ-8 provides a hint about the ages. As there are no directional data available absolute dating of archaeological artefacts seems to be difficult in the near future. Nevertheless

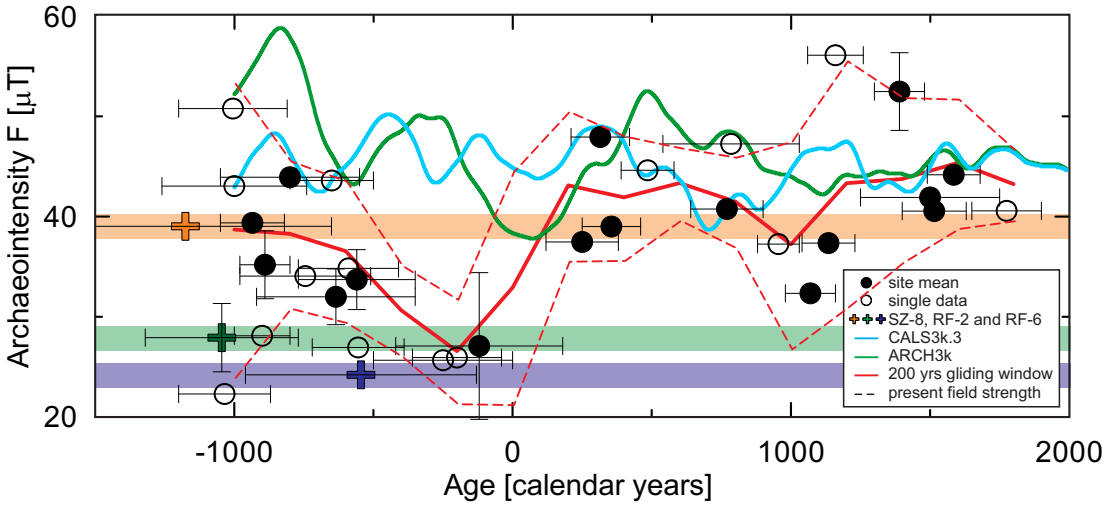

Figure 9.4: An attempt at archaeomagnetic dating of the sites RF-2, RF-6 and SZ-8 from the Santa Cruz Islands. A 200 yrs gliding window with error envelopes helps to fit in intensities in possible age intervals.

a determination of relative ages is feasible and can help archaeologists to interpret their results in particular when radiocarbon dating is not possible.

9.6 Possible occurrence of archaeomagnetic jerks in the south west Pacific and their implications

Gallet et al. (2003) coined the term "archaeomagnetic jerks" and described them as a coincidence of an erratic change of the direction and strong increase of the intensity of the Earth's magnetic field. Archaeomagnetic jerks range on a time scale between geomagnetic jerks $\sim$ 1 year (Courtillot and Le Mouel, 1988) and magnetic excurions $\sim 10^3$ years (Valet and Meynadier, 1993). The archaeointensity curve from the south west Pacific suggests two strong archaeointensity increases between 200 AD and 400 AD and 1200 AD and 1400 AD which could be a first indication of archaeomagnetic jerks (Fig. 9.5a). Unfortunately there are no measured directional data available from the SWP to compare to these intensity maxima. The closest directional data set stem from Lake Eacham in north eastern Australia (Constable and McElhinny, 1985), but even when averaging with 200 years gliding windows, strong variations of the directions obscure any real trends. Directions were therefore derived from the CALS3k.3 model (Korte et al., 2009) although the validity is very limited, as has been primarily discussed, the model is not very well constrained for this region. The directional data (Fig. 9.5b) indicate several sharp changes in directions, where two of them around 200 AD and/or 450 AD and 1160 AD and/or 1400 AD could correlate with strong increases of the archaeointensity. For these error estimations in the form of ellipses are given (Fig. 9.5b) after Korte et al. (2009).

Comparing the SWP archaeointensity curve with data from Syria and France (Genevey and Gallet, 2002; Gallet et al., 2003) reveals no significant similarities (Fig. 9.5c). Although the intensity peaks shown in both diagrams do not perfectly coincide there is a possibility of a contemporaneous occurrence within the scope of the age uncertainties. This would imply that archaeomagnetic jerks are a global phenomena and not restricted to certain regions.

Studies of Gallet et al. (2005) suggest that archaeomagnetic jerks can have an impact on interactions between cosmic radiation, like the solar wind, and the atmosphere. They correlate four potential archaeomagnetic jerks with contemporaneous cooling episodes in the North Atlantic and the occurrence of enhanced aridity in the Middle East which in turn triggered abrupt upheavals in societies in the eastern Mediterranean and Mesopotamia. Although the authors admit that these coincidences must be considered with caution they do not exclude the possibility that the geomagnetic field can indirectly influence the history of ancient civilizations.

A potential archaeomagnetic jerk in the south west Pacific correlates with the so-called "A.D. 1300 event" (Fig. 9.5a), which is regarded as a transitional period between the Medieval Climate Optimum ($\sim$ 750 AD to 1250 AD) and the Little Ice Age ($\sim$ 1350 AD to 1800 AD Nunn (2007). This event ($\sim$ 1250 AD to $\sim$ 1350 AD) is characterized by a strong centennial climatic change exhibiting a rapid cooling, sea-level fall ($\sim$ 80 cm) and possible increased storminess in the entire Pacific Basin (Kumar et al., 2006; Nunn, 2007). Most Pacific societies were affected by this rapid climate change which led to outbreaks of conflicts about food resources and also to an abrupt end to long distance inter-island voyaging during the following Little Ice Age (Nunn, 2007).

It is an interesting fact that New Zealand was not discovered for more than 2500 years after the first humans started to venture into remote Oceania. Recent radiocarbon investigations assume that New Zealand was first settled by Polynesian voyagers between 1250 AD and 1300 AD (Hogg et al., 2003; Lowe, 2008). Maybe trade winds and/or currents, which had until then isolated New Zealand from discovery, changed due to the AD 1300 effect and opened doors for the colonisation of New Zealand. Hence it is possible that by influencing the climate in a way responsible for social changes in the Middle East Gallet et al. (2006), archaeomagnetic jerks were the key to the discovery of New Zealand. Assumptions about archaeomagnetic jerks in the SWP and Europe need to be treated with caution since the resolution of the data is too small to make a firm statement. Identification of an archaeomagnetic jerk around 1250 AD uses data from three different island groups and therefore it cannot be excluded that the possible sharp intensity increase is a result of different field evolutions on these islands (see Section 9.2). Also the role of such a geomagnetic event on climate changes is not yet clarified since the climate itself has a very complex nature governed by many factors.

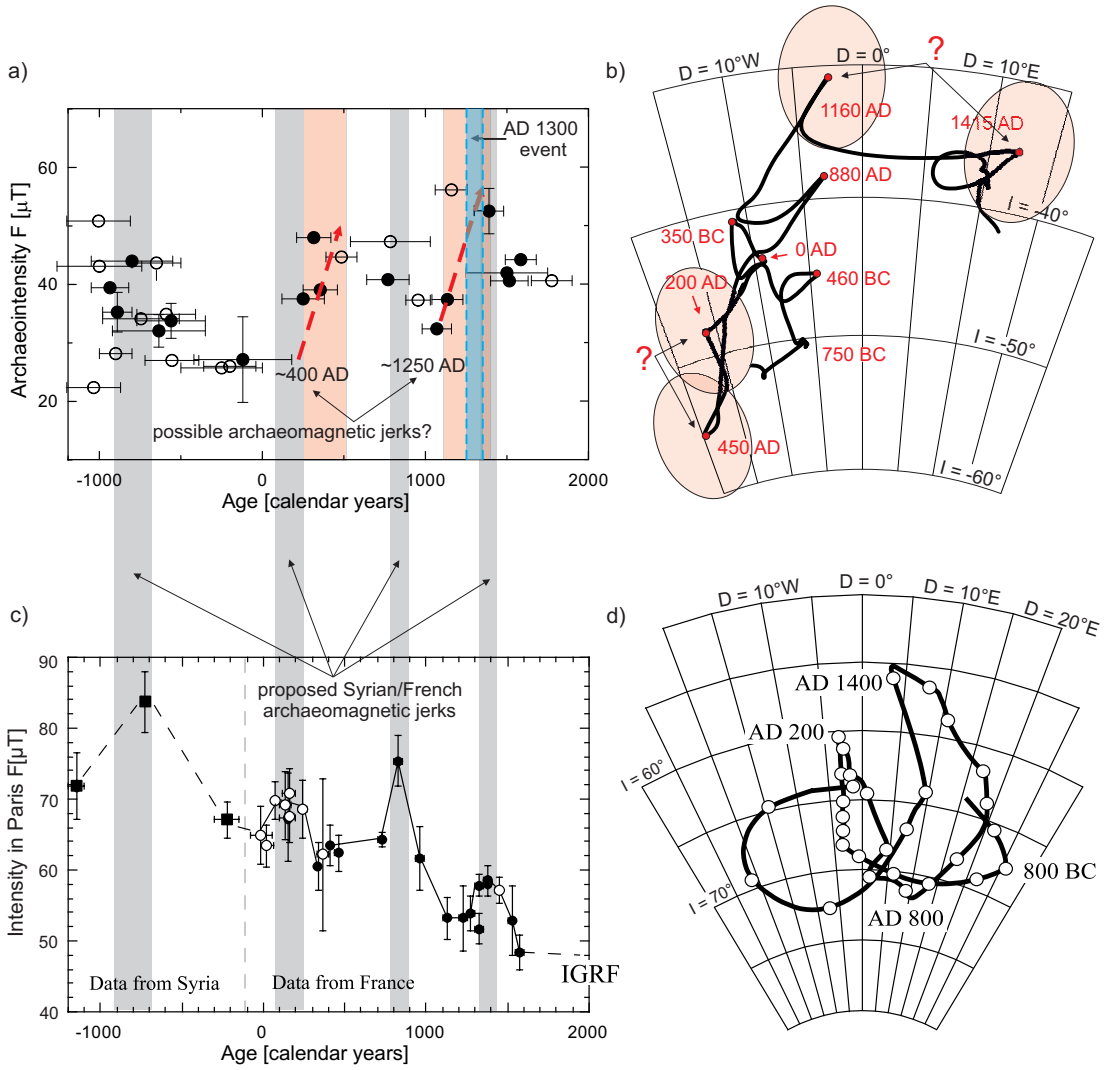

Figure 9.5: Following panels show comparisons of archaeointensity data from the SWP with directional data obtained from CALS3k.3 recalculated for Efate (Vanuatu) as well as data sets from Syria and France with their proposed archeomagnetic jerks after Gallet et al. (2003). (a) shows intensity mean values from the SW Pacific. Strong intensity rises hinting an archaeomagnetic jerks are indicated with dashed lines. The climatic AD 1300 event is highlighted in blue and coincides with an archaeomagnetic jerk. (b) exhibits proposed directional variations (inclination and declination) after CALS3k.3 (Korte et al., 2009). (c) illustrates data from Syria and France with possible archaeomagnetic jerks juxtaposed with the SW Pacific data. (d) presents the directional variations in France after (Gallet et al., 2003).

Chapter 10

Conclusions

Ceramic samples from four locations across the SW Pacific have yielded high quality archaeomagnetic field strength determinations using the microwave technique. A cross-check with the conventional Thellier technique showed good agreement. Of the 226 well dated potsherds available, 24% gave robust archaeointensity estimates. A success rate of 24% is quite low for ceramics in general, but rather high considering the crude pottery manufacturing techniques (especially the open-fire heating). Most rejected samples did not contain a stable characteristic remanent magnetization and were therefore not suitable for archaeointensity study. With the exception of samples from the Duke of York Islands, the remaining 24 potsherds from the Bismarck Archipelago did not demagnetise enough using the microwave technology and were therefore rejected.

Rock magnetic investigations, using a VFTB, revealed similar results for all studied samples from the south west Pacific islands. Typically single Curie temperatures were found between 460°C to 580°C suggesting an impure to pure magnetite phase with hysteresis parameters indicating an assemblage of pseudo single domain grains. Some samples from Efate showed Curie temperatures around both 350°C and 500°C indicating the presence of two ferrimagnetic phases, which is probably a result of a low intensity firing of the ancient pottery. After heating up to 700°C the lower phase vanishes. Additional SEM and EDX studies were performed on selected samples and revealed some differences in the clay matrix between the various island regions. This is probably a result of the different admixtures and varying clay sources. Titanomagnetite grains ($> 50\mu$m) have been found in nearly all the thin sections and were probably introduced into the clay matrix by adding beach or river sand during the manufacturing process. Nevertheless, it is considered that the stable remanence is carried by grains smaller than 1 μm, which is too small to be resolved by the SEM.

After sample pre-selection using the microwave demagnetisation technique, 51% of the archaeointensity experiments yielded acceptable results. The outcome of Thellier experiments (on preselected samples), was rather poor (success rate of 23%), due to many samples altering during the frequent heating and cooling cycles. Also the friability

of some samples resulted in some mass loss during sample mounting. Therefore the use of the microwave technique in the case of these, and possibly other SW Pacific ceramics, potentially increases the success rate considerably.

Between 1000 BC and 250 AD these new archaeointensity data from the SW Pacific, plot significantly lower than the values based on the most recently published global field models (CALS3k.3 and ARCH3k) and reveal a minimum field strength around 250 BC. There is an indication of a second minimum around 1100 AD which is only shown by the data from New Caledonia. Between 1200 AD and 1400 AD data from Fiji and Vanuatu indicate an intensity maximum. Unfortunately no data were available from New Caledonia for this time period. A strong increase of the geomagnetic field strength around 1400 AD was already reported by Genevey and Gallet (2002) for France and described as an archaeomagnetic jerk (Gallet et al., 2003). A correlation with the SWP data could be just a coincidence or could identify a global feature. Following Gallet et al. (2006), there is a possibility that a strong increase in geomagnetic field strength has an impact on atmospheric interactions with extraterrestrial radiation and thus influences the climate. A rapid climate change with implications on the islanders in the Pacific basin around 1300 AD was reported by Nunn (2007). Furthermore, the first colonisation of New Zealand by the Polynesians occurred at about this period. Further indication for a strong intensity increase between 200 AD and 400 AD was also found and seems to coincide with an archaeomagnetic jerk in France. Lacking a dense archaeointensity data coverage as well as directional data for the south west Pacific region it is not possible to make a firm statement about the occurrence of geomagnetic events like archaeomagnetic jerks at the present time.

A first attempt at archaeomagnetic dating in the SWP of potsherds from the Santa Cruz Islands (on 63 individual potsherds) using the available archaeointensity data, suggests that samples from site RF-2 and RF-6 date from before 0 AD. Additionally, low intensity values of samples from RF-2 and RF-6 contrast with a significantly higher value from potsherds found at site SZ-8, which indicates a different age for this site. Although this seems to be a very crude and inaccurate dating method it can provide vital information to archaeologists when little or no dating information are given, as is the case for the Santa Cruz Islands. It has to be admitted that the success rate ($< 10\%$) of these samples was poor.

Global models (ARCH3k and CALS3k.3) have been re-run by M. Korte using data from Fiji (Lakeba), Vanuatu and DoY, which resulted in a demonstrable impact on the models in the SW Pacific region. This clearly shows that the current models for the region are not well constrained and that even a small dataset such as this can result in significant enhancement of the global model.

This study has provided a very sound platform for future research by demonstrating the feasibility of the archaeomagnetic method in the region, identifying which

archaeological sites and ceramic materials appear to give the best chance of success, and what experimental methods are best suited to the task.

The key future research direction is the ongoing and systematic building of an archaeomagnetic master curve for the SW Pacific region to provide a new and robust dating tool for Pacific archaeological artefacts. Unfortunately, as kilns were not used in this region, recovery of the full geomagnetic vector will be problematic. Notwithstanding this, a further analysis of these and other ceramic samples from similar archaeological sites in the southern hemisphere can be expected to provide new and high quality values of archaeointensity, which will play an important role in understanding geomagnetic field behavior over the last few millenia in the SW Pacific, improving the global field models, and opening up new avenues for archaeologists by providing a new dating tool.

References

Aitken, M., Alcock, P., Bussell, G., Shaw, J., 1981. Archaeomagnetic determination of the past geomagnetic intensity using ancient ceramics: Allowance for anisotropy. Archaeometry 23 (1), 53–64.

Barbetti, M., 1977. Measurements of recent geomagnetic secular variation in southeastern Australia and the question of dipole wobble. Earth and Planetary Science Letters 36 (1), 207–218.

Barbetti, M., 1983. Results from Australia. In: Creer, K. M., Tucholka, P., Barton, C. E. (Eds.), Geomagnetism of Baked Clays and Recent Sediments. Elsevier, Amsterdam, pp. 173–175.

Barbetti, M., Polach, H. A., 1973. ANU Radiocarbon Date List V. Radiocarbon 15, 241–251.

Barton, C. E., McElhinny, M. W., 1982. Time-series analysis of the 10000 yr geomagnetic secular variation record from SE Australia. Geophysical Journal of the Royal Astronomical Society 68 (3), 709–724.

Bellwood, P., 1978. Man's conquest of the Pacific: the prehistory of Southeast Asia and Oceania. Auckland: Collins.

Bellwood, P., 1991. The Austronesian dispersal and the origin of languages. Scientific American 265 (1), 88–93.

Best, S., 1984. Lakeba: the prehistory of a Fijian island. Ph.D. thesis, University of Auckland.

Best, S., 2002. Lapita: a view from the east. New Zealand Archaeological Association Monographs 24.

Biggin, A. J., Perrin, M., Shaw, J., 2007. A comparison of a quasi-perpendicular method of absolute palaeointensity determination with other thermal and microwave techniques. Earth and Planetary Science Letters 257 (3-4), 564–581.

Biggin, A. J., Thomas, D. N., 2003. The application of acceptance criteria to results of Thellier palaeointensity experiments performed on samples with pseudo-single-domain-like characteristics. Physics of the Earth and Planetary Interiors 138 (3-4), 279–287.

Biggin, A. J., van Hinsbergen, D. J. J., Langereis, C. G., Straathof, G. B., Deenen, M. H. L., 2008. Geomagnetic secular variation in the Cretaceous Normal Superchron and in the Jurassic. Physics of the Earth and Planetary Interiors 169 (1-4), 3–19.

Bloemendal, J., King, J. W., Hall, F. R., Doh, S.-J., 1992. Rock magnetism of late Neogene and Pleistocene deep-sea sediments: Relationship of sediment source, diagenetic processes and sediment lithology. Journal of Geophysical Research 97, 4361–4375.

Böhnel, H. N., Dekkers, M. J., Delgado-Argote, L. A., Gratton, M. N., 2009. Comparison between the microwave and multispecimen parallel difference pTRM paleointensity methods. Geophysical Journal International 177 (2), 383–394.

Bol'shakov, A. S., Shcherbakova, V. V., 1979. A thermomagnetic criterion for determining the domain structure of ferrimagnetics. Izv. Acad. Sci. USSR Phys. Solid Earth, Engl. Trans. 15, 111–117.

Bowles, J., Gee, J., Hildebrand, J., Tauxe, L., 2002. Archaeomagnetic intensity results from California and Ecuador: evaluation of regional data. Earth and Planetary Science Letters 203, 967–981.

Brabers, V. A. M., 1995. Progress in spinel ferrite research. In: Buschow, K. (Ed.), Handbook of Ferromagnetic Materials. Vol. 8. Elsevier, Amsterdam, pp. 189–324.

Bronk Ramsey, C., 2001. Development of the Radiocarbon calibration program OxCal. Radiocarbon 43, 355–363, Proceedings of 17th International 14C Conference.

Bronk Ramsey, C., 2009. Bayesian analysis of radiocarbon dates. Radiocarbon 51 (1), 337–360.

Brookfield, H. C., Hart, D., 1971. Melanesia: A Geographical Interpretation of an Island World. London: Methuen & Co.

Brown, M., 2008. The Matuyama-Brunhes geomagnetic field reversal: a global and temporal perspective. Ph.D. thesis, University of Liverpool, 20841.BRO.

Brown, M. C., Shaw, J., Goguitchaichvili, A. T., 2006. Microwave palaeointensity from the R3-N3 geomagnetic field reversal. Geophysical Journal International 167 (1), 53–69.

Burr, G. S., Beck, J. W., Taylor, F. W., Recy, J., Edwards, R. L., Cabioch, G., Correge, T., Donahue, D. J., O'Malley, J. M., 1998. A high-resolution radiocarbon calibration between 11,700 and 12,400 calendar years BP derived from Th-230 ages of corals from Espiritu Santo Island, Vanuatu. Radiocarbon 40 (3), 1093–1105.

Butler, R. F., 1992. Paleomagnetism: Magnetic Domains to Geologic Terranes. Boston: Blackwell Scientific Publications.

Butler, R. F., Banerjee, S. K., 1975. Theoretical single-domain size range in magnetite and titanomagnetite. Journal of Geophysical Research 80, 4049–4058.

Casas, L., Incoronato, A., 2007. Distribution analysis of errors due to relocation of geomagnetic data using the 'Conversion via Pole' (CVP) method: implications on archaeomagnetic data. Geophysical Journal International 169 (2), 448–454, doi:10.1111/j.1365-246X.2007.03346.x.

Chauvin, A., Garcia, Y., Lanos, P., Laubenheimer, F., 2000. Paleointensity of the geomagnetic field recovered on archaeomagnetic sites from France. Physics of the Earth and Planetary Interiors 120, 111–136.

Clark, G., Anderson, A., 2009. Site chronology and review of radiocarbon dates from Fiji. In: Clark, G., Anderson, A. (Eds.), The early prehistory of Fiji. pp. 153–181.

Coe, R. S., 1967a. The determinations of paleointensities of the Earth's magnetic field with emphasis on mechanisms which could cause non-ideal behavior in Thellier's method. Journal of Geomagnetism and Geoelectricity 19, 157–179.

Coe, R. S., 1967b. Palaeointensity of the Earth's magnetic field determined from Tertiary and Quaternary rocks. Journal of Geophysical Research 72, 3247–3262.

Coe, R. S., 1974. The effect of magnetic interactions on paleointensity determinations by the Thellier's method. Journal of Geomagnetism and Geoelectricity 26, 311–317.

Coe, R. S., Grommé, S., Mankinen, E. A., 1978. Geomagnetic paleointensities from radiocarbon-dated lava flows on Hawaii and the question of the Pacific nondipol low. Journal of Geophysical Research 83, 1740–1756.

Constable, C., 1985. Eastern Australian geomagnetic-field intensity over the past 14000 yr. Geophysical Journal of the Royal Astronomical Society 81 (1), 121 – 130.

Constable, C. G., McElhinny, M. W., 1985. Holocene geomagnetic secular variation records from Northeastern Australian lake-sediments. Geophysical Journal of the Royal Astronomical Society 81 (1), 103–120.

Courtillot, V., Le Mouel, J., 1988. Time variations of the Earth's magnetic field: From daily to secular. Annu. Rev. Earth Planet. Sci. 16, 389–476.

Davies, C., 2009. Assessing the effect of mineral alteration on palaeointensities derived from volcanic rocks of Cretaceous age. Ph.D. thesis, University of Liverpool, 20941.DAV.

Day, R., Fuller, M. D., Schmidt, V. A., 1977. Hysteresis properties of titanomagnetites: Grain size and composition dependence. Physics of the Earth and Planetary Interiors 13, 260–266.

De Marco, E., Spatharas, V., Gomez-Paccard, M., Chauvin, A., Kondopoulou, D., 2008. New archaeointensity results from archaeological sites and variation of the geomagnetic field intensity for the last 7 millennia in Greece. Physics and Chemistry of the Earth 33 (6-7), 578–595, doi:10.1016/j.pce.2008.02.025.

Dickinson, W., 2009. Petrography of sand tempers in 73 Lapita vessels, Teouma, Efate, Vanuatu. Unpublished Petrographic Report WRD-282 .

Dickinson, W. R., 2006. Temper Sands in Prehistoric Oceanian Pottery: Geotectonics, Sedimentology, Petrography, Provenance. Geological Society of America Special Papers 406, 1–160.

Dodson, M. H., McClelland-Brown, E., 1980. Magnetic blocking temperatures of single-domain grains during slow cooling. Journal of Geophysical Research 85, 2625–2637.

Donadini, F., Korhonen, K., Riisager, P., L., P., 2006. Database for Holocene geomagnetic intensity information. EOS, Transactions, American Geophysical Union 87 (14), doi:10.1029/2008gc002295.

Donadini, F., Korte, M., Constable, C. G., 2009. Geomagnetic field for 0-3 ka: 1. New data sets for global modeling. Geochemistry, Geophysics, Geosystems 10, doi:10.1029/2008GC002295.

Donadini, F., Riisager, P., Korhonen, K., Kahma, K., Pesonen, L., Snowball, I., 2007. Holocene geomagnetic paleointensities: A blind test of absolute paleointensity techniques and materials. Physics of the Earth and Planetary Interiors 161 (1-2), 19–35.

Dunlop, D. J., 2002a. Theory and application of the Day plot (Mrs/Ms versus Hcr/Hc) 1. Theoretical curves and tests using titanomagnetite data. Journal of Geophysical Research 107, doi:10.1029/2001JB000486.

Dunlop, D. J., 2002b. Theory and application of the Day plot (Mrs/Ms versus Hcr/Hc) 2. Application to data for rocks, sediments, and soils. Journal of Geophysical Research 107, doi:10.1029/2001JB000487.

Dunlop, D. J., Özdemir, Ö., 1997. Rock magnetism: fundamentals and frontiers. Cambridge Univ. Press.

Encyclopaedia Britannica, 2011a. Fiji. Encyclopaedia Britannica online . URL http://www.britannica.com/EBchecked/topic/206686/Fiji

Encyclopaedia Britannica, 2011b. New Caledonia. Encyclopaedia Britannica online . URL http://www.britannica.com/EBchecked/topic/623102/Newcaledonia

Encyclopaedia Britannica, 2011c. Solomon Islands. Encyclopaedia Britannica online . URL http://www.britannica.com/EBchecked/topic/533556/Solomon-Islands

Encyclopaedia Britannica, 2011d. Vanuatu. Encyclopaedia Britannica online . URL http://www.britannica.com/EBchecked/topic/623102/Vanuatu

Fabian, K., 2003. Some additional parameters to estimate domain state from isothermal magnetization measurements. Earth and Planetary Science Letters 213, 337–345.

Felgate, M., 2003. Reading lapita in Near Oceania: Intertidal Shallow-water Pottery Scatters, Roviana Lagoon, New Georgia, Solomon Islands. Ph.D. thesis, University of Auckland.

Firth, S., 1983. New Guinea under the Germans. Carlton, Australia: Melbourne University Press.

Fisher, R. A., 1953. Dispersion on a sphere. Proc. R. Soc. London A 217, 295–305.

Fox, J. M. W., Aitken, M. J., 1980. Cooling-rate dependency of thermoremanent magnetisation. Nature 283, 462–463.

Franklin, J., Keppel, G., Whistler, A., 2008. The vegetation and flora of Lakeba, Nayau and Aiwa Islands, Central Lau Group, Fiji. Micronesia 40 (1-2), 169–225.

Fuller, B., 1987. Ferrites at Microwave Frequencies. Peregrinus, London.

Gallet, Y., Genevey, A., Courtillot, V., 2003. On the possible occurrence of 'archaeomagnetic jerks' in the geomagnetic field over the past three millennia. Earth and Planetary Science Letters 214 (1-2), 237–242.

Gallet, Y., Genevey, A., Fluteau, F., 2005. Does Earth's magnetic field secular variation control centennial climate change? Earth and Planetary Science Letters 236 (1-2), 339 – 347.

Gallet, Y., Genevey, A., Le Goff, M., Fluteau, F., Ali Eshraghi, S., 2006. Possible impact of the Earth's magnetic field on the history of ancient civilizations. Earth and Planetary Science Letters 246 (1-2), 17 – 26, doi:10.1016/S0012-821X(01)00259-X.

Gallet, Y., Genevey, A., Le Goff, M., Warmé, N., Gran-Aymerich, J., Lefèvre, A., 2009. On the use of archeology in geomagnetism, and vice-versa: Recent developments in archeomagnetism. Comptes Rendus Physique 10, 630–648.

Genevey, A., Gallet, Y., 2002. Intensity of the geomagnetic field in western Europe over the past 2000 years: New data from ancient French pottery. Journal of Geophysical Research 107, EPM1.1–EPM1.17.

Genevey, A., Gallet, Y., Constable, C. G., Korte, M., Hulot, G., 2008. ArcheoInt: An upgraded compilation of geomagnetic field intensity data for the past ten millennia and its application to the recovery of the past dipole moment. Geochemistry, Geophysics, Geosystems 9 (4).

Genevey, A., Gallet, Y., Rosen, J., Le Goff, M., 2009. Evidence for rapid geomagnetic field intensity variations in Western Europe over the past 800 years from new French archeointensity data. Earth and Planetary Science Letters 284 (1-2), 132–143.

Goldstein, J., Newbury, D., Echling, P., Joy, D., Romig, A., Lyman, C., Fiori, C., Lifshin, E., 1992. Scannning electron microscopy and X-Ray microanalysis (second edition). Plenum Press, New York.

Gratton, M., 2004. Variation of geomagnetic field intensity over the last 45,000 years in Hawaii using the microwave palaeointensity technique. Ph.D. thesis, University of Liverpool, 20441.GRA.

Green, R., 1979. Lapita. In: Jennings, J. (Ed.), The prehistory of Polynesia. Cambridge: Harvard University Press, pp. 27–60.

Green, R., 1991. Near and Remote Oceania: disestablishing "Melanesia" in culture history. In: Pawley, A. (Ed.), Man and a Half: Essays in Pacific Anthropology and Ethnobiology in Honour of Ralph Bulmer. The Polynesian Society, Auckland, pp. 491–502.

Green, R., 1993. Changes over time: recent advances in dating human colonisation of the Pacific basin area. In: Sutton, D. (Ed.), Origin of the first New Zealanders. pp. 11–42.

Green, R., Jones, M., 2008. The absolute age of SE-RF-6 (Ngamanie) and its relation to SE-RF-2 (Nenumbo): two decorated Lapita sites in the south-east Solomon Islands. New Zealand Journal of Archaeology 29, 5–18.

Green, R. C., Jones, M., Sheppard, P., 2008. The reconstructed environment and absolute dating of SE-SZ-8 Lapita site on Nendo, Santa Cruz, Solomon Islands. Archaeology in Oceania 43 (2), 49–61.

Halgedahl, S. L., Day, R., Fuller, M., 1980. The effect of cooling rate on the intensity of weak-field TRM in single-domain magnetite. Journal of Geophysical Research 85, 3690–3698.

Hill, M., 2000. The microwave palaeointensity technique and its application to lava. Ph.D. thesis, University of Liverpool, 20041.HIL.

Hill, M. J., Gratton, M. N., Shaw, J., 2002. A comparison of thermal and microwave palaeomagnetic techniques using lava containing laboratory induced remanence. Geophysical Journal International 151 (1), 157–163.

Hill, M. J., Lanos, P., Chauvin, A., Vitali, D., Laubenheimer, F., 2007. An archaeomagnetic investigation of a Roman amphorae workshop in Albinia (Italy). Geophysical Journal International 169 (2), 471–482.

Hogg, A., Higham, T., Lowe, D., Palmer, J., Reimer, P., Newnham, R., 2003. Polynesian settlement of New Zealand and the impacts of volcanism on early Maori society: an update. Antiquity 77, 116–125.

Irwin, G., 1985. The emergence of Mailu as a central place in coastal Papuan prehistory. In: Dept. of Prehistory, R. S. o. P. S. (Ed.), Terra Australis 10. Dept. of Prehistory, Research School of Pacific Studies, Canberra, pp. 253–262.

Irwin, G., 1992. The Prehistoric Exploration and Colonisation of the Pacific. Cambridge University Press, Cambridge.

Jackson, A., Jonkers, A. R. T., Walker, M. R., 2000. Four centuries of geomagnetic secular variation from historical records. Philosophical Transactions of the Royal Society of London Series a-Mathematical Physical and Engineering Sciences 358 (1768), 957–990.

Jones, M., Petchey, R., Sheppard, P., Phelan, M., 2001. The Marine δR for Nenumbo (Solomon Islands): a case study in calculating reservoir offsets from paired sample data. Radiocarbon 49 (1), 95–102.

Kirch, P., 1997. The Lapita Peoples: Ancestors of the Oceanic World. Blackwell, Cambridge.

Kirch, P., 2000. On the Road of the Winds. An Archaeological History of the Pacific Islands before European Conquest. University of California Press.

Knauft, B., 1999. From primitive to postcolonial in Melanesia and anthropology. University of Michigan Press.

Knudsen, M. F., Riisager, P., Donadini, F., Snowball, I., Muscheler, R., Korhonen, K., Pesonen, L. J., 2008. Variations in the geomagnetic dipole moment during the Holocene and the past 50 kyr. Earth and Planetary Science Letters 272 (1-2), 319–329, doi:10.1016/j.epsl.2008.04.048.

Kono, M., Tanaka, H., 1984. Analysis of Thellier's method of paleointensity determination 1: Estimation of statistical errors. J.Geomagn.Geoelectr. 36, 267–284.

Korhonen, K., Donadini, F., Riisager, P., Pesonen, L., 2008. GEOMAGIA50: an archeointensity database with PHP and MySQL. Geochemistry, Geophysics, Geosystems 9, doi:10.1029/2007GC001893.

Korte, M., Constable, C. G., 2005. Continuous geomagnetic field models for the past 7 millennia: 2. CALS7K. Geochemistry, Geophysics, Geosystems 6, doi:10.1029/2004GC000801.

Korte, M., Donadini, F., Constable, C. G., 2009. Geomagnetic field for 0-3 ka: 2. A new series of time-varying global models. Geochemistry, Geophysics, Geosystems 10, doi:10.1029/2008GC002297.

Kovacheva, M., Chauvin, A., Jordanova, N., Lanos, P., Karloukovski, V., 2009. Remanence anisotropy effect on the palaeointensity results obtained from various archaeological materials, excluding pottery. Earth Planets and Space 61 (6), 711–732.

Kovacheva, M., Hedley, I., Jordanova, N., Kostadinova, M., Gigov, V., 2004. Archaeomagnetic dating of archaeological sites from Switzerland and Bulgaria. Journal of Archaeological Science 31 (10), 1463–1479.

Krása, D., Herrero-Bervera, E., 2005. Alteration induced changes of magnetic fabric as exemplified by dykes of the Koolau volcanic range. Earth and Planetary Science Letters 240 (2), 445 – 453, doi:10.1016/j.epsl.2005.09.028.

Krása, D., Heunemann, C., Leonhardt, R., Petersen, N., 2003. Experimental procedure to detect multidomain remanence during Thellier-Thellier experiments. Phys. Chem. Earth 28, 681–687.

Krása, D., Petersen, K., Petersen, N., 2007. Variable Field Translation Balance. In: Gubbins, D., Herrero-Bervera, E. (Eds.), Encyclopedia of Geomagnetism and Paleomagnetism. pp. 977–979.

Kumar, R., Nunn, P., Field, J., de Biran, A., 2006. Human responses to climate change around AD 1300: A case study of the Sigatoka Valley, Viti Levu Island, Fiji. Quaternary International 151, 133–143.

Ladd, H. S., Hoffmeister, J. E., 1945. Geology of Lau, Fiji. Honolulu: Bernice P. Bishop Museum.

Le Goff, M., Gallet, Y., 2004. A new three-axis vibrating sample magnetometer for continuous high-temperature magnetization measurements: applications to paleo- and archeo-intensity determinations. Earth and Planetary Science Letters 229 (1-2), 31–43.

Leonhardt, R., 2006. Analyzing rock magnetic measurements: The RockMagAnalyzer 1.0 software. Comp. Geosci. 32, 1420–1431.

Leonhardt, R., Heunemann, C., Krasa, D., 2004a. Analyzing absolute paleointensity determinations: Acceptance criteria and the software ThellierTool4.0. Geochemistry, Geophysics, Geosystems 5, doi:10.1029/2004GC000807.

Leonhardt, R., Krása, D., Coe, R. S., 2004b. Multidomain behavior during Thellier paleointensity experiments: A phenomenological model. Physics of the Earth and Planetary Interiors 147, 127–140.

Leonhardt, R., Matzka, J., Menor, E. A., 2003. Absolute paleointensities and paleodirections from Fernando de Noronha, Brazil. Physics of the Earth and Planetary Interiors 139, 285–303.

Leonhardt, R., Matzka, J., Nichols, A., Dingwell, D., 2006. Cooling rate correction of paleointensity determination for volcanic glasses by relaxation geospeedometry. Earth and Planetary Science Letters 243, 282–292.

Leonhardt, R., Saleh, A., Ferk, A., 2010. Archaeomagnetic field intensity during the Roman period at Siwa and Bahryn oasis, Egypt: implications for the fidelity of Egyptian archaeomagnetic data. Archaeometry 52, 502–516, doi:10.1111/j.1475–4754.2009.00508.x.

Lowe, D., 2008. Polynesian settlement of New Zealand and the impacts of volcanism on early Maori society: an update. Lowe, D.J. (editor) Guidebook for Pre-conference North Island Field Trip A1 'Ashes and Issues'. Australian and New Zealand 4th Joint Soils Conference, Massey University, Palmerston North (1-5 Dec. 2008). New Zealand Society of Soil Science.

McClelland-Brown, E., 1984. Experiments on TRM intensity dependence on cooling rate. Geophys. Res. Lett. 11, 205–208.

McCormac, F. G., Hogg, A. G., Blackwell, P. G., Buck, C. E., Higham, T. F. G., Reimer, P. J., 2004. SHCal04 Southern Hemisphere calibration, 0-11.0 cal kyr BP. Radiocarbon 46 (3), 1087–1092.

McElhinny, M. W., Senanayake, W. E., 1982. Variations in the Geomagnetic Dipole1: the past 50,000 years. Journal of Geomagnetism and Geoelectricity 34, 39–51.

Moskowitz, B. M., 1981. Methods for estimating Curie temperatures of titanomagnetites from experimental J_s-T data. Earth and Planetary Science Letters 53, 84–88.

Nagata, T., 1943. The natural remanent magnetism of volcanic rocks and its relation to geomagnetic phenomena. Bull. Earthquake Res. Inst. Tokyo Univ. 21(1943) (p.1.).

Nagata, T., Momose, K., Arai, Y., 1963. Secular variation of geomagnetic total force during last 5000 years. Journal of Geophysical Research 68 (18), 5277–5281.

Néel, L., 1955. Some theoretical aspects of rock magnetism. Adv. Phys. 4, 191–243.

Nunn, P. D., 2007. The A.D. 1300 Event in the Pacific Basin. Geographical Review 97, 1–23, doi:10.1111/j.1931-0846.2007.tb00277.x.

O'Reilly, W., 1976. Magnetic minerals in the crust of the Earth. Report on the Progress of Physics 39, 857–908.

Özdemir, O., Dunlop, D., 1988. Crystallization remanent magnetization during the transformation of maghemite to hematite. Journal of Geophysical Research 93 (B6), 6530–6544.

Pavon-Carrasco, J., Rodriguez-Gonzales, J., Osete, M. L., Torta, J. M., 2011. A Matlab tool for archaeomagnetic dating. Journal of Archaeological Science 38, 408–419.

Petchey, F., Phelan, M., White, J. P., 2004. New Delta R values for the southwest Pacific Ocean. Radiocarbon 46 (2), 1005–1014.

Reimer, P., Baillie, M., Bard, E., Bayliss, A., Beck, J., Blackwell, P., Ramsey, C., Buck, C., Burr, G., Edwards, R., Friedrich, M., Grootes, P., Guilderson, T., Hajdas, I., Heaton, T., Hogg, A., Hughen, K., Kaiser, K., Kromer, B., McCormac, F., Manning, S., Reimer, R.W., R. D., Southon, J., Talamo, S., Turney, C., van der Plicht, J., Weyhenmeyer, C., 2009. IntCal09 and Marine09 radiocarbon age calibration curves, 0-50,000 years CAL BP. Radiocarbon 51 (4), 1111–1150.

Reimer, P., Reimer, R., 2007. Radiocarbon dating: Calibration. In: Scott, A. E. (Ed.), Encyclopedia of Quaternary Science. Elsevier, pp. 2941–2950.

Riisager, P., Riisager, J., 2001. Detecting multidomain magnetic grains in Thellier paleointensity experiments. Physics of the Earth and Planetary Interiors 125, 111–117.

Rogers, J., Fox, J. M. W., Aitken, M. J., 1979. Magnetic anisotropy in ancient pottery. Nature 277, 644–646.

Roth, K., 1935. Pottery making in Fiji. Royal Anthropological Institute of Great Britain and Ireland Vol.65, 217–233.

Sand, C., 1997. The chronology of Lapita ware in New Caledonia. Antiquity 71, 539–547.

Sand, C., 2001. Evolutions in the Lapita Cultural Complex: A View from the Southern Lapita Province. Archaeology in Oceania 36 (2), 65–76.

Schnepp, E., Lanos, P., 2005. Archaeomagnetic secular variation in Germany during the past 2500 years. Geophysical Journal International 163 (2), 479–490.

Selbekk, R. S., Trønnes, R. G., 2007. The 1362 A.D. Öræfajökull eruption, Iceland: petrology and geochemistry of large-volume homogeneous rhyolite. Journal of Volcanology and Geothermal Research 160, 42–58.

Selkin, P. A., Gee, J. S., Tauxe, L., Meurer, W. P., Newell, A. J., 2000. The effect of remanence anisotropy on paleointensity estimates: a case study from the Archean Stillwater Complex. Earth and Planetary Science Letters 183 (3-4), 403–416.

Selkin, P. A., Tauxe, L., 2000. Long-term variations in paleointensity. Phil. Trans. R. Soc. Lond. 358, 1065–1088.

Shashkanov, V. A., Metallova, V. V., 1972. Violation of Thellier's law for partial thermoremanent magnetizations. Izv. Acad. Sci. USSR Phys. Solid Earth, Engl. Trans. 3, 80–86.

Shaw, J., Share, J. A., 2007. A new automated microwave demagnetiser/remagnetiser system for palaeointensity studies. Fall Meet. Suppl., Eos Trans. AGU 88 (52) .

Shaw, J., Walton, D., Yang, S., Rolph, T. C., Share, J. A., 1996. Microwave archeointensities from Peruvian ceramics. Geophys. J. Int. 124, 241–244.

Shaw, J., Yang, S., Rolph, T. C., Sun, F. Y., 1999. A comparison of archaeointensity results from Chinese ceramics using microwave and conventional Thellier's and Shaw's methods. Geophysical Journal International 136 (3), 714–718.

Shcherbakov, V. P., McClelland, E., Shcherbakova, V. V., 1993. A model of multidomain thermoremanent magnetization incorporating temperature-variable domain structure. Journal of Geophysical Research 98, 6201–6216.

Shepard, A., 1963. Ceramics for the Archaeologist. Washington DC: Carnegie Institution of Washington .

Sheppard, P. J., Walter, R., 2006. A revised model of Solomon Islands culture history. Journal of the Polynesian Society 115 (1), 47–76.

Soffel, H. C., 1991. Paläomagnetismus und Archäomagnetismus. Springer-Verlag, Berlin, Heidelberg, New York.

Spriggs, M., 1997. The Island Melanesians. London: Blackwell Publishers.

Stark, F., Leonhardt, R., Fassbinder, J., Reindel, M., 2008. Archeointensities from Peruvian Ceramics: Implications for the occurrence of archeomagnetic jerks and their relationship to climatic changes. EGU Vienna .

Stark, F., Leonhardt, R., Reindl, M., Fassbinder, H., 2009. The field of sherds: Reconstructing geomagnetic field variations from Peruvian potsherds. In: Reindel, M., G.A., W. (Eds.), New technologies for archaeology. Multidisciplinary investigations in Palpa and Nasca, Peru, 1st Edition. Vol. First. Springer, Berlin, Heidelberg, Ch. 7, pp. 103–116.

Suttie, N., 2010. Geomagnetic field archaeointensities from Britain and the application of the microwave palaeointensity method to materials of different dielectric properties. Ph.D. thesis, University of Liverpool, 21041.SUT.

Suttie, N., Shaw, J., Hill, M. J., 2010. Direct demonstration of microwave demagnetization of a whole rock sample with minimal heating. Earth and Planetary Science Letters 292 (3-4), 357 – 362, doi:10.1016/j.epsl.2010.02.002,.

Tauxe, L., 1998. Paleomagnetic principles and practice. Kluwer Academic Publishers, London.

Tauxe, L., Mullender, T. A. T., Pick, T., 1996. Potbellies, wasp-waists, and superparamagnetism in magnetic hysteresis. Journal of Geophysical Research-Solid Earth 101 (B1), 571–583.

Teanby, N., Laj, C., Gubbins, D., Pringle, M., 2002. A detailed palaeointensity and inclination record from drill core SOH1 on Hawaii. Physics of the Earth and Planetary Interiors 131, 101–140.

Thellier, E., 1938. Sur l'aimantation des terres cuites et ses applications geophysiques. Ann. Inst. Globe Univ. Paris 16, 157–302.

Thellier, E., Thellier, O., 1959. Sur l'intensité du champ magnétique terrestre dans le passé historique et géologique. Ann. Géophys. 15, 285–376.

Thomas, D. N., Hill, M. J., Garcia, A. S., 2004. Comparison of the Coe-Thellier-Thellier and microwave palaeointensity techniques using high-titanium titanomagnetites: Results from a Tertiary basaltic intrusion from the Sydney Basin, New South Wales. Earth and Planetary Science Letters 229 (1-2), 15–29.

Turner, G. M., Lillis, D. A., 1994. A palaeomagnetic secular variation record for New Zealand during the past 2500 years. Physics of the Earth and Planetary Interiors 83 (3-4), 265–282.

Ulm, S., 2006. Australian marine reservoir effects: A guide to δR values. Australian Archaeology 63, 57–60.

Valet, J.-P., Brassart, J., Le Meur, I., Soler, V., Quidelleur, X., Tric, E., Gillot, P.-Y., 1996. Absolute paleointensity and magnetomineralogical changes. Journal of Geophysical Research 101 (B11), 25029–25044.

Valet, J.-P., Herrero-Bervera, E., LeMouel, J.-L., Plenier, G., 2008. Secular variation of the geomagnetic dipole during the past 2000 years. Geochemistry, Geophysics, Geosystems 9, doi:10.1029/2007GC001728.

Valet, J.-P., Meynadier, L., November 1993. Geomagnetic field intensity and reversals during the past four million years. Nature 366, 234–238.

Van der Plas, L., Tobi, A., 1965. A chart for determining the reliability of point counting results. American Journal of Science 263, 87–90.

Veitch, R. J., Hedley, I. G., Wagner, J.-J., 1984. An investigation of the intensity of the geomagnetic field during Roman times using magnetically anisotropic bricks and tiles. Arch. Sc. Genéve 37, 359–373.

Walton, D., 1988. The lack of reproducibility in experimentally determined intensities of the Earth's magnetic field. Reviews of Geophysics 26 (1), 15–22.

Walton, D., 2004. Avoiding mineral alteration during microwave magnetization. Geophysical Research Letters 31 (3), doi:10.1029/2003GL019011.

Walton, D., Share, J., Rolph, T. C., Shaw, J., 1993. Microwave magnetisation. Geophysical Research Letters 20 (2), 109–111.

Walton, D., Shaw, J., Share, J., Hakes, J., 1992. Microwave demagnetization. Journal of Applied Physics 71 (3), 1549–1551.

Wickler, S., 2001. The Prehistory of Buka: A stepping stone island in the northern Solomons. Terra Australis. Canberra: Department of Archaeology and Natural History and Centre for Archaeological Research, Australian National University 16.

Yang, S., Odah, H., Shaw, J., 2000. Variations in the geomagnetic dipole moment over the last 12000 years. Geophys. J. Int. 140 (1), 158–162.

Yu, Y., Dunlop, D. J., Özdemir, O., 2003. Are ARM and TRM analogs? Thellier analysis of ARM and pseudo-Thellier analysis of TRM. Earth and Planetary Science Letters 205, 325–336.

Yu, Y., Tauxe, L., Genevey, A., 2004. Toward an optimal geomagnetic field intensity determination technique. Geochemistry, Geophysics, Geosystems 5, doi:10.1029/2003GC000630.

Appendix A

VFTB investigations on SW Pacific ceramics

Table A.1: Results of the rock magnetic investigations of SW Pacific ceramics

Sample	Weight (mg)	M_{rs}	M_s	B_c	B_{cr}	M_{rs}/M_s	B_{cr}/B_c	S-300	shape	T_{C1}(HC)	T_{C2}(HC)	T_{C1}(CC)	T_{C2}(CC)
Fiji Lau Group													
Lakeba													
F2800-7	90	0.000589	0.005072	8.65	29.94	0.12	3.46	0.96	-0.9	530	0	526	0
F2800-6	40	0.000706	0.006424	7.98	27.37	0.11	3.43	0.97	-0.84	531	0	538	0
F2800-5	110	0.002029	0.008913	21.1	50.07	0.23	2.37	0.99	-0.96	510	0	523	0
F2800-4	100	0.001858	0.018262	8.83	34.62	0.1	3.92	0.97	-0.88	530	0	544	0
F2800-3	90	0.000687	0.004586	12.99	42.09	0.15	3.24	0.98	-0.88	522	0	517	0
F2800-2	110	0.000837	0.004674	12.21	36.86	0.18	3.02	0.97	-0.71	521	0	517	0
F2800-1	70	0.0002	0.000907	18.7	52.68	0.22	2.82	0.92	-0.74	511	0	527	0
F2700-5	90	0.004125	0.01729	18.33	42.17	0.24	2.3	1	-0.86	509	0	509	0
F2700-4	70	0.000495	0.002934	12.49	37.4	0.17	3	0.98	-0.77	527	0	520	0
F2700-3	60	0.000798	0.003728	12.76	34.4	0.21	2.7	0.98	-0.76	550	0	509	0
F2700-2	70	0.000504	0.002487	12.26	33.49	0.2	2.73	0.98	-0.6	530	0	545	0
F2700-1	100	0.003783	0.019838	18.12	48.47	0.19	2.67	0.99	-0.93	501	0	528	0
F2250-5	120	0.000198	0.001026	10.11	37.88	0.19	3.75	0.92	-0.32	519	0	519	0
F2250-4	100	0.001399	0.005548	18.56	40.88	0.25	2.2	0.98	-0.83	511	0	527	0
F2250-3	50	0.001337	0.006242	12.06	34.77	0.21	2.88	0.97	-0.65	539	0	521	0
F2250-2	70	0.000472	0.002124	17.2	50.05	0.22	2.91	0.98	-0.76	510	0	524	0
F2250-1	70	0.000154	0.000761	10.41	35.43	0.2	3.4	0.94	-0.2	537	0	535	0
F2230-4	180	0.000672	0.002223	25.71	56.17	0.3	2.18	0.98	-0.8	532	0	545	0
F2230-3	165	0.000122	0.000619	9.72	29.02	0.2	2.98	0.96	-0.5	561	0	563	0
F2230-2	130	0.00007	0.000274	12.57	37.78	0.26	3.01	0.89	0.1	555	0	552	0
F2230-1	90	0.000168	0.000719	12.07	31.23	0.23	2.59	0.95	-0.46	542	0	558	0
F1930-4	120	0.000621	0.003474	7.21	18.77	0.18	2.61	0.97	-0.96	556	0	558	0
F1930-3	170	0.002015	0.008299	22.75	49.6	0.24	2.18	0.99	-0.98	504	0	509	0
F1930-2	130	0.000354	0.00136	20.58	55.2	0.26	2.68	0.98	-0.75	506	0	509	0
F1500-5	100	0.000119	0.000426	23.38	67.61	0.28	2.89	0.93	-0.43	542	0	519	0
F1500-4	170	0.000239	0.001016	15.18	41.65	0.24	2.74	0.95	-0.57	544	0	521	0

Continued on Next Page...

Table A.1 – Continued

Sample	Weight (mg)	M_{rs}	M_s	B_c	B_{cr}	M_{rs}/M_s	B_{cr}/B_c	S-300	shape	T_{C1}(HC)	T_{C2}(HC)	T_{C1}(CC)	T_{C2}(CC)
F1500-3	130	0.002143	0.008673	18.08	44.32	0.25	2.45	0.98	-0.79	529	0	517	0
F1500-2	140	0.000239	0.001269	8.3	23.79	0.19	2.87	0.94	-0.39	556	0	566	0
F1500-1	160	0.000582	0.002703	9.94	23.13	0.22	2.33	0.98	-0.88	552	0	551	0
F930-4	100	0.002011	0.006272	26.81	53.25	0.32	1.99	0.99	-0.89	525	0	517	0
F930-3	110	0.000238	0.001157	12.08	35.81	0.21	2.97	0.97	-0.69	544	0	546	0
F930-2	60	0.000521	0.002849	12.34	45.07	0.18	3.65	0.98	-0.64	525	0	514	0
F930-1	120	0.000683	0.002497	14.29	30.87	0.27	2.16	0.99	-0.86	581	0	579	0
F500-6	90	0.001394	0.009424	8.63	25.27	0.15	2.93	0.98	-0.76	515	0	505	0
F500-5	140	0.000243	0.001256	8.27	27.86	0.19	3.37	0.95	-0.39	524	0	513	0
F500-4	110	0.00033	0.001611	10.5	27.06	0.21	2.58	0.98	-0.4	541	0	534	0
F500-3	100	0.000399	0.001663	15.99	35.71	0.24	2.23	0.98	-0.79	544	0	539	0
F500-2	110	0.00021	0.001141	8.64	24.84	0.18	2.87	0.97	-0.64	541	0	535	0
F500-1	80	0.00037	0.001534	12.11	27.64	0.24	2.28	0.97	-0.69	574	0	570	0
Nayau Island													
FN001	100	0.00002	0.00009	16.83	42.83	0.22	2.55	0.92	-0.31	531	0	515	0
FN002	210	0.000117	0.000676	15.31	44	0.17	2.87	0.96	-0.67	493	0	489	0
FN003	200	0.000621	0.009294	5.9	28.82	0.07	4.88	0.95	-0.81	510	0	507	0
FN004	180	0.000116	0.000678	12.39	37	0.17	2.99	0.97	-0.7	521	0	504	0
FN005	60	0.00066	0.011655	4.21	33.83	0.06	8.03	0.96	-0.42	426	0	423	0
FN006	60	0.000129	0.000548	11.62	30.69	0.24	2.64	0.97	-0.5	549	0	546	0
FN007	80	0.000155	0.000715	9.63	29.7	0.22	3.08	0.92	-0.25	559	0	561	0
Aiwa Islands													
FA008	140	0.000223	0.00099	10.53	29.31	0.23	2.78	0.94	-0.54	529	0	531	0
FA009	120	0.000036	0.000165	15.22	41.33	0.22	2.72	0.92	-0.31	486	0	474	0
FA010	120	0.000101	0.00041	16.15	41.49	0.25	2.57	0.94	-0.56	496	0	495	0
FA011	120	0.000272	0.001238	11.91	32.93	0.22	2.76	0.96	-0.57	533	0	525	0
FAL12	80	0.000084	0.000359	12.91	32.59	0.23	2.52	0.95	-0.7	536	0	544	0
FAL13	120	0.000147	0.000777	9.06	27.47	0.19	3.03	0.96	-0.57	521	0	509	0
FAL14	120	0.000171	0.000821	11.1	44.07	0.21	3.97	0.93	-0.28	519	0	520	0

Continued on Next Page...

Table A.1 – Continued

Sample	Weight (mg)	M_{rs}	M_s	B_c	B_{cr}	M_{rs}/M_s	B_{cr}/B_c	S-300	shape	T_{C1}(HC)	T_{C2}(HC)	T_{C1}(CC)	T_{C2}(CC)
FAL15	120	0.000071	0.000243	18.22	52.51	0.29	2.88	0.92	-0.29	531	0	529	0
FAL16	80	0.000028	0.000111	14.43	40.93	0.26	2.84	0.96	-0.42	549	0	530	0
FAL17	120	0.000111	0.000469	11.6	32.55	0.24	2.81	0.96	-0.33	531	0	519	0
FAL18	140	0.00009	0.000396	11.92	31.99	0.23	2.69	0.95	-0.36	503	0	493	0
Vanuatu													
Efate Island													
VE001g	130	0.0001	0.001935	3.94	20.9	0.05	5.31	1	-0.94	464	344	489	0
VE001r	140	0.000247	0.002066	10.95	37.77	0.12	3.45	0.98	-0.94	494	0	490	0
VE002	210	0.000085	0.002253	3.03	18.21	0.04	6.01	0.97	-0.85	340	470	494	0
VE004	230	0.000844	0.002915	5.99	31.79	0.29	5.31	0.98	0.17	484	0	492	0
VE005	140	0.000326	0.001745	19.63	43.84	0.19	2.23	0.99	-1.16	504	0	497	0
VE006	180	0.000314	0.001825	15.53	40.67	0.17	2.62	1	-1.01	500	0	491	0
VE007	180	0.000108	0.002706	3.25	19.15	0.04	5.88	0.96	-0.62	342	482	490	0
VE008	120	0.000122	0.002858	3.46	20.79	0.04	6.01	0.95	-0.95	468	328	492	0
VE009	100	0.000513	0.002657	20.58	43.97	0.19	2.14	0.99	-1.1	500	0	497	0
VE010	80	0.000119	0.00209	4.74	27.34	0.06	5.76	0.97	-0.88	462	345	494	0
VE011	150	0.000155	0.005085	2.45	17.18	0.03	7.02	0.93	-0.45	474	357	491	0
VE012	180	0.000216	0.00217	8.64	36.39	0.1	4.21	0.98	-0.73	484	0	487	0
VE013	110	0.000165	0.003849	3.55	19.36	0.04	5.46	0.95	-0.5	470	358	488	0
VE014	180	0.000108	0.001842	4.38	21.23	0.06	4.84	0.94	-0.99	350	470	491	0
VE015	130	0.00011	0.002433	3.72	20.89	0.05	5.61	0.96	-1.05	470	348	499	0
VE016	190	0.000287	0.002075	12.43	39.07	0.14	3.14	0.99	-0.9	496	0	494	0
VE017	130	0.000162	0.003157	4.68	31.05	0.05	6.63	0.96	-0.77	474	0	492	0
VE018	170	0.000199	0.002161	7.64	33.09	0.09	4.33	0.96	-1.01	480	0	490	0
VE019	140	0.000129	0.003206	3.47	25.68	0.04	7.39	0.97	-0.53	476	0	485	0
VE020	140	0.000325	0.002529	14.1	42	0.13	2.98	0.98	-1.1	484	0	490	0
VE021	170	0.000049	0.001304	3.11	21.53	0.04	6.92	0.98	-0.86	484	0	493	0
VE022	140	0.000243	0.002941	6.57	33.81	0.08	5.14	0.97	-0.79	480	0	490	0
VE022	140	0.000243	0.002941	6.57	33.81	0.08	5.14	0.97	-0.79	480	0	490	0

Continued on Next Page...

Table A.1 – Continued

Sample	Weight (mg)	M_{rs}	M_s	B_c	B_{cr}	M_{rs}/M_s	B_{cr}/B_c	S-300	shape	T_{C1}(HC)	T_{C2}(HC)	T_{C1}(CC)	T_{C2}(CC)
VE024	200	0.000474	0.00288	16.01	39.42	0.16	2.46	0.97	-0.99	480	0	480	0
VE025	210	0.000175	0.005427	2.51	16.21	0.03	6.45	0.95	-0.54	344	464	490	0
VE026	160	0.000111	0.00456	1.79	24.82	0.02	13.87	0.92	-0.44	330	458	491	0
VE027	160	0.000456	0.00477	7.3	33.79	0.1	4.63	0.97	-0.93	480	0	490	0
VE028	230	0.000134	0.004606	2.43	20.4	0.03	8.39	0.95	-0.21	478	0	488	0
VE029	120	0.000171	0.00428	3.6	32.07	0.04	8.92	0.95	-0.63	439	0	414	0
VE030	160	0.000146	0.003816	2.89	19.42	0.04	6.71	0.93	-1.2	472	372	479	419
VE031	150	0.000161	0.003289	3.91	22.14	0.05	5.66	0.96	-1.23	476	0	485	0
VE032	160	0.000504	0.003463	13.18	36.45	0.15	2.77	0.97	-1.04	494	0	491	0
VE033	190	0.000129	0.001637	6.48	26.33	0.08	4.06	0.98	-0.51	332	465	500	0
VE034	140	0.000103	0.002039	3.49	17.67	0.05	5.06	0.96	-0.48	474	0	492	0
VE035	110	0.000128	0.002653	3.67	18.82	0.05	5.13	0.97	-0.23	344	464	415	485
VE036	150	0.000033	0.000277	5.75	21.68	0.12	3.77	0.93	-0.64	318	518	512	0
VE037	120	0.001598	0.015447	8.57	40.99	0.1	4.78	0.98	-0.84	464	0	487	0
VE038	180	0.000269	0.003253	6.89	35.81	0.08	5.2	0.98	-0.86	352	476	492	412
VE039	140	0.002325	0.033649	6.42	28.31	0.07	4.41	0.98	-0.7	0	0	0	0
VE040	150	0.000589	0.003962	12.51	36.14	0.15	2.89	0.98	-0.84	474	0	489	0
VE041	130	0.001762	0.054489	3.46	28.33	0.03	8.18	0.96	-0.21	0	0	0	0
VE042	120	0.000384	0.008679	3.43	29.23	0.04	8.51	0.95	-0.55	344	467	489	419
VE043	140	0.000083	0.000788	8.37	33.84	0.11	4.04	0.96	-0.93	494	0	498	0
Malekula													
VM044	100	0.000239	0.001024	12.51	44.48	0.23	3.56	0.93	-0.29	512	0	509	0
VM045	130	0.000942	0.003283	15.07	37.1	0.29	2.46	0.97	-0.67	530	0	510	0
VM046	110	0.000545	0.002166	16.82	41.53	0.25	2.47	0.98	-0.72	550	0	530	0
VM047	110	0.000151	0.001737	5.74	23.46	0.09	4.09	0.96	-0.87	513	0	485	0
VM048	90	0.000141	0.001478	5.68	20.07	0.1	3.53	0.99	-0.96	495	0	490	0
VM049	120	0.000059	0.000257	16.96	51.66	0.23	3.05	0.93	-0.55	529	0	492	0
Vao Island													
VV050	160	0.001385	0.013399	9.97	39.25	0.1	3.94	0.97	-0.93	515	0	520	0

Continued on Next Page...

Table A.1 – Continued

Sample	Weight (mg)	M_{rs}	M_s	B_c	B_{cr}	M_{rs}/M_s	B_{cr}/B_c	S-300	shape	T_{C1}(HC)	T_{C2}(HC)	T_{C1}(CC)	T_{C2}(CC)
VV051	160	0.001576	0.01303	10.94	40.02	0.12	3.66	0.98	-0.97	504	0	511	0
VV052	120	0.000439	0.002464	7.73	23.75	0.18	3.07	0.96	-0.64	534	0	519	0
VV053	150	0.000545	0.003484	6.54	24	0.16	3.67	0.96	-0.54	534	0	521	0
VV054	70	0.003173	0.017525	16.46	42.72	0.18	2.59	0.99	-0.98	494	0	483	0
VV055	80	0.000611	0.0029	21.96	48.75	0.21	2.22	0.98	-1.02	495	0	501	0
VV056	130	0.003346	0.088805	6.1	31.44	0.04	5.15	1	-0.98	0	0	0	0
VV057	130	0.004499	0.053845	11.24	39.21	0.08	3.49	1	-0.75	0	0	0	0
VV058	140	0.002541	0.014865	17.05	44.22	0.17	2.59	0.98	-0.95	510	0	512	0
Santo Island													
VS059	150	0.000549	0.003354	13.68	38.47	0.16	2.81	0.98	-1	494	0	481	0
Uripiv Island													
VU060	210	0.000396	0.001804	13.4	30.51	0.22	2.28	0.98	-0.78	575	0	536	0
Ambae Island													
VA061	160	0.000717	0.001999	27.38	69.68	0.36	2.55	0.98	-0.66	546	0	546	0
VA062	110	0.000132	0.001536	6.81	34.46	0.09	5.06	0.96	-0.76	534	0	528	0
Bismarck Archipelago													
Duke of York Islands													
Y2940-7	80	0.000908	0.016304	4.34	31	0.06	7.14	0.96	-0.66	345	497	412	497
Y2940-6	140	0.000939	0.016139	4.37	30.03	0.06	6.87	0.97	-0.63	354	493	407	496
Y2940-5	140	0.00085	0.015588	4.01	28.3	0.05	7.05	0.96	-0.79	352	505	417	497
Y2940-4	180	0.000082	0.000928	10.55	37.61	0.09	3.56	0.97	-1.04	552	0	559	0
Y2940-3	140	0.000123	0.001925	5.95	34.67	0.06	5.82	0.97	-0.87	325	472	399	503
Y2940-2	200	0.00022	0.002064	9.58	42.01	0.11	4.39	0.93	-0.79	492	0	489	0
Babase Island													
BB-6-1	120	0.000332	0.004155	6.47	28	0.08	4.33	0.97	-0.91	468	0	448	0
BB-6-2	120	0.000956	0.006561	12.29	36.53	0.15	2.97	0.99	-0.87	475	0	464	0
BB-6-3r	130	0.001157	0.011439	7.67	30.02	0.1	3.91	1	-0.73	445	0	464	0
BB-6-4g	140	0.000978	0.01154	7.01	30.64	0.08	4.37	0.98	-0.78	515	0	498	0
BB-6-4r	60	0.00103	0.010638	8.05	32.02	0.1	3.98	1	-0.89	490	0	483	0

Continued on Next Page...

Table A.1 – Continued

Sample	Weight (mg)	M_{rs}	M_s	B_c	B_{cr}	M_{rs}/M_s	B_{cr}/B_c	S-300	shape	T_{C1}(HC)	T_{C2}(HC)	T_{C1}(CC)	T_{C2}(CC)
BB-6-5	130	0.000501	0.006346	6.34	29.87	0.08	4.71	0.97	-0.76	462	0	0	0
BB-6-6	120	0.000327	0.005621	5.15	27.83	0.06	5.41	0.96	-1	435	0	430	0
BB-9-1	180	0.000451	0.003841	9.29	32.81	0.12	3.53	0.98	-0.83	455	0	467	0
BB-9-2	180	0.000129	0.003809	2.66	22.37	0.03	8.4	0.97	-1.16	337	456	390	492
BB-9-3r	70	0.000101	0.000763	10.13	30.32	0.13	2.99	1	-0.94	436	0	455	0
BB-9-4	140	0.000172	0.003771	4.63	27.63	0.05	5.97	0.98	-1.07	434	0	444	0
BB-9-5	140	0.00048	0.007494	5.42	25.81	0.06	4.76	1.02	-0.99	443	0	457	0
BB-9-6g	60	0.000586	0.004708	9.84	31.44	0.12	3.2	0.99	-1.02	476	0	456	0
BB-9-6r	100	0.000428	0.002592	12.38	32.56	0.16	2.63	0.98	-0.96	438	519	464	0
Ambitle Island													
BA-1	100	0.000405	0.008266	4.52	26.97	0.05	5.96	0.96	-0.69	462	0	472	0
BA-2	150	0.000128	0.000747	10.69	33.76	0.17	3.16	0.96	-0.7	521	0	513	0
BA-3	140	0.000892	0.008443	8.64	35.09	0.11	4.06	0.98	-0.75	460	0	468	0
BA-4	140	0.000299	0.003317	8.86	36.09	0.09	4.07	0.97	-1.08	0	0	0	0
BA-5	120	0.000706	0.006787	8.7	32.44	0.1	3.73	0.98	-0.9	510	0	480	0
BA-6	110	0.00043	0.002337	10.01	27.42	0.18	2.74	0.99	-0.83	535	0	533	0
Emira Island													
BE-1	130	0.000274	0.001469	8.33	21.91	0.19	2.63	0.99	-0.6	557	0	555	
BE-2	150	0.00017	0.001434	9.18	34.09	0.12	3.71	0.96	-0.97	554	0	514	
BE-3	160	0.000049	0.000277	7.04	22.32	0.18	3.17	0.97	-0.57	572	0	558	
BE-4g	80	0.000184	0.001067	9.67	28.87	0.17	2.99	0.99	-0.59	562	0	550	
BE-4r	130	0.000079	0.000444	9.47	29.41	0.18	3.1	0.97	-0.63	544	0	540	
BE-5	120	0.000259	0.001959	10.56	32.77	0.13	3.1	0.98	-0.77	584	0	581	
BE-6	130	0.000091	0.000584	7.74	24.79	0.16	3.2	0.95	-0.67	572	0	575	
New Caledonia													
Kone													
NC-19	120	0.000288	0.001675	6.32	19.95	0.17	3.15	0.96	-0.66	522	0	526	0
NC-20	110	0.000437	0.002338	7.36	19.03	0.19	2.59	0.99	-0.97	542	0	545	0
NC-21	140	0.000079	0.000532	5.8	20	0.15	3.45	0.95	-0.64	518	0	520	0

Continued on Next Page...

Table A.1 – Continued

Sample	Weight (mg)	M_{rs}	M_s	B_c	B_{cr}	M_{rs}/M_s	B_{cr}/B_c	S-300	shape	T_{C1}(HC)	T_{C2}(HC)	T_{C1}(CC)	T_{C2}(CC)
NC-22	110	0.000252	0.001132	10.52	25.49	0.22	2.42	0.97	-0.62	540	0	557	0
NC-23	110	0.000165	0.000773	10.54	28.45	0.21	2.7	0.97	-0.79	546	0	524	0
NC-24	110	0.00027	0.001256	8.84	20.95	0.21	2.37	0.99	-0.9	515	0	553	0
Tiouandé													
NC-25	170	0.000018	0.000146	6.61	28.82	0.12	4.36	0.99	-0.82	535	0	516	0
NC-26	160	0.000035	0.000247	7.04	20.19	0.14	2.87	0.97	-0.98	522	0	533	0
NC-27	160	0.00001	0.000153	4.52	23.03	0.07	5.09	0.89	-0.5	409	0	414	0
NC-28	220	0.000124	0.000786	6.64	22.29	0.16	3.36	0.96	-0.73	515	0	505	0
NC-29	240	0.00018	0.001882	3.26	18.02	0.1	5.53	0.98	-0.42	527	0	526	0
NC-30	60	0.000224	0.001322	6.61	19.21	0.17	2.91	0.98	-0.88	512	0	515	0
NC-31	260	0.000252	0.001249	6.58	17.94	0.2	2.73	0.98	-0.82	512	0	505	0
NC-32	210	0.000073	0.000357	9.76	24.17	0.2	2.48	0.98	-0.82	554	0	536	0
NC-33	150	0.000138	0.000852	6.42	18.64	0.16	2.91	0.98	-0.98	532	0	536	0
NC-34	130	0.000215	0.001455	6.23	22.41	0.15	3.6	0.94	-0.62	517	0	500	0
NC-35	190	0.000138	0.0008	7.43	22.56	0.17	3.04	0.97	-0.84	502	0	516	0
NC-36	190	0.000046	0.000233	10.16	36.97	0.2	3.64	0.94	-0.39	522	0	526	0
NC-37	170	0.000147	0.000515	14.48	35.29	0.29	2.44	0.98	-0.68	504	0	0	0
NC-38	170	0.00033	0.001576	7.92	20.61	0.21	2.6	0.97	-0.91	553	0	564	0
NC-39	130	0.000052	0.000359	5.62	35.38	0.15	6.3	0.71	-0.51	544	0	547	0
NC-40	170	0.000088	0.000392	8.34	23.95	0.23	2.87	0.85	-0.6	574	0	577	0
NC-44	200	0.000092	0.000676	6.07	19.61	0.14	3.23	0.97	-0.86	582	0	589	0
NC-45	130	0.000053	0.000534	6.1	26.38	0.1	4.33	0.95	-0.75	574	0	584	0
NC-46	80	0.00008	0.000421	8.18	22.21	0.19	2.71	0.97	-0.8	576	0	579	0
NC-47	180	0.000105	0.000603	6.24	18.72	0.17	3	0.98	-0.74	574	0	575	0
NC-48	100	0.000295	0.00189	8.25	31.73	0.16	3.85	0.96	-0.56	574	0	577	0
NC-49	190	0.000314	0.00145	9.65	22.17	0.22	2.3	0.98	-0.9	584	0	584	0
NC-50	90	0.000122	0.000629	9.51	24.12	0.19	2.54	0.96	-0.68	584	0	585	0
NC-51	70	0.000914	0.005086	9.34	24.87	0.18	2.66	0.98	-0.93	584	0	589	0
NC-52	170	0.000116	0.000677	9.22	27.87	0.17	3.02	0.95	-0.58	574	0	577	0

Continued on Next Page...

Table A.1 – Continued

Sample	Weight (mg)	M_{rs}	M_s	B_c	B_{cr}	M_{rs}/M_s	B_{cr}/B_c	S-300	shape	T_{C1}(HC)	T_{C2}(HC)	T_{C1}(CC)	T_{C2}(CC)
NC-53	190	0.000067	0.000286	11.83	26.9	0.24	2.27	0.96	-0.67	574	0	577	0
NC-54	180	0.000314	0.001687	8.61	21.29	0.19	2.47	0.99	-0.87	584	0	576	0
NC-55	210	0.00038	0.00214	7.11	19.23	0.18	2.7	0.99	-0.82	574	0	574	0
NC-56	140	0.000357	0.001838	9.12	23.86	0.19	2.62	0.98	-0.9	574	0	577	0
NC-57	200	0.00053	0.002485	9.04	21.92	0.21	2.42	0.98	-0.77	574	0	572	0
NC-58	200	0.000241	0.001335	6.33	17.55	0.18	2.77	0.98	-0.92	566	0	574	0
NC-59	170	0.00003	0.000192	9.06	28.06	0.15	3.1	0.96	-0.8	590	0	584	0
NC-60	190	0.00062	0.003082	6.11	16.76	0.2	2.74	0.97	-0.79	567	0	565	0
NC-61	120	0.000066	0.00043	9.57	27.61	0.15	2.89	0.97	-0.68	584	0	583	0
NC-62	160	0.000097	0.000524	7.4	20.31	0.18	2.75	0.96	-0.59	574	0	581	0
NC-63	80	0.000512	0.002642	7.49	21.37	0.19	2.85	0.98	-0.72	572	0	560	0
Pindai													
NC-64	110	0.000641	0.003458	6.34	17.45	0.19	2.75	0.96	-0.82	564	0	561	0
NC-65	110	0.000193	0.001339	5.73	19.57	0.14	3.41	0.95	-0.65	554	0	556	0
NC-66	120	0.000432	0.002355	8.29	23.12	0.18	2.79	0.98	-0.68	574	0	577	0
NC-67	160	0.000496	0.002685	6.84	19.6	0.18	2.87	0.96	-0.95	575	0	568	0
NC-68	180	0.000297	0.001596	6.72	18.8	0.19	2.8	0.97	-0.92	564	0	568	0
NC-69	110	0.000238	0.001494	6.66	19.52	0.16	2.93	0.98	-0.8	564	0	566	0
NC-70	110	0.000379	0.002372	5.41	16.22	0.16	3	0.97	-0.81	564	0	567	0
NC-71	80	0.000381	0.002119	7.35	21.05	0.18	2.86	0.97	-0.6	564	0	567	0
NC-72	80	0.00034	0.002072	6.21	18.84	0.16	3.04	0.97	-0.8	544	0	556	0
NC-76	150	0.000265	0.001687	6.01	17.44	0.16	2.9	0.98	-0.97	564	0	567	0
NC-77	190	0.000269	0.001554	7.16	19.69	0.17	2.75	0.97	-0.75	574	0	565	0
NC-78	180	0.000144	0.000829	7.55	20.56	0.17	2.72	0.97	-0.79	564	0	567	0
NC-79	100	0.000006	0.000053	6.77	28.36	0.12	4.19	0.94	-0.5	564	0	558	0
NC-80	80	0.00018	0.000941	8.88	28.7	0.19	3.23	0.97	0.03	552	0	569	0
NC-81	140	0.000414	0.00234	8.24	22.25	0.18	2.7	0.97	-0.86	584	0	585	0
NC-82	100	0.000258	0.002082	6.31	23.99	0.12	3.8	0.97	-0.76	554	0	556	0
NC-83	180	0.000163	0.001033	7.84	31.94	0.16	4.07	0.97	-0.65	574	622	565	0

Continued on Next Page...

Table A.1 – Continued

Sample	Weight (mg)	M_{rs}	M_s	B_c	B_{cr}	M_{rs}/M_s	B_{cr}/B_c	S-300	shape	T_{C1}(HC)	T_{C2}(HC)	T_{C1}(CC)	T_{C2}(CC)
NC-84	80	0.000423	0.002792	5.28	18.7	0.15	3.54	0.98	-0.65	555	0	566	0
NC-85	170	0.000095	0.000724	4.61	22.34	0.13	4.85	0.94	-0.75	564	0	555	0
NC-86	130	0.000094	0.00059	5.69	19.86	0.16	3.49	0.95	-0.76	555	0	0	0
Nepou													
NC-87	160	0.000115	0.000684	9.79	41.4	0.17	4.23	0.96	-0.63	525	0	547	0
NC-88	170	0.000112	0.00061	8.29	21.53	0.18	2.6	0.98	-0.91	575	0	567	0
NC-89	150	0.0005	0.002704	8.37	23.76	0.18	2.84	0.97	-0.81	574	534	580	0
NC-90	80	0.00011	0.000304	31.87	65.63	0.36	2.06	0.98	-0.83	527	0	536	0
Nouville													
NC-91	120	0.000274	0.002144	6.22	26.98	0.13	4.34	0.9	0.02	555	0	552	0
NC-92	140	0.000236	0.001459	7.49	27.96	0.16	3.73	0.95	-0.69	575	0	565	0
NC-73	90	0.000344	0.002086	7.92	31.74	0.17	4.01	0.96	-0.61	544	0	556	0
NC-74	80	0.000329	0.002019	7.33	26.4	0.16	3.6	0.96	-0.47	544	0	559	0
Nessaidou													
NC-93	140	0.000149	0.00094	6.27	19.43	0.16	3.1	0.97	-0.51	565	0	578	0
NC-94	130	0.000179	0.000935	8.07	21.26	0.19	2.64	0.98	-0.86	565	0	571	0
NC-95	170	0.000343	0.001863	10.06	32.26	0.18	3.21	0.96	-0.66	574	0	588	0
NC-96	70	0.000196	0.001065	9.62	30.51	0.18	3.17	0.94	-0.52	554	0	576	0
Goro													
NC-97	120	0.000393	0.001864	8.6	21.5	0.21	2.5	0.97	-0.6	542	0	550	0
NC-98	120	0.000576	0.003053	7.94	27.49	0.19	3.46	0.97	-0.7	574	0	567	0
NC-41	120	0.000216	0.000974	9.11	21.5	0.22	2.36	0.98	-0.68	584	0	585	0
NC-42	180	0.000087	0.0007	5.49	18.19	0.12	3.32	0.98	-0.87	554	0	554	0
NC-43	160	0.000153	0.000955	7.17	20.42	0.16	2.85	0.98	-0.86	542	0	548	0
Solomon Islands													
New Georgia (Hoghoi)													
HG1	120	0.000171	0.001804	8.31	32.96	0.09	3.97	0.95	-0.95	499	606	0	0
HG2	80	0.000159	0.001195	13.43	40.1	0.13	2.99	0.97	-0.91	510	606	512	0
HG3	130	0.000027	0.000138	8.92	30.5	0.19	3.42	0.95	-0.37	609	499	576	0

Continued on Next Page...

Table A.1 – Continued

Sample	Weight (mg)	M_{rs}	M_s	B_c	B_{cr}	M_{rs}/M_s	B_{cr}/B_c	S-300	shape	T_{C1}(HC)	T_{C2}(HC)	T_{C1}(CC)	T_{C2}(CC)
HG3g	130	0.00001	0.000058	10.07	35.52	0.17	3.53	1	-0.45	609	499	607	0
HG3r	100	0.000027	0.000149	8.9	32.63	0.18	3.67	0.97	-0.31	597	477	542	452
NG251	60	0.000401	0.001963	8.97	26.29	0.2	2.93	0.97	-0.64	555	0	561	0
NG252	100	0.000143	0.001103	5.17	18.59	0.13	3.59	0.95	-0.84	575	0	565	0
NG253	100	0.000465	0.002538	8.34	26.91	0.18	3.23	0.95	-0.64	555	0	558	0
Santa Cruz (Nendo)													
SZ1	120	0.000646	0.006814	5.34	21.46	0.09	4.02	0.99	-0.7	533	0	538	0
SZ2	120	0.000417	0.002426	8.91	22.44	0.17	2.52	0.99	-0.85	553	0	553	0
SZ3	140	0.000456	0.003042	8.27	26.18	0.15	3.17	0.98	-0.78	569	0	536	0
SZ8-1	100	0.000247	0.001394	10.84	28.27	0.18	2.61	0.99	-0.89	567	0	560	0
SZ8-2	90	0.000895	0.003169	14.82	34.68	0.28	2.34	0.98	-0.74	593	0	577	0
SZ8-3	110	0.000811	0.006747	7.72	27.71	0.12	3.59	0.98	-0.84	513	0	527	0
SZ8-4b	120	0.000528	0.003967	10.1	35.56	0.13	3.52	0.99	-0.95	549	0	536	0
SZ8-5	110	0.000334	0.00208	8.27	21.77	0.16	2.63	0.99	-1	559	0	554	0
SZ8-6	130	0.000492	0.003744	9.27	32.2	0.13	3.47	0.97	-0.88	547	0	524	0
SZ8-7	150	0.000447	0.002496	12.92	38.25	0.18	2.96	0.98	-0.85	517	0	519	0
SZ8-8	140	0.000186	0.000885	11.61	32.74	0.21	2.82	0.98	-0.67	549	0	553	0
SZ8-9	130	0.000746	0.003822	8.65	22.95	0.2	2.65	0.99	-0.76	569	0	564	0
SZ8-10	120	0.000481	0.002701	7.52	23.93	0.18	3.18	0.99	-0.73	559	0	550	0
SE-1	130	0.000146	0.000825	11.23	30.84	0.18	2.75	0.96	-0.78	557	0	536	0
SE-2	120	0.000315	0.001315	12.29	27.72	0.24	2.25	0.99	-0.86	553	0	557	0
SE-3	130	0.000319	0.001667	10.47	25.73	0.19	2.46	1	-0.97	555	0	545	0
SE-4	140	0.000113	0.000733	9.86	30.46	0.15	3.09	0.99	-0.9	567	0	546	0
SE-5	130	0.000217	0.001345	7.83	25.39	0.16	3.24	0.98	-0.7	545	0	508	0
SE-6	150	0.00019	0.001088	12.06	35.3	0.17	2.93	0.96	-0.75	545	0	546	0
SE-7	160	0.00037	0.001914	8.87	25.65	0.19	2.89	0.99	-0.67	549	316	550	0
SE-8	160	0.000091	0.000603	8.98	29.34	0.15	3.27	0.98	-0.78	547	0	535	0
SE-9	120	0.000171	0.001361	8.59	33.86	0.13	3.94	0.98	-0.85	487	0	500	0
SE-10	120	0.000975	0.003772	12.4	27.08	0.26	2.18	1	-0.83	567	0	564	0

Continued on Next Page...

Table A.1 – Continued

Sample	Weight (mg)	M_{rs}	M_s	B_c	B_{cr}	M_{rs}/M_s	B_{cr}/B_c	S-300	shape	T_{C1}(HC)	T_{C2}(HC)	T_{C1}(CC)	T_{C2}(CC)
SZS-1b	150	0.000505	0.002561	9.45	25.76	0.2	2.73	0.98	-0.88	557	0	546	0
SZS-2	140	0.000262	0.001639	9.22	25.05	0.16	2.72	0.97	-0.93	577	0	564	0
SZS-3	130	0.000746	0.006959	8.32	33.26	0.11	4	0.98	-0.81	507	0	515	0
SZS-4	130	0.00103	0.005149	10.02	27.59	0.2	2.75	0.95	-0.65	527	0	526	0
SZS-5	140	0.000482	0.003087	9.31	28.01	0.16	3.01	0.98	-0.8	547	0	565	0
SZS-6	130	0.000253	0.001089	11.8	29.78	0.23	2.52	0.96	-0.69	577	0	560	0
SZS-7	140	0.000329	0.002375	9.78	33.15	0.14	3.39	0.96	-0.78	545	0	520	0
SZS-8	130	0.001092	0.003552	14.89	29.1	0.31	1.95	0.99	-0.94	575	0	565	0
SZS-9	140	0.000615	0.003418	11.99	35.44	0.18	2.96	0.97	-0.77	517	0	526	0
SZS-10	120	0.000447	0.002835	10.72	30.11	0.16	2.81	0.99	-1	609	519	562	0
Santa Cruz (Reef Islands)													
RF6-1	120	0.000496	0.002621	12.31	35.15	0.19	2.85	0.99	-0.85	537	0	536	0
RF6-2	120	0.001025	0.006805	11.25	29.16	0.15	2.59	0.99	-0.82	507	0	504	0
RF6-3	130	0.000207	0.000969	13.93	37.63	0.21	2.7	0.97	-0.8	537	0	524	0
RF6-4	140	0.000538	0.002449	11.81	29.96	0.22	2.54	0.98	-0.84	567	0	546	0
RF6-5	120	0.000381	0.001719	11.16	29.53	0.22	2.65	0.98	-0.77	567	0	546	0
RF6-6b	130	0.000365	0.002523	11.41	36.26	0.14	3.18	0.97	-0.83	543	345	565	0
RF6-7	140	0.000288	0.001498	9.8	28.12	0.19	2.87	0.97	-0.63	562	323	576	0
RF6-8	130	0.000108	0.001086	6.89	28.29	0.1	4.11	0.97	-0.91	557	0	525	0
RF6-9	140	0.000512	0.002386	12.39	32.92	0.21	2.66	0.98	-0.76	565	0	546	0
RF6-10	130	0.000309	0.002025	11	33.48	0.15	3.04	0.99	-0.86	507	0	515	0
RF251-1	120	0.000927	0.005464	10.64	31.54	0.17	2.96	0.97	-0.84	537	0	525	0
RF251-2	140	0.001095	0.004207	12.31	28.77	0.26	2.34	0.98	-0.8	593	0	546	0
RF251-4	100	0.000629	0.00706	8.48	33.13	0.09	3.91	0.99	-1	515	0	525	0
RF251-5	140	0.000263	0.001079	11.69	26.38	0.24	2.26	0.97	-0.64	577	0	566	0
RF251-6	110	0.000406	0.004317	6.33	26.43	0.09	4.17	0.97	-0.85	487	0	475	0
RF251-7	120	0.000559	0.003429	9.91	28.48	0.16	2.87	0.98	-0.81	557	0	546	0
RF251-8	150	0.001008	0.005327	10.83	28.92	0.19	2.67	0.99	-0.68	527	0	524	0
RF251-9	120	0.000851	0.004794	8.21	26.27	0.18	3.2	1	-0.67	547	0	543	0

Continued on Next Page...

Table A.1 – Continued

Sample	**Weight (mg)**	$\mathbf{M}_{rs}$	$\mathbf{M}_s$	$\mathbf{B}_c$	$\mathbf{B}_{cr}$	$\mathbf{M}_{rs}/\mathbf{M}_s$	$\mathbf{B}_{cr}/\mathbf{B}_c$	**S-300**	**shape**	$\mathbf{T}_{C1}$**(HC)**	$\mathbf{T}_{C2}$**(HC)**	$\mathbf{T}_{C1}$**(CC)**	$\mathbf{T}_{C2}$**(CC)**
RF251-10	180	0.000607	0.003615	6.74	24.9	0.17	3.69	0.99	-0.63	549	0	549	0
RF251-11	120	0.000403	0.002022	9.48	27.03	0.2	2.85	0.97	-0.57	545	0	516	0
RF252-1	130	0.000213	0.001207	7.01	26.66	0.18	3.8	0.92	-0.47	537	0	525	0
RF252-3	150	0.000495	0.002472	8.6	22.28	0.2	2.59	0.98	-0.82	567	0	563	0
RF252-4	140	0.001206	0.008525	5.69	20.87	0.14	3.66	0.97	-0.59	577	0	575	0
RF252-5	130	0.00036	0.002097	7.69	24.15	0.17	3.14	0.96	-0.68	547	0	546	0
RF252-6	130	0.000418	0.002466	9.63	33.33	0.17	3.46	0.88	-0.72	537	0	543	0
RF252-7	120	0.001017	0.006523	8.13	28.95	0.16	3.56	0.9	-0.72	587	0	546	0
RF252-8	130	0.000331	0.002533	8.9	39.82	0.13	4.47	0.85	-0.74	517	0	524	0
RF252-9	130	0.000396	0.00513	5.72	29.07	0.08	5.09	0.97	-0.58	485	0	476	0
RF252-10	110	0.00031	0.003247	6.9	34.67	0.1	5.02	0.94	-0.73	517	0	526	0

Results from magnetic mineralogical investigations on prehistoric ceramics from the south west Pacific using a Variable Field Translation Balance (VFTB). M_{rs}, M_s, B_c, B_{cr}, M_{rs}/M_s, B_{cr}/B_c denotes hysteresis parameter and their ratios. S-300 is a coercivity parameter after Bloemendal et al. (1992). "shape" describes the appearance of hysteresis loops after Fabian (2003). T_C(HC) and T_C(CC) are Curie temperatures obtained from the heating and/or cooling curves.

Appendix B

Results of petrographic investigations of Efate potsherds

Table B.1: Identity of petrographically investigated thin sections of ceramics from Efate island.

SITE	GROUP A T_{C1} & T_{C2} *(reliable AI)*	GROUP B T_{C1} & T_{C2} *(unreliable AI)*	GROUP C T_{C1} only *(reliable AI)*	GROUP D T_{C1} only *(unreliable AI)*
Mangaasi	VE-02 & VE-10	VE-25	VE-09 & VE-31	VE-21
Arapus		VE-35	VE-32	
Teouma		VE-38		VE-40

Ten potsherds from three different sites on Efate were divided in four different groups depending on the occurrence of one or two Curie temperatures and their capability yielding reliable archaeointensity (AI) results (courtesy of W.R.Dickinson, (2011)).

Table B.2: Frequency percentages of grain types in ceramics from Efate island of Table B.1.

	GROUP A		GROUP B			GROUP C			GROUP D		
sherd	VE-02	VE-10	VE-25	VE-35	VE-38	VE-09	VE-32	VE-31	VE-21	VE-40	SDCE[3]
site[1]	M	M	M	A	T	M	A	M	M	T	
plg[2]	81	67	73	62	54	75	69	71	58	50	4-5
cpx[2]	-	-	8	5	18	1	7	2	4	20	1-4
opa[2]	6	6	8	12	6	7	5	7	8	4	2-3
VRF[2]	13	27	11	21	22	17	19	20	30	26	3-5

[1]A, Arapus; M, Mangaasi; T, Teoma. [2]plg, plagioclase feldspar; cpx, clinopyroxene (augite); opa, opaque iron oxides; VRF, volcanic rock fragments (mostly vitric with minor plagioclase microlites embedded in felsic volcanic glass). [3]standard deviation of counting error = $[p(100\text{-}p)/n]^{\frac{1}{2}}$ where n (grains counted) = 100 per sherd (Van der Plas and Tobi, 1965) (courtesy of W.R.Dickinson, (2011)).

Table B.3: Mean frequency percentages of grain types in Efate sherds of Table B.2 from different archaeological sites.

site	Mangaasi	Arapus	Teouma	SDCE
N	N=6	N=2	N=2	
plg	71±8	66±4	52±2	4-5
cpx	3±3	6±1	19±1	1-4
opa	7±1	8±4	5±1	2-3
VRF	20±8	20±1	24±2	3-5

N is number of sherds. ± is the standard deviation. SDCE from Table 2 (courtesy of W.R.Dickinson, (2011)).

Appendix C

Archaeomagnetic dating of an Icelandic lava flow

Introduction

This study shows how well established secular variation curves (directions) can be used for a determination of the age of a Holocene volcanic lava flow and thus aids for a better understanding and risk assessment of potential hazardous volcanoes. Since a deepener investigation of this study is beyond the scope of this thesis, only the results, possibilities and limitations of archaeomagnetic dating are described. For the age determination a "Matlab" tool for archaeomagnetic dating developed by Pavon-Carrasco et al. (2011) was used.

The investigated lava flow was produced by the Öræfajökull volcano in south east Iceland which is on the southern margin of the Vatnajökull ice cap (63.6° N, 16.5° W). The Öræfajökull is an ice-clad stratovolcano which erupted twice during the history of the Icelandic settlement in 1362 AD and 1727 AD (Selbekk and Trønnes, 2007). Rapid retreat of the margin of the outlet glaciers of the Öræfajökull ice cap in the last decade has led to the uncovering of an extensive lava flow $\sim$ 0.8 to 1 km in length (Richard Chiverell pers. comm. 2011). The age and relative order of the lava flow events in the region is not fully understood and here the potential for archaeomagnetic dating in solving this problem is assessed.

Sampling

Twenty-five samples (2.54 cm cores) were drilled from 5 different sections along the 2 km intermittent exposure of a probable continuous single lava flow on the southern lateral margin of the Virkisjökull outlet glacier of Öræfajökull.

A large number of independent samples are important for obtaining a statistically robust result of the direction. The core orientation in the field was determined using a sun-compass (y-sight) and orientation device (dip).Laboratory analysis comprised the samples being demagnetised in 25°C steps from room temperature to 350°C and

Table C.1: Directional and dating results from an Icelandic lava flow.

Code	Fitted Dec	Fitted Inc	MAD	Dec_{mean}	Inc_{mean}	α_{95}	Age estimation
Virkisjökul, Iceland (63.5759° N, 16.4754° W)							
VS02	1.4	66.1	0.3	5.3	64.9	3.0	1208 AD - 1482 AD
VS03	8.6	64.0	0.3				
VS04	7.4	62.1	0.5				
VS05	3.2	67.2	0.6				
Virkisjökul, Iceland (63.5759° N, 16.4756° W)							
VS08	350.2	66.2	0.9	348.6	64.8	2.1	1345 AD - 1405 AD
VS09	355.9	64.7	0.5				
VS11	346.4	65.1	0.7				
VS13	346.2	64.1	0.8				
VS14	344.5	63.7	0.9				
Virkisjökul, Iceland (63.5757° N, 16.4801° W)							
VS15	7.4	64.1	0.9	6.9	68.3	4.3	479 AD - 626 AD
VS17	356.8	69.0	1.2				1078 AD - 1565 AD
VS18	13.7	70.1	1.9				
VS19	10.0	69.7	1.1				
Virkisjökul, Iceland (63.5746° N, 16.4849° W)							
VS21	351.6	55.0	1.1	357.2	63.8	8.3	245 AD - 483 AD
VS23	347.7	55.3	0.6				1144AD - 1538 AD
VS24	3.1	68.6	0.6				
VS25	5.1	70.8	0.4				
VS26	7.7	68.3	0.3				
Virkisjökul, Iceland (63.5735° N, 16.4913° W)							
VS33	352.1	65.4	1.3	349.7	65.4	4.8	1295 AD - 1450 AD
VS34	0.1	67	0.7				
VS35	0.1	64.7	0.8				
VS36	343.4	66.4	1.2				
VS37	334.7	61.9	1.3				
Mean values of all results (63.58° N, 16.48° W)							
				356.6	65.5	2.2	†1328 AD - 1427 AD

Table C.1: Fitted Dec and Inc describe mean directions determined using "Plotcore 2.1" by Alan McCormack. MAD denotes the mean angular deviation. Dec_{mean} and Inc_{mean} are the mean values from a sampled section. The α_{95} describes the radius of a 95% confidence cone. Age estimations show the estimated age levels for each section at a 95% confidence level. †The final age estimation is determined by using mean values of all results.

measured with a JR6 magnetometer. The directional data were afterwards determined by recalculating the sun-compass data and using the software "Plotcore 2.1" by Alan McCormack. In order to estimate the age of the lava flow, the directional data (inclination and declination) together with the determined α_{95} were compared to the secular variation (SV) curves from France. The SV curves with age intervals from 950 BC to 1800 AD cover both volcanic eruptions. The age was computed using a "Matlab" tool for archaeomagnetic dating developed by Pavon-Carrasco et al. (2011).

Results and Discussion

Twenty-three samples revealed reliable directions with MAD's < 1.9. Two samples were rejected due to a significant overprint which was probably drilling induced. All age determination results are shown in Table C.1 and illustrated in Fig. C.1. The lava

flow was sampled over a length of 2 km and partly not exposed. Consistent mean values from each sampled section suggest that one single lava flow was sampled. Using all 23 successful results in a mean directional value with a low α_{95} value (2.2°) (Fisher, 1953). Comparing the mean inclination and declination obtained from the lava flow with the secular variation curve from France recalculated for Iceland (Fig. C.1a and b) reveal two probability densities on a 95% confidence level (Fig. C.1c and d). Whereas the declinational data exhibit several possibilities for an age, the inclinational data resulted in a distinct age interval. Combining these two results gives an age interval between 1321 AD to 1401 AD which suggests that the 1362 AD eruption produced this lava flow and not the 1727 AD eruption (Fig. C.1f). An overview map with the origin of the SV curve and the investigated site is shown in (Fig. C.1e).

It has to be acknowledged that the age determination is solely governed by the inclination which is even shallower than predicted by the French secular variation curve. The result, however, is still within the error envelope calculated from the α_{95} value. There is also a likelihood that the investigated lava flow is a result of an earlier eruption which is not covered by the secular variation curve.

Conclusion

This study has shown the feasibility of archaeomagnetic dating of a lava flow. Due to the limited coverage of the SV curve the 1362 AD eruption cannot be verified. Nevertheless, it seems to be unlikely that the 1727 AD eruption caused the investigated lava flow at Virkisjökull. Though the age assignment of the Virkisjökull lava flow by archaeomagnetic dating remains at present ambiguous, the recovery of a coherent signal from 2km of discontinuous exposure suggests that with improved spatial and temporal coverage of SV data the technique has considerable potential in constraining the timing of historic and prehistoric eruptions thereby informing hazard awareness.

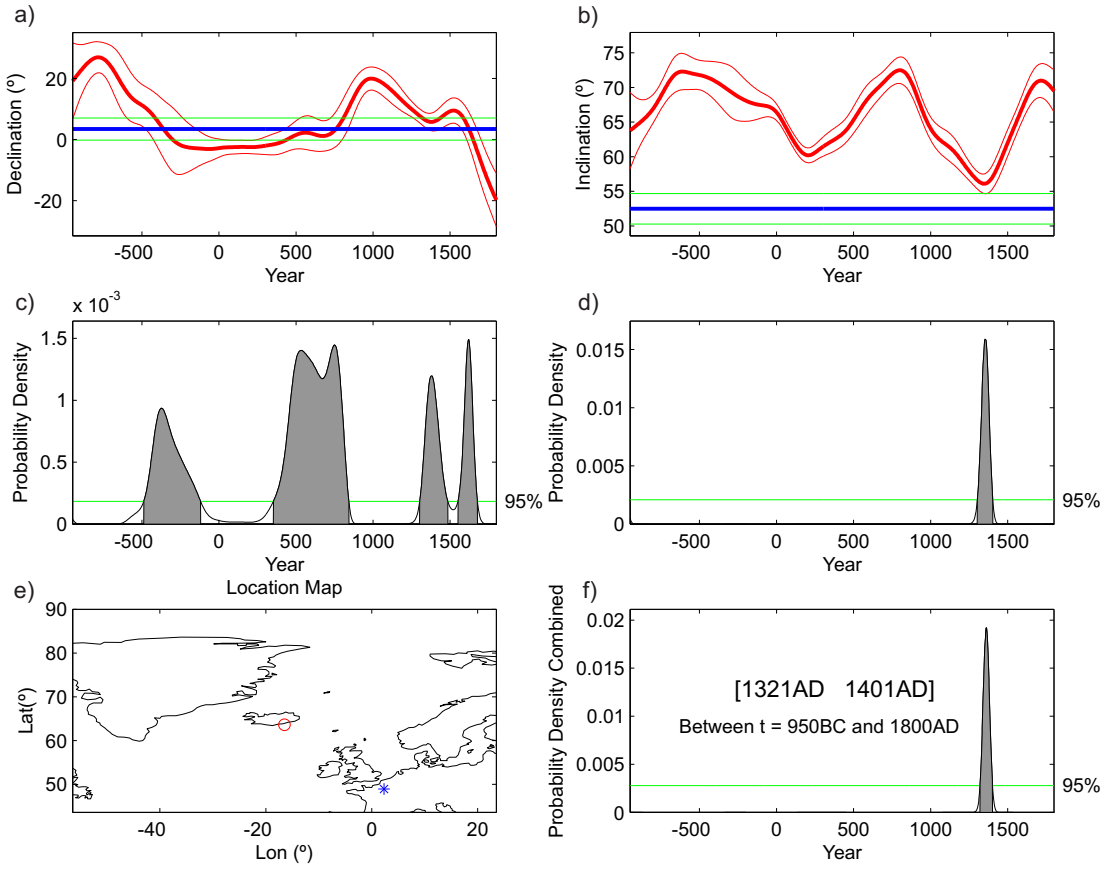

Figure C.1: Archaeomagnetic dating of an Icelandic lava flow. Panel (a) and (b) exhibit both declination and inclination (blue) with error envelops (green) using the α_{95} parameter as well as secular variations (red) from the UK. (c) and (d) show probability densities determined by superposing the measured declinations and inclinations with the secular variation curves. A location map with the origin of the secular variation curve (blue asterisk) and the investigated site (red circle) are illustrated in (e). A combination of the probability densities with an age estimation is shown in (f).